Czech University of Life Sciences Prague
Faculty of Engineering

2020

Proceeding of 22nd International Conference of Young Scientists 2020

Czech University of Life Sciences Prague – Faculty of Engineering

Sept. 14th – Sept. 15th 2020

CZECH UNIVERSITY OF LIFE SCIENCES PRAGUE

FACULTY OF ENGINEERING

22ND INTERNATIONAL CONFERENCE OF YOUNG SCIENTISTS 2020

PROCEEDING OF 22ND INTERNATIONAL CONFERENCE OF YOUNG SCIENTISTS 2020

September 14th 2020 – September 15th 2020

Prague

Czech Republic

Editors: Rostislav Chotěborský, Jiří Kuře

ISBN 978-80-213-3037-5

22nd International Conference of Young Scientists 2020

September 14th 2020 – September 15th 2020

Conference ICYS publishes research in engineering and physical sciences that represent advances in understanding or modelling of the performance of biological and physical systems for sustainable developments in land use and the environment, agriculture and amenity, bioproduction processes and the food chain, logistics systems in agriculture, manufacturing and material systems in design of agriculture engineering.

Conference venue:

Faculty of Engineering, Czech University of Life Sciences Prague, Kamýcká 129, Praha 6, Prague, 165 21, Czech Republic

Scientific committee:

prof. Ing. Vladimír Jurča, CSc.

prof. Ing. David Herák, Ph.D.

doc. Ing. Rostislav Chotěborský. Ph.D.

doc. Ing. Jiří Mašek, Ph.D.

prof. Ing. Zdenko Tkáč, PhD.

doc. RNDr. Vlasta Vozárová, PhD.

doc. Ing. Pavel Beňo, PhD.

prof. Ing. Roman Gálik, PhD.

CONTENT

The impact of different tillage on selected wheat varieties by using the UAV

K. Balážová[1], J. Kumhálová[2], J. Chyba[1], J. Mašek[1]

[1]Department of Agricultural Machines, Faculty of Engineering, Czech University of Life Sciences Prague, Prague, Czech Republic

[2]Department of Machinery Utilization, Faculty of Engineering, Czech University of Life Sciences Prague, Prague, Czech Republic

Abstract

Multi-spectral images taken by unmanned aerial vehicles (UAVs) can help to assess the characteristics of selected crops in different phenological stages. Two cultivars, the Khorasan and the Kabot wheat, in three different tillages were monitored by an eBee X UAV equipped by a MicaSense RedEdge-MX camera. A normalized difference vegetation index (NDVI) was selected to assess the vitality of crops. The measurement took place in three phenological stages: tillering, stem elongation, heading. No statistically significant difference was found between the variants except the early phase of both wheat varieties growth, however, the variant with the plowing and Kabot variety reached higher average values than other variants.

Key words: Unmanned Aerial Vehicles, tillage, wheat, vegetation indices

INTRODUCTION

The grain of Khorasan wheat has an amber colour and high vitreosity and it excels in the impressive size of the grain compared to the other types of wheat. In the most cases the WTS (weight of thousand seeds) is greater than 50 g, but there are cases where the WTS exceeds the limit of 60 g. In general, the Khorasan crop is taller than other wheat varieties. Wheat Khorasan is suitable for ecological agriculture systems, although it is less adaptable, especially to low temperatures and powdery mildew. It is also necessary to monitor unnecessarily large inputs of nitrogen fertilizers which increase the effect of susceptibility to disease. The advantage of this wheat is higher habitus and rapid development of young plants which creates very good competition against unwanted weeds (QUINN et al., 1999; GIANOTTI et al., 2012; LORETO et al., 2017).

Tillage is a basic process in crop growing that contributes to stable and high yields. In the long-term perspective the tillage is an important process of caring for soil and its fertility. By tillage, the soil should ensure that crops receive the best possible conditions for their growth and

development. At the same time the negative impact on the habitat should be minimized (HŮLA et al., 2010). Until the early 1990s the conventional ploughing tillage with subsequent pre-sowing preparation was a key agricultural technology (KÖLLER & LINKE, 2006). JAVOREK (2006) states that ploughing eliminates the germination of some weeds because their seeds are moved to greater depths by ploughing. It also incorporates plant residues and fertilizers into the soil. It should also ensure stable yields and enable seamless sowing which is not always easy. After the early 1990s due to growing economic pressure and ever-increasing positive response to farming without ploughing, the whole range of tillage systems including latest trends such as direct sowing began to expand (KÖLLER & LINKE, 2006). Minimization technologies are characterized mainly by the unification of several work operations into one, but they are also characterized by the replacement of ploughing by shallow tillage of the soil. There has been a change not only in the technologies themselves, the changes were also made on the machines used for the crop establishment (MAŠEK, 2006).

Today remote sensing is a very important technique for obtaining valuable information not only for farmers themselves, but also for general public which is interested in the issue. Collecting images that are in the different spectral bands plays an important role. Three remote sensing methods are commonly used: satellite, aerial and UAVs. Satellite methods are a good helper in crop yield, chlorophyll and nitrogen content estimation (JELÍNEK et al. 2020; VINCINI et al. 2016). The negative factor for the mentioned method is the spatial resolution (KUMHÁLOVÁ et al. 2014). UAV imaging provides practical monitoring of the crop conditions, especially in various experiments where is important to have a constant overview. Aerial photography not only provides a comprehensive results of vegetation vitality, but also time saving tool as a reliable replacement for manual sampling (DUAN et al. 2017).

The NDVI is so-called differentiated ratio of reflectance between the red (absorbed by vegetation) and near infrared light (NIR – reflected by vegetation) (ROUSE et al. 1974; TUCKER, 1979) and is quite often used in research and in commercial agronomic applications (MARTI et al. 2007). NDVI serves as a means of obtaining valuable information on crop yield, biomass estimation, structure, crop vigour, leaf area in wheat but also more often in other less common crops of all kind. It is also a good tool for monitoring the dynamic changes of biomass during the growing season in different types of crops which can help to not only breeding companies but it is also a modern solutions for precision agriculture (MARTI et al. 2007; TESTER & LANGRIDGE, 2010; MCKINNON & HOFF 2017). Estimates are obtained from different patterns of reflectivity of green plant and soil. The index output is usually assigned to a colour from the colour range and creates a coherent image (ERDLE et al.,2011).

MATERIALS AND METHODS

Study area

The experiment was established in the village of Čenovice located in the Vysočina region (N 49˚79'46.367", E 15˚11'37.622") in Czechia. On the experimental area were founded six plots, each of them represents individual variant that were treated by different tillage technologies and sown by different cultivars. Each variant has an area 4×50 m. Between each variant is a separating strip 4 m wide. Variants 1 to 3 were sown with ancient spring wheat Khorasan (*Triticum turgidum ssp. Turanicum*) while variants 4 to 6 were sown by modern and efficient spring wheat Kabot, which is characterized by a very high WTS. With regards to tillage the variants 1 & 4 were treated conventionally by ploughing, variants 2 & 5 by minimization technique using a coulter cultivator and variants 3 & 6 by minimization technique using disc cultivator.

UAV equipment and flight configuration

Aerial photography was carried out using a flying wing eBee X (senseFly SA, Cheseaux-Lausanne, Switzerland). The flying wing was equipped with a MicaSense RedEdge-MX multispectral camera (MicaSense, Inc. Seattle, WA, USA) which contains five spectral bands with a resolution of 1.2 Mpx. Imaging took place in three phenological phases of wheat, during tillering (18.5.2020), stem elongation (11.6.2020) and heading (3.7.2020). The flights were performed at an altitude of 90 m above ground with a spatial resolution of 7 cm per pixel. Mission planning was carried out using eMotion software (SW, senseFly, Lausanne). All flights were scheduled so that the individual images have 65% lateral and 80% longitudinal overlap.

The images were processed using postflight tool in eMotion SW. Subsequently the images were consolidated into orthophoto by SW Pix4D from which the spectral index NDVI was derived. Another adjustment of the orthophoto was performed in the SW QGIS where the plots were clipped, furthermore, by using tool Zonal Statistics the descriptive statistics of monitored experiment were derived.

RESULTS AND DISCUSSION

Summary statistics of crop vitality are in Figure 1 where a significant statistical difference occurred only between terms of measurement the lower values in term 18.5.2020 occurred because early stage of development of crops and thus less coverage by green plants. Nevertheless, the variant 4 (Kabot with ploughing) showed the highest average NDVI value through all variants. There was no statistically significant difference in phenological phases. All variants in terms of variety and tillage have very similar NDVI values.

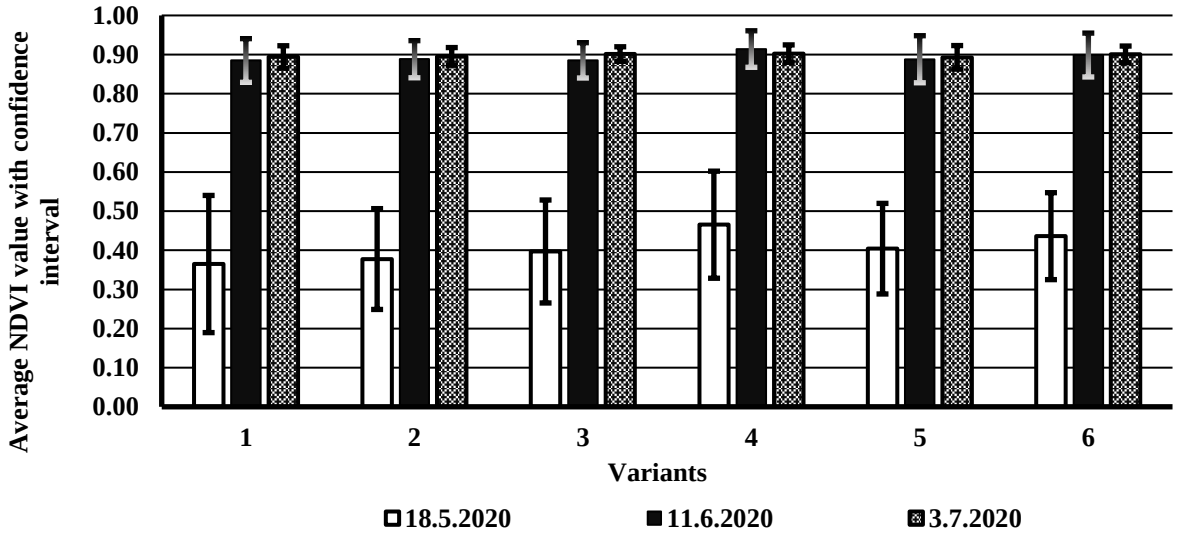

Fig. 1 Average NDVI values generated from aerial photos taken in three terms at different phenological phases in two varieties of wheat Kamut (1 to 3) and Kabot (4 to 6) under different tillage processing: 1 & 4 ploughing, 2 & 5 coulter cultivator, 3 & 6 disc cultivator

Figure 2 shows NDVI indices for all measured variants. From the figure is visible that the variant 4 (ploughing with variety Kabot) has best NDVI results. This is especially evident in term b (11.6.2020).

Comparing the condition of the crop within different tillage using UAV and NDVI has not been much studied yet for spring wheat. In addition, the results should be supported by sample collection before harvest or by yield mapping. For example, comparison of WTS within variants, laboratory analysis, comparison of size and conditions of selected plants and focus on the collection and analysis of soil samples. These additional measurements should provide more comprehensive output data and a better insight into the issue. YEOM et al. (2019) examined the difference in tillage for two selected crops (cotton and sorghum) using various RGB and NIR VIs (vegetation indices). Data from UAV DJI Phantom 4 Pro and DJI Matrice 100 with high resolution of VIs were used to measure the effect of tillage on plant vitality. The

measurement took place every week during the season. The results showed clear difference in VIs between tillage throughout the growing season. NIR-based VIs showed better discrimination performance than RGB-based VIs. The results also showed clear differences in Vls between conventional tillage and no-tillage throughout the cotton and sorghum growth period. Plots with no tillage showed higher Vls values in most variants.

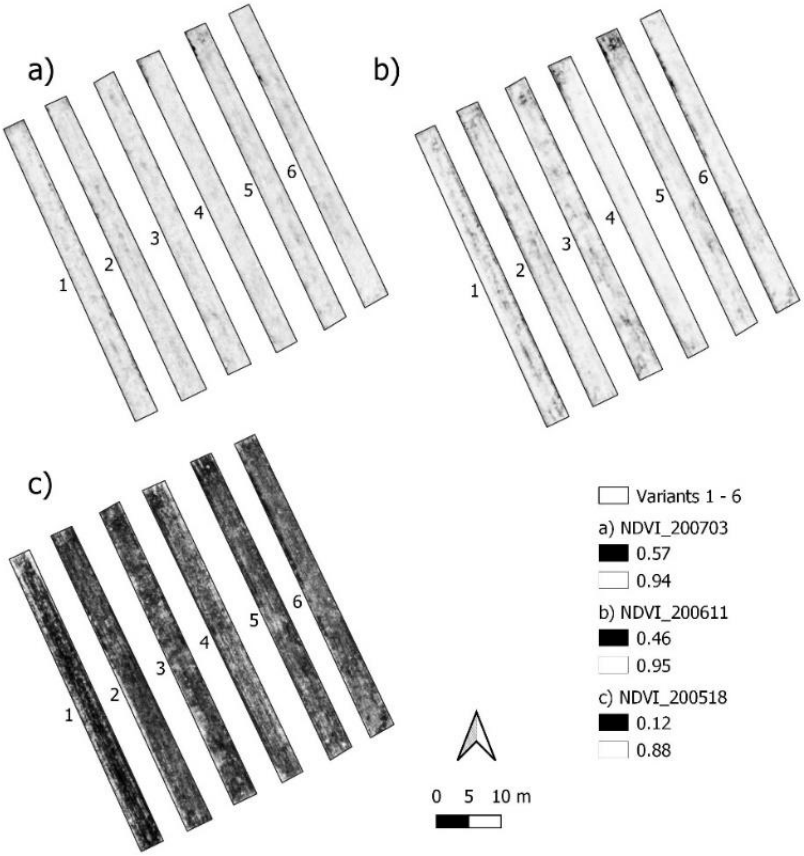

Fig. 2 NDVI values for all variants during monitored terms with two varieties of wheat Kamut (1 to 3) and Kabot (4 to 6) under different tillage processing: 1 & 4 ploughing, 2 & 5 coulter cultivator, 3 & 6 disc cultivator. Terms: a – 3.7.2020, b – 11.6.2020, c – 18.5.2020

CONCLUSION

The use of UAVs and vegetation indices is a good complement to gaining a new knowledge about the state of the crop during the vegetation, especially in their early stages. In comparing the difference in the effect of different tillage on plant vitality, there were no significant statistical difference in the measurements through different phenological phases. There was a significant statistical difference only between the measurement date, especially in the period of 18.5.2020 when the index values were very low. Which could be expected, due to the early stage of plant development, when the green plant cover was very small. In figure 2 the variant 4

(Kabot and ploughing) showed the highest average values. The results therefore indicate that different tillage does not have such a large impact on NDVI in this research and is necessary to complete the growing season with supporting measurements such a crop yield, WTS etc. and then draw conclusion over the past season.

REFERENCES

1. DUAN, T., CHAPMAN, S. C., GUO, Y., & ZHENG, B. 2017. Dynamic monitoring of NDVI in wheat agronomy and breeding trials using an unmanned aerial vehicle. *Field Crops Research*, *210*, 71-80.
2. ERDLE, K., MISTELE, B., SCHMIDHALTER, U., 2011. Comparison of active and passive spectral sensors in discriminating biomass parameters and nitrogen status in wheat cultivars. *Field Crops Res*. 124, 74–84. http://dx.doi.org/10.1016/j.fcr.2011.06.007.
3. HŮLA, J., PROCHÁZKOVÁ, B., BADALÍKOVÁ, B., DRYŠLOVÁ, T., HORÁČEK, J., JAVŮREK, M., KOVAŘÍČEK, P., KROULÍK, M., KUMHÁLA, F., SMUTNÝ, V., TIPPL, M., WINKLER, P. 2010. Dopad netradičních technologií zpracování půdy na půdní prostředí, Výzkumný ústav zemědělské techniky, v.v.i., Praha 6 Ruzyně, str. 58, SBN 978-80-86884-53-0.
4. JAVOREK, F. 2006. Technika pro půdoochranné systémy. *Zemědělec*, č. 6, Profi Press, Praha, str. 15-17.
5. JELÍNEK, Z., BALÁŽOVÁ, K., STARÝ, K., CHYBA, J., & KUMHÁLOVÁ, J. (2020). Comparing RGB-based vegetation indices from UAV imageries to estimate hops canopy area.
6. KÖLLER, K. & LINKE, CH. 2006, Úspěch bez pluhu. Vydavatelství *Zemědělský týdeník*, Praha, str. 191. ISBN 80-87002-00-8.
7. KUMHÁLOVÁ, J., ZEMEK, F., NOVÁK, P., BROVKINA, O. & MAYEROVÁ, M. 2014. Use of Landsat images for yield evaluation within a small plot. *Plant Soil Environment* 11, 501-506.
8. MARTI, J., BORT, J., SLAFER, G. A., ARAUS, J. l., 2007. Can wheat yield be assessed by early measurements of Normalized Difference Vegetation Index? *Annals of Applied biology*, *150*(2), 253-257. http://dx.doi.org/10.1111/j.1744-7348.2007.00126.x.
9. MAŠEK, J. 2006. Zakládání porostů polních plodin. *Mechanizace zemědělství*, č. 2, *Profi Press*, Praha, str. 46-49.

10. MCKINNON, T., & HOFF, P. 2017. Comparing RGB-based vegetation indices with NDVI for drone based agricultural sensing. *Agribotix. Com*, 1-8.
11. ROUSE J.W., HAAS R.H., SCHELL J.A., DEERING D.W. (1974): Monitoring vegetation systems in the Great Plains with ERTS. In: Proceedings Third ERTS-1 Symposium, NASA Goddard, NASA SP-351, 309–317.
12. TESTER, M., LANGRIDGE, P., 2010. Breeding technologies to increase crop production in a changing world. *Science* 327 (5967), 818–822. http://dx.doi.org/10.1126/science.1183700.
13. TUCKER, C.J., 1979. Red and photographic infrared linear combinations for monitoring vegetation *Remote Sensing of Environment*. 8, 127–150. http://dx.doi.org/10.1016/0034-4257(79)90013-0
14. VINCINI, M., CALEGARI, F. & CASA, R. 2016. Sensitivity of leaf chlorophyll empirical estimators obtained at Sentinel-2 spectral resolution for different canopy structures. *Precision Agriculture* 17, 313-331.
15. YEOM, J., JUNG, J., CHANG, A., ASHAPURE, A., MAEDA, M., MAEDA, A., & LANDIVAR, J. (2019). Comparison of vegetation indices derived from UAV data for differentiation of tillage effects in agriculture. *Remote Sensing*, *11*(13), 1548.

Corresponding author:
Ing. Kristýna Balážová, Department of Agricultural Machines, Faculty of Engineering, Czech University of Life Sciences Prague, Kamýcká 129, Praha 6, Prague, 16521, Czech Republic, tel: +420224383137, email: balazovak@tf.czu.cz

Production line material flow optimization through discrete-event simulation

R. Bambura[1], E. Sujová[1], P. Aláč[2]

[1]*Department of Manufacturing Technology and Quality Management, Faculty of Technology, Technical University in Zvolen, Slovakia*

[2]*Department of Economics, Management and Business, Faculty of Wood Sciences and Technology, Technical University in Zvolen, Slovakia*

Abstract

This article is focused on optimization of manufacturing processes and material flow in woodworking industry. Optimization was done using Tecnomatix Plant Simulation (TPS) software from Siemens. This research was performed in a production plant in Slovakia.

Key words: optimization, manufacturing, discrete-event simulation

INTRODUCTION

One of the most common optimization tasks in production is optimization od production processes and material flow optimization (SUJOVÁ et al. 2020). The increasing demands of the market environment force businesses to optimize production processes to ensure faster manufacturing. (ALAVI, HABEK 2016). The company must work in such a way that the input-output transformation proceeds with the optimal consumption of production inputs, the optimal choice of production processes, resources, and optimal utilization of production capacity (SIMANOVA, GEJDOS, 2016). Optimization of production processes is commonly done with the use of simulation software to create discrete-event simulation (DES) models of a production line. The DES model can be characterized as a system that mimics the actual idea of the real production line and its movement with defined objects, configurations, and sequences identical to physical world. Therefore, DES is an efficient tool for planning, operating, and evaluating manufacturing systems (GREGOR et al. 1999).

DES is viable optimization method for woodworking industry that provides support for decision making with fast analysis of various production scenarios in a relatively short time (RAHMAN et al. 2018; ALI AND ZULKIFLI, 2017; JURCZYK-BUNKOWSKA, 2019). TPS simulation software enables to create DES models to help user define system characteristics and optimize performance. Various scenarios of future production system and processes can be simulated

without disturbing existing production. The simulation provides the information needed for quick and reliable decision making.

MATERIALS AND METHODS

The aim of this article is to optimize material flow in woodworking company through DES created in TPS. Analysis of current stare of production was performed before actual creation of DES. Human interaction was not considered for simplification. Production line consists from 7 manufacturing blocks. Each block consists from specific machines (Tab. 1).

Tab. 1 Production line workstations

Manufacturing cell	Number of machines	Operation
MC1	2	Sawing
MC2	1	Planing
MC3	2	Milling
MC4	2	Gluing
MC5	1	Sealing
MC6	1	Sanding
MC7	1	Final surface treatment

Production line is used to manufacture 5 different types of windows (W1, W2, W3, W4, W5) (Tab. 2). All manufacturing cells operates at single shift production plan.

Tab. 2 Process times

Manufacturing cell	Process times [hrs]				
	W1	**W2**	**W3**	**W4**	**W5**
MC1	2	4	7	6	8
MC2	3	3	5	3	4
MC3	1.8	2.3	2.4	1.1	1.3
MC4	1	3	4	3	2
MC5	1.2	1.4	1.8	1.6	1.4
MC6	2	2	3	3	2
MC7	1.8	2.1	2.8	2.6	2

RESULTS AND DISCUSSION

The aim of this research is to optimize material flow in Slovak woodworking industry focused on windows manufacturing. With the use of real production line data, DES model of current state of production was made in TPS software for production of 5 products. DES model of original production line is shown in Fig. 1.

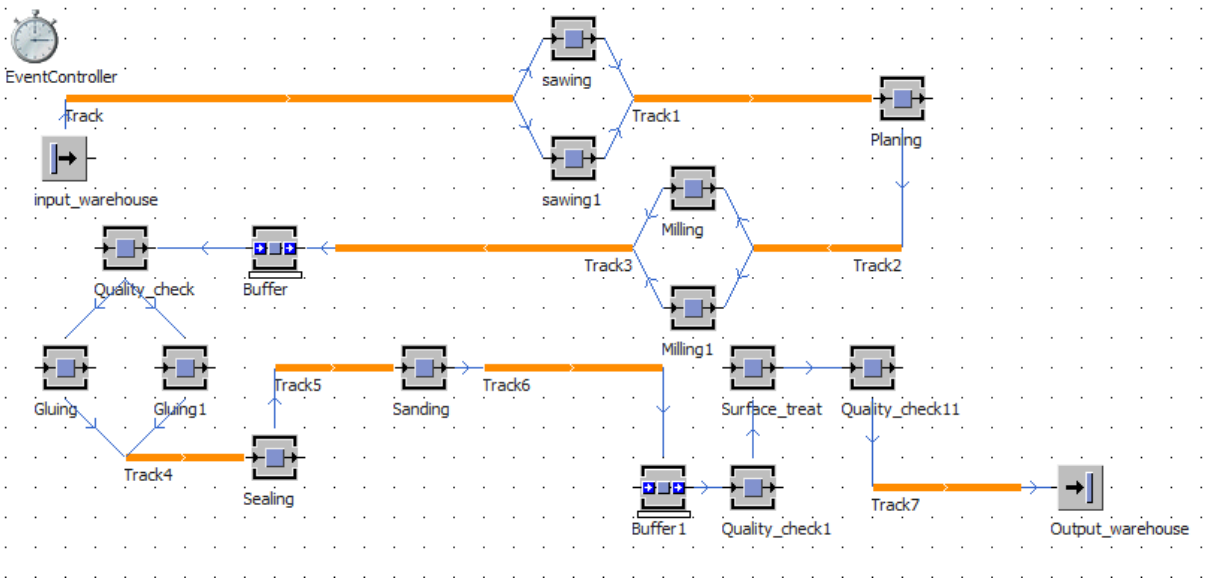

Fig. 1 Original production line DES

Results from initial DES shown that total production time is 160.8 hrs. First optimization of production line material flow consists from reduction of necessity for storage of workpieces between operation in buffers and quality control between operations. One final quality check is sufficient for whole production process which will reduce unwanted downtimes. Second significant optimization of material flow is done through merging of two manufacturing cells MC4 an MC5 into one manufacturing cell, which is achieved by purchasing a new machine, which can perform two operations in succession, thus eliminating unnecessary downtime caused by transfer from operation to operation and the overall processing time is reduced. Optimized production line DES is shown in Fig. 2. With production line optimization we were able to reduce total production time from 160.8 hrs to 120.5 hrs.

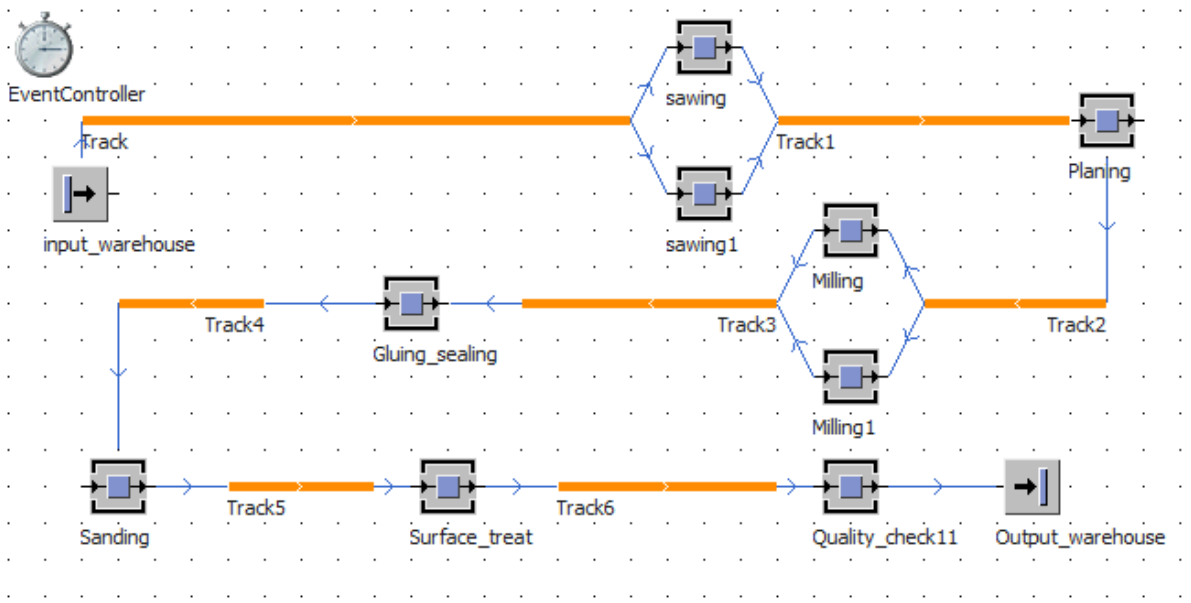

Fig. 2 Optimized production line DES

CONCLUSION

Our research shows that creation of DES models for production systems can provide data to mirror actual production and subsequently innovate production lines material flow without disruption of real production. DES models allows to respond quickly to requirements of customers and perform analysis and tests of future production. Our case study presented creation of DES model of real production line in woodworking industry focused on window manufacturing. The optimization of material flow through DES results into reduction of total production time needed to create selected products.

ACKNOWLEDGEMENT

The authors would thank the APVV Agency for their support via project APVV-17-0400, “Enhancing the Ethical Environment in Slovakia (Institutional Procedures, Actors, Risks, Strategies).” This paper was created as part of the aforementioned project.

REFERENCES

1. ALAVI, H., AND HABEK, P.: Optimizing outcome in the university – industry technology transfer projects,” Management Systems in Production Engineering, 22(2), 2016, 94 - 100

2. SIMANOVA L., AND GEJDOS, P.: The process of monitoring the quality costs and their impact on improving the economic performance of the organization, Enterprise Management, 3, 2016, 172-179
3. SUJOVA, E., BAMBURA, R., AND CIERNA, H.: Case Study Of Real Manufacturing System Improving Through Simulation Models, MM Science Journal, 2020, 3779–3783
4. KOSTURIAK, J., AND GREGOR, M.: Simulation in production system life cycle, Computers in Industry, 38(2), 1999, 159-172
5. ALI, A. T. B., AND ZULKIFLI, M. F.: A study on the cycle time of an assembly workstation using application of arena simulation software in a furniture industry in: Proceedings of the International Conference on Industrial Engineering and Operations Management, Bristol, UK, 2017, pp. 67-76
6. JURCZYK-BUNKOWSKA, M.: Using discrete event simulation for planning improvement in small batch size manufacturing system, Sustainable Production: Novel Trends in Energy, Environment and Material Systems, Springer, Cham, 2020, 9-43,
7. RAHMAN, A., SARKER, S., AND ISLAM, M. T.: Simulating Cutting Line of a Furniture Industry," in: 2018 International Conference on Production and Operations Management Society, Peradeniya, Sri Lanka, 2018, pp. 1-7

Corresponding author:
Roman Bambura, Department of Manufacturing Technology and Quality Management, Faculty of Technology, Technical University in Zvolen, Slovakia, Študentská 26, Zvolen, 96001, Slovakia, email: bambura.r@gmail.com

Influence of cutting parameters to vibrations and roughness of machined surface

M. Baráth[1], J. Žitňanský[1]

[1]*Department of Quality and Engineering Technologies, Faculty of Engineering, Slovak University of Agriculture in Nitra, Slovakia*

Abstract

This paper deals with influence of cutting parameters to vibration during turning of steel on CNC lathe. We observed the effect of changing cutting parameters to machine vibration and the quality of the machined surface. Cutting parameters were changed in three steps. Cutting speed, feed and depth of cut were subsequently changed. We used piezoelectric accelerometer MMF KS78.100 to sense vibrations, data acquisition unit Adlink USB 2405 was used for recording and processing signals from accelerometers. Recorded signals were transformed by Fast Fourier Transform from time domain to frequency domain. Software Visual Signal DAQ Express was used to perform this transformation.

Key words: vibration, turning, cutting parameters, roughness, acceleration

INTRODUCTION

The theory of vibrations and chatter has been known for long time. However, new transducers and their improvements have occurred, as well as new possibilities in data acquisition and computing equipment, which make methodologies and approaches to avoid vibrations more reliable and suitable for industrial application (Kuljanić et al., 2008). Vibrations have negative effect to whole process of chip machining. Badiola et al. (2019) determine these problems:
Chatter vibration is a common problem in almost all cutting operations which limits productivity of machining processes. Chatter vibrations cause poor workpiece surface finishing, premature tool wear, and breakage of cutting tools. Furthermore, due to this phenomenon, the machine tool life, reliability, and safety of the machining operation are affected negatively. Chatter vibrations have been researched for more than a century and it is still a major obstacle in achieving automation for most of the machining processes.

MATERIAL & METHODS

For the purposes of our experiments we used measuring device which consist from accelerometers MMF KS78.100 connected to signal acquisition module Adlink USB 2405 and PC with software Visual Signal DAQ Express. Block diagram of this device is shown in Fig.1.

Fig. 1 Block diagram of measuring device

Adlink USB 2405

The USB-2405 shown in Fig. 2 is a 24-bit high-performance dynamic signal acquisition USB module equipped with 4 analog input channels providing simultaneous-sampling at up to 128 kS/s per channel. The USB-2405 also features software selectable AC or DC coupling input configuration and built-in high precision 2 mA excitation current to measure integrated electronic piezoelectric (IEPE) sensors such as accelerometers and microphones. The USB-2405 is USB bus powered and equipped with BNC connectors and removable spring terminals for easy device connectivity (Adlink, 2020).

Fig. 2 Adlink USB 2405 signal acquisition module (Adlink 2020)

Accelerometer

Piezoelectric accelerometers use piezoelectric material in their design to create a charge proportional to the mechanical stresses caused by acceleration. Piezo crystal charge is measured either directly by external electronics with a high input impedance value, or more often the internal sensor electronics converting the charge to a low impedance voltage output. The

disadvantage of these accelerometers is that they cannot be used to measure frequencies below 0.1 Hz. One side of the piezoelectric material is attached to a solid sensor base. The part named as seismic mass is attached to the piezo-sensor. If the accelerometer is exposed to acceleration (vibration, shock), the generated force F, which acts on the piezoelectric element, will generate a charge, respectively voltage at the sensor output (Hudák, 2009). We used two accelerometers MMF Ks78.100 shown in Fig.3.

Fig. 3 Accelerometer MMF KS 78.100

Visual Signal DAQ Express software

Visual Signal is a signal processing software developed to provide time-frequency analysis solutions in an intuitive way. The design eliminates the complicated ways of writing a program to produce visual process control components, and instead provides a variety of visual process control components to be utilized. This gives users the ability to create a presentation of their own ideas for analysis without the limitation of needing to be able to code it (http://www.ancad.com/VisualSignal/overview.html).

Mitutoyo Surftest 301

Mitutoyo Surftest 301 is a portable measuring instrument that allows you easily and accurately measure surface roughness. It performs roughness analyses conform to various international standards (EN ISO, VDA, ANSI, JIS) and customized settings. Display range: Ra, Rq: 0.01 µm - 100 µm; Ry, Rz, Rt, Rv, R3z, Rk, Rpk, Rvk, R, Rp, Rx, AR, W, Wx, Wte: 0.02 µm - 350 µm; S, Sm: 2 µm - 4000 µm; HSC, Pc: 2.5/cm - 5000/cm; Ppi: 6.35 - 12700/inch; dc: - 350 µm - + 350 µm; Lo: 0.1 mm - 99999 mm; mr, Mr 1, Mr 2: 0 - 100 % ;A1, A2: 0 – 15000;

(https://shop.mitutoyo.eu/web/mitutoyo/en/mitutoyo/$catalogue/mitutoyoData/PR/178-952-4D/datasheet.xhtml;jsessionid=C93A6E5D8F471B473B5680F42FF833CE).

CNC Turning center Doosan Lynx 220A

Vibration measurements were performed on CNC machine presented on Fig. 4.

Technical parameters of the machine:

Control system: FANUC 0i - TC

Working range:

- Maximum turning diameter above support - 290 mm
- Maximum turning diameter above the bed - 510 mm
- Maximum diameter of turned rod - 45 mm
- The maximum length of turning with chuck - 322 mm

Fig. 4 CNC turning center Doosan Lynx 220A

RESULTS AND DISCUSSION

As a specimen of the material for turning we used a shaft made from STN 412-050 steel with a diameter of 39.55 mm. The shaft was divided into sections with a length 15 mm. During the measurements we changed only one of the cutting parameters (cutting speed, feed, depth of cut), keeping other cutting parameters unchanged. We changed all parameters in three levels.

Change of depth of cut

We changed depth of cut as a first parameter. Cutting parameters for case change of depth of cut are shown in Tab. 1.

Tab. 1 Cutting parameters for case change of depth of cut

Step number	Cutting speed [m.min^{-1}]	RPM [min^{-1}]	Depth of cut [mm]	Feed [mm.rev^{-1}]
1	150	1240	0.1	0.15
2	150	1240	0.3	0.15
3	150	1240	0.5	0.15

In Fig. 5 shows an example of vibrations during turning with 0.1 mm depth of cut. On Y-axis is acceleration of vibration an on X-axis is frequency of vibration. We measured vibrations on two part of machine, on tailstock upper graph in Fig. 5 and on cutting tool bottom graph in Fig. 5.

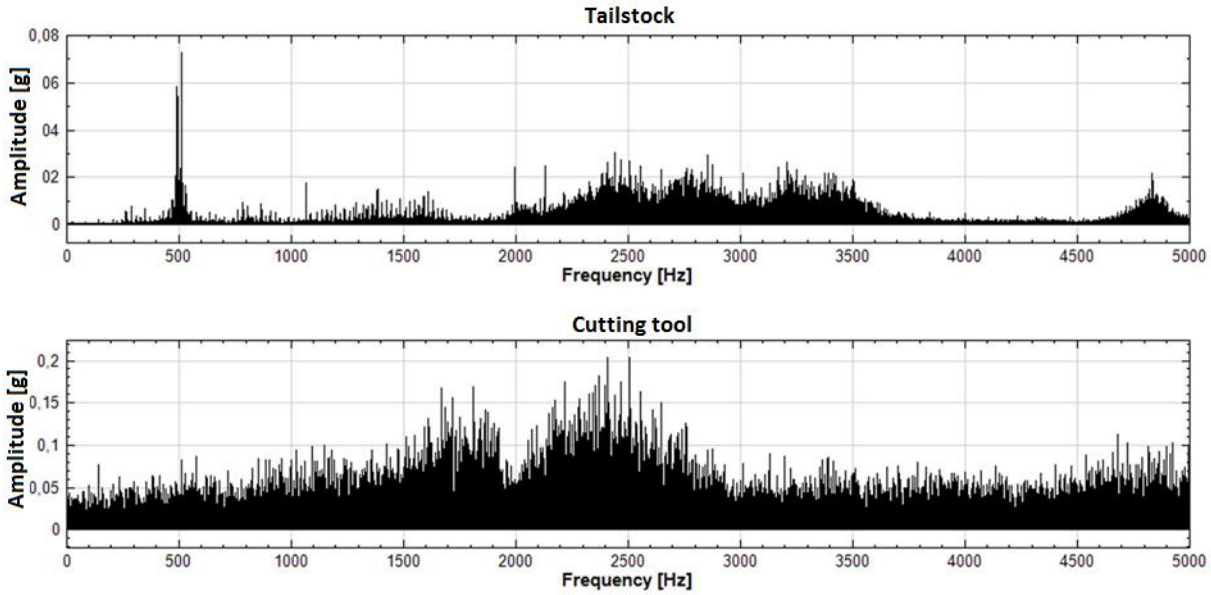

Fig. 5 Vibrations during turning with 0.1 mm depth of cut

Roughness of machined surfaces, created during turning with different depth of cut is shown in Tab. 2. As we can see increasing depth of cut had almost no effect to surface roughness and vibrations.

Tab. 2 Roughness of machined surfaces

Depth of cut [mm]	Roughness Ra [μm]
0.1	0.35
0.3	0.36
0.5	0.37

Change of feed

Next case was measurement of vibration during turning with changing of feed. Only feed was changed, similarly to previous case. Cutting parameters for this case are shown in Tab. 3.

Tab. 3 Cutting parameters for case change of feed

Step number	Cutting speed [$m.min^{-1}$]	RPM [min^{-1}]	Depth of cut [mm]	Feed [$mm.rev^{-1}$]
1	150	1240	0.5	0.15
2	150	1240	0.5	0.25
3	150	1240	0.5	0.35

During turning with feed per revolution 0.35 mm was reached the highest level of vibrations. This case is shown in Fig. 6. We can clearly see relation between level of vibrations and roughness of machined surface from Tab. 4 and Fig. 6. Surface roughness was increase almost two-time by increasing from feed per revolution 0.25 mm to feed per revolution 0.35 mm, amplitude of vibrations had similar behavior.

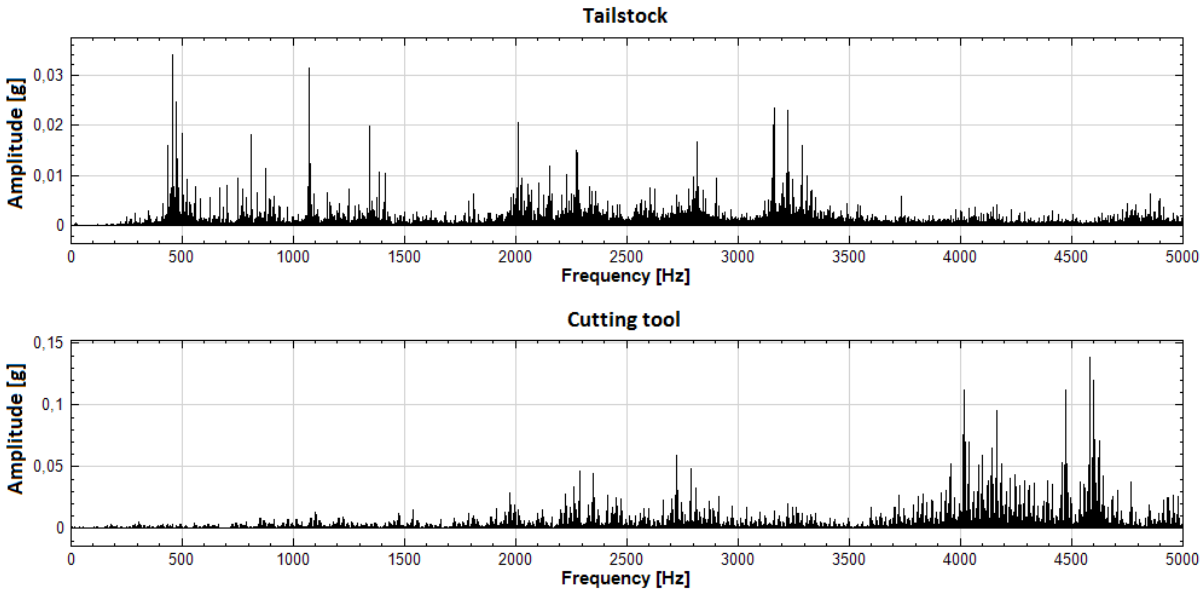

Fig. 6 Vibrations during turning with feed per revolution 0.35 mm

Tab. 4 Roughness of machined surfaces

Feed [mm.rev^{-1}]	**Roughness Ra [µm]**
0.15	0.21
0.25	0.28
0.35	0.51

Change of cutting speed

In the last case we measure vibrations during turning with changing cutting speed. Only cutting speed was changed, similarly to previous two cases. Cutting parameters for this case are shown in Tab. 5.

Tab. 5 Cutting parameters for case change of cutting speed

Step number	**Cutting speed [m.min^{-1}]**	**RPM [min^{-1}]**	**Depth of cut [mm]**	**Feed [mm.rev^{-1}]**
1	175	1410	0.5	0.15
2	200	1610	0.5	0.15
3	225	1810	0.5	0.15

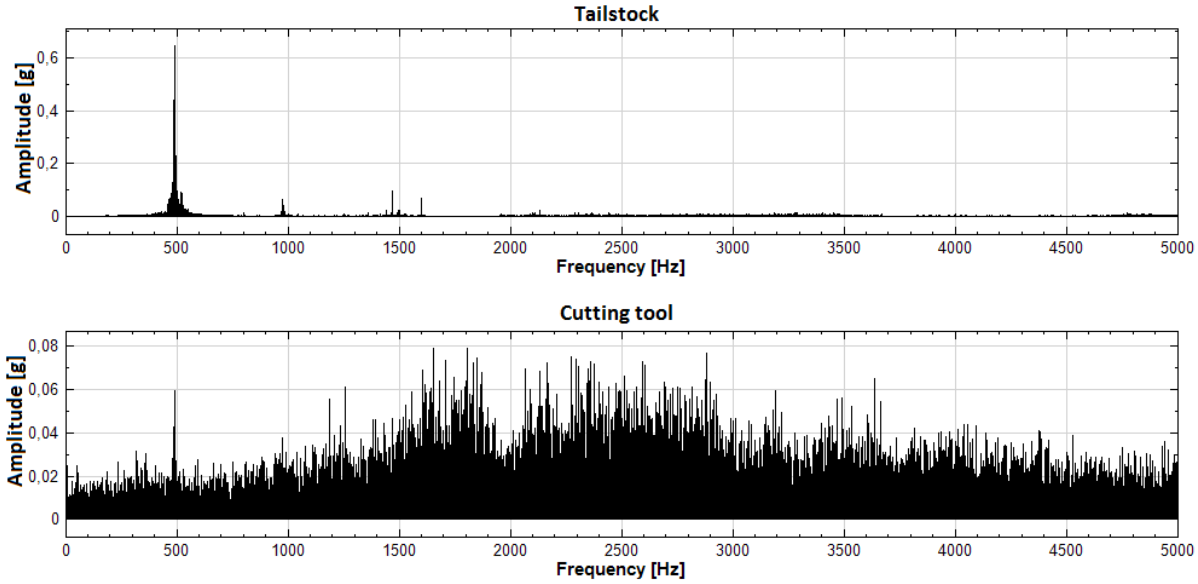

Fig. 7 Vibrations during turning with cutting speed 200 m.min^{-1}

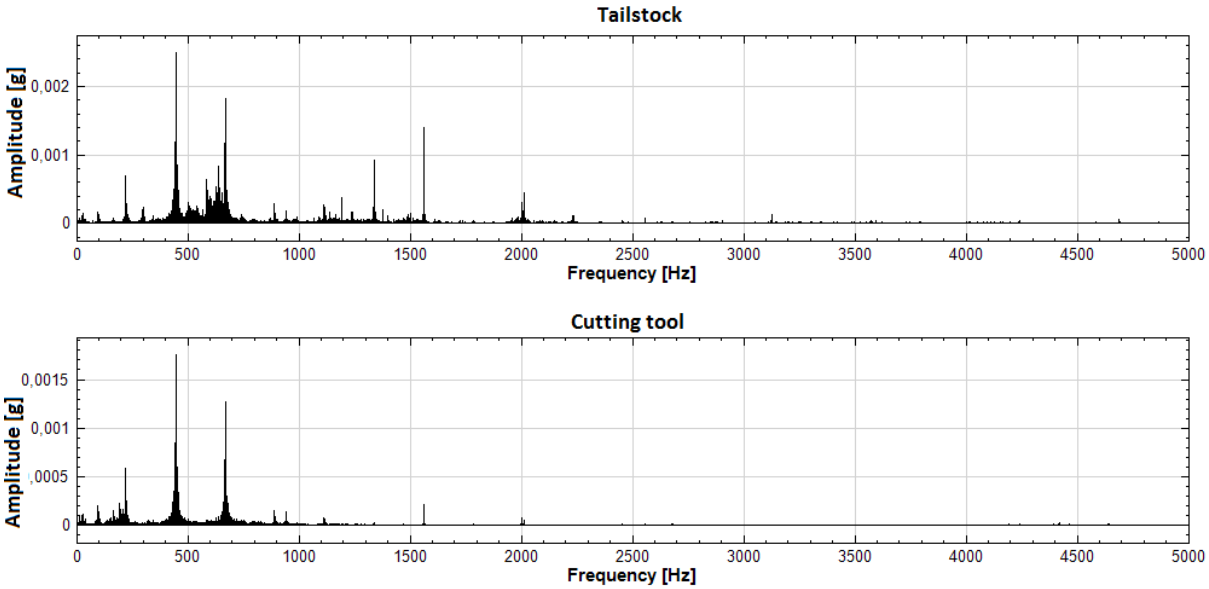

Fig. 8 Vibrations during turning with cutting speed 225 m.min^{-1}

Tab. 6 Roughness of machined surfaces

Cutting speed [m.min^{-1}]	**Roughness Ra [µm]**
175	0.24
200	0.32
225	0.16

In this case was reached the highest difference between vibration levels. As you can see in Fig. 7 vibrations are multiple time higher than in Fig. 8. Also you can see in Tab. 6 roughness of surface is two-time higher. Sivaraman et al. (2017) studied effect of vibration to surface texture. Despite of the fact that they use different material and conventional lathe, they had similar results "By increasing the spindle speed from 40 $m.min^{-1}$ to 100 $m.min^{-1}$ the vibration is getting reduced this is evidenced from the decrease in acceleration values for 100$m.min^{-1}$ compared to 40$m.min^{-1}$".

CONCLUSION

In this paper we researched the influence of cutting parameters on vibration and quality of machined surface during turning on a CNC lathe. We changed the parameters in three levels. We changed the depth of cut as the first parameter. From the graphs of measured vibrations and the measured roughness of the machined surface, it can be concluded that changing the depth of cut had almost no effect on the vibrations level and roughness of the machined surface. In second case, we changed feed. The vibration graphs and surface roughness values clearly show that vibrations increase and the quality of the machined surface decreases by increasing the feed. Especially with the last increase of feed, the decrease in surface quality is the most noticeable. In last case we changed the cutting speed. The attached graphs of vibrations and surface roughness show that increasing the cutting speed from 175$m.min^{-1}$ to 200$m.min^{-1}$ brought a deterioration of the surface quality and a significant increase of vibrations. However, further increase in cutting speed has brought a significant improvement in surface quality, the roughness of the machined surface has fallen to half the value, and vibration has also decreased considerably. Based on these facts, we can conclude that the greatest influence on the surface roughness and vibration has the cutting speed. For the future, it would be useful to research the influence of cutting speed in a wider range and in more levels.

REFERENCES

1. *Adlink. 2020. USB 2405* datasheet [online]. 2020 [cit. 25 March 2020]. Available from: <https://www.adlinktech.com/Products/Data_Acquisition/USBDAQ/USB-2405?lang=en>

2. BADIOLA, X.- ITURROSPE, A.- ABETE J.M. 2019. . State–space analysis of mode-coupling workpiece chatter. In *The International Journal of Advanced Manufacturing Technology* [online], vol 103, pp 2773 – 2781 [cit. 2019-03-17]. ISSN: 0268-3768. Available from: <https://doi.org/10.1007/s00170-019-03737-8>.
3. BEJAXHIN, A.B.H., PAULRAJ, G. 2019. Experimental investigation of vibration intensities of CNC machining centre by microphone signals with the effect of TiN/epoxy coated tool holder. *In J Mech Sci Technol* [online], vol 33**,** pp. 1321–1331 [cit. 25 March 2020]. ISSN 1976-3824. Available from: <https://doi.org/10.1007/s12206-018-1232-3>
4. KULJANIĆ Elso, TOTIS, GIOVANNI, SORTINO, MARCO. 2008. *AMST'08 Advanced Manufacturing Systems and Technology*. Udine: International Centre for Mechanical Sciences. 666 s. ISBN 978-88-85137-22-9
5. TU Košice. 2009. Akcelerometre [online]. 2009 [cit. 2019-03-17]. Available from: <:http://www.senzorika.leteckafakulta.sk/?q=node/175.>.
6. VASILKO Karol. 2009. *Teória a prax trieskového obrábania*. Prešov: Fakulta výrobných technológií Technickej univerzity v Košiciach, so sídlom v Prešove. 532 s. ISBN 978-80-553-0152-5
7. V.SIVARAMAN, L.VIJAYARAGHAVAN, S.SANKARAN. 2017. Effect of Vibration on Surface Texture during Machining Multiphase Microalloyed Steel. In *Procedia Manufacturing* [online], vol 10, pp. 429-435 [cit. 5. April 2020]. ISSN: 2351-9789. Available from: https://www.sciencedirect.com/journal/procedia-manufacturing/vol/10

Corresponding author:

Ing. Martin Baráth., Department of Quality and Engineering Technologies, Faculty of Engineering, Slovak University of Agriculture in Nitra, Tr. A. Hlinku 2, 949 76 Nitra, Slovakia, tel: +421 37 641 5690, email: xbarath@uniag.sk

Effect of stand establishment technology on tillage erosion

P. Brož[1], J. Hůla[1], P. Novák[1]

[1]Department of Agricultural Machines, Faculty of Engineering, Czech University of Life Sciences Prague, Prague, Czech Republic

Abstract

The article is concentrated on the tillage erosion, which causes adverse effects on the soil environment and long-term declines in crop yields. The field experiment was focused on the evaluation of soil particles transfer in conventional tillage technology. The most soil particles after tillage were found in the range of 0.00 to 0.03 m. The relationship of the tracer weight to a distance from the original location can be described by an exponential function. The part of the tracers were found after conventional tillage more than about 3 m from their original location in the upper soil layer. The acquired knowledge will be used in the next study of tillage erosion processes.

Key words: soil, soil translocation, soil erosion, soil tillage, tiller, degradation

INTRODUCTION

In the Czech Republic are approximately 3.5 million ha arable soil, a large part of this area is characterized by a high average slope. For this reason, most research is focused on water and wind erosion. This erosion is very often discussed and it is given considerable attention, both in the professional and non-professional part of the public. However, this does not apply to tillage erosion. Tillage erosion contributes to changes in the soil, especially to the deterioration of fertility and other properties of the soil (MORGAN, 2005). Research on soil erosion during soil tillage does not have a long history (GOVERS et al. 1999). CULS has been studying of soil erosion since 2010 (HŮLA, NOVÁK et al. 2011).

This article is focused on the above-mentioned the tillage erosion. It examines the effect of erosion in conventional tillage technology. Conventional technology can be divided into the areas of primary tillage and secondary tillage. In the article we deal with secondary tillage using mouldboard plough and soil preparation using cultivator with harrows.

The soil experiment was created in the locality of Nesperská Lhota in the Central Bohemian Region. The experiment was established to measure the longitudinal displacement of soil particles and the weight of the relocated soil.

MATERIALS AND METHODS

The tillage erosion was measured in July after harvest of spring oats in the green ripeness phase. Basic data on a field where measurements were done: the locality Nesperska Lhota near Vlasim, altitude of 420 m a.s.l., sandy loamy Cambisol. Before the translocation of soil particles started to be measured, soil samples were taken to determine the basic physical properties of soil at a depth of its tillage. A digital clinometer (BMI, Germany) was used to measure the angle of slope of a part of the field where measurements were performed. The average slope is 2.7°. For tillage passes was chosen direction "downslope orientation“. The machines that were chosen to measure: mouldboard plough Ross PH-1-535 five-share of working width 1.75 m and cultivator Kovo-Novák with two levelling bars and harrows of working width 3 m. The tractor Zetor 130 HSX 16V was used. To indicate the translocation of soil particles white limestone grit (particle size 10-16 mm) was used (LOGSDON, 2013). Grits were incorporated into grooves 0.20 m in width and 1 m in length. The longer side of the grooves was oriented perpendicularly to the direction of passes of tillage machines. The groove depth was chosen to match the working depth of tools of tillage machines. Soil tillage depth: mouldboard plough - 0.20 m and cultivator with two levelling bars and harrows- 0,05 m. The working speed of machines in the field was chosen according to the manufacturers' recommendations: mouldboard plough 4.5 $km.h^{-1}$, cultivator with two levelling bars and harrows 5.5 $km.h^{-1}$. After passing the tractor with the tillage machine across the field, the tracers were picked by hand from the soil in segments of 0.30 m in the direction of machine movement. The segments were divided into three segments of 0.33 m also in a crosswise direction. By weighing the tracers their weight was determined in each segment as an indicator of soil particle translocation by soil tillage. Data were processed by the programmes MS Excel (Microsoft Corp., USA).

RESULTS AND DISCUSSION

The measured values after tillage by the mouldboard plough and cultivator Kovo-Novák with two levelling bars and harrows are presented in figure (Fig. 1) and (Fig. 2).

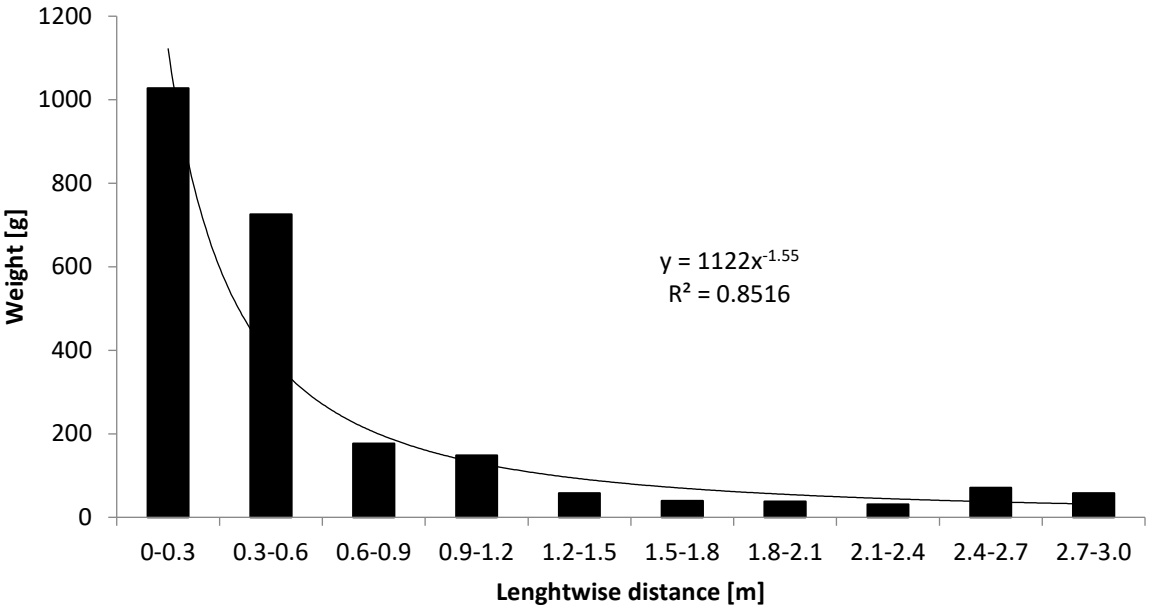

Fig. 1 Average values of particle translocation in a lengthwise direction

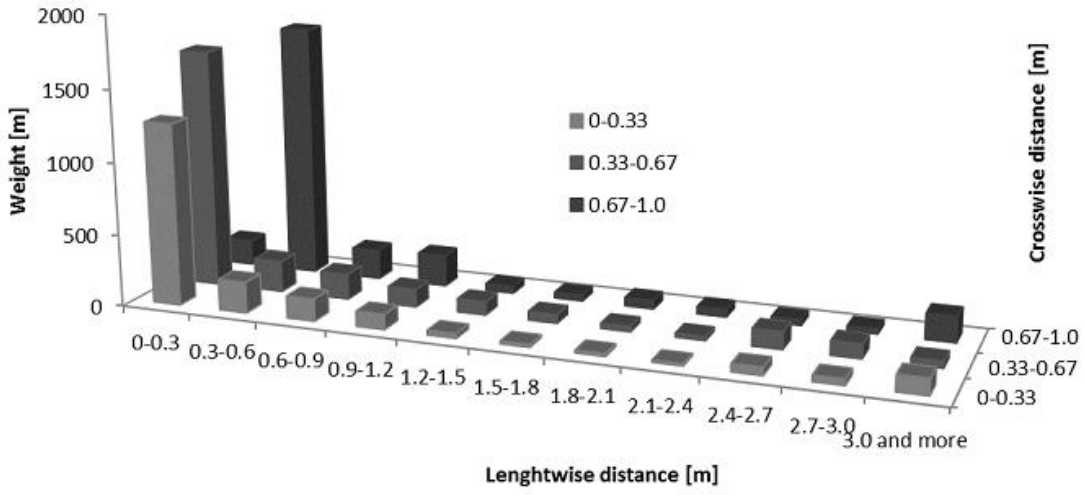

Fig. 2 Particle translocation in three crosswise segments

The evaluation of acquired data shows a noticeable translocation of particles in the direction of the machine movement. Fig. 1 shows the curve representing the average values of translocation in the particular segments. There is a steep fall in the weight of translocated particles at a longer distance from the original location. The relationship of the tracer weight to a distance from the original location can be described by an exponential function. The graph shows that the particles are translocated by the working tools of the cultivators to distances more than 3 m.

As reported by (VAN MUYSEN et al. 2002), on average, the largest movement of soil particles occurs in the range from 0 to 0.9 m. However, these results were obtained by (VAN MUYSEN et al. 2002) in the study of tools used for primary tillage. Our results in the tested technology are similar. In studys evaluate the influence of different machine design on the displacement of soil particles (TIESSEN et al. 2007), (LI et al. 2007). The results are also similar, the type and geometry of working tools has an effect on the magnitude of displacement of soil particles. The longest distance of the displaced particle according to (VAN MUYSEN et al. 2006) was measured at about 10 m, but it was again a primary tillage using discs. This was not confirmed during the tested technology - the farthest particles were found at a distance of 3 m.

CONCLUSION

During primary and secondary tillage, a large amount of soil is set in motion. It was found that the soil translocation is very variable and depended on the type of machine and the chosen technology. The largest displacement of soil particles was in the range of 0.00 to 0.03 m. Surprisingly, the most distant particles after conventional tillage were found more than about 3 m from their original location in the upper soil layer. These findings should be taken into account in further study of erosion processes.

ACKNOWLEDGEMENTS

Supported by the Faculty of Engineeering (CULS) - IGA no. 2020:31160/1312/3101.

REFERENCES

1. GOVERS, G., LOBB, D.A., QUINE, T.A.: Tillage erosion and translocation: emergence of a new paradigm in soil erosion research. Soil and Tillage Research, 1999, 167-174
2. HŮLA, J., NOVÁK, P., KOVAŘÍČEK, P., STANĚK, L.: Indikátory vodní eroze půdy při pěstování kukuřice. Mechanizace zemědělství, 2011, 152-158 (in Czech)
3. LI, S., LOBB, D.A., LINDSTROM, M.J.: Tillage translocation and tillage erosion in cereal-based production in Manitoba, Canada. Soil & Tillage Research, 2007, 164-182
4. LOGSDON, S.D.: Depth dependence of chisel plow tillage erosion. Soil and Tillage Research, 2013, 119-124
5. MORGAN, R.P.C.: Soil Erosion and Conservation, Blackwell Publishing, Oxford, UK., 2005, 304 pp

6. TIESSEN, K.H.D., LOBB, D.A., MEHUYS, G.R., REES, H.W.: Tillage erosion within potato production in Atlantic Canada: II. Erosivity of primary and secondary tillage operations. Soil and Tillage Research, 2007, 320-331
7. VAN MUYSEN, W.V., & GOVERS, G.: Soil displacement and tillage erosion during secondary tillage operations: the case of rotary harrow and seeding equipment. Soil and tillage research, 2002, 185-191
8. VAN MUYSEN, W.V., OOST, K.V., GOVERS, G.: Soil translocation resulting from multiple passes of tillage under normal field operating conditions. Soil and Tillage Research, 2006, 218-230

Corresponding author

Ing. Pavel Brož, Department of Agricultural machines, Faculty of Engineering, Czech University of Life Sciences Prague, Kamýcká 129, Praha 6, Prague, 16521, Czech Republic, tel: +420721402927, email: brozp@tf.czu.cz

Analysis of the flow of liquid in the suction pipe of the radial centrifugal pump

J. Černý[1], D. Sitte[1]

[1]Department of Mechanical Engineering, Faculty of Engineering, Czech University of Life Sciences Prague, Prague, Czech Republic

Abstract

This article focuses on the analysis of the liquid speed field at suction pipe flow by the Laser Anemometry PIV (Particle Image Velocity) method in the selected areas power characteristics of the selected radial centrifugal pump on the real hydraulic test circuit. The achieved of experiment results are detailed vector maps of real liquid flow, they show that with increasing total head, the fluid flow in the suction pipe in front of the pump is significantly affected. The results will be used for optimizing the model of digital flow simulation (ANSYS CFD) and in the next stages of developing pump innovations to increase performance and efficiency.

Key words: Particle image velocimetry (PIV), centrifugal pump, hydraulic performance

INTRODUCTION

The main task of this work is to analyze the field of fluid velocity at the flow through the suction pipe using the method of laser anemometry PIV in a real hydraulic circuit to determine how the impeller affects the flow of fluid in the suction pipe at the pump inlet depending on the change total head.

In centrifugal pumps, the geometry of the impeller blades is a major component of the conversion of mechanical energy into hydraulic pressure energy. [1], [2]

The results of the studies show that the fluid flow through the impeller of a rotary centrifugal pump at partial load creates vortices that directly affect the hydraulic performance of the pump. Clockwise vortices on the suction side of the vane and counterclockwise vortices on the pressure side of the vane. While the counterclockwise vortices move toward the impeller output, the clockwise vortices move to the opposite side. Turning the vortex counterclockwise increases energy loss, while turning the vortex clockwise will positively affect the pump head. [3], [4]

Swirling flow in pump intake has been the subject of discussion for decades due to the detrimental effects brought about by its existence. Among the effects of swirling flow are reduced pump efficiency, cavitation, excessive vibration and load imbalance at the pump impeller which are caused by hydraulic problems associated to swirling flow. [5], [6], [7], [8],

[9] It is necessary to deal in detail with the causes of vortices in the suction pipe to be able to design such solutions that guarantee an even flow of liquid into the pump.

MATERIALS AND METHODS

Experimental verification of pump performance parameters

Verification of performance characteristics and operating parameters in the development, manufacture and supply of pumps is described in ISO 9906. The standard specifies hydraulic power tests for all rotodynamic pumps. And it can be used for pumps of all sizes and on which wheels pumped liquids that behave like pure cold water. Testing of the pump used here was based on this standard. [10]

A cast iron pump has been selected for laboratory testing, the geometry of the wheel in the spiral cabinet together with the parameters of the pump are specified in figure (Fig. 1).

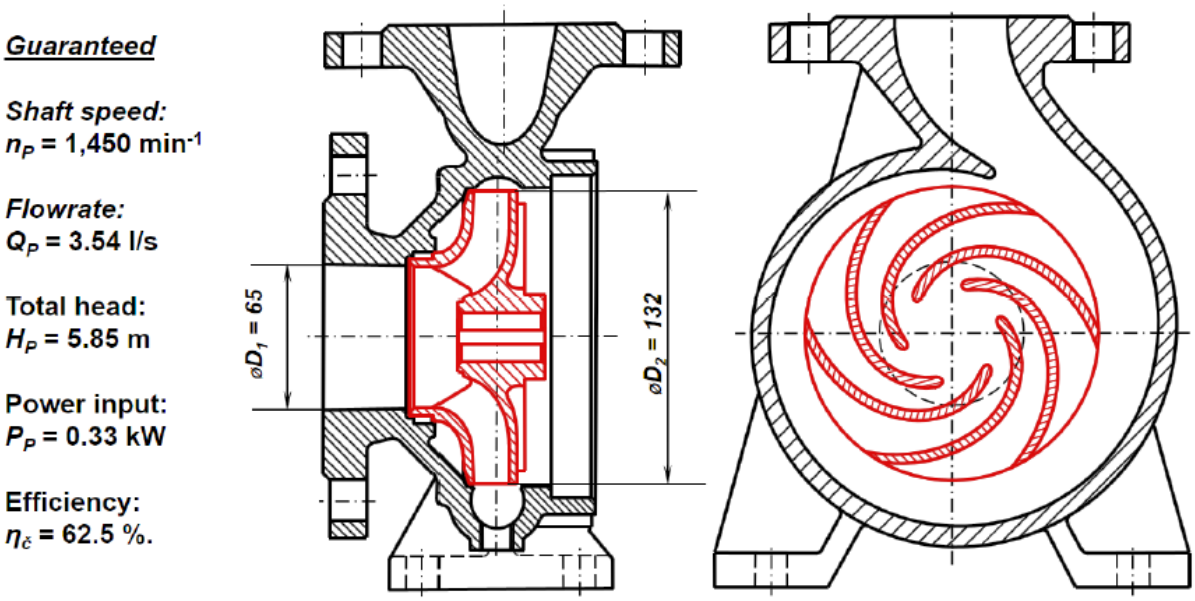

Fig. 1 Cast iron impeller in spiral housing and parameters of pump [11]

Hydraulic testing

A hydraulic test circuit was used for the experimental examination of the hydrodynamic flow of liquid in the suction pipe by the particle image rate (PIV) method in the context of the pump performance characteristics. The diagram of the circuit in figure (Fig. 2).

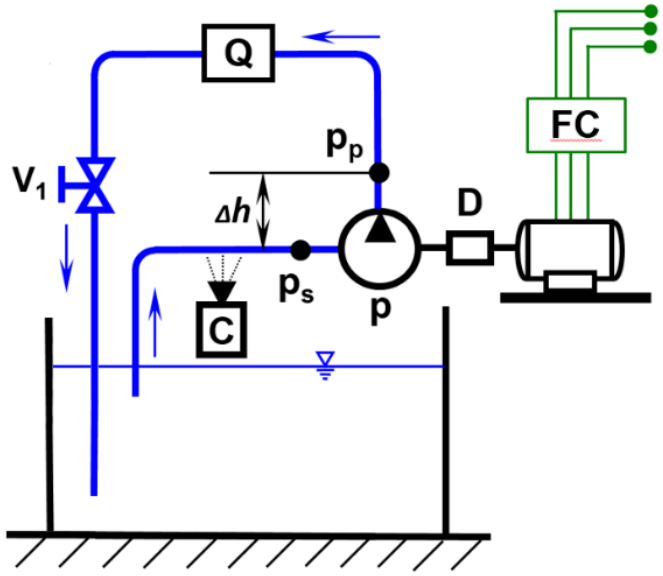

Fig. 2 Hydraulic circuit scheme [12]

Q – flow meter,
P – tested pump, V1, – control valves,
Pp, Ps – pressure sensors,
D – dynamometer, FC – frequency converter, C – camcorder PIV.

The hydraulic test circuit consisted of tank, connecting pipes, control and measuring elements and the pump tested (P). The water flows in the direction of the arrows and forms a closed circuit. Gradual closing of valve V1 simulated an increase in the total head for the tested pump. The pump was powered by a three-phase asynchronous electric motor with continuous shaft speed control using the LSLV0055s100-4EOFNS frequency converter. The torque on the pump shaft was measured by the torque sensor (D) Magtrol TMB 307/41 (accuracy 0.1%). The water flow rate was measured using the electromagnetic flow meter (Q) SITRANS F M MAG 5100 W (accuracy 0.5%). Pressures in suction pipe (p_s) and pressure pipe (p_p) were measured by pressure sensors HEIM3340 (accuracy 0.5 %) installed according to the measurement requirement 1. accuracy class (ISO 9906).

The PIV laboratory equipment from company TSI consisted of laser, optics, synchronizer, camera, computer, software and fluorescent substance. The system was used to obtain a two-dimensional array of speeds. For measurements, a vertical plane in the axis of the suction pipe at the pump inlet was selected. The field of view covered the entire cross-section of the pipeline to reveal the overview structures of the flow. A Double pulse Nd:YAG laser (YAG100-100-LIT) with a wavelength of 532 nm was used to illuminate the vertical plane. During the measurement, the time delay between the two laser pulses was adjusted to 50 μs. The light beams have been adjusted to a perfectly thin light sheet in the Light Sheet Optics 610026 optical device. A Powerview Cameras 630092 camera was used to capture images. The camera was placed in the perpendicular direction to a laser light sheet. LaserPulse Synchronizer Model 610036 was provided by laser and camera timing control. The computer provided storage and preliminary evaluation of the measured data by the COMPUTER for PIV 600054-64 with

INSIGHT™ 4G-2DTR Data Acquisition software. A glass powder coated with 100-SLVR silver was used as a fluorescent substance.

The measurement was carried out at constant speeds (1,450 rpm.min^{-1} or 2,950 rpm.min $^{-1}$) set by the frequency converter. Gradually closing of the V2 valve increased the resistance of the discharge pipe. During the measurement, values of the flow, engine speed, torque on the engine shaft, fluid pressures at the pump inlet and outlet were recorded. From the measured values, the performance parameters were continuously calculated and the images of PIV were recorded at selected points of these graphs, see figure (Fig. 3 and Fig. 4) [10], [12]

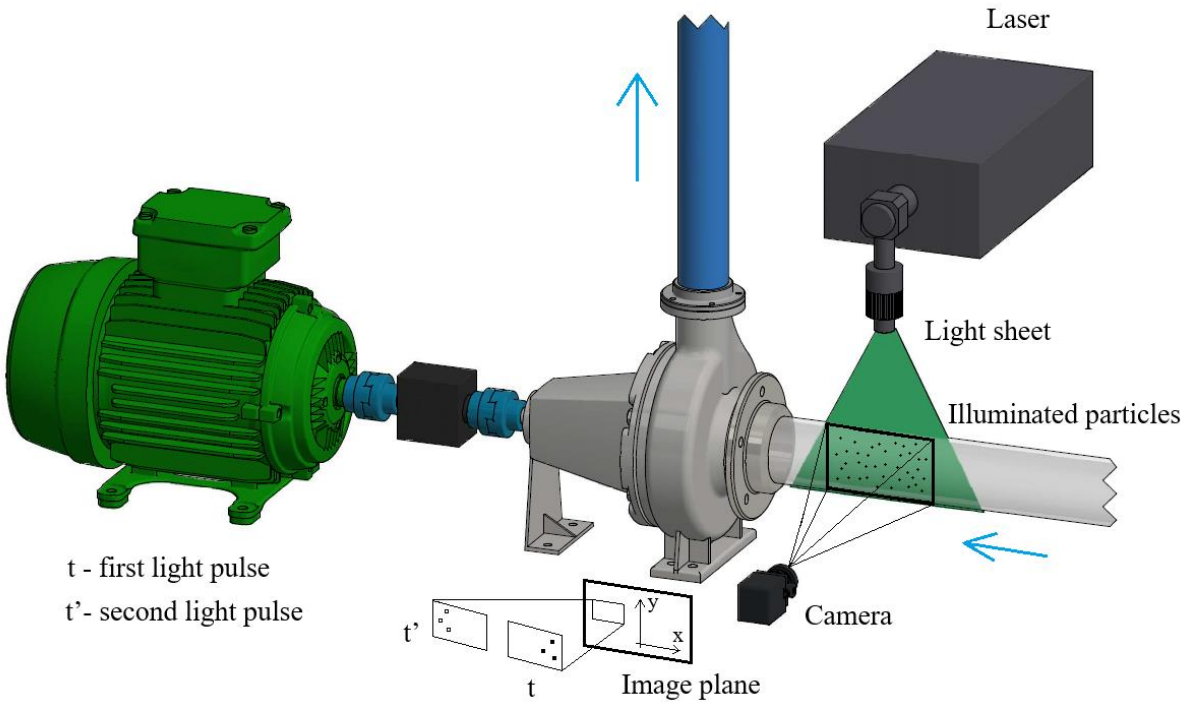

Fig. 3 Diagram of Particle Image Velocity (PIV)

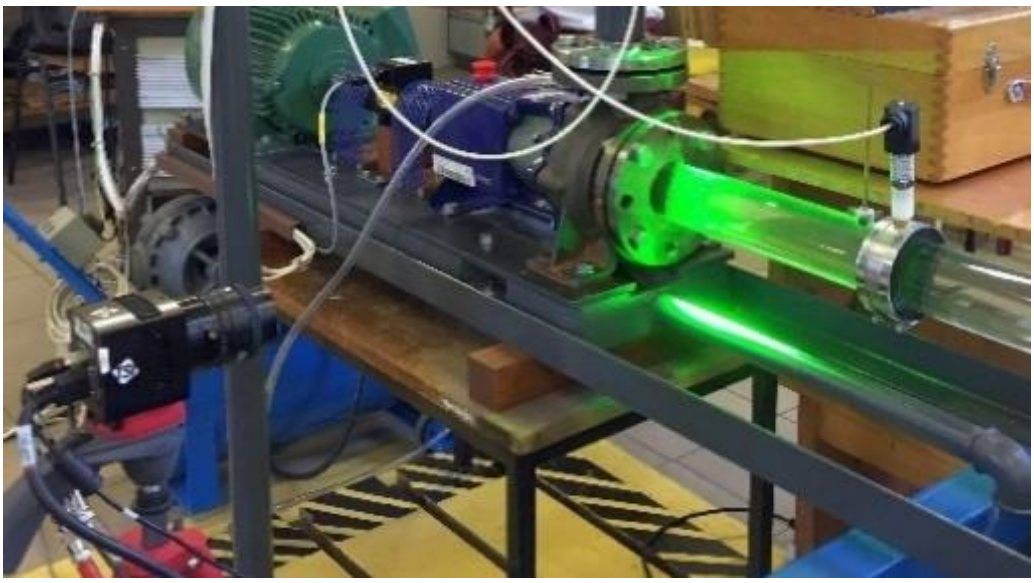

Fig. 4 Testing of Particle Image Velocity

Calculation of relations

From Bernoulli's equation between intake (ps) and displacement (pp) of the pump and the continuity equation, the pump's variable energy was calculated:

$$0 + \frac{p_s}{\rho} + \frac{{v_s}^2}{2} + Y_p = g \cdot h + \frac{p_p}{\rho} + \frac{{v_p}^2}{2} \qquad [J \cdot kg^{-1}] \qquad (1)$$

$$Q = v \cdot S \qquad [m^3 \cdot s^{-1}] \qquad (2)$$

$$Y_p = \frac{p_p - p_s}{\rho} + \frac{{v_p}^2 - {v_s}^2}{2} + g \cdot h \qquad [J \cdot kg^{-1}] \qquad (3)$$

Nomenclature

p – liquid pressure at a given location	[Pa]
ρ – specific mass of liquid	$[kg \cdot m^{-3}]$
v – medium fluid speed at a given location	$[m \cdot s^{-1}]$
Y_p – specific pump energy	$[J \cdot kg^{-1}]$
g – gravitational acceleration	$[m \cdot s^{-2}]$
h – vertical pressure relief	[m]
Q – volumetric flow rate	$[l \cdot s^{-1}]$
S – flow cross-section at a given location	$[m^2]$
d – inner diameter of the pipe at a given location	[m]

Test circuit input parameters

- inner diameter of suction pipe: ds = 65 mm
- inner diameter of pressure pipe: dp = 50 mm
- vertical pressure relief: h = 290 mm

RESULTS AND DISCUSSION

The pump was tested by dual rotation of the ordinary wheel 1.450 rpm.min-1 and 2.950 rpm.min-1, see figure (Fig. 5 and Fig. 6) shows the performance characteristics.

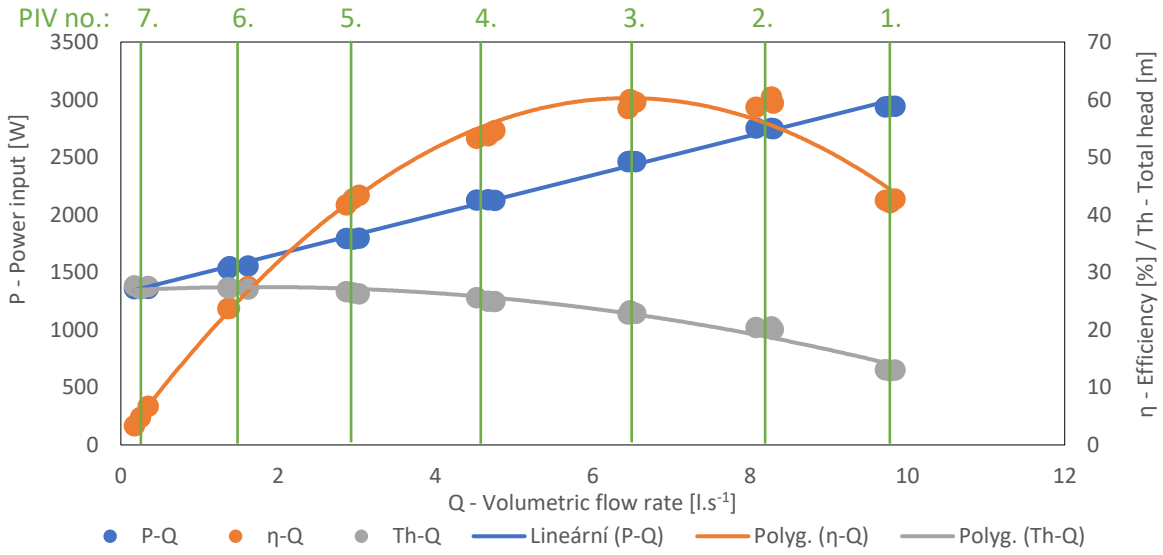

Fig. 5 Performance characteristic at 2.950 rpm.min-1, volumetric flow rate depending on efficiency, total head and power input

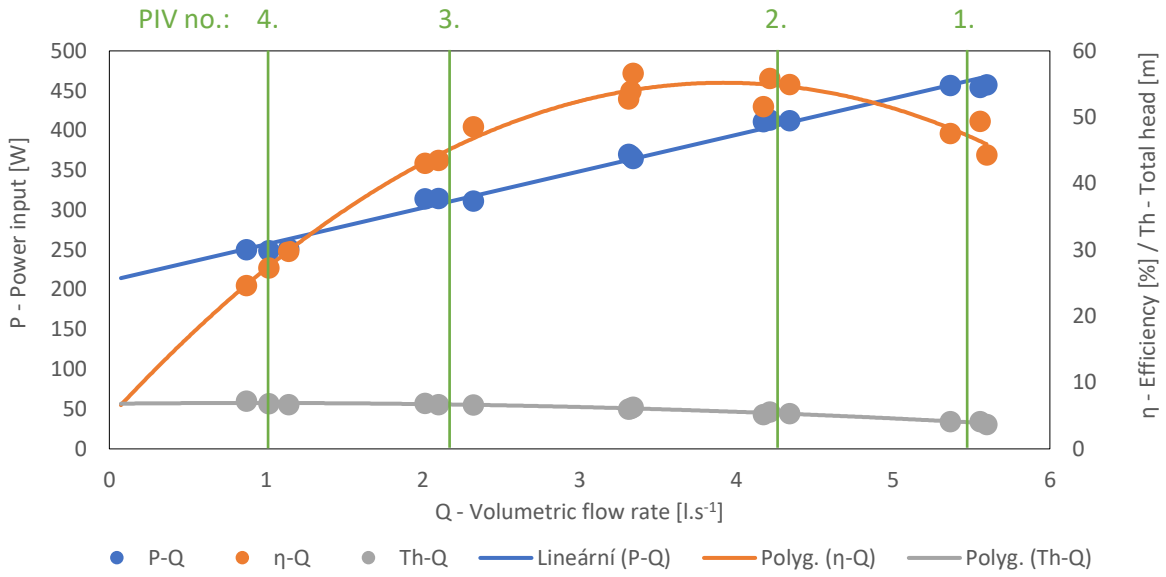

Fig. 6 Performance characteristic at 1.450 rpm.min-1, volumetric flow rate depending on efficiency, total head and power input

In the graph the green points show the record of the flow in the suction pipe by the testing method PIV. Each measurement is presented by one vector field plot. Vector field plot for measurement at 2.950 rpm.min^{-1} is identical with measurement at 1.450 rpm.min^{-1}. Figures (Fig. 7 to Fig. 9) show some of those vector field plots. The areas with the highest flow to areas with the highest effectiveness. see figure (Fig. 7). Particle measured by PIV create streamlines moving parallelly and not intermingling, in the cross-section of the pipe they do not move with the same speed, the highest speed (v=3,23 m.s^{-1}) was measured in the axis of the pipe and in the direction to the edge of the pipeline the speed declines. That is basic premise in designing of pumps where the steady flow of liquid is desirable.

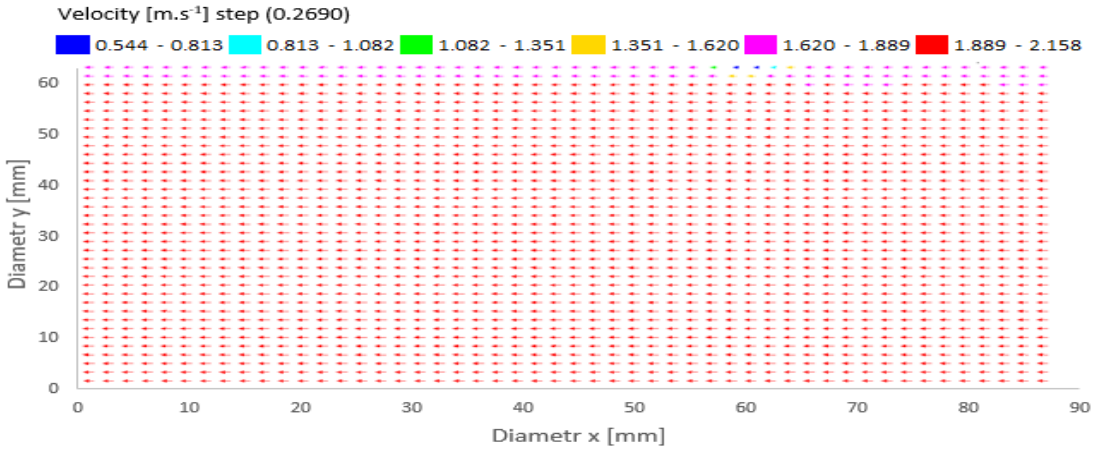

Fig. 7 Vector field plot, performance characteristic at 2.950 rpm.min^{-1}, PIV no. 3.

The first differences from the steady flow of liquid towards the pump occur at point PIV no. 3. In areas near the suction of the pump is measured higher speed up to 100 % towards the pump.

The figure (Fig. 8) shows that increase relates to the short section of the liquid therefore by the sides of pipe is lower or negative flow which causes minor local whirls by the sides. If the rotations are higher, the whirls are more significant.

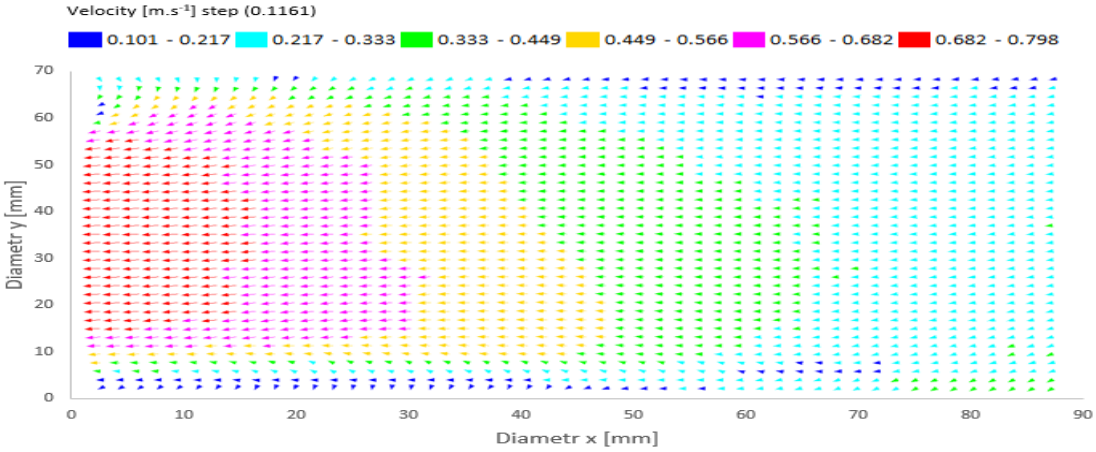

Fig. 8 Vector field plot, performance characteristic at 1.450 rpm.min^{-1}, PIV no. 3.

If the flow approaches zero and total head is maximal, similar phenomenon is visible in both regimes of the pump. The figure (Fig. 9) shows the upper part of the pipeline in proximity of the pump with significant whirl which affects the flow in the entire length of tested pipeline so that in the entire upper part there are visible local minor whirls.

The other significant whirl is located in further from the pump on the opposite side of the pipe and has the opposite direction of rotation. These whirls affect the transport of the liquid towards the pump, streamlines are not parallel, the direction is affected by the whirls.

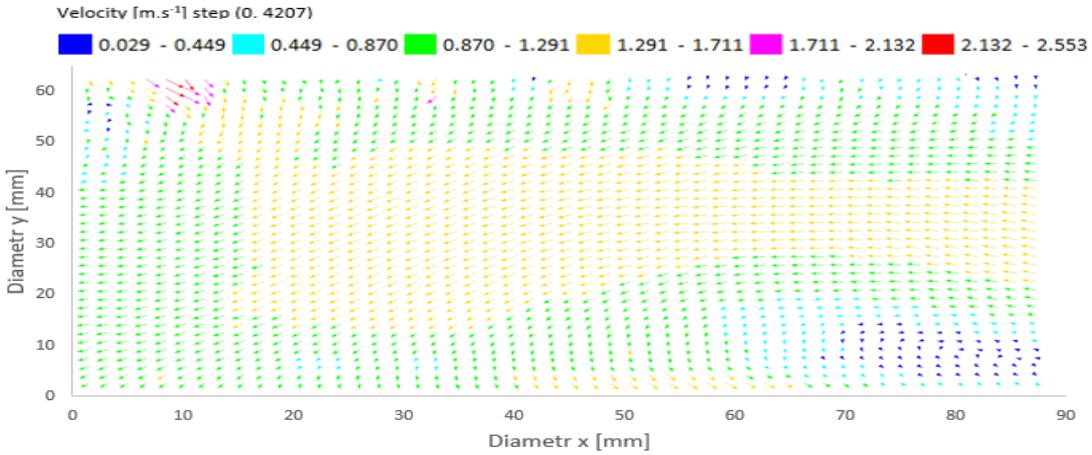

Fig. 9 Vector field plot, performance characteristic at 2.950 rpm.min^{-1}, PIV no. 7.

Vector field plots show speeds and directions of the flow of the liquid only in the plane of the axis of the pipeline. The result is an overview of the shape of the streamlines in the mentioned plane. It is possible to see the condition for designing the pump the steady flow of liquid towards the pump at highest efficiency. In the area from the first differences of the uniform flow of liquid to the pump to the area where the flow is close to zero and the discharge height is

maximum are located the position of the created whirl and the influence of the whole liquid flow are determined. These conclusions are possible to use in order to increase the effectiveness of the pump. To better represent of the liquid flow, the measurement can be extended by a second set of measuring equipment (laser and a camera) for measuring the other area. In case of measuring two areas which are perpendicular, the result will show three-dimensional illustration of the flow, due to the financial demands of the equipment, this measurement variant was not carried out. Results of PIV measuring can be compared with numerical models of CFD programs. The output of mathematical model CFD is three-dimensional illustration of the flow which can be used to reach the optimization of the pump model.

CONCLUSION

The measuring validates the uniformity of the flow of the liquid in the suction pipeline of the pump at the point of the highest effectiveness. The result of the measurements are detailed vector maps and description of real liquid flow in front of the pump. In decreasing of the flow and increasing the transport height of the pump up to the limits of the highest effectiveness of the pump, the whirls occur disrupting the steady flow of the liquid towards the pump. The whirls are measured by PIV methods and described in the chapter Results. The results can be compared with the results of the numerical model of the flow on CFD program to reach the optimization.

Acknowledgements

The authors thank the Internal grant agency 2020 of the Czech University of Life Sciences Prague for funding from the project Liquid flow analysis in hydrodynamic pump and pump in turbine mode, 2020:31130/1312/3114.

REFERENCES

[1] D. Li, H. Wang, Y. Qin, Z. Li, X. Wei, and D. Qin, “Mechanism of high amplitude low frequency fluctuations in a pump-turbine in pump mode,” *Renew. Energy*, vol. 126, pp. 668–680, Oct. 2018.

[2] C. Wang *et al.*, “Optimal design of multistage centrifugal pump based on the combined energy loss model and computational fluid dynamics,” *Appl. Energy*, vol. 187, pp. 10–26, Feb. 2017.

[3] X. Li, B. Chen, X. Luo, and Z. Zhu, “Effects of flow pattern on hydraulic performance and energy conversion characterisation in a centrifugal pump,” *Renew. Energy*, vol. 151, pp. 475–487, May 2020.

[4] W. Cao, Z. Jia, and Q. Zhang, "Near-Wall Flow Characteristics of a Centrifugal Impeller with Low Specific Speed," *Processes*, vol. 7, no. 8, p. 514, Aug. 2019.

[5] Z. Harun, M. A. Akbar Batcha, T. A. Norizan, Z. Zainol Abidin, and W. H. M. Wan Mohtar, "Vortex Measurement at Bell-Shaped Pump Inlet Using Particle Image Velocimetry," *J. Kejuruter.*, vol. 30, no. 2, pp. 209–217, Oct. 2018.

[6] T. A. Norizan, Z. Harun, S. Abdullah, and W. H. M. W. Mohtar, "Effects of floor splitter height on the effectiveness of swirl angle reduction in pump intake," *J. Adv. Res. Fluid Mech. Therm. Sci.*, vol. 57, no. 1, pp. 32–39, 2019.

[7] Z. Harun, T. Ariffin Norizan, and W. Hanna Melini Wan Mohtar, "Application of Vortex Control Principle at Pump Intake," in *Vortex Dynamics [Working Title]*, IntechOpen, 2020.

[8] T. A. Norizan, W. H. M. W. Mohtar, Z. Harun, and S. Abdullah, "Characteristics of swirl angle in pump intake flow near the minimum inlet submergence," in *ASME-JSME-KSME 2019 8th Joint Fluids Engineering Conference, AJKFluids 2019*, 2019, vol. 3B-2019.

[9] S. Ajai, K. Kumar, P. M. Abdul Rahiman, V. S. Sohoni, and V. S. Jahagirdar, "Vortex prediction in a pump intake system using computational fluid dynamics," *Int. J. Innov. Technol. Explor. Eng.*, vol. 8, no. 10, pp. 3158–3163, 2019.

[10] International Organization for Standardization, "ISO - ISO 9906:2012 - Rotodynamic pumps — Hydraulic performance acceptance tests — Grades 1, 2 and 3." International Organization for Standardization, Geneva, Switzerland, p. 59, 2012.

[11] M. Polák, "Experimental evaluation of hydraulic design modifications of radial centrifugal pumps," *Agron. Res.*, vol. 15, no. Special Issue 1, pp. 1189–1197, 2017.

[12] M. Polák, "The influence of changing hydropower potential on performance parameters of pumps in turbine mode," *Energies*, vol. 12, no. 11, 2019.

Corresponding author:

Ing. Jan Černý, Department of mechanical engineering, Faculty of Engineering, Czech University of Life Sciences Prague, Kamýcká 129, Praha 6, Prague, 16521, Czech Republic, email: cernyjan@tf.czu.cz

Evaluation of losses in the mechanized harvesting of grapes

M. Dočkalik[1], J. Jobbágy[1]

[1]Department of Machines and Production Biosystems, Faculty of Engineering, Slovak University of Agriculture in Nitra

Abstract

This article is focused on monitoring and evaluation of losses arising from the mechanized harvesting of grapes in the two years 2017 and 2018. Measurements were performed in the conditions of Slovak viticulture in the company Pivnica Radošina s. r. o., when using the Pellenc 8090 SP trailed harvester on the Traminer variety. In 2017, losses of 274.12 kg.ha^{-1} were found, which represented 2.03%, and in 2018 it was 137.34 kg.ha^{-1}, which accounted for 1.47% at a higher frequency of oscillations of the harvesting system. All research measurements were conducted during full grapes harvesting operation in the company.

Key words: mechanized grape harvesting, losses, evaluation of harvest,

INTRODUCTION

Slovak viticulture and viniculture have a long tradition. After the more demanding nineties of the 20th century, viticulture in Slovakia stabilized. Slovak wine has a high quality and quality value at the world level. However, at this time, the cultivation of must and the wine sector face problems of cheap competition. These problems can be solved by greater support for the sector, but also by optimizing production processes, reducing the amount of need for human labor, which is expensive and insufficient today. Related to this is the use of viticulture mechanization as much as possible, which will increase the efficiency of processes and ultimately reduce the costs themselves and increase the competitiveness of Slovak viticulture. Therefore, it is necessary to introduce mechanization in those processes, which for many years were associated only with the need for human labor. One such operation in the grape growing process is harvesting, which is one of the most demanding operations. Because grape harvesting is the most demanding operation in vineyard technology and significantly affects the quality of the final product, i.e. wine, it is necessary to carry it out in the shortest possible time of the optimal date of harvest, with the highest quality of harvested material. This can be achieved by modern mechanized means for grape harvesting - grape harvesters, which are manufactured as self-propelled or semi-trailer machines attachable to a tractor. In Slovakia, however, mechanized

grape harvesting is applied to a much lesser extent, such as in the Czech Republic. This can result in higher harvesting costs. However, there are voices from practitioners that mechanized harvesting leads to large losses or damage to vegetation or a reduction in the quality of the harvested product. Therefore, the issue of mechanized grape harvest involves several authors in the world, but also in the Czech Republic and Slovakia, to examine and evaluate the quality and effects of mechanized grape harvesting.

To spread mechanized harvesting in Slovakia, it is necessary to bring this method of harvesting to the attention of winegrowers, to highlight its advantages in comparison with manual harvesting. However, this requires research in this area, which is mainly addressed by foreign authors, where mechanized grape harvesting is more widespread. Potential users of grape harvesting technology are also interested in harvesting losses. Therefore, the research aimed to monitor and evaluate the losses of grapes that occur when using a new modern harvesting machine used in the current conditions in Slovakia.

The choice of mechanical harvesting of wine grapes depends on many factors including vineyard location, value of the crop, the availability and cost of hand labour, the efficiency of fruit removal, and transporting the harvested product (Clary et al., 1990). Interaction between the machine and vine is one of the more promising lines of research to improve the performances of grape harvesters. The machine–plant relationship affects the results of the grape harvest in terms of yield, product quality and preservation of the vineyard (Intrieri and Poni, 1990; Pezzi et al., 2005).

The primary factor for introducing mechanization is a reduction in the amount of human labour and a reduction in annual costs, even if the initial costs are high (Jobbágy, Findura, 2013; Bates and Morris, 2009; Pezzi, Martelli, 2015).

MATERIALS AND METHODS

Our monitoring aimed to assess the losses incurred during the harvest by falling into the soil and not harvesting, in a year-on-year comparison. The research measurements took place in the vineyards of the company Pivnica Radošina s. r. o. on the variety Traminer. The vine is grown on a middle line with a flat harvest shape. The supporting structure consists of galvanized steel posts, suitable for mechanized collection. The vineyards are south-oriented and reach a slope of 3 – 7%. Measurements took place in October 2017 and September 2018.

The PELLENC 8090 SP trailed harvester in aggregation with the SAME Frutteto3 100 vineyard tractor was used for harvesting. The Pellenc 8090 SP grape harvester is suitable for small and medium-sized businesses. It is an over-the-counter grape harvester that achieves lower

performance compared to self-propelled machines. The combine is connected to the tractor utilizing a lower link via special swivel drawbars, which allows good maneuverability of the set. The construction of the machine is portal. The machine works on the vibrating principle of shaking. The harvesting device consists of bilaterally mounted pairs of shaking rods anchored at two points. These are rods of elongated shape. The catch device is lamellar with an inclination on both sides. Each side of the catch ramp contains 19 slats, which are attached to flexible joints. The volume of the tanks is 3000 l. The control of the machine and the setting of working parameters is performed utilizing a control unit consisting of a screen for displaying information, a combined joystick control and a control for navigating and setting parameters. The working speed of the set was in the range of 2.5 – 3.1 $km.h^{-1}$.

Each year, 3 experimental measurements were performed. In selected experimental rows, PE foils were distributed in the area of the anvil strip in a section of 10 m wide 2.8 m, 1.4 m on each side of the row of vines. Thus, one measurement represented one 10 m measured section. After passing through the harvester through the measured section, the fallen berries were collected in containers and then the berries were collected from the trusses that remained after passing through the harvester. The total losses per 1 hectare of vineyard were determined by weighing and calculation and also expressed as a percentage of the harvest.

The vineyard is planted in a 2.4 x 1.0 m clip, which represents 4200 trusses per hectare.

RESULTS AND DISCUSSION

Before performing the measurements, the machine parameter was set to the values recommended by the manufacturer. However, frequency is the most important factor influencing the amount of harvesting losses. Therefore, the frequency of shaking was set based on passing through the first row of the vine, when we determined, based on visual assessment, the value of the frequency at which the lowest losses occurred with the least damage to the berries. By observing, we confirmed what Pezzi and Caprara (2009) state that visible losses decreased with increasing frequency. The following machine parameters were set for measurements in 2017: frequency 450 $.min^{-1}$, oscillation amplitude 90%, shaker spacing 20 mm, separation fan speed 1600 rpm. Working speed ranged from 2.5 to 3.1 $km.h^{-1}$.

From the measurements, we evaluated that the total absolute value of losses was 274.12 kg per hectare, which represented a percentage of 2.03% with the achieved fertility. The average yield per hectare was 13.5 $t.ha^{-1}$.

Tab. 1 Harvest losses 2017

Measurement 2017 - Traminer		
The Measurement	**Losses incurred**	
	Slumped, [kg]	**Non-harvested, [kg]**
1.	0.396	0.43
2.	0.383	0.142
3.	0.502	0.105
Average	0.427	0.226
Losses for hectare, [kg.ha^{-1}]	179.34	94.78
Percentage, [%]	1.33%	0.70%
Total losses for hectare [kg.ha^{-1}]	**274.12**	
Total losses in %	**2.03%**	

During the harvest in 2018, slightly different parameters of the machine were set based on visual evaluation. Oscillation frequency 490 .min^{-1}, oscillation amplitude 100%, shaker spacing 20 mm, separation fan speed 1600 rpm. Working speed in the range of 2.5 - 3.1 km.h^{-1}. Lower losses were measured this year. The specific value was 137.34 kg per hectare. With an average fertility of 9.36 tons, this represented a percentage of 1.47%.

Tab. 2 Harvest losses 2018

Measurement 2018 - Traminer		
The Measurement	**Losses incurred**	
	Slumped, [kg]	**Non-harvested, [kg]**
1.	0.265	0.052
2.	0.252	0.041
3.	0.235	0.136
Average	0.251	0.076
Losses for hectare, [kg.ha^{-1}]	105.28	32.06
Percentage, [%]	1.12%	0.34%
Total losses for hectare [kg.ha^{-1}]	**137.34**	
Total losses in %	**1.47%**	

The results of measurements show that in 2018 lower percentage losses were achieved by almost 28%. We can therefore say that the statement of Pezzi and Caprara (2009) that the losses decreased with increasing frequency was also confirmed here in terms of values. However, it is not possible to increase the frequency enormously, as hidden losses in the form of increased berry damage may subsequently occur. This results in splashing of berries and increased hidden losses. It is therefore necessary to identify a medium, reasonable frequency at which losses are minimized. This can be traced to the condition of the harvested product in the container.

The maximum losses were at the level of 2%, which are particularly good values comparable to the results of other authors (Jobbágy et al. 2018; Pezzi, Martelli 2015; Novák, Burg 2013; Zemánek, Burg 2005). Even, such loss values are lower compared to losses that result from manual harvesting, as reported by Clary et al. (1990), where in their research the losses of manual harvesting reached up to 2.64%.

In addition to the frequency of oscillations and working speed, other factors also influence the amount of losses, such as degree of ripening of the grapes. If the grapes have a smaller amount of water (degree of ripening and precipitation), the berries hold more firmly on the bunches, so it is necessary to shift the frequency of oscillations to higher values. This means that the operational setting of the machine changes each year for each variety, even within one variety of the same season at different harvest times.

CONCLUSION

The work aimed to evaluate the mechanized harvesting of grapes, especially the losses that occur during the harvesting of the overhead grape harvesters. A Pellenc 8090 SP harvester was used for the measurements. Measurements were performed in two years on the variety Traminer. The monitoring revealed that lower losses were achieved by almost 28% year-on-year in the given company. This could be achieved by a higher value of the oscillation frequency of the shaking rods. Total losses reached 2.03%, respectively 1.47%. The amount of losses is influenced by many factors from the ripeness of the grapes to the appropriate setting of the machine parameters, but also compliance with agrotechnical requirements for mechanized harvesting. Mechanized harvesting of grapes can be considered as an efficient method of harvesting, which achieves higher performance, comparable or lower losses. From the acquired knowledge we can conclude that it is very important to first monitor the losses visually at lower frequency values and find the optimal frequency when there is minimal visual loss, to achieve the minimum hidden losses.

REFERENCES

1. BATES, T – MORRIS, J. 2009. Mechanical Cane Pruning and Crop Adjustmen Decreases Labor Costs and Maintains Fruit Quality in New York "Concord" Grape Production. In *HortTechnology.* Vol. 19, no. 2, 247 – 253 p. ISSN 1943-7714
2. CLARY, Carter D. et al. 1990. Evaluation of machine vs. hand-harvested Chardonnay, In *American journal of enology and viticulture.* vol. 41, pp. 176 – 181, ISSN 0002-9254. Available on: <https://ajevonline.org/content/ajev/41/2/176.full.pdf >.
3. INTRIERI C. – Poni S. 1990. New integrated approach between training systems and machines for the management of high-quality vineyards. In *Accademia Italiana della Vite e del Vino*, 42, 295–323.
4. JOBBÁGY, Ján. et al. 2018. Evaluation of the mechanized harvest of grapes with regards to harvest losses and economical aspects. In *Agronomy research* [online], vol. 16, no. 2, pp. 426 – 442. Available on : <https://doi.org/10.15159/AR.18.056>.
5. PEZZI F. – BERARDINELLI A. – BORDINI F. – GIUNCHI A. – RAGNI L. 2005. Mechanical grape harvesting: a study of the correlations between work quality, operating conditions and transmission of vibrations to the plant. In *Rivista di Ingegneria Agraria*, 4, 25–34.
6. JOBBÁGY, Ján – FINDURA, Pavol. 2013. *Mechanizácia vinárstva.* 1. ed. Nitra: Slovenskápoľnohospodárskauniverzita v Nitre, 2013. 165 p.ISBN 978-80-552-0996-8.
7. NOVÁK, Pavel – BURG, Patrik. 2013. Evaluation of Harvest Losses Within a Full Mechanised Grape Harvest. In *Acta Universitatis Agriculturae Et Silviculturae Mendelianae Brunensis.* Vol. 61, no. 3, pp. 751-756. ISSN 2464-8310
8. PEZZI, F – MARTELLI, R. 2015. Technical and economic evaluation of mechanical grape harvesting in flat and hill vineyards. Trans ASABE 2015; 58 (2):297–303.
9. PEZZI, F – CAPRARA, C. 2009. Mechanical grape harvesting: Investigation of the transmission of vibrations, In *Biosystems Engineering*, vol. 103, pp. 281 – 286.
10. ZEMÁNEK, Pavel – BURG, Patrik. 2005. Hodnocení mechanizované sklízně hroznu. In *Acta Universitatis Agriculturae Et Silviculturae Mendelianae Brunensis.* Vol. 53, no. 4, 191 – 194 . ISSN 2464-8310.

We would like to thank Pivnica Radošina s. r. o. for enabling the carrying out of research work. We would also like to thank Agroplast Mýtna Nová Ves for providing a part of the material support of the research.

Corresponding author:

Ing. Martin Dočkalik, Department of Machines and Production Biosystems, Faculty of Engineering, Slovak University of Agriculture in Nitra, Tr. A. Hlinku 2, 949 76, Nitra Slovakia, email: xdockalik@uniag.sk

The work was created within the preparation and solution of the project KEGA no. 012SPU-4/2020 "Innovation of the educational process and implementation of knowledge from practice with a focus on viticulture and viticulture" solved at the Department of Machines and Production Biosystems SUA in Nitra in 2020-2022.

Backscatter analysis of a corn field using Sentinel-1 data

J. Dvořák[1], V. Novák[1]

[1]Czech University of Life Sciences Prague (CULS), Faculty of Engineering, Department of Machinery Utilization, Kamýcká 129, CZ165 21 Prague, Czech Republic

Abstract

Monitoring of agricultural crops is already an integral part of precision agriculture. The radar system with a synthetic aperture enables continuous monitoring of the vegetation during the growing season. Radar data can provide information of crop type or estimate biophysical parameters. The Copernicus program offer opportunity to monitor crops systematically every 6 - 12 days in the Czech Republic. In this study, VV / VH SAR images with high temporal resolution were used to compare the two life cycles of maize. A time series analysis was performed that compares the growing seasons of maize with significantly different meteorological conditions. Different fertilization variants were also compared using backscatter.

Key words: radar, weather, maize, time series, backscatter, polarization

INTRODUCTION

Due to the growing demand for food, the demands on farmers are constantly increasing. Earth remote sensing is a tool that helps farmers in various areas of interest. Earth remote sensing can be divided into several areas of use. Estimation of crop yield, precise farming, where maximum yield is required, evaluation of cultivated crop, mapping of losses and yields, and control of agriculture (Henderson, Floyd M., Lewis, 1998) (Sivakumar et al., 2003). Remote sensing of the Earth is most often performed using optical or radar data. Crop analysis using optical data is already well developed and offers a lot of tools for crop analysis. However, optical data has a shortcoming that is addressed by radar data. Optical data work mainly with the visible part of the electromagnetic spectrum, which cannot penetrate the clouds due to its very short wavelength (Vreugdenhil et al., 2018).

Radar systems working with Synthetic Aperture Radars solve this problem. These systems work with the microwave part of the frequency band, which allows the penetration of clouds and rain. (Steele-Dunne et al., 2017). The SAR emits a pulse of electromagnetic radiation and then records the amplitude and phase that return reflected from Earth. The backscatter

coefficient σ^0 describes the strength of the recorded radar signals. (Atzberger, 2013). However, interpreting the data is very difficult, but a great benefit for this field is the Copernicus program from the European Space Agency, which offers data from its satellites free of charge. (Kim & Van Zyl, 2009)

MATERIALS AND METHODS

The cornfield is located in Sloveč in Central Bohemia Region. The date of sowing corn was 14.4. and the date of harvest 27.8. in 2015. In 2018 the date of sowing was 10.4. and 3.8. was the harvest date. The cornfield was divided into ten variants of the fertilization system. Variants shown in tab. 1 adhered to the same fertilization management at all times. The NPK is a typical fertilizer (nitrogen, phosphorus, potassium), SOL (PRP Technologies, France) was used as the soil activator. FIX (PRP Technologies, France) was used as the activator of the biological transformation of manure.

Tab. 1 Variants of feritilization

Variant number	***Type of fertilization***
1	cow manure with FIX + NPK
2	cow manure with FIX + SOL+ NPK
3	cow manure + NPK
4	cow manure + SOL+ NPK
5	SOL + NPK
6	NPK (control)
7	pig manure with FIX + NPK
8	pig manure with FIX + SOL+ NPK
9	pig manure + NPK
10	pig manure + SOL+ NPK

The calculation of backscatter σ^0 was demonstrated using the Sentinel Application Platform (*SNAP*). The timeline was processed from one Sentinel 1 satellite mission, meaning that the timeline has a step of 14 days. The images were calibrated, and a Lee Speckle filter was applied to increase the image quality. The images were compared with the Terrain Correction function. The resulting images have a resolution of 10 x 10 pixels and contain backscatter values (Jin et

al., 2015). The image was converted to a logarithmic level using the dB unit. Values in VV (vertical polarization), VH (vertical/horizontal polarization) was available for backscatter purposes. In Figures 1 and 2 you can see the time series from the year of backscatter σ^0 in VH polarization for all ten tested variants.

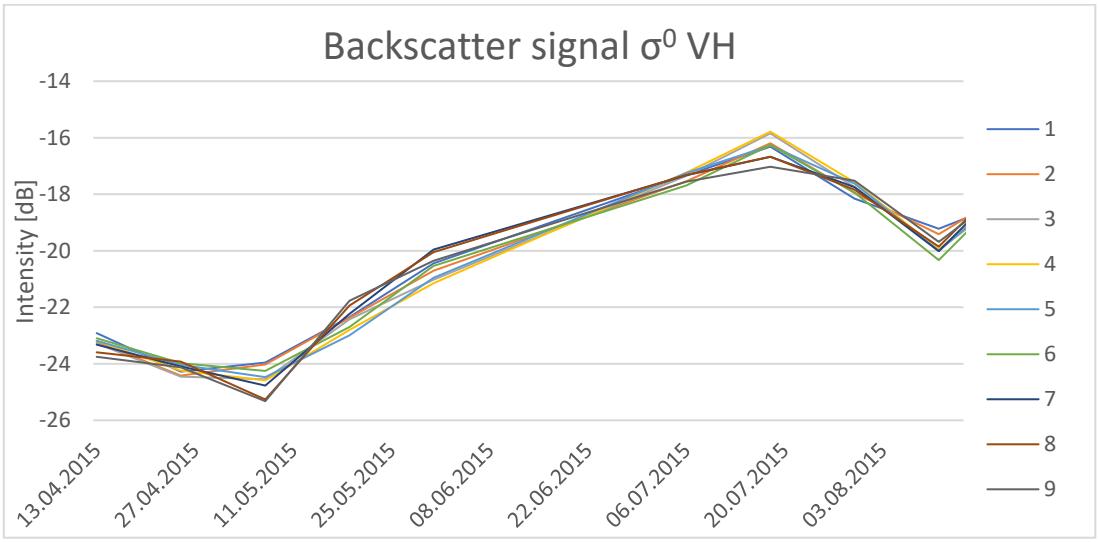

Fig. 1 Time series of backscatter signal σ^0 VH 2015

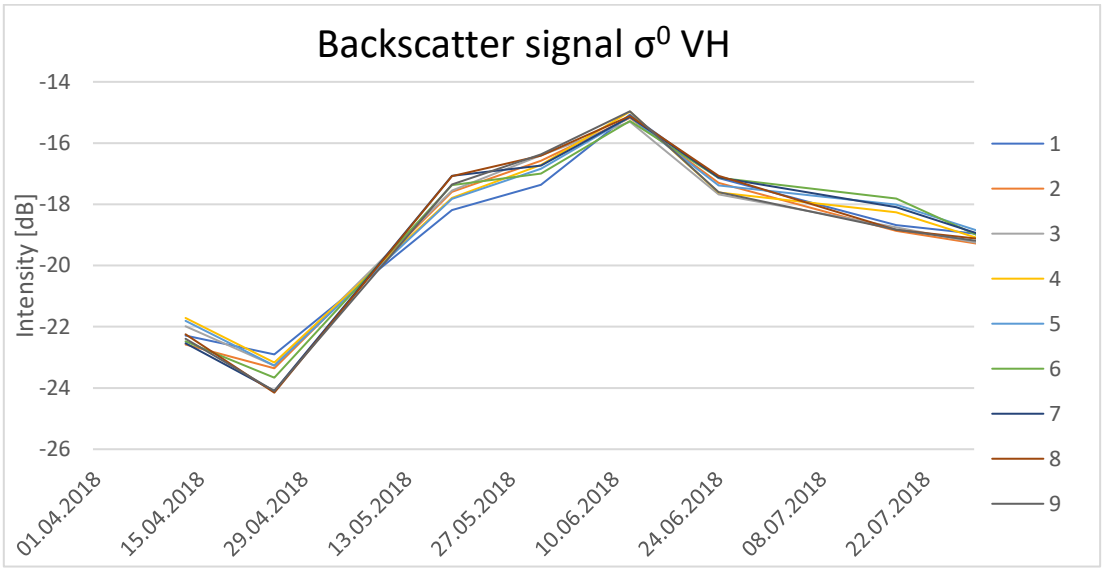

Fig. 2 Time series of backscatter signal σ^0 VH 2018

Backscatter monitoring is very sensitive to moisture changes. Due to rainfall must be taken into account in the analysis. The nearest meteorological station, which records the frequency of rainfall, is located in the town of Poděbrady, which is 17 km from the measured field. The average rainfall in the area from April to August is 1.47 mm of rainfall per day (average from

1961 - 2019). In 2015, rainfall in the measured period was 1.62 mm per day and a total of 221 mm of rainfall in the measured period. In 2018, 1.13 mm per day and 131 mm of rainfall in total were measured for the measured period (*ČHMÚ*).

RESULTS AND DISCUSSION

When comparing the backscatter from 2015 and 2018, large differences can be observed. These differences are mainly caused by different total rainfall. In 2015, the backscatter curve grows more slowly, indicating a more even total precipitation. From 30.7. From 2015 to 15.8. 2015, no rain was recorded in the area, which is immediately shown in the graph. Just before harvest, the daily total rainfall was very high, which could affect the backscatter value. The year 2018 was rainfall poorer than the average in the area. There was only one day during the growth of the crop, when more than 25 mm of rain fell, which indicates that light rain prevailed during the period. According to the data, the graph is clearly influenced mainly by 12.6. 2018, where the backscatter reaches high values due to humidity, which is caused by that very day with a very high total precipitation, namely 30.3 mm per day. Pre-harvest values are almost declining in 2015 and 2018, but in 2018 they are not affected by rain.

The back dispersion of fertilization variants in 2015 differed before harvest by a maximum of 6.47% for VH and by 5.16% for VV. The data suggest that fertilization variants 7 and 8 should have the highest yield according to VH and according to VV variants 2 and 6. In 2018, VH differed by 2.27% and VV by 8.92%. According to the data, variants 1 and 2 should have the highest yield according to VH and VV.

CONCLUSION

This study evaluated the backscatter sensitivity of Sentinel-1 SAR. Two maize growing seasons from 2015 and 2018 in the same field were compared. Different fertilization variants were also compared. Time series analysis demonstrated the sensitivity of the backscatter to vegetation variables. The differences in σ^0 backscatter between 2015 and 2018 were caused by different rainfall intensities, but also by other factors, such as the application of activators of biological transformation of organic matter applied to soil in 2014, the effect of which is more pronounced over the years. According to available data, the yield after conversion to 38% of dry matter in 2018 was higher by 11.9%. Before harvest the backscatter values vary very little between years, but in 2015 the data may be affected by heavy rain before the last image was taken just before harvest. This phenomenon can also be seen 12.6. 2018, when heavy rain certainly affected the

measured data. Data on total rainfall were obtained from a hydrometeorological station 17 km away from the measuring point. Therefore, rainfall data may not be completely accurate.

Evaluations of individual fertilization variants according to backscatter show that the polarizations of VH and VV differ in the analysis of maize. In 2015, the backscatter analysis incorrectly identified the fertilization variants in VV polarization. For VH, the variant with the highest yield was identified correctly. For 2018, the polarizations VV and VH evaluated the first two variants with the highest yield correctly. According to the data on yields from the combine harvester, the first two variants were significantly withdrawn. The other variants had very similar yields, here the data no longer correlate completely.

The results could be refined if both satellites from the Sentinel-1 mission were used. Images taken from different satellites do not provide exactly the same information, but would halve the timeline interval, that is, every approximately seven days.

REFERENCES

1. Atzberger, C. (2013). Advances in remote sensing of agriculture: Context description, existing operational monitoring systems and major information needs. In *Remote Sensing* (Vol. 5, Issue 2, pp. 949–981). https://doi.org/10.3390/rs5020949
2. Henderson, Floyd M., Lewis, A. J. (1998). *Principles and Applications of Imaging Radar (Manual of Remote Sensing, Volume 2): Henderson, Floyd M., Lewis, Anthony J.: 9780471294061: Amazon.com: Books*. https://www.amazon.com/Principles-Applications-Imaging-Manual-Sensing/dp/0471294063
3. Jin, X., Yang, G., Xu, X., Yang, H., Feng, H., Li, Z., Shen, J., Lan, Y., & Zhao, C. (2015). Combined Multi-Temporal Optical and Radar Parameters for Estimating LAI and Biomass in Winter Wheat Using HJ and RADARSAR-2 Data. *Remote Sensing*, *7*(10), 13251–13272. https://doi.org/10.3390/rs71013251
4. Kim, Y., & Van Zyl, J. J. (2009). A time-series approach to estimate soil moisture using polarimetric radar data. *IEEE Transactions on Geoscience and Remote Sensing*, *47*(8), 2519–2527. https://doi.org/10.1109/TGRS.2009.2014944
5. *Portál ČHMÚ : Historická data : Počasí : Denní data : Denní data dle z. 123/1998 Sb.* (n.d.). Retrieved July 26, 2020, from http://portal.chmi.cz/historicka-data/pocasi/denni-data/Denni-data-dle-z.-123-1998-Sb#
6. Sivakumar, M. V. K., Roy, P. S., Harmsen, K., & Saha, S. K. (2003). *Satellite Remote Sensing and GIS Applications in Agricultural Meteorology World Meteorological Organization (WMO) India Meteorological Department (IMD) Centre for Space*

Science and Technology Education in Asia and the Pacific (CSSTEAP) Indian Institute of Remote Sensing (IIRS) National Remote Sensing Agency (NRSA) and Space Application Centre (SAC). http://www.bishensinghbooks.com

7. *SNAP Download | STEP*. (n.d.). Retrieved July 28, 2020, from http://step.esa.int/main/download/snap-download/
8. Steele-Dunne, S. C., McNairn, H., Monsivais-Huertero, A., Judge, J., Liu, P. W., & Papathanassiou, K. (2017). Radar Remote Sensing of Agricultural Canopies: A Review. In *IEEE Journal of Selected Topics in Applied Earth Observations and Remote Sensing* (Vol. 10, Issue 5, pp. 2249–2273). Institute of Electrical and Electronics Engineers. https://doi.org/10.1109/JSTARS.2016.2639043
9. Vreugdenhil, M., Wagner, W., Bauer-Marschallinger, B., Pfeil, I., Teubner, I., Rüdiger, C., & Strauss, P. (2018). Sensitivity of Sentinel-1 Backscatter to Vegetation Dynamics: An Austrian Case Study. *Remote Sensing*, *10*(9), 1396. https://doi.org/10.3390/rs10091396

ACKNOWLEDGMENT
This study was supported by TAČR TH02030169 and IGA 2020:31180/1312/3103.

Corresponding author:

Ing. Jakub Dvořák, Czech University of Life Sciences Prague (CULS), Faculty of Engineering, Department of Machinery Utilization, Kamýcká 129, CZ165 21 Prague, Czech Republic
tel: +420777948882, email: jakubdvorak@tf.czu.cz

Comparison of two MPC methods using membranes with different diameters

J. Effenberk[1]

[1]*Department for Quality and Dependability of Machines, Faculty of Engineering, Czech University of Life Sciences Prague, Prague, Czech Republic*

Abstract

This article is focused on the comparison of two Membrane Patch Colorimetry (MPC) methods using membranes with different diameters. Test performed on bigger membrane is standardized. The smaller membrane is not. The main aim of this study is to find out if it is possible to use smaller membrane to get the same results and if so under which conditions. The main motivation for this change are benefits in the form of cost and time savings.

Key words: deformation characteristics, mechanical, physical, properties, pressing, tangent curve, varnish

INTRODUCTION

Membrane patch colorimetry (MPC) is a method standardized by ASTM D7843 to determine the propensity for a lubricant to form varnish deposits. It is recommended to test all critical installations on monthly basis. The test is straightforward and can be used not only as a part of already existing analysis method but for rapid on-site application as well. It is suited to turbines, compressors and hydraulic systems.

The standardized MPC test consists of the parts:

a) Filtration is performed under prescribed conditions. The apparatus and consumables are defined in the standard. It includes anything from heating and storing to detailed hardware requirements. The mixture of 50 ml of the lubricant and equal volume of petroleum ether is filtered through a 0.45 μm nitrocellulose patch which is then rinsed with petroleum and dried.

b) Color measurement is a process of setting the difference of the intensity and the color between the dried membrane and control patch. The measuring device is called spectrophotometer and the result is ΔE value which is then evaluated according to an MPC scale.

MPC scale is a guideline to assess lubricant´s potential for varnish formation. It has 4 levels:

a) Good (ΔE<15),

b) Monitor (ΔE = 15-25),

c) Abnormal (ΔE = 25-35),

d) Critical (ΔE >35).

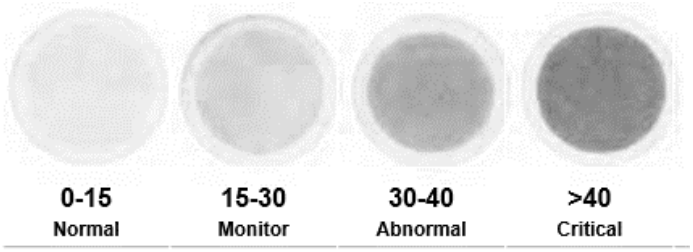

Fig. 1 MPC rating scale

The higher the MPC value, the higher the amount of varnish deposits and precursors dissolved in the lubricant and the greater the potential for the lubricant to form harmful varnish deposits (EPT Clean Oil, 2016). The trend of MPC values of modern lubricants is not linear anymore and the degradation process tends to speed up in the very end of their lifespan. Modern oils have better overall performance and total life span but once the level of antioxidants decrease under certain level then volume of pollutants starts to increase exponentially in very short time frame (NOVÁK, 2013).

Increment in MPC value means accumulation of dissolved oil breakdown products called varnish precursors (KON, 2018) produced by oxidation and thermal degradation (ALS). This process begins from the very first moment the lubricant is put in the machine and never stops. Each lubricant has its finite saturation point dependent on often changing lubricant temperature, pressure and flow which is basically a capacity to hold these dissolved oxidation products in solution. When the lubricant is fully saturated then excess breakdown products are forced from the fluid formatting the harmful varnish deposits. Those deposits are highly acidic and can have different form from soft and sticky sludges to hard and shiny varnishes (NOVÁK, 2013), (Wear Check, 2009). All of them has natural attraction to coat metal surfaces, reduce mechanical clearances, impair lubricant film, decrease equipment performance and in the worst scenario it can lead to machine failure in sensitive mechanical areas (EPT Clean Oil, 2016), (NOVÁK, 2013).

The most often affected parts and related problems:

- valves - jamming,
- pumps,
- hydromotors – slip-stick effect,
- bearings – higher wear rate,
- filters – shorten lifespan and clogging,
- gears – higher wear rate,
- cooler surfaces – lower efficiency (NOVÁK, 2013), (ALS).

There are several advantages brought by this method in form of time and money savings:

- less lubricants needed,and optimization of their lifespan,
- less downtimes,
- less missed opportunities and missed incomes,
- more environmentally friendly approach (NOVÁK, 2013), (ALS).

On today's market it is possible to buy a smaller but not standardized device which offers the same advantages while keeping the buying price lower. Moreover the cost per measurement should be lower as well. This device follows the same methodology and principles but uses smaller 25 mm membrane patches and smaller volume of the mixture. The volume recommended by the supplier is 25 ml of lubricant and 25 ml of petroleum ether. However this volume doesn´t provide the same results as standardized tests. This problem rises some questions about its suitability and interchangeability.

MATERIALS AND METHODS

There were 9 hydraulic oil samples used in this experiment. The samples were taken from hydraulic machines used in leading Czech automotive company. All the tests were performed in the tribotechnical laboratory under supervision of certified tribodiagnostician.

There were four partial objectives defined to answer the question of both methods suitability and interchangeability:

a) To find out if the methods are interchangeable without optimization.
b) To find out if there is direct proportion between membrane surface and MPC value.
c) To find out what relationship is between sample volume and MPC value.
d) To set the optimal sample volume needed to get good results on smaller membrane.

The first set of measurements was performed on both apparatuses. Tests done on smaller one were done according to recommendations from the supplier. The mixture consisted of 25 ml of lubricant and 25 ml of petroleum ether. Testing on bigger membrane was done in line with ASTM D7843 standard, namely mixture of 50 ml of lubricant and 50 ml petroleum ether. The main purpose was to confirm if the methods are interchangeable.

Then the useful surface of membranes was measured. The useful surface is the part of membrane where the mixture is filtered through. The ratio between both membranes was calculated as a division of their useful surfaces. This ratio was compared to the average relative difference of results from both membranes.

The process of best curve fitting was used to define the relationship between sample volume and MPC value. The main criteria was a value of correlation coefficient R. Prior to this the additional measurements with 3 different sample volumes were done (5, 10 and 15 ml of lubricant and the same volume of petroleum ether). Once the relationship is known then its equation and coefficients were used to calculate the average optimal sample volume.

This optimal sample volume value was then verified with 3 different samples and compared to standardized procedure. The both MPC values should be as close as possible. In the end there are briefly mentioned the benefits of the smaller membrane taking into count the average prices of the materials using for both methods.

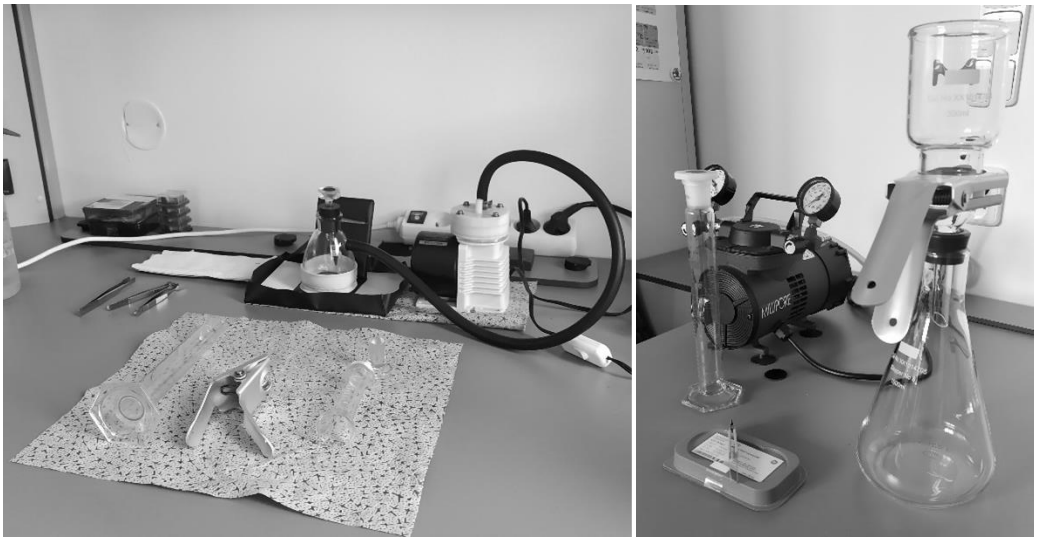

Fig. 2 Smaller and bigger apparatuses used for measurements

RESULTS AND DISCUSSION

The first set of measurements was performed on both membranes and the differences could be seen by the eye. Sample 186 was taken out of the experiment because the whole sample volume did not go through on both methods.

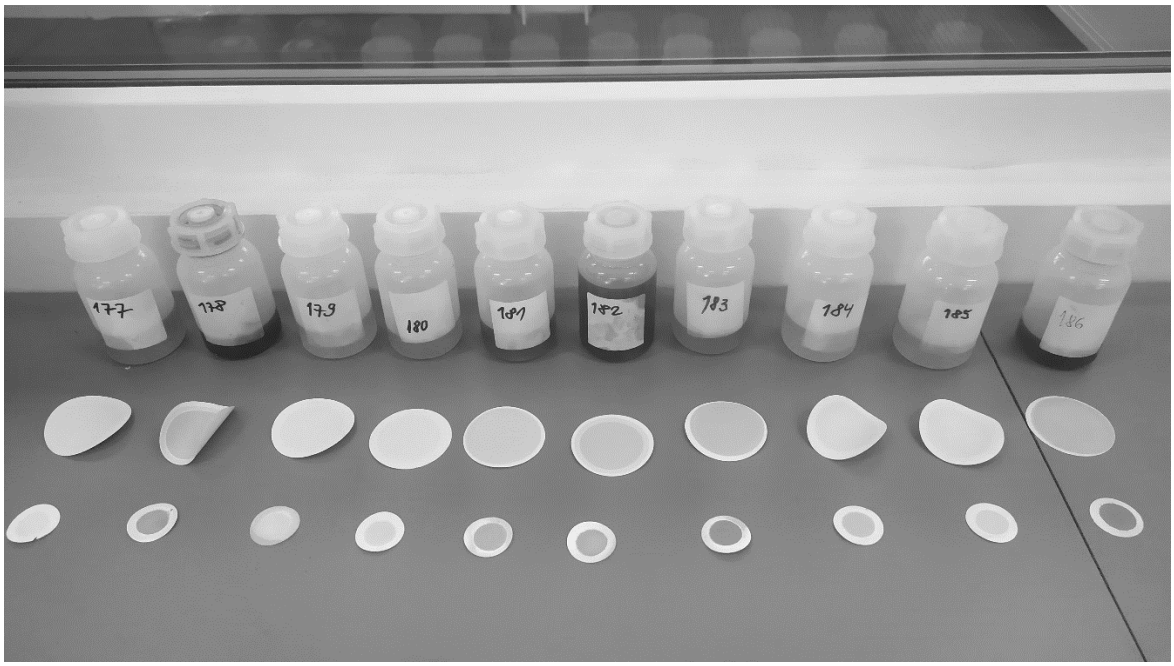

Fig. 3 The first set of measurements performed under recommended conditions

The exact values are presented in a table (Tab. 1). The average relative difference of both methods was 95.56 %. The methods are not interchangeable when the tests performed on smaller membrane are performed in line with supplier recommendations.

Tab. 1 MPC results measured on both smaller and bigger membrane

Sample	Membrane Ø 25 mm [ΔE]	Membrane Ø 47 mm [ΔE]	Absolute difference [ΔE]	Relative difference [%]
177	9.3	5.4	3.9	72.22
178	36.5	20.8	15.7	75.48
179	14.6	6.5	8.1	124.62
180	17.4	6.9	10.5	152.17
181	36.1	20.2	15.9	78.71
182	34.4	18.8	15.6	82.98
183	40.8	21.0	19.8	94.29
184	21.8	9.8	12.0	122.45
185	13.2	8.4	4.8	57.14
AVG	-	-	**11.8**	**95.56**

The membrane surfaces needed to be calculated to be able to decide if there is a direct proportion between membrane surface and MPC value. According to results in the tables (Tab. 1 and Tab. 2) the average relative difference does not correspond with useful surface ratio. It indicated that there is not a direct proportion between these two parameters.

Tab. 2 Membrane surface comparison

Membrane	Useful diameter [mm]	Total surface [mm^2]	Useful surface [mm^2]
Ø 25 mm	16	490.87	201.06
Ø 47 mm	35	1734.94	962.11
Ratio	2.19	3.53	**4.79**

To define the relationship between MPC values and sample volume additional testing with different sample volumes was done as shown in Tab. 3.

Tab. 3 Measured MPC values and calculated optimal sample volume for each sample

Volume [ml]	Sample [ΔE]								
	177	**178**	**179**	**180**	**181**	**182**	**183**	**184**	**185**
5	1.5	11.0	7.5	3.6	11.6	9.6	11.8	5.3	4.0
10	6.0	18.0	9.5	6.0	18.0	16.5	19.8	7.9	6.3
15	8.4	26.4	11.5	9.7	23.5	21.0	29.7	12.9	8.6
25	9.3	36.5	14.6	17.4	36.1	34.4	40.8	21.8	13.2
50	5.4	20.8	7.9	6.9	20.2	18.8	21.0	9.8	8.4
a	*0.3634*	*1.2794*	*0.3537*	*0.7034*	*1.2183*	*1.2223*	*1.4566*	*0.8474*	*0.4600*
b	*1.3029*	*5.3829*	*5.9114*	*0.4971*	*5.5486*	*3.5686*	*5.4971*	*0.3229*	*1.7000*
R	*0.7907*	*0.9870*	*0.9614*	*0.9922*	*0.9994*	*0.9957*	*0.9835*	*0.9908*	*1.0000*
OPT	11.27	12.05	5.62	9.10	12.03	12.46	10.64	11.18	14.57

The results were used to find the best fitting curve for all 9 samples. All 9 samples were best fitted with linear curve as shown in Fig. 4. The main criteria was a value of correlation coefficient R. The equation confidents and R coefficient are mentioned in Tab. 3.

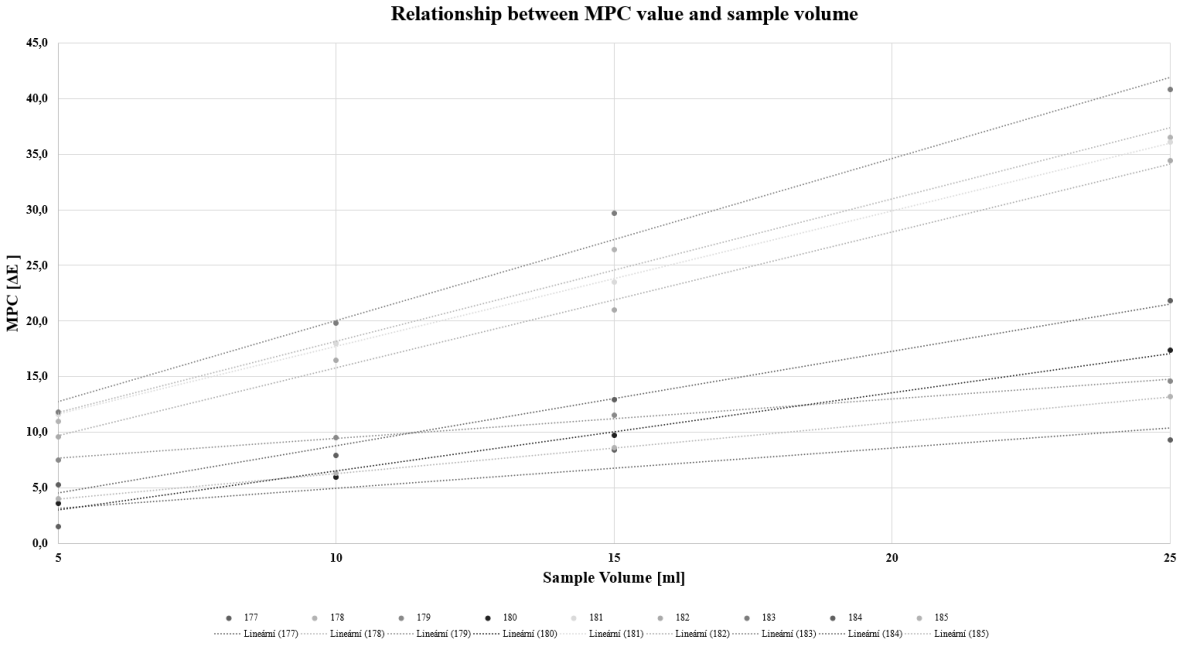

Fig. 4 Measured MPC values in relation to sample volume

The equations were used for a calculation of the optimal sample volume for each sample. The desired value for each sample was a MPC value received by standardized method done with 50 ml of lubricant. This value is mentioned in Tab. 3. The average optimal sample size was 10.99 ml. This calculated value was then experimentally verified with 3 randomly chosen samples different from 9 samples used for in previous steps. The results are shown in Tab. 4.

Tab. 4 Verification results

Sample	Membrane Ø 25 mm [ΔE]	Membrane Ø 47 mm [ΔE]	Absolute difference [ΔE]	Relative difference [%]
170	12.6	14.7	2.1	14.29
171	34.4	33.1	1.3	3.93
172	11.6	11.4	0.2	1.75
AVG	-	-	**1.2**	**6.66**

Results of all three samples were very similar to the standardized method. The average relative difference was 6.66 %. The difference was small enough to correctly assess all three samples to the same MPC category as the standardized method.

CONCLUSION

The optimal lubricant sample volume calculated in this study is 10.99 ml. Mixed with the same volume of petroleum ether and filtered through 25 mm membrane it shows satisfying results in accuracy of smaller membrane.

This solution brings benefits mainly in form of money. Taking into account the current market prices of consumable materials the savings from the membranes could go up to 50 % and savings from the lower consumption of petroleum ether up to 75 %.

Other benefit is overall sample volume which makes this method more suitable for equipment with smaller lubricant tanks. Considering the fact that the mixture is not reusable than the whole method is becoming more environmentally friendly due to lower volume of the total chemical waste.

REFERENCES

1. EPT Clean Oil: MPC Varnish Potential Testing (ASTM D7843), 2016, 5pp
2. NOVÁK J.: Moderní oleje a nový přístup k jejich analýze, TECHMAGAZÍN Tribotechnické informace, 2013, 12 pp
3. ALS: Varnish Testing by Colour Evaluation – Membrane Patch Colorimetry (MPC), Malaysia, 1 pp
4. KON T., HONDA T., SASAKI A.: Influence of Solvents, Oil Temperature, and Incubation Period on Membrane Patch Color, Bunkyo, Fukui, Japan, 2018, 7 pp
5. Wear Check: Varnish Potential Testing, USA, 2009, 2 pp

Monitoring of selected parameters for gasoline vehicle while using the testing substance

P. Feriancová[1], J. Polerecký[1], R. Janoušková[1], P. Kuchar[2]

[1]Department of Transport and Handling, Faculty of Engineering, Slovak University of Agriculture in Nitra, Nitra, Slovak Republic

[2]Department of Building Equipment and Technology Safety, Faculty of Engineering, Slovak University of Agriculture in Nitra, Nitra, Slovak Republic

Abstract

The aim of the experiment was to carry out a research on the tested substance MPG BOOST in laboratory conditions. The MPG BOOST was tested on a Škoda Fábia 1.4 MPi with a combustion engine. The methodology of the experiment with the selection of suitable measuring and evaluation devices and with the characteristics of the measured object are specified in the experiment. The results of the paper include the evaluation of the measured values.

Key words: petrol engine, emissions, emission limits, testing substance, dynamometer, combustion engine

INTRODUCTION

At the present, environmentalist and energy industries belong to substantial problems in society (KOSIBA et al. 2017). Traffic has an eminent effect on generating of undesirable emissions, as well as energy load (MARKIEWICZ-PATALON et al. 2018). Transportation is participant in air pollution in the range circa up 13% to 20 %. We can therefore state, that transport sector is ranked among the most serious problem in term of power consumption (JABLONICKÝ et al. 2019). The European Union had to take measures, that would have secure reducing the production of greenhouse gases (MARKIEWICZ-PATALON et al. 2019). The European Union defines emission limits for motor vehicles since 1992 (MARKIEWICZ-PATALON et al. 2018). To reduce emissions more effectively, standard hydrocarbon fuels should be replaced by alternative fuels and alternative propulsion (TOMIC et al. 2014). At the present, many technologies are being used to reduce emissions, including engine modifications, emission control devices and the use of alternative fuels (JANOŠKO et al. 2019). One of the alternatives for reducing emissions and improving fuel quality is to add additives (PUŠKÁR et al. 2019).

MATERIALS AND METHODS

An accurate procedure for performing the tests with the testing substance has been established, a suitable vehicle for testing has been identified, an appropriate measurement method and a measuring equipment were determined.

Methodology of emission measurement, simulated driving test and performance in use testing substance

Measurement methodology of vehicle emission status with testing substance, alongside with simulated driving test were realized according to items listed below:

1. Initial status of vehicle emission status before using of testing substance in accordance with the Act no. 106/2018 CA during first measurement,
2. Measurement performance of petrol engine before application testing substance,
3. Execution of simulated driving test before application of testing substance,
4. Fill-up full tank container – until shutdown of fuel nozzle,
5. Addition of the testing substance according to the specified quantity after fill-up full fuel tank– 15 ml,
6. Another measurement of emission status and simulated driving test was carried out after driving 500 km ± 50 km,
7. Repeating of measurement (4 times), always after driving 500 km ± 50 km,
8. Measurement of combustion engine performance,
9. Evaluation of results (Methodical instruction No. 32/2018, 2018).

The above measurements were performed in the Laboratory of Bioenergy Resources. The measurement of the emission status will be performed in keeping with the valid legislation (Act no. 106/2018 Coll.).

The methodology of the simulated driving test will be performed according to the proposed procedure, as follows:

1. Steady speed of the vehicle – 90 $km.h^{-1}$,
2. Measurement time at steady speed – 5 min.
3. Driving position engaged – 5,
4. Load during the simulated driving test – 200 N.

Measurement of emission status

Petrol engine emissions were measured by five-gas analyzer MAHA MGT 5 (Fig. 1). The analyzer measures contents of CO, CO_2 and HC based on non-dispersive infrared absorption. The analyzer also measures the share of O_2 and NO_X by using of electrochemical cells. Analyzed gas is sampled by a probe from a vehicle exhaust. After that, water and combustion gases are separated, and they flock into the measuring chamber.

Fig. 1 Five-gas analyzer MAHA MGT 5 and smoke tester MDO – 2 Lon Euro

Characteristics of the testing substance

Function of testing substance is secondary addition of motor petrol which quality defined by European standard. This substance influences the combustion process, increase the burning temperature and by that, better combustion of mixture is obtained, which decrease exhaust fumes emissions. Another function of testing substance is to decarbonize engine combustion chamber, the zone of the first pistol ring and to keep the fuel supply system clean. Combustion chamber of engine bestrews with microscopic layer and it does not create harmful compounds after decarbonization. Appropriate mixture of petrol and testing substance are shown in the following Tab. 1.

Tab. 1 Mixing ratios of fuel and testing substance

Fuel volume (petrol), l	**Dose of testing substance, ml**
23 – 40	15
41 – 59	22
60 – 85	29.5
86 – 108	37
109 – 130	44.5

Fig. 2 Testing substance

Characteristics of the vehicle used for the measurement

A vehicle with a kilometer reading more than 250000 km was selected for the measurement. Parameters of testing vehicle are listed in Tab. 2.

Tab. 2 Test vehicle parameters

Vehicle	Škoda Fabia Combi 6Y
Year of production	2002
Engine type	BBZ
Engine cylinder capacity	1390 cm^3
Catalyzer	RKAT
Highest engine power	74.00 kW
rpm	6000 min^{-1}
Maximum torque	126 N.m / 4400 min^{-1}
Gearbox/ number of stages	MT/5
ABS	yes
Size and type of tires	185/60 R14 82H
Manufacturer's maximum speed	186 $km.h^{-1}$
Emission ES/EHK	1999/102A (EURO 3)
Fuel consumption	6.7 l/100 km

Dynamometer MSR MAHA

Dynamometer MAHA MSR 500 (Fig. 3) was used to measure torque and power.

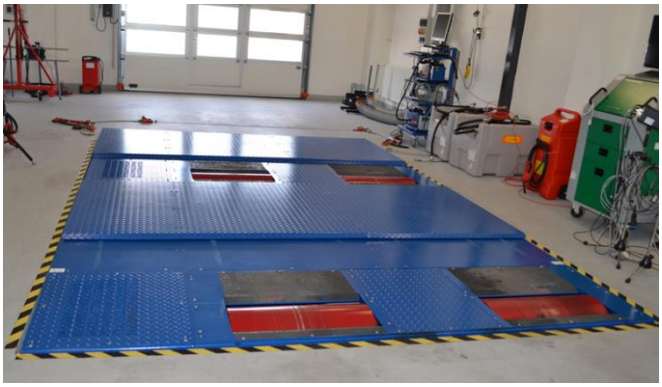

Fig. 3 Dynamometer MAHA MSR 500

Calculation of the correction factor Ka

When determining the correction factor Ka, the absolute temperature (T) of the induced air into the engine and dry atmospheric pressure (p) are measured. The parameter Ka is determined according to the relationships below.

EWG 80/1269

$$Ka = \frac{(\ 990\ )^{1,2}}{p[mbar]} . (\frac{T\ [K]}{298})^{0,6} \quad (1)$$

Where:

Ka is correction factor,

P is atmospheric pressure in test room expressed in mbar (1mbar = 0,001bar, 1bar = 0,1MPa),

T is temperature of air in test room expressed in Kelvins (0°C = 273K).

RESULTS AND DISCUSSION

Mentioned vehicle has, by regulations, specified levels of emissions that are indicated by the manufacturer. The range of allowed values specified by the manufacturer are listed in Tab. 3. Measured emission values of CO, HC, O_2 and CO_2 are listed in Tab. 4, and also the value of excess-air coefficient λ without and with testing substance was established.

Graphical waveforms of the measured emission values and the coefficient of excess-air at the idle speed are shown in Fig. 4 to Fig. 8.

Tab. 3 The range of allowed values of emissions at the idle speed (data from the manufacturer)

Emission	Minimum value	Maximum value
HC	-	100 ppm
CO_2	14.5 vol.%	16 vol.%
O_2	0.1 vol.%	0.5 vol.%
CO	-	0.3 vol.%
Lambda	0.97	1.03

Tab. 4 Measured average values of emissions at the idle seed

Idle speed		CO	HC	Lambda	O_2	CO_2
Without testing substance		0.10	37	0.997	0.3	15.85
With testing substance	1. measurement	0.08	54	0.996	0.2	15.43
	2. measurement	0.12	52	0.994	0.16	15.50
	3. measurement	0.09	43	0.996	0.16	15.52
	4. measurement	0.12	27	0.995	0.18	15.72
	5. measurement	0.04	25	1.001	0.2	15.47

At the idle speed, the CO value varied from 20% to 60% (Fig. 4). At the first measurement, it decreased by 20% from the original state, subsequently, in the second measurement, the measured value was 20% higher than before the addition of the testing substance. At the last measurement, the CO emission value stabilized at a value 60% lower than before the addition of the testing substance. The CO emissions did not overpassed the permissible value specified by the combustion engine manufacturer.

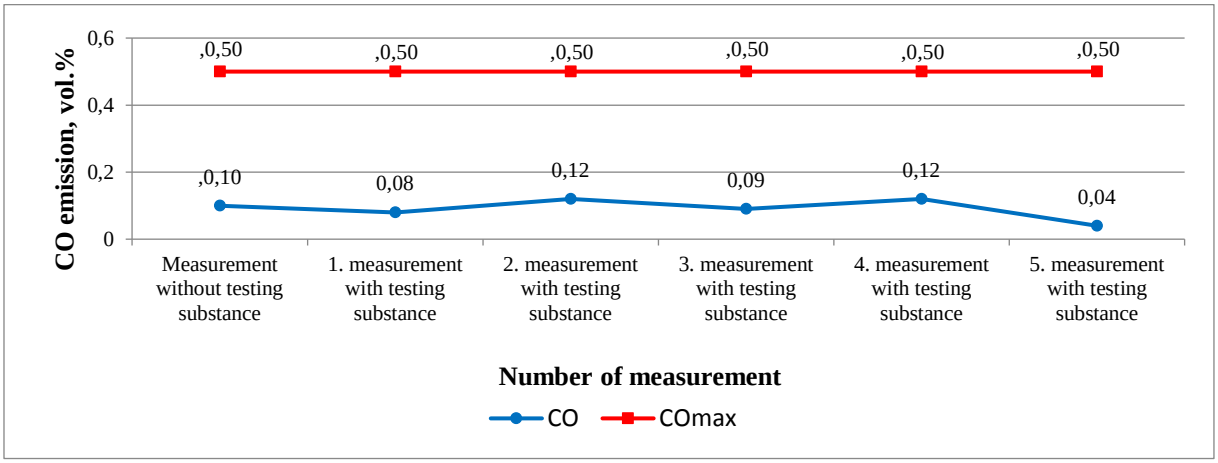

Fig. 4 Measured CO values at the idle speed

HC emission values (Fig. 5) increased by 45.95% after adding the testing substance at the first measurement. Subsequently, they began to decline and in the third measurement they were increased by only 16.22% as before adding the testing substance. In the fifth measurement, the value of hydrocarbons was 32.43% lower than the original condition. HC emissions values did not exceed the permissible value specified by the combustion engine manufacturer.

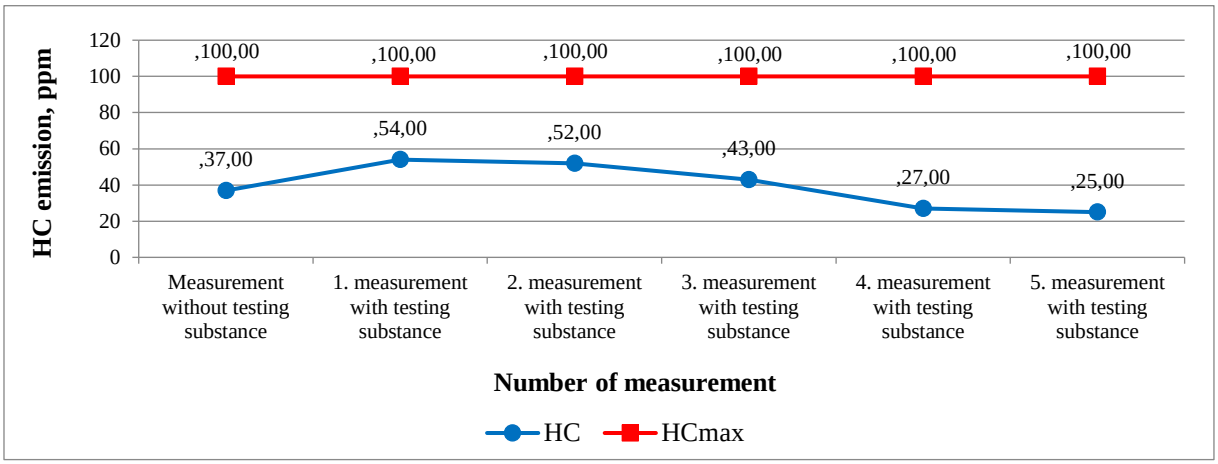

Fig. 5 Measured HC values at the idle speed

For the next monitored component O_2 (Fig. 6), values at the first measurement showed a decrease of 33.33%, in the second to third measurements, there was a decrease of 46.67% from the original condition. In the fourth measurement, the value was 40% lower and in the fifth measurement, the value was 33.33% lower before adding the testing substance. O_2 emissions values did not exceed the permissible value specified by the combustion engine manufacturer.

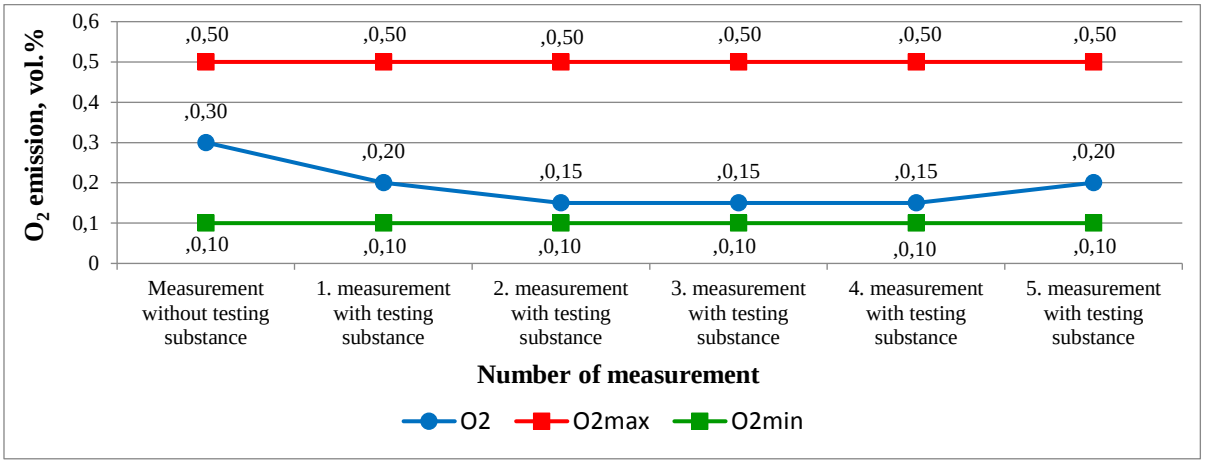

Fig. 6 Measured O_2 values at the idle speed

The last component, CO_2 emissions values (Fig. 7) decreased after adding the testing substance. In the third measurement, it was 2.08% lower than the original condition. . In the third measurement, it was 0.82% lower and in the last measurement, it was 2.40% lower before adding the testing substance. CO_2 emissions values did not exceed the permissible value specified by the combustion engine manufacturer.

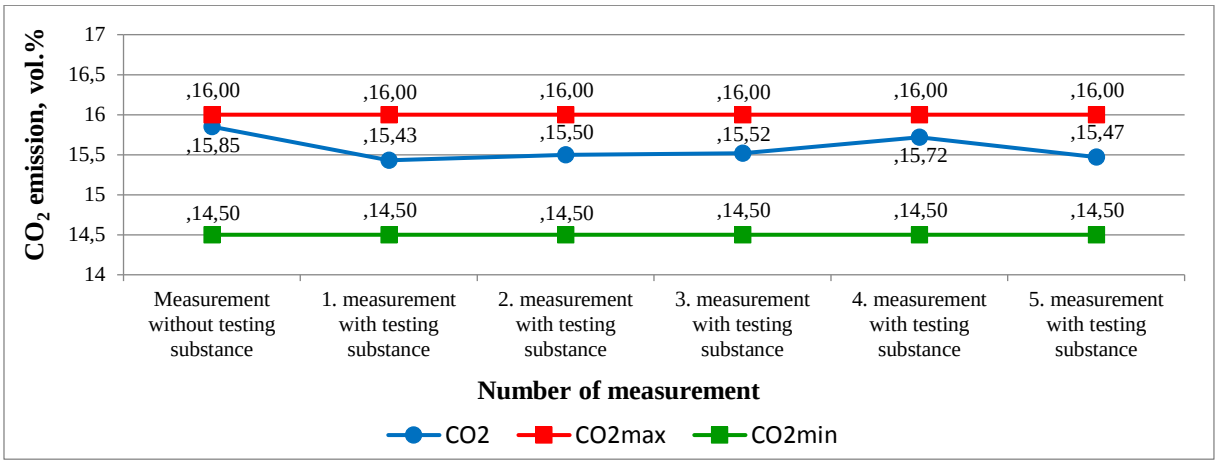

Fig. 7 Measured O_2 values at the idle speed

The values of the excess-air coefficient λ gradually decreased by 0.1% at the first measurement, by 0.3% at the second measurement and in the third measurement, it was 0.1% lower from the original condition. In the last measurement, the value of excess-air coefficient increased by 0.4% comparing the state before adding the testing substance. values of excess-air coefficient did not exceed the permissible value specified by the combustion engine manufacturer.

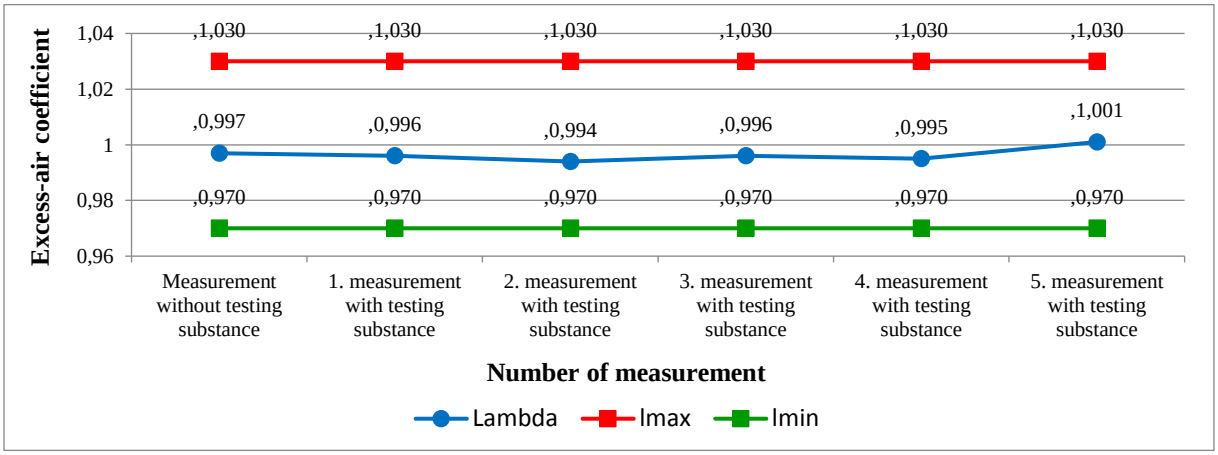

Fig. 8 Measured excess-air coefficient values at the idle speed

After adding the testing substance and driving 2500 km, a power measurement was performed. When measuring the power with the testing substance, the power reached the value of 77.7 kW at a speed of 6380 min^{-1}. The torque reached 128 Nm at 4390 min^{-1}. From the measured results after application of the test substance, it can be stated that the testing substance has no significant effect on the performance parameters of the combustion engine. A comparason of the course of the torque and the standard power without and with the added testing substance is shown in Fig. 9.

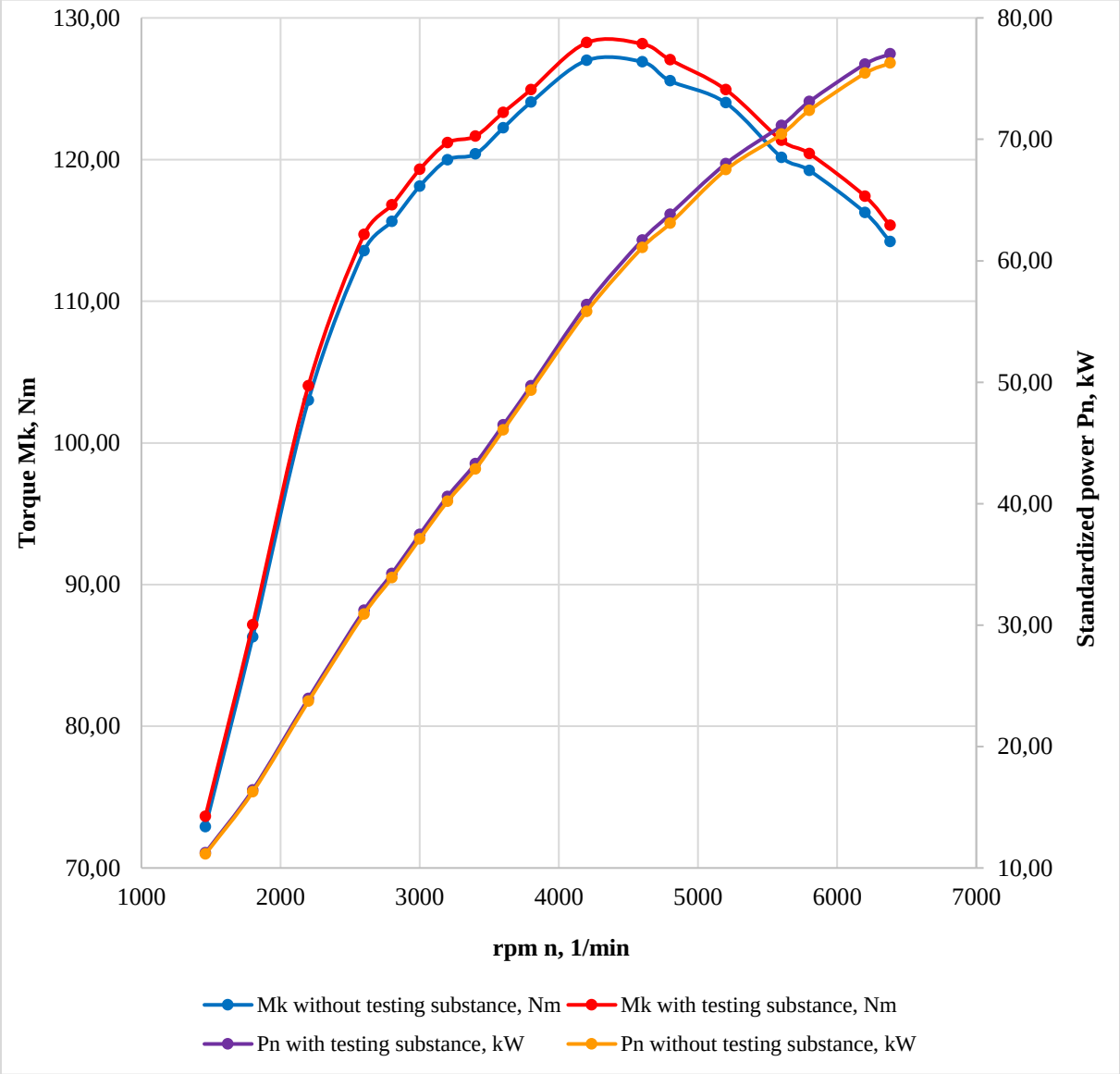

Fig. 9 External speed characteristic of the combustion engine

CONCLUSION

The exact methodological measurement procedure was determined in the work methodology, which we followed. A total of 6 measurements were performed. The first measurement was performed before adding the testing substance and another five measurements were performed after adding the testing substance. During the testing of the substance, it was driven 2500 km. Measurements were performed in the Laboratory of Bioenergy Resources. Measurements of performance parameters showed that the Škoda Fábia 1.4 MPi is in good technical condition, however, the results also show that the testing substance does not have a significant effect on engine performance. After application of the test substance, we can evaluate that the measured values of CO emissions at the idle speed were 60% lower, hydrocarbons decreased by 32.43%,

O_2 emissions decreased by 33.33% and carbon dioxide decreased by 2.4%. The value of the excess-air coefficient increased by 0.4% at the idle speed. The measured values did not exceed the permitted values specified by the legislation. In the simulated driving test, the specific fuel consumption was also assessed, which decreased by 0.23%. Testing on other vehicles would be needed for a more objective assessment of the MPG BOOST testing substance, which have driven more than 250000 km.

REFERENCES

1. JANOŠKO, I., MOJŽIŠ, M.: The impact of fuel additive (II) on combustion diesel engine parameters. (KOKA 2019), Brno, MENDELU, 2019, 240 pp
2. PUŠKÁR, M. JAHNÁTEK, A., KURIC, I., KADAROVA, J., KOPAS, M., ŠOLTÉSOVÁ, M.: Complex analysis focused on influence of biodiesel and its mixture on regulated and unregulated emissions of motor vehicles with the aim to protect air quality and environment. Air Quality, Atmosphere & Health, 2019, 12: 855–864
3. Methodical instruction no. 32/2018 for carrying out regular emission control of motor vehicles with petrol engine, with an unenriched emission system, with petrol engine with advanced emission system and with a diesel engine. Methodical instruction, Section of road transport and communication over land, Ministry of transport, construction and regional development, 2018, Bratislava: Ministry of transport, construction and regional development, 55 pp
4. MARKIEWICZ, M. AND MUŚLEWSKI, Ł.: Analysis of toxic combustion components of the diesel engine powered with a blend of diesel fuel and biodiesel. Trends in agricultural engineering, 2019, Praha, Česká zemědělská univerzita, 225-230 pp
5. MARKIEWICZ-PATALON, M., MUŚLEWSKI, Ł., KASZKOWIAK, J., KNOPIK, L.: Analysis of selected operating parameters of engine powered by a mixture of bio components and diesel oil. Journal of Kones Powertrain and Transport, 2018, 25: 240-244
6. MARKIEWICZ-PATALON, M., MUŚLEWSKI, Ł. KASZKOWIAK, J., SÓJKA M.: Analysis of efficiency of the vehicle transport facilities powered with diesel oil with additive of bicomponent. KONMOT, Kraków, 2018, 42-53 pp
7. JABLONICKÝ, J., POLERECKÝ, J., BERNÁT, R., KOLLÁROVÁ, K.: Assessment of alternative fuel samples applied in a test combustion engine. 1ed st. Lüdenscheid, RAM-Verlag, 2019, 163 pp

8. KOSIBA, J., HUJO, Ľ.: Research of degradation processes of ecological fluids in process tests. Slovak university of agriculture, Nitra, 2017, 98 pp
9. TOMIC, M., SAVIN, L., MICIC, R., SIMIKIC, M., FURMAN, T.: Possibility of using biodiesel from sunflower oil as an additive for the improvement of lubrication properties of low-sulfur diesel fuel. Elsevier, 2014, 65: 101-108 pp

This work was supported by project APVV SK-PL-18-0041 „The Development of Scientific Cooperation in the Study of the Effects of Biofuels in Road Transport, Including Environmental Impact."
This work was supported by AgroBioTech Research Centre built in accordance with the project "Building the AgroBioTech Research Centre" ITMS 26220220180.

Corresponding author:
Ing. Patrícia Feriancová, Department of Transport and Handling, Faculty of Engineering, Slovak University of Agriculture in Nitra, Tr. A. Hlinku 2, Nitra, 94976, Slovak Republic, tel: +421908430544, email: xferiancova@is.uniag.sk

Evaluation of electromobility energy consumption with the support of geoinformatics tools

T. Hajlich[1], J. Kumhálová[1], F. Kumhála[2]

[1]Department of Machinery Utilization, Faculty of Engineering, Czech University of Life Sciences Prague, Prague, Czech Republic

[2]Department of Agricultural Machinery, Faculty of Engineering, Czech University of Life Sciences Prague, Prague, Czech Republic

Abstract

Battery Electric Vehicles (BEVs) have great potential to reduce fossil fuel consumption in relation to transport, as well as pollutant and greenhouse gas (GHG) emissions, as they can use electricity from renewable sources as their only energy source. The widespread use of BEVs is therefore seen as a positive means of alleviating environmental problems (e.g. air pollution and climate change) resulting from transport activities. However, the faster spread of BEVs is hindered by the widespread myth of the range of current BEVs and the incoherent - sparse network of charging stations. For this reason, the paper deals with the comparison of the actual BEV energy consumption of three different routes between two identical points. The route from Horoměřice, Prague West (Czech Republic) to Uggl, Uttendorf (Austria) was compared using BEV TESLA S 100D in these tests. The results showed that with an 87% share of the motorway, the total distance travelled and energy consumption were the highest, the total time was the shortest and the time spent by charging was the longest.

Key words: Battery electric vehicles, energy conception, landscape relief, geoinformatics

INTRODUCTION

Information on theoretical calculations of BEV energy consumption under various conditions is available in the literature. For example, acceleration was studied by Yao et al. (2014), deceleration (possibility of recuperation - recharging) by Genikomsakis and Mitrentsis (2017), speed by Fiori, Ahn and Rakha (2016), road slope, climatic conditions by Kambly and Bradley (2015). Information on measuring actual BEV energy consumption in cities, including various climatic conditions, is also available in the literature, i.e. Yuan et al. (2017) or Zhang et al. (2020). However, there is little information available on the behaviour of BEVs at different

pathways between two targets. That is why the main aim of this article was to study energy consumption of BEV that travelled the route between two identical points by three different routes.

MATERIALS AND METHODS

BEV TESLA S 100D was used for the tests. Electricity consumption according to the NDEC methodology cycle is 189 $Wh.km^{-1}$, which results in a total range of 529 km with a battery capacity of 100 kWh. The tests covered a total of 12792 km. Experimental routes between the two points, Horoměřice, Prague West (Czech Republic) and Uggl, Uttendorf (Austria) were created based on the share of road classes.

1st route: Horoměřice, motorway D7, D0 (city ring road), D5 direction Rozvadov, A93 Munich, Rossenheim, Kufstein and then on 1st class roads via Kitzbuhel and Mittersill to Uggl. Total distance travelled 562 km, of which on motorways 490 km, on 1st and 2nd class roads 82 km.

2nd route: Horomerice, motorway D7, D0 (city ring road), D5 direction Pilsen, road no. 26 direction Folmava, Germany B20, A94 Muhldorf, Austria A8, St. Johann in Tirol and Kitzbuhel to Uggl. Total distance travelled 477 km, of which on motorways 110 km, on 1st and 2nd class roads 367 km.

3rd route: Horoměřice, motorway D7, D0 (city ring road), D4 direction Písek, E49 České Budějovice, E55 Dolní Dvořiště, Austria A7 Linz, A1 Salzburg and No. 311 Zell am See to Uggl. Total distance travelled 511 km, of which on motorways 286 km, on 1st and 2nd class roads 225 km.

The following data were collected at the beginning, during and at the end of the tests: Date, Route type, Vehicle type, Number of passengers, Load in kg (including persons), Starting point, Target point, Initial state of the battery [kWh], Transit points, Data recording time [h], Mileage [km], Outdoor temperature [°C], Internal temperature [°C], Sunny, Cloudy, Rain, Snowfall, Icing, Steering wheel heater, Seat heating, Heated front window, Heated rear window, Washer heating, Air conditioning, Communication class, Energy consumption [$Wh.km^{-1}$]. Recording climatic conditions in and out of the vehicle was important for objective evaluation by comparing route types under approximately climatically identical conditions.

RESULTS AND DISCUSSION

Results were calculated from the recorded data. Obtained results are presented in Table 1. The results for each of the routes were always calculated as the averages of two measurements.

Tab. 1. Results calculated from three experimental routes.

Variables of the routes	**1st route**	**2nd route**	**3rd route**
Total distance [km]	562	477	511
Motorways [km]	490	110	286
1st and 2nd class roads [km]	82	367	225
Share of motorways [%]	87	23	56
Total travel time [hours]	7.2	7.7	7.7
Driving time [hours]	5.5	6.6	6.3
Average speed [km.h^{-1}]	102.2	72.6	81.1
Max. speed	177.4	149.7	147.3
Total consumption [kWh]	145	106.5	102.5
Average consumption [Wh.km^{-1}]	257.8	223.3	200.5
Number of recharges [-]	3	2	2
Total charging time [h]	1.7	1.1	1.4
Energy at start of the journey [kWh]	55	97.5	54.5
Energy at end of the journey [kWh]	33.6	66	68.5
Altitude gained [m a.s.l.]	3557	3886	3246
Altitude lost [m a.s.l.]	3926	3404	3731

From the results shown in Table 1, it is clear that on the 1st route with an 87% share of the motorway, the total observed travelled distance and energy consumption was the highest, the total time necessary for reaching end point of the route was the shortest and the time spent by charging BEV batteries was the longest. In the contrary, with a 23% share of the motorway (2nd route), the total distance travelled was the shortest and the time spent recharging is also the shortest. However, the total travel time, including recharging the BEV batteries, was longer. Interesting results were found on the 3rd route with a share of motorways of 56%. It was the most energy efficient route. In comparison with the 1st route, total travel time was about 7% longer, but average energy consumption to 1 km was about 22% lower. Total travel time was the same as in the case of 2nd route, nevertheless, average energy consumption to 1 km of the route was 10% lower, although the average speed of the 3rd route was higher than the 2nd route. As a possible explanation for this finding, it can be deduced from other measured data that this was due primarily to the different relief of the two routes. In the case of 2nd route, altitude gained in meters above sea level was 3886 but in the case of 3rd route it was 3246 m a.s.l. only and in

contrary, in the case of 2nd route altitude lost was 3404 m a.s.l. only in comparison with 3731 m a.s.l. of 3rd route. From this consideration, based on the measured data, it can be deduced that the relief of the route itself can have a significant effect on the energy consumption of BEV and this should be taken into account when planning the energy-optimal route. Geoinformatics tools can help significantly in planning such a route.

CONCLUSION

From three different experimental routes between the same two points passed by BEV under similar weather conditions it was found that in addition to the share of motorways and cruising speed, the relief of the route can also have a significant effect on the optimization of BEV energy consumption. This finding is important for planning the optimal route. This can increase market acceptance of BEVs and reduce greenhouse gas emissions from route transport. Geoinformatics can help significantly in this process.

REFERENCES

1. FIORI, C., AHN, K. A RAKHA, H. A. (2016) „Power-based electric vehicle energy consumption model: Model development and validation", *Applied Energy*, 168. doi: 10.1016/j.apenergy.2016.01.097.
2. GENIKOMSAKIS, K. N. A MITRENTSIS, G. (2017) „A computationally efficient simulation model for estimating energy consumption of electric vehicles in the context of route planning applications", *Transportation Research Part D: Transport and Environment*. doi: 10.1016/j.trd.2016.10.014.
3. KAMBLY, K. A BRADLEY, T. H. (2015) „Geographical and temporal differences in electric vehicle range due to cabin conditioning energy consumption", *Journal of Power Sources*. Elsevier B.V., 275, s. 468–475. doi: 10.1016/j.jpowsour.2014.10.142.
4. YAO, E. *et al.* (2014) „Estimating energy consumption on the basis of microscopic driving parameters for electric vehicles", *Transportation Research Record*. doi: 10.3141/2454-11.
5. YUAN, X. *et al.* (2017) „Method for evaluating the real-world driving energy consumptions of electric vehicles", *Energy*. doi: 10.1016/j.energy.2017.11.134.
6. ZHANG, J. *et al.* (2020) „Energy consumption analysis and prediction of electric vehicles based on real-world driving data", *Applied Energy*. Elsevier Ltd, 275. doi:

10.1016/j.apenergy.2020.115408.

Corresponding Author:

Ing. Tomáš Hajlich, Department of Machinery Utilization, Faculty of Engineering, Czech University of Life Sciences Prague, Kamýcká 129, Praha 6, Prague, 16521, Czech Republic, tel: +420602368800, email: tomas.hajlich@seznam.cz

Felling knife thickness analysis in the process of chipless wood cutting

P. Harvánek[1], J. Kováč[1]

[1]Department of Environmental and Forestry Machinery, Faculty of Technology, Technical University in Zvolen, Zvolen, Slovakia.

Abstract

This article is focused on the research of the influence of different thickness of cutting knives in the area of chipless cutting of woody plants. Chipless wood cutting is defined as the penetration of a cutting tool into the wood in a direction perpendicular to the growth of fibers. The task of the article is to follow the course of the magnitude of the cutting force required for the division of samples from different woody plants in a direction perpendicular to the growth of tree fibers. The measurement was performed on wood samples from spruce (Picea abies), beech (Fagus sylvatica) and willow (Salix caprea). For the measurement, flat single-acting cutting knives of the same material were used, with the same cutting edge but with different knife thicknesses (6 mm, 8 mm and 10 mm). The measurement was performed on a hydraulic stand to maintain the cutting kinematics. The results from the measured data were processed by the statistical software STATISTICA 12. From the results of measurements it was found that in the process of chipless felling of woods, is the most advantageous use a knife with 10 mm thickness

Key words: chipless cutting, chipless cutting head, cuting knives, knife thickness analysis.

INTRODUCTION

There is a very rapid development of science and especially technology in the world, which is also related to the development of production, which results in an increasingly intensive extraction of natural resources. To ensure rational forest management, it is necessary to use more and more modern techniques of wood felling, which would bring with them less waste generation when cutting trees are. One of the possible solutions is the use of chipless wood cutting in the actual harvesting of fast-growing wood (Kováč et al., 2017). Chipless wood cutting in the forestry process is mainly used in machines intended for machine delimbing of trees. Increasingly, chipless wood cutting is used in the form of chipless cutting heads in single-operating machines. The author discussed the construction, advantages of use and modeling of cutting processes using cutting heads (Hatton et al., 2015, Hatton et al., 2017).In comparison

with the current state of equipment and machines used in forest management, there is an increasing emphasis on the use of light machines and adapters for base machines, which can reduce the pressure on the soil (Suchomel et al., 2012, Cavalli et al., 2014). The importance and justification of the solution of the given issue clearly follows from the above. The transverse division of wood with a knife is based on the ability of the wood to deform. The wood shows a relatively low resistance to deformation when the wedge is pushed into it. When the cutting tool is pressed into the wood, the cutting edge breaks the bonds between the fibers, while no waste chips are formed and the cutting joint is equal to zero (Marko and Holík, 2000). An illustration of the basic scheme of chipless cutting with a single-acting flat knife is shown in (Fig. 1).

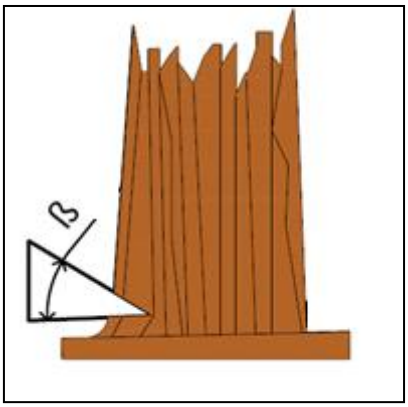

Fig. 1 Scheme of chipless wood cutting (Krilek et al., 2018)
β- angle of the cutting wedge

The principle of the chipless cutting head is based on pushing the cutting wedge (cutting tool) into the trunk in a direction perpendicular to the growth of the tree fibers. Very often, this principle is used when splitting wood is, but with the difference in splitting wood kinematic. In wood splitting is cutting wedge pushed into the trunk in a direction parallel to the growth of the tree fibers. With the chipless cutting method, no waste chips are formed.

MATERIALS AND METHODS

The whole course of laboratory measurements was carried out on the hydraulic stand of the KELT department in the TUZVO workshop. All measuring devices were used from the available stocks of the Faculty of Technology of the Technical University in Zvolen (Barcík et al., 2016). Cutting knives with different thicknesses were gradually attached to the stand. As

far as laboratory conditions are concerned, the size of the cutting knives was smaller in comparison with the cutting knives used for chipless cutting heads.

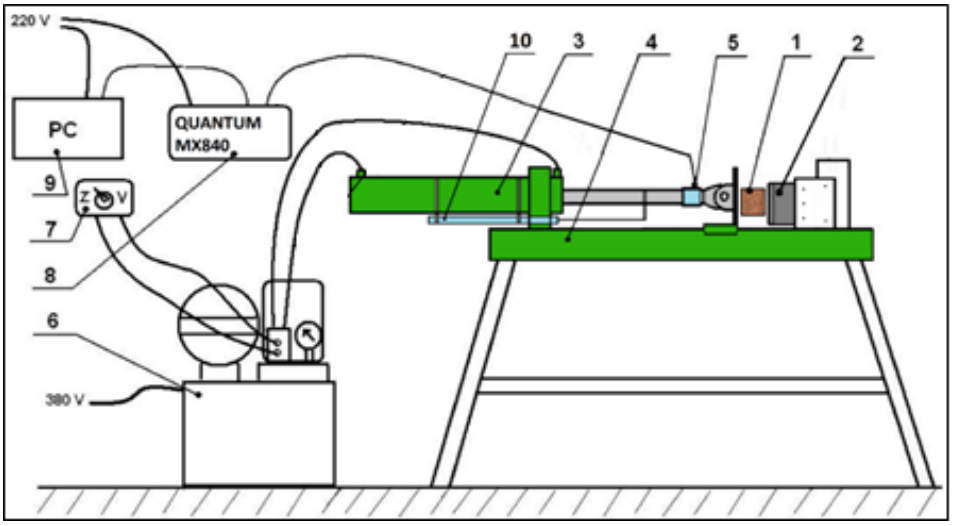

Fig. 2 Schematic of measuring device
1-sample material, 2-cutting knife, 3-line hydraulic motor, 4-beam, 5-strain force sensor, 6-hydrogenerator, 7-stroke control of the hydraulic cylinder piston, 8-measuring control panel, 9-PC evaluation device, 10- path sensor.

The process of chipless cutting of woods in the direction perpendicular to the growth of fibers will provide a rectilinear hydraulic motor (3), which is placed on the beam (4) and will be driven by the pressure of the liquid from the hydrogenerator (6). The direction of movement of the piston rod of the linear hydraulic motor is secured from the control panel (7). To ensure the correct cutting kinematics, the rectilinear hydraulic motor will push the wood (1) into the cutting knife (2). The entire chipless cutting process will be recorded using the QUANTUM MX840 (8). During the chipless cutting process, the force will be monitored depending on the path of the piston rod. The force will be recorded indirectly due to the deformations of the piston rod of the rectilinear hydraulic motor by means of a strain gauge force sensor (5). Thanks to the path sensor (10), it will be possible to monitor the course of the measured force depending on the depth of penetration of the cutting knife into the wood. The whole experimental measurement will be evaluated in PC (9).

When wood samples are cutting with a flat single-acting knife, the cutting force can be defined from the following formulas:

$$F_c = F_N + F_D + F_{CH} + F_{Č} = 30.032 + 17.73 + 0.075 + 2.18 = 20[kN] \quad (1)$$

where:

F_N - force of cutting the fibers by the cutting edge of the knife [kN],

F_D - deformation force of wood at the front of the knife) [kN],

F_{CH}– force to overcome the resistance on the back of the knife [kN],

$F_Č$ - force to overcome the resistance on the knife face [kN].

Calculation of the force at the outlet of the hydraulic cylinder:

$$F = P.S = 16\,000\,000 \cdot 0.005 = 80 \text{ [kN]} \quad (2)$$

where :

F- force [N],

p - working pressure of the hydraulic cylinder [MPa]

S - drilling area of the hydraulic cylinder [m^2].

Chipless cutting knife.

The most important part of a chipless cutting head is the cutting knife. The advantage of such cutting heads is mainly the simple construction of the cutting mechanism in contrast to harvester heads, where the cutting mechanism represents a set of hydraulic motors together with a cutting chain. Older types of cutting harvester heads used the principle of the circular for cutting and thus the rotation of the toothed saw blade around its axis (Kováč et al., 2014). In the experimental measurement, 6mm, 8mm and 10mm thick cutting knives were used, but the shape of the cutting edge and the material of the knife were always the same. However, as found in previous studies, the use of a cutting knife with a cutting edge angle of 30 ° is most preferred (Marko, 1996, Johansson, 1996) and therefore all cutting knives used will have this cutting edge angle.

Tab. 1 Technical parameters of chipless cutting knives

Nr.	Knife thickness s (mm)	Cutting wedge angle β (°)	Cutting edge shape
1	6	30	Straight line
2	8	30	Straight line
3	10	30	Straight line

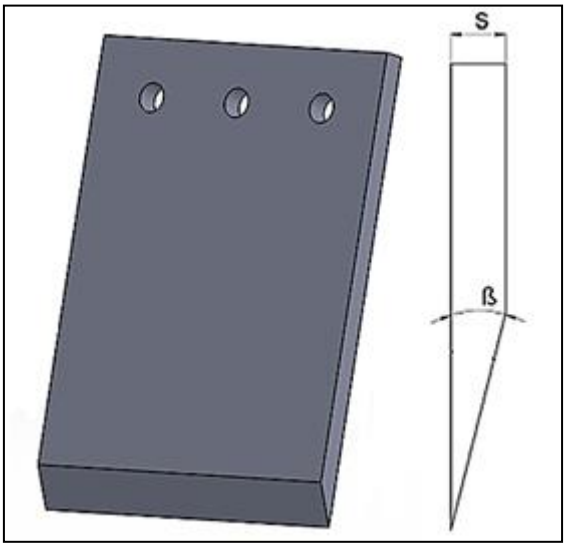

Fig. 3 Model and geometry of a single-acting flat cutting knife
s- knife thickness, β- cutting wedge angle

Steel 19 191 (STN 41 9191) or DIN C105W1 (SLAVIA STEEL s.r.o, 979 01 Rimavská Sobota Slovakia) was used for cutting knives. Steel 19 191 is suitable for smaller-shaped cutting tools for wood, rubber, and plastics. The mechanical properties of steel are described in Table 1 (Leinveber and Vavra 2011). Steel 19 191 is suitable for use in mowing machines but also for use in the cutting process due to high hardness and wear resistance (Ťavodová and Kalincová 2018).

Tab. 2 Mechanical properties of DIN C105W1 steel.

Quantity	Value	Unit
Young's modulus	200000 - 200000	MPa
Tensile strength	650 - 880	MPa
Elongation	8 - 25	%
Fatigue	275 - 275	MPa
Yield strength	350 - 550	MPa

The measurement was performed on wood samples from spruce (Picea abies), beech (Fagus sylvatica) and willow (Salix caprea) .

RESULTS AND DISCUSSION

The criteria used for the analysis was the maximum force required to cut the wood sample in a direction perpendicular to the growth of the tree fibers. For each tree sample, a graph of 95% confidence interval for mean values of cutting force depending on knife thickness was produced separately where it was possible to separately observe the amount of cutting force for each cutting knife thickness. A similar measurement theory was used by Kováč et al. (2014), Kováč (2002), Kuvik et al. (2018), Kuvik et al (2017) and Krilek et al. (2015).

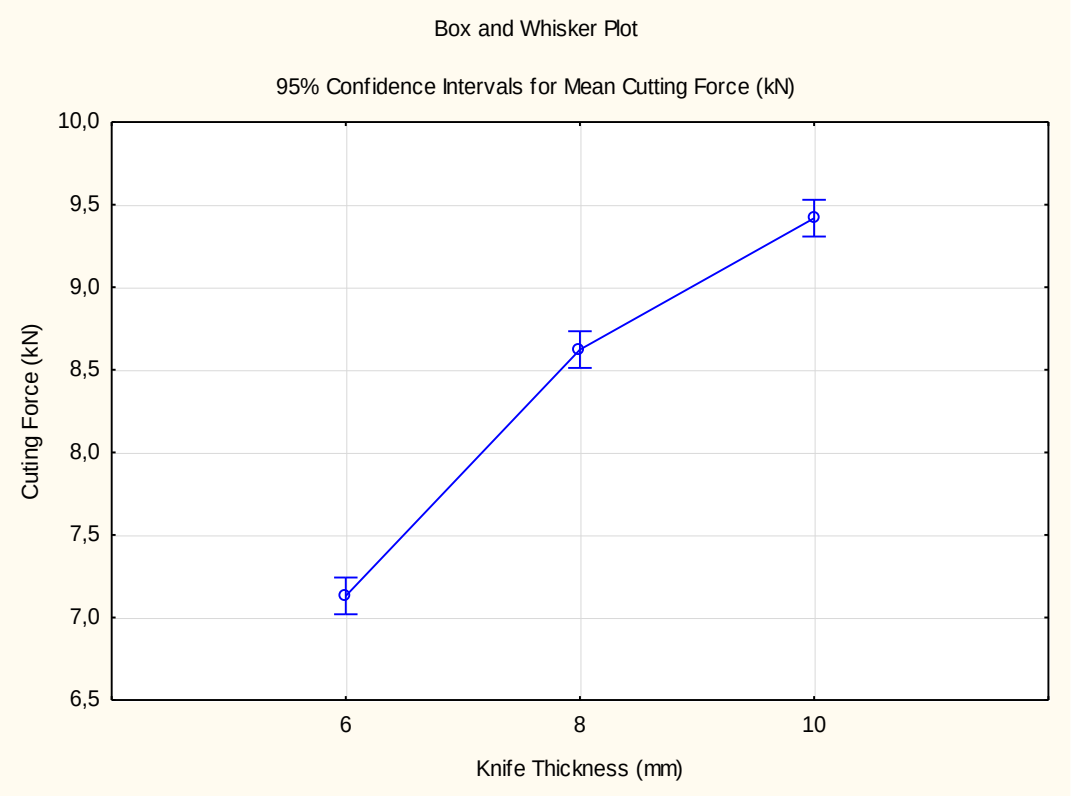

Fig. 4 Graph of 95% confidence intervals for mean values of cutting force depending on knife thickness

In Fig. 4 it is possible to see an increasing cutting force due to a change in the thickness of the cutting knives. The greatest force was recorded with a 10mm thick cutting knife. A more detailed view of the issue is shown in Fig. 5.

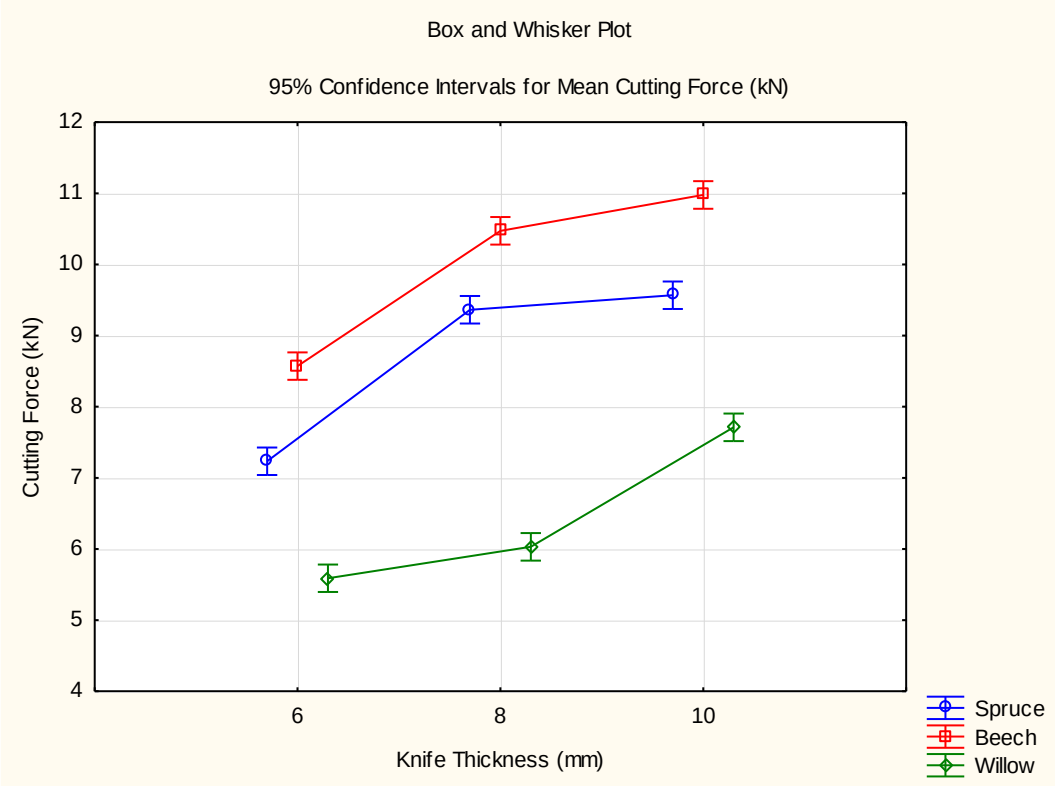

Fig. 5 Graph of 95% confidence intervals for mean values of cutting force depending on knife thickness for spruce, beech and willow wood.

Fig. 5 shows the dependence of the knife thickness and the type of wood on the size of the cutting force. It can be clearly stated from the graph that the greatest cutting force was achieved with a 10 mm thick cutting knife for all wood types. On the contrary, the lowest cutting force was always achieved with a 6mm thick cutting knife. Despite the fact that the cutting force was at least with the 6 mm thick knife, the use for cutting in the process of chipless felling is inappropriate from the point of view of the material strength of the knife. As the difference in the size of the cutting force between the thickness of the knives of 8 mm and 10 mm for spruce and beech woods was minimal and statistically insignificant, it is advantageous from the point of view of material safety to use knives of thickness 10 mm.

CONCLUSION

Recently, when great emphasis is placed on the protection of the environment, the method of wood chipless cutting comes to the forefront. The purpose of this article was to determine the effect of the thickness of the cutting knife on the amount of cutting force required to cut the sample in a direction perpendicular to the fiber growth. Different wood samples with the different size were used for the experiment. From this analysis and experimental measurement,

it has been shown that varying thickness of the cutting knife has a statistically significant effect on the size of the cutting force. The size of this cutting force is always different with the above-mentioned tree species. From the results of experimental measurement, it can be argued that for chipless wood cutting of spruce, beech or willow It is best to use a 10 mm knife.

REFERENCES

1. CAVALLI, R., GRIGOLATO, S., SGARBOSSA, A., 2014: JOURNAL OF AGRICULTURAL ENGINEERING. Productivity and quality performance of an innovative firewood processor. S. 32-36. 2014.
2. KOVÁČ,J., KRILEK, J.,JOBBÁGY, J., DVOŘÁK, J., 2017: Technika a mechanizácia v lesníctve, Technická univerzita vo Zvolene, 2017. ISBN 978-80-228-3021-8
3. KRILEK, J., KOVÁČ. J., DVOŘÁK, J., MIKLEŠ, J.,2018 : Výskum rezných mechanizmov v lesníctve. Zvolen : Vedecká monografia. Technická univerzita vo Zvolene.ISBN 978-80-228-3056-0
4. LEINVEBER, J. VAVRA, P. 2011. Strojnícke tabuľky. Praha: Vydavateľstvo ALBRA. 2011. 927s. ISBN 978-80-736-1081-4.
5. MARKO, J. 1996: Problematika hodnotenia rezných mechanizmov pre výchovné zásahy. 1. vyd. Zvolen: Technická Univerzita vo Zvolene, 1996. 49s. ISBN 80-228-0586-8.
6. MARKO, J., HOLIK, J. 2000: Teoria delenia dreva. 1. vyd. Zvolen: Technická Univerzita vo Zvolene, 2000. 66s. ISBN 80-228-0891-1.
7. SUCHOMEL, C., SPINELLI, R., MAGAGNOTTI, N., 2012: CROATIAN JOURNAL OF FOREST ENGINEERING. Productivity of processing hardwood from coppice forests. S. 39-47. ISSN: 1845-5719. 2012.
8. ŤAVODOVÁ, Miroslava - KALINCOVÁ, Daniela Possibility of lifetime increasing of functional places of cutting knives In Kolokvium ku grantovej úlohe č. 1/0826/15 Technická univerzita vo Zvolene, 2018. - ISBN 978-80-228-3128-4. - S. 122-128 [CD-ROM].
9. HATTON, B., BOUZGARROU, J., FAUROUX, V., GAGNOL, V., GOGU, G., 2017: Springer International Publishing AG. An approach for modelling harvester head mechanism in the harvesting process of hardwood stands. S. 133-141. 2017.
10. HATTON, B., POT, G., BOUZGARROU, B., GAGNOL, V., GOGU, G., 2015: Croatian journal of forest engineering. Experimental determination of delimbing forces and deformations in hardwood harvesting. s.43-53. ISSN: 1845-5719. 2015.
11. BARCÍK, Š.,NEUPAUEROVÁ, A.,KOLEDA, P.,SUJOVÁ, E.,MINÁRIK, M.,2016: Katalóg zariadení. Technická univerzita vo Zvolene. ISBN 978-80-228-2869-7
12. KOVÁČ, J., KRILEK, J., KUČERA, M., AND BARCÍK, S. 2014. "The impact of design parameters of a horizontal wood splitter on splitting force," Drvna Industrija 65(4), 263-271. DOI: 10.5552/drind.2014.1335

13. JOHANSSON, J., 1996: Forestry, Case studies on farm tractors as base machines for single-grip thinnings harvester heads. S. 229-244. ISSN: 0015-752X. 1996.
14. KOVÁČ, J. 2002. Aplikácia Beztrieskového Delenia v Procese Odvetvovania Stromov [Application of Chipless Wood Cutting in Tree Delimbing], Technical University in Zvolen, Zvolen, Slovakia, pp. 52-64.
15. KOVÁČ, J., KRILEK, J., KUČERA, M., AND BARCÍK, S. 2014. The impact of design parameters of a horizontal wood splitter on splitting force, Drvna Industrija 65(4), 263-271.
16. KRILEK. J., KOVÁČ. J., BARCÍK. Š., SVOREŇ. J., ŠTEFÁNEK. M., KUVIK. T. 2015: The influence of chosen factors of a circular saw blade on the noise level in the process of cross cutting wood. Wood research 61 (3): 2016. 475-486.
17. KUVIK, T., KRILEK, J., AND KOVÁČ, J. 2018. Výskum Rezných Mechanizmov Pri Priečnom Rezaní Dreva [Research of Cutting Mechanisms in Cross-Cutting of Wood], Technical University in Zvolen, Zvolen, Slovakia.
18. KUVIK. T., KRILEK. J., KOVÁČ. J., ŠTEFÁNEK. M., DVOŘÁK. J. 2017: impact of the selected factors on the cutting force when using a chainsaw. Wood research 62 (5): 2017. 807-814.

Corresponding author:

Ing. Pavol Harvánek, Department of Environmental and Forestry Machinery, Faculty of Technology, Technical University in Zvolen, Študentská 26, Zvolen, 960 01, Slovakia, tel: +421918325541, email: pavol.harvanek@gmail.com

Heat load in dairy cows housing

A. Hauliková[1], J. Lendelová[1], Š. Mihina[1]

[1]Department of Building Equipment and Technology Safety,
Faculty of Engineering, Slovak University of Agriculture in Nitra, Trieda Andreja Hlinku 2,
949 76 Nitra, Slovak Republic

Abstract

High temperature during the summer makes heat load on cattle which could cause heat stress with a negative impact on the health and production mainly of dairy cows. This can be detected by observing microclimatic parameters like temperature and humidity. The thermal humidity index (THI) is most often used to detect heat load in cows, but this index does not consider the climatic factor as the speed of air flow. Heat Load Index (HLI) considering not only temperature and relative humidity but also the air flow rate. In our experiment, we have measured air temperature and relative humidity in the barn to calculate the THI index in animal buildings and the air flow rate, to calculate the HLI index. We compared these results with the recommended values. We found that the THI (ranged from 82 to 85) and LHI (ranged from 81 to 87) values were out of the limit, although the air exchange was intensified by installing fans with a capacity of 15 000 $m^3.h^{-1}$. We have concluded that there is a need to increase the efficiency of ventilation and change the direction of the air to flow to the animal zone.

Key words: cattle, heat load, temperature – humidity index, cooling.

INTRODUCTION

In the last decades, climate change has become a serious issue. Global temperature rises from year to year. Compared to 2010, the worldwide average temperature can rise by 1.1 – 6.4 °C in 2100 (SHEIKH et al., 2017). Global warming has a negative impact on livestock production because hot weather causes heat load on dairy cows followed by heat stress. Many scientific studies have shown that heat stress has a significant effect on dairy cow's health and production (BERMAN, 2005, BROUČEK et al., 2007, ZIMBELMAN et al., 2009). Heat stress in dairy cows adversely affects reduced milk production, reduced animal reproduction, reduced growth of young animals, changes in animal behaviour, worsening of animal health and welfare (POGRAN et al., 2011). In southern regions, animals are frequently exposed to high temperatures for more than 5 months a year (DOLEŽAL et al., 2010). STRAPÁK et al. (2013),

claimed that the microclimatic parameters in barns are determined mostly by the farmer. Shielding, ventilation and soaking are some of the basic cooling systems which can reduce the effects of heat stress (POGRAN, et al., 2011). The level of thermal load in dairy farms can be estimated by monitoring of some weather conditions like temperature, humidity, air flow rate, and sunlight (BRANDL, 2018). During the summer heat days, the dairy cows suffer and therefore it is necessary to estimate when period of heat load begins (BERMAN, 2005). Temperature and relative humidity are the significant climatological factors in assessing the welfare of cows in summer. To detect heat stress in cattle, farmers most often use the THI table, which demonstrates the level of heat load (ARMSTRONG, 1994). Thermal - humidity index (THI) combines relative humidity and temperature into one value. In the case of dairy cows, it is usually considered stressful when the THI exceeds 72. If the THI value is above this level, it can be expected that this will be unpleasant for cows (BROUK et al., 2003). The table below is used as a guideline for cattle breeders, where: THI <71 is value considered as a thermal comfort zone, 72 <THI <79 as mild heat stress, 80 <THI < 90 as moderate heat stress and THI> 90 as severe heat stress (ARMSTRONG, 1994). Thermal - humidity index is shown in Fig. 1. THI shows the relationship of temperature and humidity. But does not consider airflow velocity and solar radiation. Dairy cows are usually kept in open buildings and therefore sunlight and air velocity have a great influence on the microclimate in barns (BRANDL, 2018). Heat Load Index (HLI) considering not only temperature and relative humidity but also the air flow rate. According to the determined HLI value, the indoor environment can be divided into four categories: thermoneutral zone HLI < 70, heat zone HLI = 70.1 – 77, area of hot environment HLI = 77.1 – 86, area of very hot environment HLI > 86 (POGRAN et al., 2011). When evaluating the microclimate, it is necessary to consider that the temperature in barns can differ significantly from the outside temperature. SCHÜLLER (2013) compared to climatic conditions of seven dairy farms with the climate recorded at the nearest official weather station. The ambient temperature, relative humidity, and THI were compared in each barn. The results showed that the measured temperature values in barns were different to those obtained from the nearest weather stations. The conclusion of the study indicated that in assessing heat stress in dairy cows, microclimatic air parameters should be observed directly in the barn. This article is an example of work in one barn, which specifies the methodological procedures and methods on which we will proceed in our research. In the PhD study, we would like to continue in this issue.

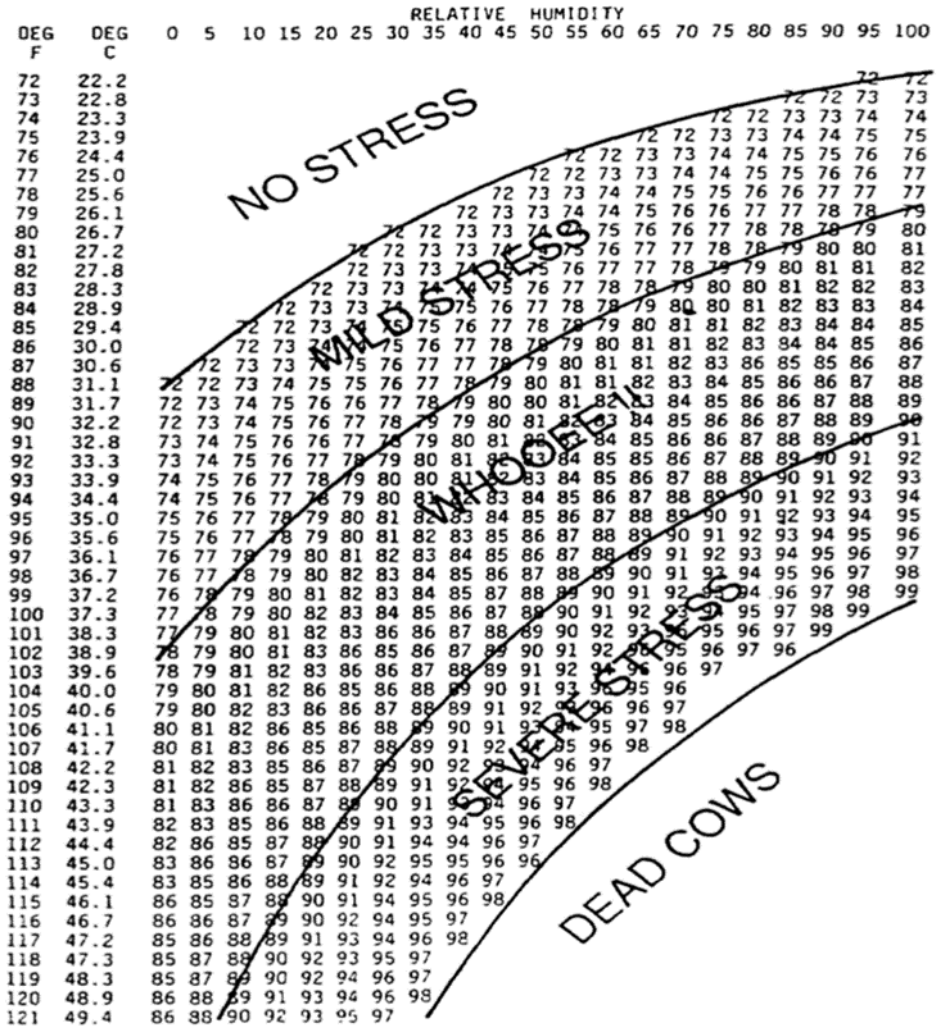

Fig. 1 The temperature and humidity index (Armstrong, 1994)

MATERIALS AND METHODS

The aim of the research was to measure microclimatic parameters, such as air temperature, relative humidity, and air flow rate, in barn for dairy cows during the summer. Based on the measured data, we evaluated the behaviour of the indoor microclimate for barn through the THI and LHI quality assessment indices. The measurement took place at the end of June 2019 on an experimental farm. There are three identical barns on the farm, of which the one closest to the milking parlour is called barn 1. We tested the effect of a new building layout and technological equipment. The barn 1 is with natural ventilation, partially supported by forced ventilation.

The barn 1 underwent a partial reconstruction in 2019. The roof was rebuilt, where continuous ridge slot with deflectors was installed. The walls in barn 1 also underwent a partial reconstruction, where the solid walls along with a little non-opening windows were replaced by 3 gate openings measuring 2 m x 2 m and 32 window free openings measuring 0.9 m x 0.9 m

on both sides of the barn. In the barn 16 basket fans: model VS36DFA, diameter 91 cm, electrical input 0.375 kW transported air volume 15 000 m^3/h, single-phase motor 230 V have been installed there. For measurement purpose we divided the barn space into two section, A and B (Fig. 2). Twelve measurement positions were set in each section (Fig. 3). The number of measuring points were chosen based on the layout of the barn. We performed the measurement with the ALMEMO 2590-4S device. We measured on an outpatient basis at 2-minute intervals. The ALMEMO 2590-4S measures air temperature, relative humidity, and air velocity. Accessories used: FHAD 46 - 2 probe humidity measurement with a range of 0 - 100% of the anemometric probe FVAD 35 TH4 with a range from 0.05 m/s^{-1} to 2.00 m/s^{-1}. We measured in the animal's life zone, at a height of 0.5 m in resting area and 1.2 m above the floor in moving and feeding area. The height of 0.5 m is the level of the animal's head when cow lying down, and the height is 12 m the level of the head when the animal is standing. From the measured data, we calculated the quality index of the evaluation of the indoor environment THI and HLI and then created a graphical representation of the behaviour of the indoor microclimate at individual locations in barn.

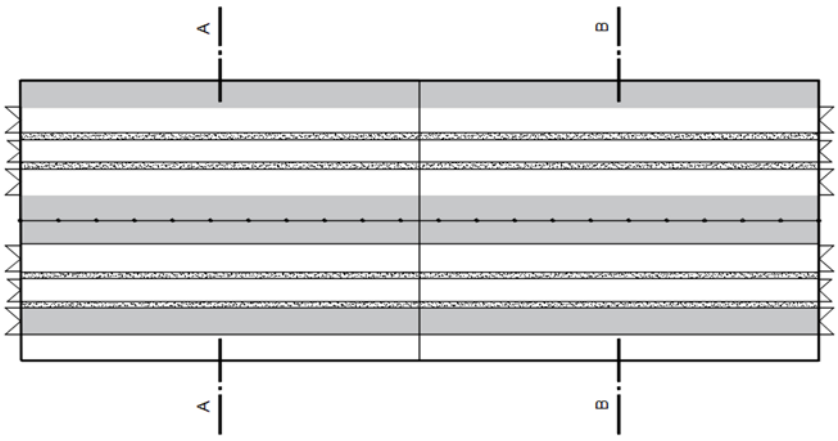

Fig. 2 Scheme of barn by sections A and B

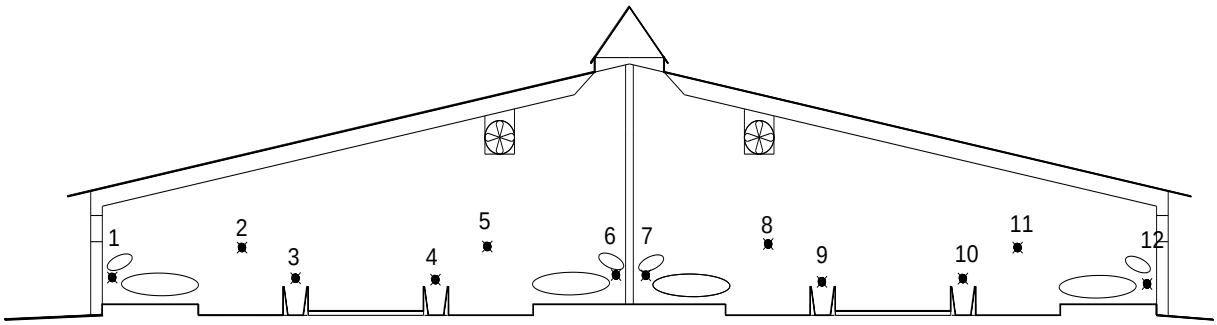

Fig. 3 Cross section of the barn

THI equation (National Research Council) for cattle is shown in equation (1)

$$THI = (1{,}8 \cdot T + 32) - [(0{,}55 - 0{,}0055 \cdot \varphi) \cdot (1{,}8 \cdot T - 26)] \quad (1)$$

Where: φ - relative humidity, %

T - temperature, °C (Pogran et al., 2011)

HLI equation for cattle is shown in equation (2)

$$HLI = 34{,}1 + (0{,}26.\theta_{BGT}) + (1{,}3.\theta_{BGT}) \quad (0{,}82.v^{0{,}1}) \quad \ln 0{,}4^{(0{,}0001+v.^2)} \quad (2)$$

Where: φ - relative humidity, %

θ_{BGT} - temperature measured with a ball thermometer, °C

v - air flow rate, $m.s^{-1}$ (Pogran et al., 2011)

$$BGT = (1{,}33.\theta_{ai}) \quad (2{,}65.\sqrt{\theta_{ai}}) + 3{,}21.\log(r+1) + 3{,}5 \quad (3)$$

Where: θ_{ai} - temperature, °C

r - solar radiation, $MJ.m^{-2}$

v - air flow rate, $m.s^{-1}$

$$HLI_{BG \geq 25} = 8{,}62 + (0{,}38.\varphi) + (1{,}55.BGT) - (0{,}55.v) + e^{2{,}4-v}$$

$$HLI_{BG < 25} = 10{,}66 + (0{,}28.\varphi) + (1{,}3.BGT) - v \quad \text{(Pogran et al., 2011)}$$

RESULTS AND DISCUSSION

The results of the measured values of air temperature, relative humidity, air flow, THI and LHI in the barn 1 from sections A and B are shown in Fig. 4, 5, 6, 7, 8 and in the Tab. 1.

Resulting values of air temperature at measuring points (Fig. 3). Both the lowest daily air temperatures (31.84 °C) and the highest air temperatures (33.48 °C) were found in section A (Fig. 4). The given calculations show that the average air temperatures ranged from 32.58 °C to 32.79 °C, while the recommended air temperature for dairy cows is from 16 °C to 22 °C.

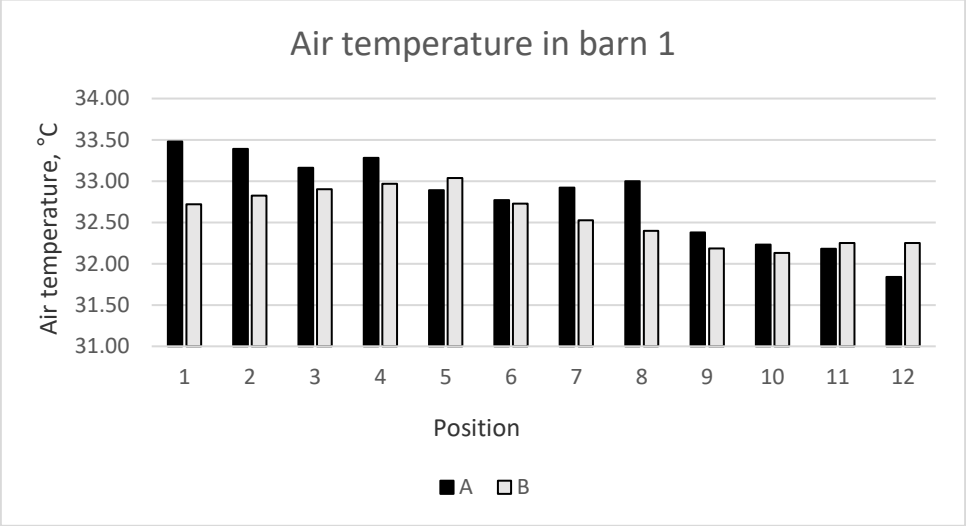

Fig. 4 Measurement results of air temperature in barn 1

Resulting values of relative humidity at measuring points (Fig. 3). Both the lowest relative humidity (54.33 %) and the highest relative humidity (62.65 %) were found in section A (Fig. 5). The average values of relative humidity ranged from 58.09 % to 56.27 %, while the recommended relative humidity for dairy cows is from 50 % to 70 %.

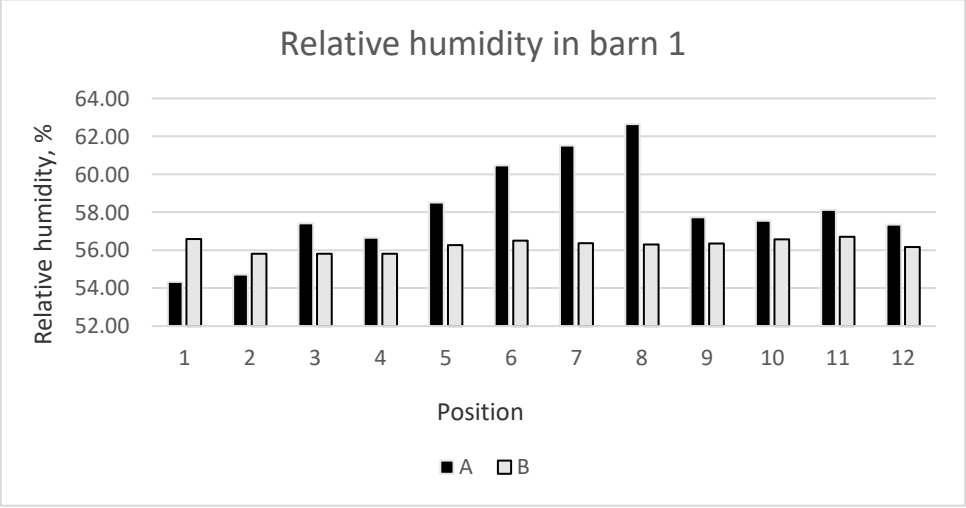

Fig. 5 Measurement results of relative humidity in barn 1

Resulting values of air flow rate at measuring points (Fig. 3). The lowest flow velocity was measured in section A, 0.21 $m.s^{-1}$ and the highest air flow velocity was measured in section B, 1.77 $m.s^{-1}$. The average values of the air flow rate ranged from 0.51 $m.s^{-1}$ to 0.80 $m.s^{-1}$ (Fig. 3).

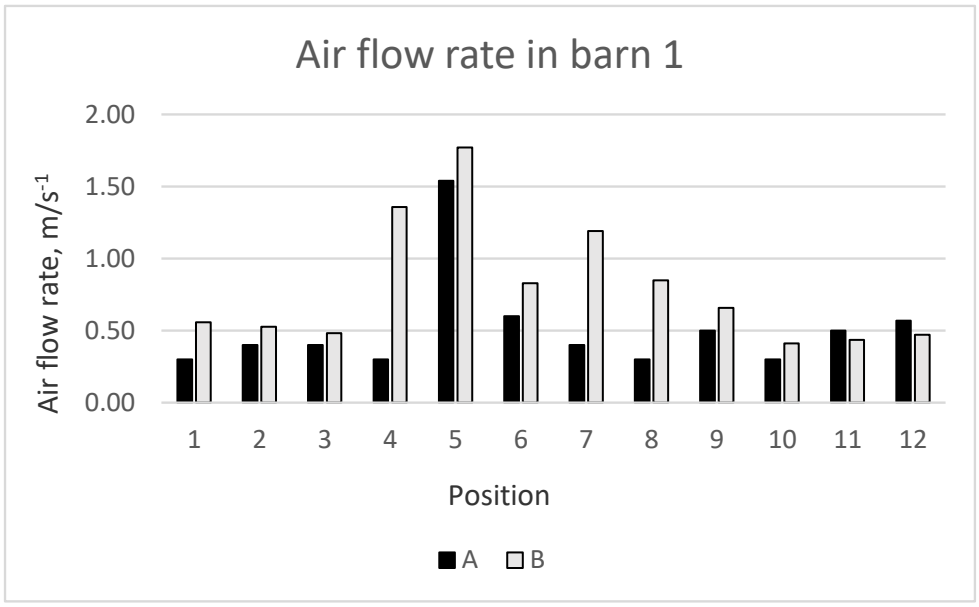

Fig. 6 Measurement results of air flow rate in barn 1

THI values in barn, ranged from 82 to 85. The given results show that the THI results in barn 1 significantly exceed the set THI limit of 72 (Fig. 7).

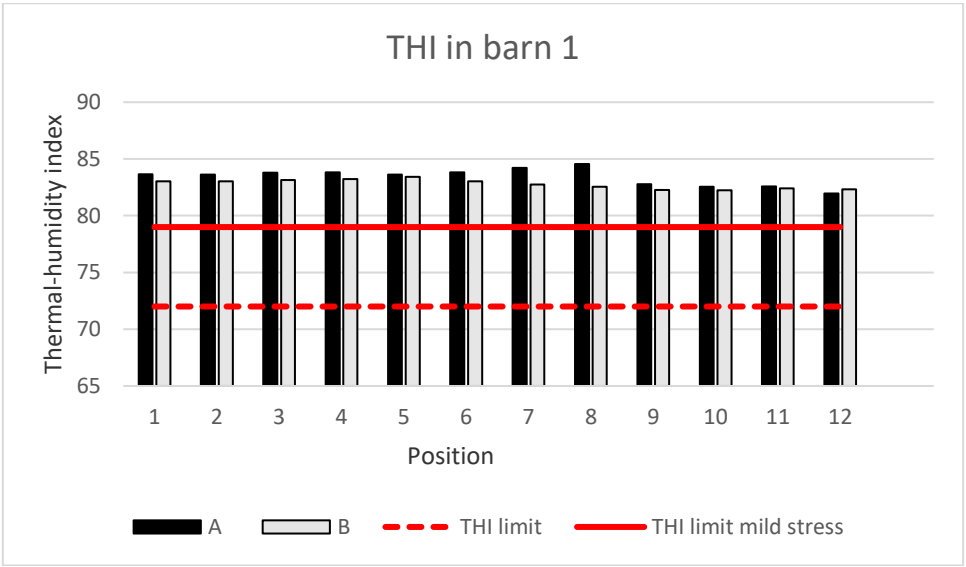

Fig. 7 Results of the calculation Thermal – humidity index in barn 1

HLI values ranged from 81 to 87. The given results show that the results of HLI in barn 1, significantly exceed the set limit HLI of 70 (Fig. 8).

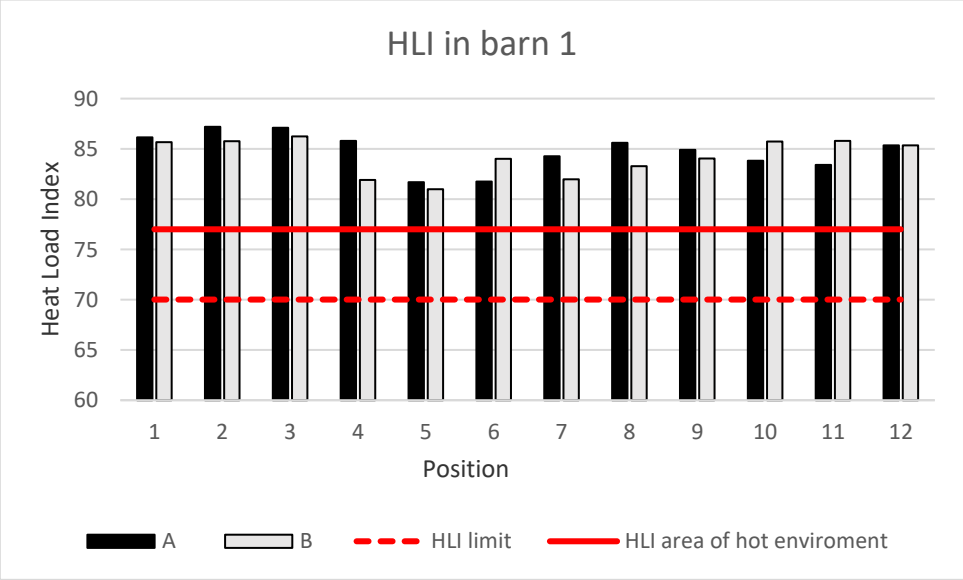

Fig. 8 Results of the calculation Heat load index in barn 1

Tab. 1 Results of measuring of climatic parameters

	Section A	Section B
Air temperature		
AVG	32.79	32.58
min	31.84	32.13
max	33.48	33.04
STDEV.S	0.53	0.33
Relative humidity		
AVG	58.09	56.27
min	54.33	55.81
max	62.65	56.70
STDEV.S	2.47	0.32
Air flow rate		
AVG	0.51	0.80
min	0.30	0.41
max	1.54	1.77
STDEV.S	0.34	0.43
THI		
AVG	83	83
min	82	82
max	85	83
STDEV.S	0.77	0.42
HLI		
AVG	85	84
min	82	81
max	87	86
STDEV.S	1.83	1.82

CONCLUSION

Despite the fact that considerable funds were invested in experimental barn 1, to improve the quality of the environment, the results of the THI and LHI did not show a demonstrable improvement in air quality in the barn and this reconstruction did not have a sufficient effective benefit. We found, that during hot summer days, THI and LHI were highly above the limit athough air exchange through the installation of fans with a capacity of 15 000 $m^3.h^{-1}$, has been intensified. This we conclude that it is necessary to pay attention to direct the flow of air to the animal zone and increase the performance of ventilation. Besides a collection and evaluation of data, mentioned above, this work has served also to examine and to improve measurement procedure for other experiments of my PhD study dealing with technological solutions to minimize heat load of dairy cows.

REFERENCES

1. ARMSTRONG, D.V. 1994. Heat stress interaction with shed and cooling. In: Journal of Dairy Science, vol. 77, n. 7, pp. 2044-2050
2. BERMAN, A. 2005. Estimates of heat stress relief needs for Holstein dairy cows. In: Journal of Animal Science. vol. 83, n. 6, pp. 1377-1384
3. BROUČEK, J. - MIHINA, Š.- RYBA, Š.- UHRINČAŤ, M.- TRÁVNIČEK, J.- ŠOCH, M. 2007. Effects of high temperatures on milk production of dairy cows in east central Europe. In: ASABE, Publication Number 701P0507e
4. BRANDL, B. T. M. 2018. Understanding heat stress in beef cattle. In: Revista Brasileira de Zootecnia Brazilian. Journal of Animal Science. vol. 47, pp. 1–9. e20160414. ISSN 1806-9290
5. DOLEŽAL, O. a spolupracovníci. 2010. Metody eliminace tepelného stresu-významná chovatelská rezerva. Praha, 41 pp
6. POGRAN, Š. - BIEDA, W. - GÁLIK, R. - LENDELOVÁ, J. - ŠVENKOVÁ, J. 2011. Kvalita vnútorného prostredia ustajňovacích objektov. 1. ed. Nitra: SPU, 2011. 242 p. ISBN 978–80–552–0557–1
7. SHEIKH, A. A.- BHAGAT, R. – ISLAM, S. T. - DAR, R. R. - SHEIKH, S. A. - WANI, J.M. – DOGRA, P. 2017. Effect of climate change on reproduction and milk production performance of livestock. In: Journal of Pharmacognosy and Phytochemistry vol. 6, n. 6, pp. 2062-2064. E-ISSN: 2278-4136

8. SCHÜLLER, L. K. - BURFEIND, O. - HEUWIESER, W. 2013. Short communication: Comparison of ambient temperature, relative humidity, and temperature-humidity index between on-farm measurements and official meteorological data. In: J. Dairy Sci. vol. 96, n. 12, pp. 7731–7738
9. STRAPÁK, P. a kolektív. 2013. Chov hovädzieho dobytka. Nitra 2013. 624 p. ISBN 978-80-552-0994-4
10. ZIMBELMAN, R. B. – RHOADS, R. P. – RHOADS, M. L. – DUFF, G.C. – BAUMGARD, L. H. - COLLIER, R. J. 2009. A re – evaluation of the impact of temperature humidity index (THI) and black globe humidity index (BGHI) on milk production in high producing dairy cows. In: Southwest Nutrition and Managment Conference. pp 158–169

Corresponding author:

Ing. Ana Hauliková, Department of Building Equipment and Technology Safety, Faculty of Engineering, Slovak University of Agriculture in Nitra, Trieda Andreja Hlinku 2, 949 76 Nitra, Slovak Republic, e – mail: xhaulikova@uniag.sk

Unique photovoltaic power plants

M. Havrlík[1], V. Beránek[2], V. Poulek[1], J. Sedláček[1], R. Belza[1], M. Libra[1]

[1]Department of Physics, Faculty of Engineering, Czech University of Life Sciences Prague, Prague, Czech Republic

[2]Solarmonitoring, Ltd., Prague, Czech Republic

Abstract

We have recently developed a unique monitoring system for photovoltaic power plants and have gradually improved it in recent years. The system is installed at about 80 power plants in several European countries and at one power plant in Chile. We collect and evaluate all data in our laboratory. In this paper we describe the unique design of three photovoltaic power plants and we present the evaluated data.

Key words: Photovoltaics, PV power plant, data monitoring

INTRODUCTION

The amount of electricity generated is significantly influenced by the design of the photovoltaic (PV) power plant and its location. Monitoring data from PV systems is important for the operator. For example, the works [1,2] talk about monitoring data from PV power plants. We have also developed our own monitoring system Solarmon-2.0 [3], which is already installed on about 80 PV power plants in the Czech Republic and abroad (Romania, Slovakia, Hungary, Chile). Data are continuously collected and evaluated and some results have already been published in previous works [4]. We compare our data with predicted values according to the internationally used internet application Photovoltaic Geographical Information System [5] (https://re.jrc.ec.europa.eu/pvg_tools/en/tools.html). This application predicts the expected values of electricity generated according to the location and the basic design of the PV power plant.

MATERIALS AND METHODS

The PV system in Cuz Cuz in Chile (see Fig. 1) is installed in a subtropical half-desert area in a location with excellent solar conditions. Its coordinates are 31.66° S, 71.22° W, altitude 275 m. Chinese BYD PV panels based on polycrystalline silicon with a nominal output power

of 305 W_p, type P6C-36, were used. The nominal output power of the whole PV system is about 3000 kW_p. The tracking axes are oriented horizontally in the north-south direction.

Fig. 1 PV system in Cuz Cuz (Chile), advanced construction with tracking stands of PV panels with horizontal tracking axis.

Fig. 2 PV system in Prague (Czech Republic) with standard construction with fixed stand of PV panels inclined to the south at an angle of 35°.

The PV system in Prague-Suchdol (see Fig. 2) is installed on the roof of our Faculty of Engineering. Its coordinates are 50,13° N, 14,37° E, altitude 280 m. PV panels Renesola, GmbH of German production based on polycrystalline silicon with a nominal output of 260 W_p, type JC 260M-24/Bb were used. The PV system has a standard construction with fixed PV panels inclined to the south at the angle of 35°. The nominal output power of the whole PV system is about 10 kW_p.

Fig. 3 PV system in Prague (Czech Republic) with standard construction with PV panels laid horizontally without supporting stands.

The PV system in Prague-Vršovice (see Fig. 3) is located approximately 10 km from Prague-Suchdol, so it is in a location with similar solar conditions. Flexible waterproof PV foils VAEPLAN V Solar 432 with a nominal power of 432 W_p were used for the construction. They lie nearly horizontally on the roof of a football stadium without supporting stands. A total of 1040 foils are connected to eight independent sections and these are connected to eight merge switchboards. 26 strings are connected into each switchboard and each string consists of 5 PV foils. The total nominal output power of the PV power plant is therefore approximately 449 kW_p.

All these PV systems are connected to the AC grid via DC/AC inverters. PV systems are connected to our above-mentioned Solarmon-2.0 monitoring system. Data collection and

evaluation takes place in our laboratory. For better comparison, the values of generated electricity are calculated per 1 kW_p of installed nominal power.

RESULTS AND DISCUSSION

Fig. 4 shows the amount of electricity produced in said PV systems during one year. The values are given by months and for the whole year. In the southern hemisphere of Cuz Cuz, the seasons of the summer and winter are opposite to that of Europe, so there are the highest values of electricity produced in December and January and the lowest values are in May and June. It can be also seen that the total annual value of the generated electricity (2043 $kWh.kWp^{-1}.year^{-1}$) in Cuz Cuz is almost double compared to the PV system in Prague-Suchdol with fixed PV panels inclined to the south at an optimal angle (1145 $kWh.kWp^{-1}.year^{-1}$). And the value is nearly triple compared to the PV system in Prague-Vršovice with fixed PV panels placed horizontally (746 $kWh.kWp^{-1}.year^{-1}$).

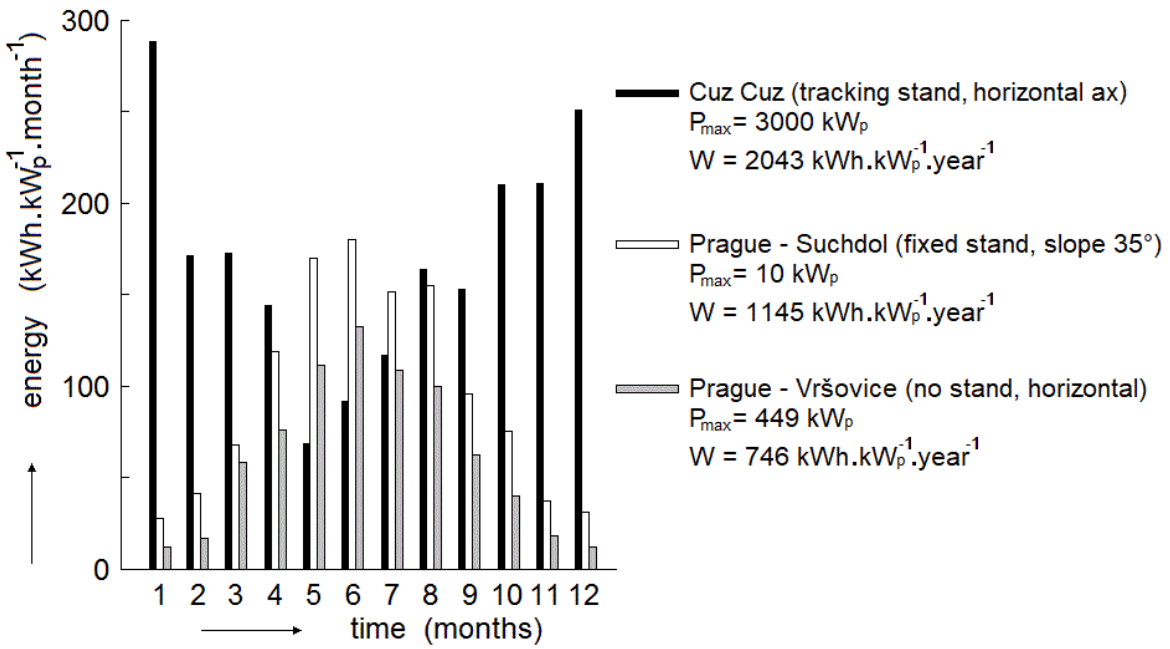

Fig. 4 The amount of electricity produced in the said PV systems during one year.

The high value of electricity generated in Cuz Cuz is certainly related to the location with excellent solar conditions as well as to the advanced design of the PV system with tracking stands of PV panels. In the half-desert region, PV panels are often dusty with desert dust, but still the value of the electricity generated is high. It can also be seen that in subtropical locations the percentage differences between these values between summer and winter months are

smaller than in Central Europe. Sun tracking racks of PV panels can increase the annual value of generated electricity by up to 30% [6].

In the case of PV systems installed in Prague, the values of electricity generated correspond to the values according to the above-mentioned and internationally used internet application Photovoltaic Geographical Information System [5]. In the case of a PV system in Prague-Suchdol, the actual annual value is slightly higher than expected (1145 $kWh.kWp^{-1}.year^{-1}$ versus 1015 $kWh.kWp^{-1}.year^{-1}$), which can be explained by high-quality PV panels with high efficiency of energy conversion. In the case of the PV system in Prague-Vršovice, the actual annual value is slightly lower than expected (746 $kWh.kWp^{-1}.year^{-1}$ as opposed to 850 $kWh.kWp^{-1}.year^{-1}$). This we have seen in the previous work (Libra et al., 2016) and it was explained by the dusty environment near the railway track and by a slight rounding of the roof, where all PV panels are not completely horizontal.

CONCLUSION

In this paper, we compared and discussed the evaluated data from power plants in locations with very different solar conditions. The location in the half-desert area in northern Chile is, according to all forecasts, one of the places with excellent solar conditions, as confirmed by our data.

Sun tracking stands slightly increase the amount of electrical energy produced, but at higher latitudes they must have an inclined polar axis. The individual racks must be set apart from each other so that they do not shield each other. In this way, however, the use of the area of the PV power plant is reduced and the price of the area is high in Central Europe. Conversely, in subtropical half-desert regions, the rotational axis can be oriented horizontally, thereby minimizing shielding. In addition, the price of the power plant area is lower.

In densely populated areas of Central Europe, we recommend installing PV systems on roofs and facades of buildings and not on farmland. In the desert and half-desert areas, installation on open areas is also suitable with regard to the lower price of the PV power plant area.

REFERENCES

1. AYOMPE, L.M., DUFFY, A., McCORMACK, S.J., CONLON, M.: Measured performance of a 1.72 kW rooftop grid connected photovoltaic system in Ireland. Energy Conversion and Management, 2011, 52: 816-825.
2. MADETI, S.R., SINGH, S.N.: Monitoring system for photovoltaic plants: A review. Renewable and Sustainable Energy Reviews, 2017, 67: 1180-1207.

3. BERÁNEK, V., OLŠAN, T., LIBRA, M., POULEK, V., SEDLÁČEK, J., DANG, M.Q., TYUKHOV, I.I.: New Monitoring System for Photovoltaic Power Plants' Management. Energies, 2018, 11: Article ID 2495.
4. LIBRA, M., BERÁNEK, V., SEDLÁČEK, J., POULEK, V., TYUKHOV, I.I.: Roof photovoltaic power plant operation during the solar eclipse. Solar Energy, 2016, 140: 109-112.
5. Photovoltaic Geographical Information System [online], 2020. Available from: https://re.jrc.ec.europa.eu/pvg_tools/en/tools.html. [Accessed 3rd June 2020].
6. POULEK, V., LIBRA, M.: New solar tracker. Solar Energy Materials and Solar Cells, 1998, 51: 113-120.

Corresponding author:

Ing. Matouš Havrlík, Department of Physics, Faculty of Engineering, Czech University of Life Sciences Prague, Kamýcká 129, Praha 6, Prague, 16500, Czech Republic, email: m.havrlik@seznam.cz

3D printing covid mask

P. Hnízdil[1], J. Mašek[2], R. Chotěborský[1]

[1]*Department of Material Science and Manufacturing Technology, Prague, Czech Republic*

[2]*Department of Agricultural Machines, Prague, Czech Republic*

Abstract

The non-standard use of 3D printing technology was used during the Covid19 pandemic. This new situation brought the need to address completely new procedures for the application of printed protective equipment. The subject of the solution was the design of a suitable design of the protective mask, the use of a suitable material and the method of disinfecting the surface of the mask. Due to mass production, it was necessary to optimize the printing time. The concept became very successful on social networks, we actively working with feedbacks. The masks were used at a later stage by the general public and were also distributed to hospitals. The result is a proven concept that is being prepared for mass injection production (by injection).

Key words: 3D printing, covid19 mask, pandemie, filament, filters, desifection

INTRODUCTION

With the development of additive production technologies in rapid prototyping area, small-scale production of functional products from 3D printers is beginning to be applied to a lesser extent. The widest expansion was in the field of continuous application of molten plastic (FFF method).

It is therefore reasonable to propose a successful adaptation of 3D printing technologies to the materials used, which could allow a simple way of producing printing with suitable material properties with lower production costs and a high degree of automation. Because it is possible to precisely place the reinforced structure of the composite parts in each layer, it is possible to obtain innumerable possibilities for designing the optimization of individual parameters of the printed object. Recently, new application possibilities have opened up, both in the personal production market and in the production of light parts for industry (Basgul et al., 2020).

Towards the end of 2019, COVID-19 began to spread, challenging the need for health protection needs around the world. The basic measures were, in particular, the observance of

strict hygienic measures, the wearing of protective veils and social distancing. However, according to the guidelines of the World Health Organization (WHO), protective equipment was necessary for all healthcare providers, especially effective face masks with at least a protective FFP2, especially for doctors, nurses, dentists and other health professionals. The problem was the acute lack of these protective masks. Thus, an effort has been made to engage with 3D mask concepts that could effectively replace existing masks on the market and could be reused (Swennen et al., 2020). The advantage of synthetic polymeric materials is easy availability and cost-effectiveness. The cost of a 3D printer varies, but is a good investment as a supplement to work, healthcare organizations or, in the event of an emergency, to the home, helping to produce protective equipment for healthcare professionals and all people facing the COVID 19 pandemic in the first line (Ishack & Lipner, 2020).

MATERIALS AND METHODS

Design

The design was created in the program Trimble Sketchup Pro. Compared to other masks, which were designed with an insufficient filter area, emphasis was placed on the largest possible filter area, due to the comfortable breathing of the mask user. The design was intended for the simplest possible production on the most widespread home 3D printers. A simple filter replacement procedure was designed regardless of the selected type and purpose of the filter element. From the point of view of design, the mask is designed as a universal protective aid, which consists of three printed pieces.

Material

The mask is designed for printing from PET G, ABS, PLA and ASA. Filter material: Perlan, nanofiber (), antibacterial filters for vacuum cleaners. Filtration capacity more than 95%.

Printing

The design of the mask is designed for printing on conventional FFF printers with a print layer of 0.25 mm, which should be sufficient.

The first model of the designed mask works as a better veil, but does not replace a respirator. It is washable (alcohol). The filters were chosen antibacterial, commonly used in vacuum cleaners, which is good to change often. The mask is not for all-day wear, only for short-term (trade, refueling etc.). PETG was recommended as the printing material, printing with a layer

of 0.25 mm, which should be sufficient. The printing time of one mask was about eight hours. It is an alternative to sewn veils for more technically people.

RESULT AND DISCUSSION

First and second version of mask was not so ideal for filter area, every stage of design enlarged filter area, next was upgraded shape of mask for pleasant using. Also was upgraded filter replacement system to easy way as in figure 3.

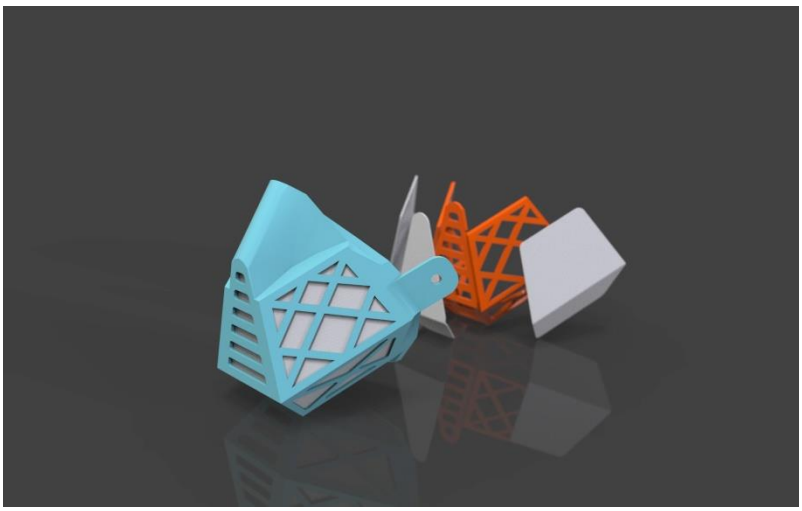

Fig.1 The first designed mask model with a variable filter and side rubber holes.

Fig, 2 The second design of the mask with larger vents and a more pleasant seal.

Fig. 3 The final design of the mask, with the optimal vent part for longer wear, is intended for mass production.

- size of vents – for easy breath must be design of mask customized for largest area as possible.
- enlargement, taking into account feedback from users of the first models and adaptation to needs – upgrade mask for used friendly, that´s mean easy change filter.
- more pleasant design and seals – facelift of mask to more anatomical shape and smooth surface.
- filter solutions – universal solution of design mask for different filters

CONCLUSION

After research and testing some designs of covid masks, is prepare best concept for industrial production on an injection molding machine.

AKNOWLEDGEMENT

Authors would like to thank TAČR GAMA TPO1010050 for financial support on this project.

REFERENCES

1. BASGUL, C., YU, T., MACDONALD, D. W., SISKEY, R., MARCOLONGO, M., & KURTZ, S. M. (2020). Does annealing improve the interlayer adhesion and structural integrity of FFF 3D printed PEEK lumbar spinal cages?. *Journal of the mechanical behavior of biomedical materials*, *102*, 103455.

2. SWENNEN, G. R., POTTEL, L., & HAERS, P. E. (2020). Custom-made 3D-printed face masks in case of pandemic crisis situations with a lack of commercially available FFP2/3 masks. *International Journal of Oral and Maxillofacial Surgery*.

3. ISHACK, S., & LIPNER, S. R. (2020). Applications of 3D Printing Technology to Address COVID-19 Related Supply Shortages. *The American Journal of Medicine*.

Corresponding author:

Ing. Petr Hnízdil, *Department of Material Science and Manufacturing Technology, Prague, Czech Republic*, Czech University of Life Sciences Prague, Kamýcká 129, Praha 6, Prague, 16521, Czech Republic, tel: +420774789767, email: hnizdilp@tf.czu.cz

The use of fuzzy regulator to control movement of mobile robot

D. Horňák[1], R. Srnánek[1], M. Olejár[1], D. Hrubý[1]

[1]*Department of Electrical Engineering, Automation and Informatics, Slovak University of Agriculture in Nitra, Tr. A. Hlinku 2, 949 76 Nitra, Slovakia*

Abstract

Designing proper regulator is crucial part in movement control of mobile robot. Regulator must be efficient and reliable in terms of navigating mobile robot in its work area. This paper is focused on designing a fuzzy regulator capable of navigating mobile robot in working area. Regulator must be able to get a mobile robot in to required position with minimal offset, minimal deviation of straight route and without becoming unstable. We've also created a mathematical model of differential drive based mobile robot with similar behavior as our mobile robot EN20 and simulated measured data.

Key words: fuzzy, mobile robot, differential drive, kinematics, simulation

INTRODUCTION

Autonomous control makes it possible to ensure constant presence of the robot in the production area or on the field in which it's deployed. By appropriately selected and designed algorithm to control mobile robot we can achieve increased quality of work output, accuracy and thus a possible reduction of unwanted losses in time or material.

Of all the software-calculation methods used to control autonomous mobile robots, fuzzy logic combined with neural network elements has proven to be one of the most effective mobile robot regulator. It has best tolerance for external interference and for errors made by sensor subsystem. Several successful implementations of a pure neural system for controlling an autonomous mobile robot have been created. That system has some drawbacks and suffers from slow convergence, lack of generalization due to a limited number of patterns representing complex environments. The advantages and disadvantages of each system have led to the creation of a new neuro-fuzzy system that provides the synergy between the two paradigms. Above all, it is about imitating the decision-making of human expertise in a fuzzy system and learning from the previous experience of a mobile robot in neural networks.

MATERIALS AND METHODS

Mobile robot chassis kinematics is selected according to environment in which the robot will operate and according its purpose. EN 20, that we used, is based on a differential drive chassis. Robots' wheels can move independently of each other at different speeds and directions. These speeds are measured by incremental encoders connected to measuring wheels respectively on both sides. Both driving wheels are connected to drives through gearbox as shown on fig. 1.

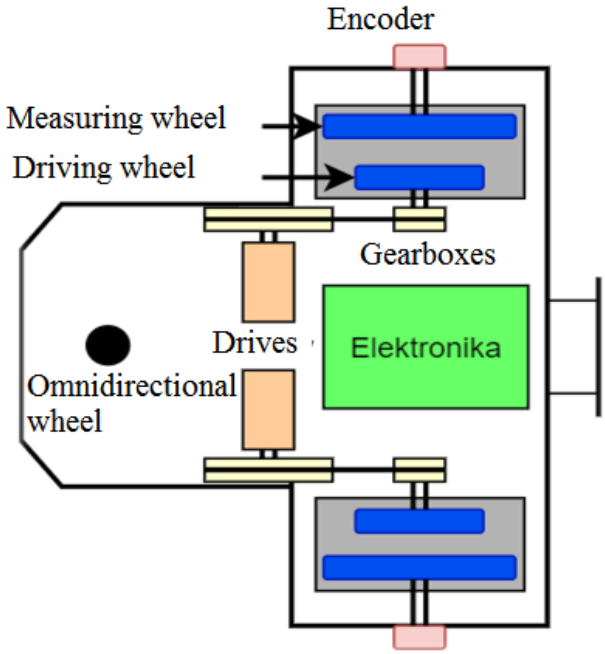

Fig. 1 Mobile robot EN 20 schematics based on differential (Olejár, 2017)

Communication between individual modules such as motors, sensors, power supply and control is managed via SPI communication protocol in a 4-wire connection with data rate of 1 Mbps. Primary communication module IM1.0 ensures communication between the individual modules and PC. IM1.0 is single-chip microcontroller C8051F340 that incorporates both UART and SPI communication protocol. UART serial line is used only for communication with the PC via Xbee protocol with full duplex communication and communicate at 2.4 GHz. SPI communication line is set as MASTER and it can provide connection to eight SLAVE devices. The MASTER always checks if all individual SLAVE devices are in running order right after the start of the mobile robot and also stores information about their addresses. Then it collects, sends control commands and robot status information (Cviklovič, 2013).

This functionality and communication between individual modules od mobile robot EN 20 are shown in block diagram in fig. 2.

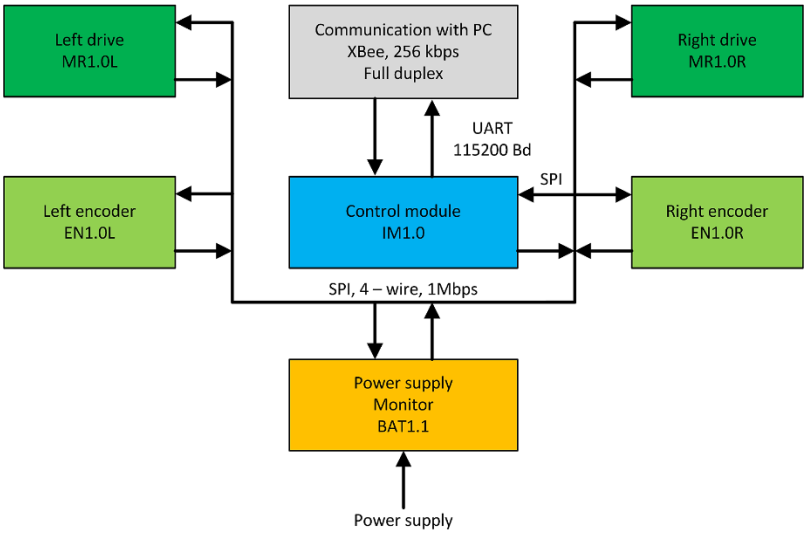

Fig. 2 Block diagram of mobile robot EN 20 (Olejár, 2017)

EN 20 mobile robot uses BLDC motors BLY171S 24V-4000 as drives. These motors are controlled by MR1.0R and MR1.0L control modules.

For measuring traveled distance, robots' rotation angle and rotation of the individual wheels of mobile robot there are hall sensors located on the stator of BLDC motors and there are also two incremental encoders TP 6.35 1024 BZ TTL on each side respectively for more accurate measurement of traveled distance. Measuring wheel rotates rotor of encoders and thus we can calculate traveled distance by number of impulses counted by incremental encoder. Incremental encoder has a resolution 1024 impulses per rotor revolution and operates on optical principle. This measurement is providing us with information needed to calculate actual location of robot and desired location.

For these calculations we have to know kinematics of mobile robot, in our case differential kinematics (fig. 3), and equations 1, 2 and 3 to calculate coordinates.

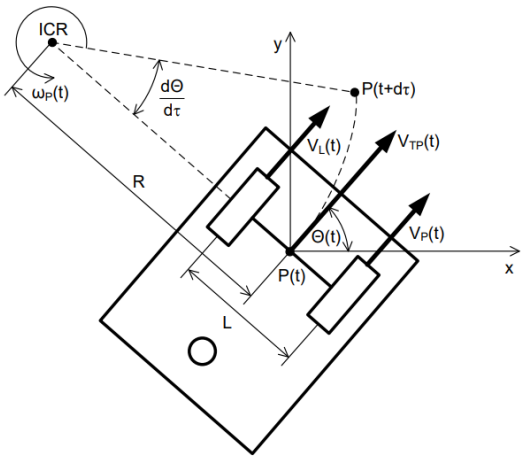

Fig. 3 Schematic of mobile robot with differential drive (Olejár, 2017)

$$\theta(k) = \frac{V_P(k) - V_L(k)}{L}.T + \theta(k-1) \quad (1)$$

$$x(k) = \frac{V_P(k) + V_L(k)}{2}.\cos[\theta(k)].T + x(k-1) \quad (2)$$

$$y(k) = \frac{V_P(k) + V_L(k)}{2}.\sin[\theta(k)].T + y(k-1) \quad (3)$$

Where: *x(k)* – current sample of path traveled on x-axis, m,

x(k-1) – previous sample of path traveled on x-axis, m,

y(k) – current sample of path traveled on y-axis, m,

y(k-1) – previous sample of path traveled on y-axis, m,

Θ(k) – current rotation angle of the mobile robot, °,

Θ(k-1) – previous rotation angle of the mobile robot, °,

$V_P(k)$ – current sample of right wheel velocity, $m.s^{-1}$,

$V_L(k)$ – current sample of left wheel velocity, $m.s^{-1}$,

L – wheelbase length, m,

T – timing period, s.

To create a fuzzy regulator we're using MATLAB, which has function called "Fuzzy Logic Designer" to create fuzzy regulator with graphic interface and also, you're able to create a fuzzy regulator in code. With code programing of fuzzy regulator you have to learn corresponding commands to create membership functions and rules. This way it's easier to adjust rules "on the move" to create more efficient regulator.

In this paper we're going to focus on Mamdani and Sugeno types of regulators. Our basic schematic used to create fuzzy regulator is shown on fig. 4.

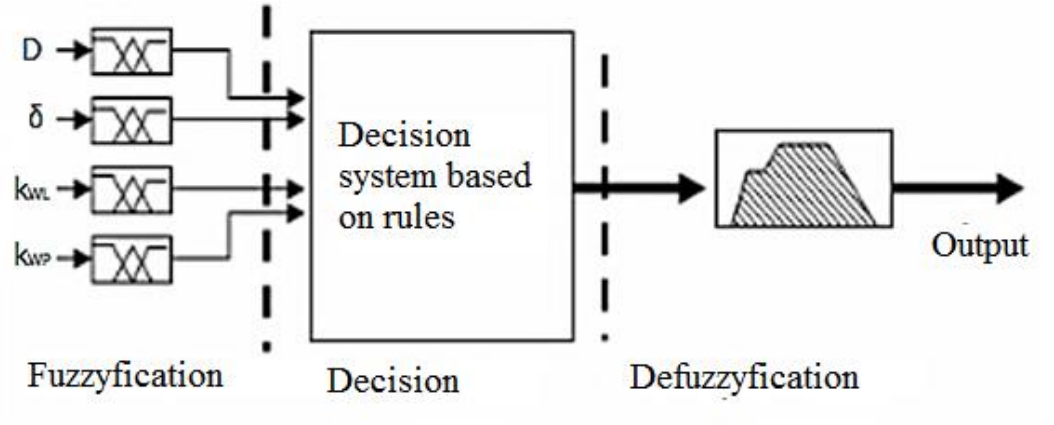

Fig. 4 Basic principle of fuzzy regulator to control mobile robot

RESULTS AND DISCUSSION

To control any type of mobile robot and to create appropriate regulator we must know its construction and mainly it's kinematics. Our mobile robot EN 20 is based on differential drive kinematics so we must use appropriate equations so we would be able to calculate its location and rotation angle so we can adjust speed of each wheel of particular mobile robot.

To determine *x* and *y* coordinates, we had to first calculate the path, that both wheels have traveled:

$$s = \frac{i}{k} \tag{4}$$

Where: s – distance traveled, m,
i – number of impulses from encoder, -,
k – calibration constant determining the number of impulses per meter, m^{-1}.

After calculation of traveled distance of both wheels we can calculate incremental value of path *dr* (eq. 5) and also angle of rotation of the mobile robot θ (eq. 8).

$$dr = \frac{s_{pm}(k) + s_{lm}(k)}{2} - \frac{s_{pm}(k-1) + s_{lm}(k-1)}{2} \tag{5}$$

Where: dr – incremental value of distance traveled, m,
s_{pm} – distance traveled by right wheel, m,
s_{lm} – distance traveled by left wheel, m.

Incremental value of the path traveled (eq. 5) and current rotation angle (eq. 8) of the mobile robot allow us to calculate current coordinates and thus determine the distance traveled in X (eq. 6) and Y (eq. 7) axis respectively by following equations:

$$x(k) = \cos[\theta(k)]dr + x(k-1) \tag{6}$$

$$y(k) = \sin[\theta(k)]dr + y(k-1) \tag{7}$$

$$\theta = \frac{s_{pm} - s_{lm}}{k_u} \tag{8}$$

Where: x(k) – current sample of path traveled on x-axis, m,
x(k-1) – previous sample of path traveled on x-axis, m,
y(k) – current sample of path traveled on y-axis, m,
y(k-1) – previous sample of path traveled on y-axis, m,
θ(k) – current rotation angle of the mobile robot, °,
dr – incremental value of distance traveled, m.
θ – angle of rotation of the mobile robot, °,
ku – calibration constant to determine the direction angle of the mobile robot, m/°.

MATLAB R2018a and newer versions support Mobile Robotics Simulation Toolbox for MATLAB, that already has all the equations needed to create mathematical model of mobile robots based on many different kinematics. You have to just input wheel velocities, wheel radius and wheelbase length.

Fuzzy regulator input is angle of deviation from desired position δ (eq. 11), ranging +/- 180°, and distance of mobile robot from desired position D (eq. 9) that has range from 0 to 10m. Output from fuzzy regulator are multiples ranging from 0 to 1 which regulate our maximal speed that we set in the beginning.

$$D = \sqrt{(x - x_{end})^2 + (y - y_{end})^2} \tag{9}$$

Where: D – distance of mobile robot from desired position, m,
x_{end} – x coordinate of desired position, m,
y_{end} – y coordinate of desired position, m,
x – current x coordinate of mobile robot, m,
y – current y coordinate of mobile robot, m.

Before we can calculate deviation angle of mobile robot from desired position, we must firstly calculate the angle of the target point with respect to current position of mobile robot.

$$\theta_{end} = \left(arcsin\frac{y_{end} - y}{D}\right)\frac{180}{\pi} \tag{10}$$

Where: θ_{end} – the angle of the target point with respect to current position of mobile robot, °.

Now we can calculate deviation angle of mobile robot from desired position δ

$$\delta = \theta - \theta_{end} \tag{11}$$

Where: θ_{end} – angle between current position and desired position, °,
θ – rotation angle of mobile robot, °,
δ – deviation angle of mobile robot from desired position, °.

To compare quality of regulation we are going to calculate area created by path of mobile robot with X axis as reference.

Criterion of absolut regulation area (eq.12)

$$I_{AE} = \int_0^{\infty} |e(t) - e(\infty)|\mathrm{dt} \tag{12}$$

Where I_{AE} is absolut regulated area.

This criterion is usable in all cases, because it add up every partial regulated area, under and above regulated variation.

Criterion of quadratic regulation area (eq. 13)

$$I_{SE} = \int_0^{\infty} [e(t) - e(\infty)]^2 \mathrm{dt} \tag{13}$$

Where I_{SE} is quadratic regulated area.

It's application is less difficult than absolut regulation area, but it lacks overvaluation of large and undervaluation of small regulation areas.

Fuzzy regulator

Our first designed fuzzy regulator was created in MATLAB with Fuzzy Logic Designer as Mamdani type. Has 25 interference rules, for which we must propose linguistic variables for inputs and outputs.

Linguistic variables were designed as follows in tab. 1.

Tab. 1 Linguistic variables for input D, δ and output k_{vp}, k_{vl} for mamdani fuzzy regulator

$\boldsymbol{D}$	$\boldsymbol{\delta}$	$\boldsymbol{k_{vp}, k_{vl}}$
N – zero distance from end point	N – no deviation angle	N – zero multiple of speed
M – small distance from end point	KS – positive average deviation angle	M – little multiple of speed
S – average distance from end point	KV – positive high deviation angle	P – average multiple of speed
V – large distance from end point	ZS – negative average deviation angle	V – high multiple of speed
VV – very large distance from end point	ZV – negative high deviation angle	VV – very high multiple of speed

After declaration of linguistic variables, we defined membership functions for *D* (fig. 5), δ (fig. 6), k_{vp} (fig. 7), k_{vl} (fig. 7)

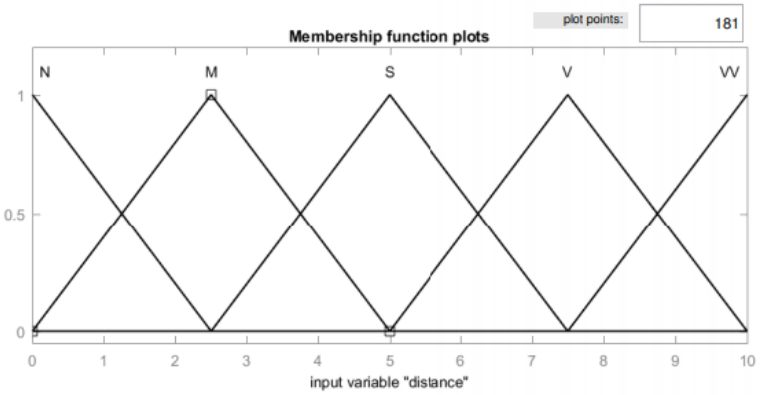

Fig. 5 Membership function of linguistic variables for distance from desired position

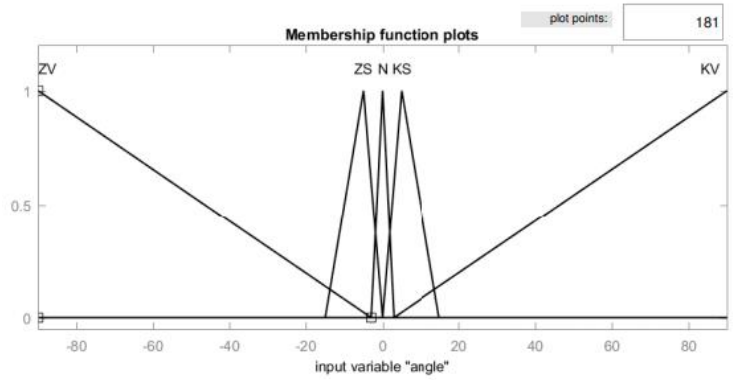

Fig. 6 Membership function of linguistic variables for deviation angle of mobile robot

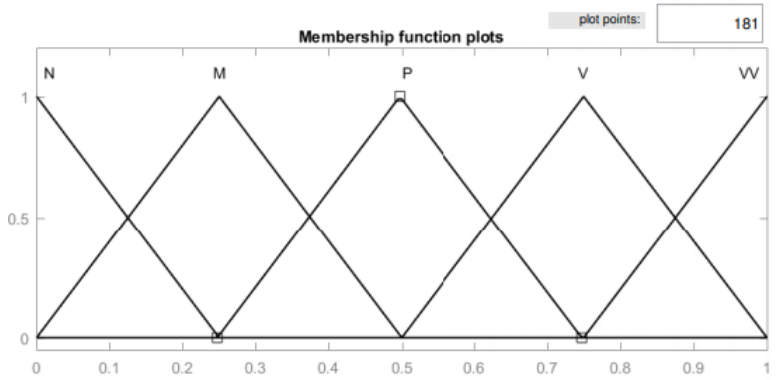

Fig. 7 Membership function of linguistic variables for multiples to regulate speed of left and right engine

After all these steps we must specify rules (tab. 2) by which our regulator will decide how will output from fuzzy regulator look. We have created fuzzy regulator with 25 rules, which is effective and sufficient number of rules to control movement of mobile robot. Less rules would mean that regulation would be less precise and instability could occur. More rules would mean that we would need more computing power to get more precise regulation and better trajectory.

Tab. 2 10 out of 25 fuzzy regulator base rules

1. If (distance is N) and (angle is N) then (vp is M)(vl is M)
2. If (distance is M) and (angle is N) then (vp is P)(vl is P)
3. If (distance is S) and (angle is N) then (vp is V)(vl is V)
4. If (distance is V) and (angle is N) then (vp is VV)(vl is VV)
5. If (distance is VV) and (angle is N) then (vp is VV)(vl is VV)
6. If (distance is N) and (angle is KS) then (vp is N)(vl is M)
7. If (distance is M) and (angle is KS) then (vp is M)(vl is P)
8. If (distance is S) and (angle is KS) then (vp is P)(vl is V)
9. If (distance is V) and (angle is KS) then (vp is V)(vl is VV)
10. If (distance is VV) and (angle is KS) then (vp is V)(vl is VV)

As a result, we have got regulation surfaces (fig. 8) for both engines. On these regulation surfaces we can see which output value belongs to combination of two inputs.

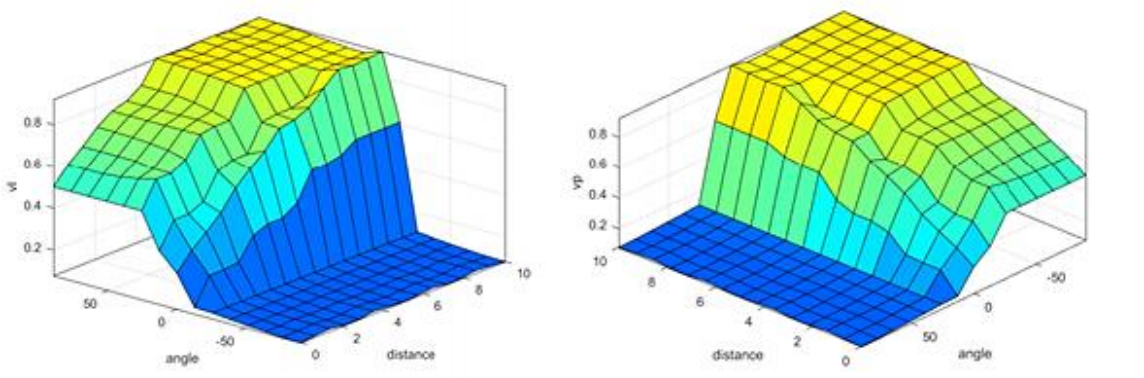

Fig. 8 Regulation surface of mamdani type fuzzy regulator for A) left engine, and B) right engine

Designing a sugeno type fuzzy regulator is very similar in membership functions of input. Only thing that is completely different is output, because sugeno has more linear output and we must assign to every output membership function parameter (Fig. 9).

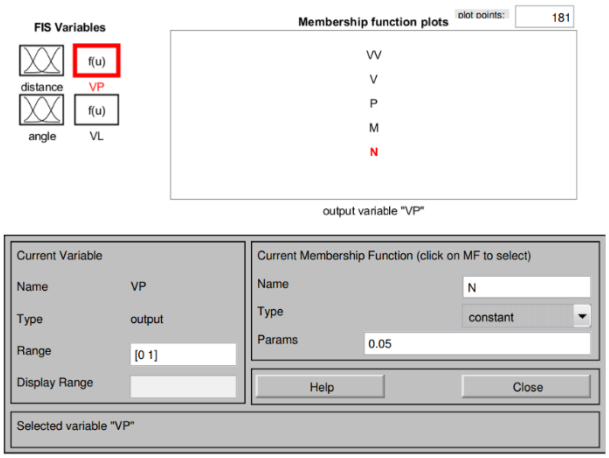

Fig. 9 Sugeno output membership parameters

We assigned parameters as follows: VV – 1; V – 0,75; P – 0,5; M – 0,25; N – 0,05.

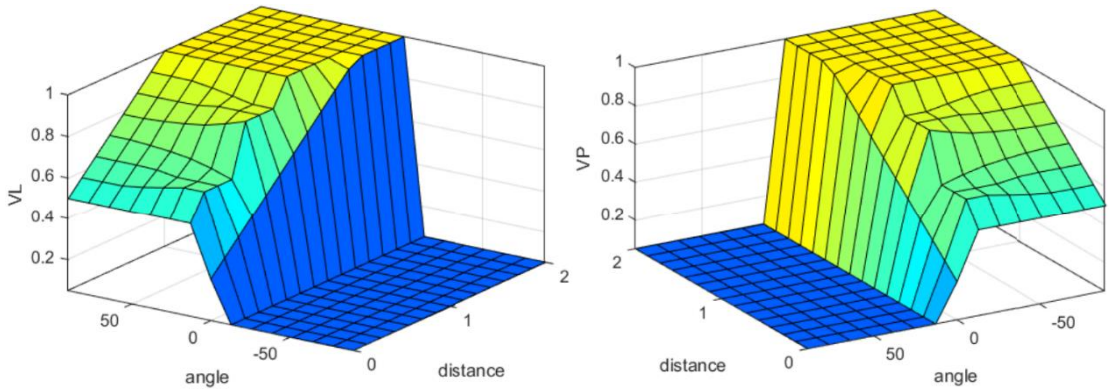

Fig. 10 Regulation surface of sugeno type fuzzy regulator for A) left engine and B) right engine

As result we have got smoother and more linear relation surface as is shown on fig. 10.

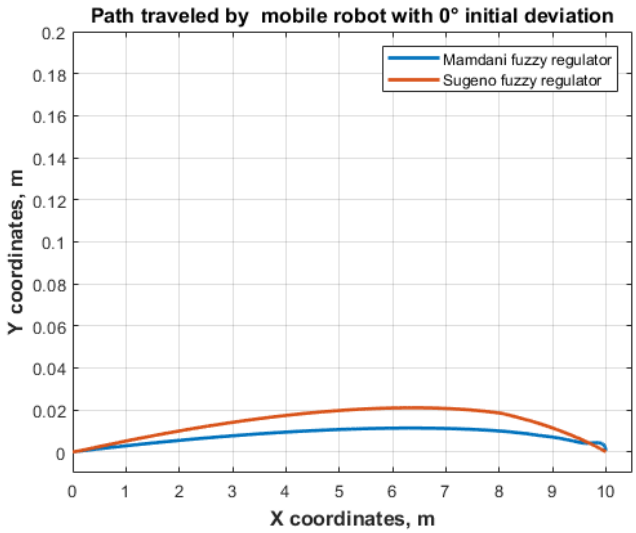

Fig. 11 Comparison of traveled distance of mobile robot with 0°initial deviation

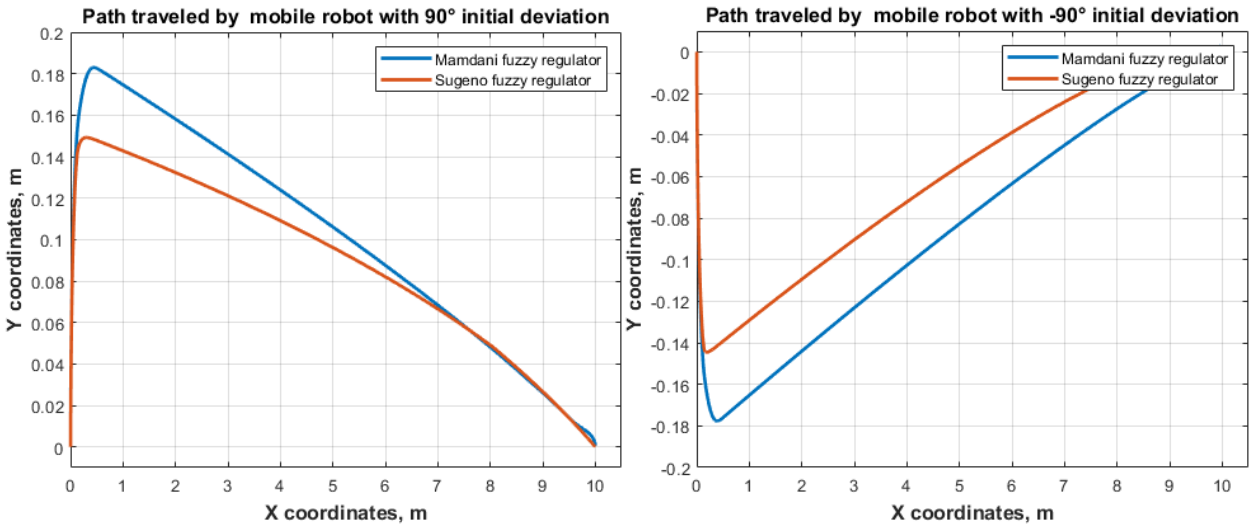

Fig. 12 Comparison of traveled distane of mobile robot with A) 90° inidtial deviation, B) -90° initial devition

As we can see on fig. 11 mamdani type of regulator is more efficient in compensating speed irregularity of both wheels and maintains flatter line. Mamdani type reached maximal value of Y_{max} 0,0113m where sugeno went to 0,0209m. But regulation time for mamdani was 34,36s and for sugeno it was 31,99s.

On fig. 12 we can see that mobile robot firstly has to correct its initial angle to get in to desired possition. With initial devitation of 90° to the target mamdani reached maximum value of Y_{max} 0,1830m and sugeno 0,1492m. With -90°deviation mamdani reached maximum Y_{max} 0,1777m and sugeno 0,1446m. Regulation times in both cases was approximately 35,3s for mamdani type and 32,8s for sugeno type. More precise comparison is shown in tab. 3.

Tab. 3 Numeric comparison of both fuzzy regulators and calculated area covered by robots trajectory

Regulator type	Initial angle deviation δ_0, (°)	Time of regualtion t_{reg}, (s)	Absolute regulation area I_{AE}, (1)	Quadratic regulation area I_{SE}, (1)	Max. deviation y_{max}, (m)
Mamdani	90°	35.3220	3.2795	0.4170	0.1830
	0°	34.3580	0.2539	0.0022	0.0113
	-90°	35.2800	2.7137	0.3218	0.1777
Sugeno	90°	32.8280	2.6592	0.2865	0.1492
	0°	31.9930	0.4114	0.0068	0.0209
	-90°	32.8170	1.7816	0.1684	0.1446

CONCLUSION

In this paper we have managed to create and design two similar fuzzy regulators based on Mamdani and Sugeno types of regulators and compared trajectories traveled by mobile robot. We have concluded that, Sugeno type is more suitable for our application and in our conditions. This conclusion is based on measured path that mobile robot traveled, and regulation time which shows how long it took regulator to navigate mobile robot to target location even with different initial angles. Sugeno type was 2,494 seconds faster and deviated by 0,0338m less from its straight path than Mamdani with 90° and -90° initial deviation. With 0° initial deviation Sugeno traveled longer distance and deviated by 0,0096m more than Mamdani, but it reached its target location by 2,365 seconds faster than Mamdani type.

In the table 3 we can observe that Sugeno type created smaller regulation areas except with 0° initial deviation. It also reached target location faster in every case because of smoother regulation.

As next step we are going to use Sugeno type of fuzzy regulator to create Neuro-fuzzy system, that adjust membership functions and base rules itself based on quality of regulation to achieve smaller traveled area and to reach target location faster.

Acknowledgments: This paper was created within the project VEGA no. 1/0720/18 Research of Alternative Navigation Algorithms for the Control of Autonomous Robots in Plant Production.

REFERENCES

1. CVIKLOVIČ, V., OLEJÁR, M., HRUBÝ, D., LUKÁČ, O. Odometry in Navigation of Autonomous Mobile Robots, 1st ed., ser. 1. Slovakia: SUA Nitra, Slovakia, vol. 1, Oct. 2013.
2. OLEJÁR, M. Implementation Possibilities of Control Surfaces of Fuzzy Controller to Central Control System of the Mobile. 2017. Habilitation thesis. Slovak university of agriculture (Nitra, Slovakia), Faculty of engineering, Department of Electrical Engineering, Automation and Info rmatics. (Možnosti implementácie riadiacich plôch fuzzy regulátora do centrálneho riadiaceho systému mobilného robota).
3. SICILIANO, B., ET. AL., (2009). Robotics modelling, planning and control. 2009. London: Springer, pp 29-31, doi:10.1007/978-1-84628-642-1.
4. TZAFESTAS, S. 2014. Chapter 2. Mobile Robot Kinematics. In Introduction to Mobile Robot Control. Athenes, Elsevier, pp. 31-67. ISBN 9780124170490.
5. ZADEH, L.A., 1965, "Fuzzy Sets", Inform. and Control, 8:338–353.
6. CVIKLOVIČ, V., OLEJÁR, M., HRUBÝ, D., PALKOVÁ, Z., LUKÁČ, O., HLAVÁČ, P. 2016. Navigation algorithm using fuzzy control method in mobile robotics. In Acta technologica agriculturae. ISSN 1335-2555, 2016, vol. 19, no. 1, s. 19-23.
7. YAHMEDI, A. – FATMI, M. 2011. Fuzzy Logic Based Navigation of Mobile Robots [online]. In Recent Advances in Mobile Robotics, pp. 287-310. ISBN 978-953-307-909-7. Available on: <http://cdn.intechopen.com/pdfs/24926/InTechFuzzy_logic_based_navigation_of_mobile_robots.pdf >
8. HRUBÝ, D. – AMRICH, M.: 2008. Application of control algorithms in agricultural conditions. (Aplikácie fuzzy riadiacich algoritmov v poľnohospodárskej praxi). Monograph. Nitra: SUA, 2008, 123s.
9. ABDELMOULA, C. - ROUABEH, H. – MASMOUDI, M.: Behavior control of a new designed mobile robot based on fuzzy logic and neuro fuzzy approaches for monitoring wall. International Journal of Intelligent Engineering & Systems, vol. 6, no. 3, pp. 17–26, 2013.

Corresponding author:

Ing. Dominik Horňák, Department of Electrical Engineering, Automation and Informatics, Faculty of Engineering, Slovak University of Agriculture in Nitra, Tr. A. Hlinku 2, 949 76, Nitra, Slovakia, mob: +421905112863, email: xhornakd@uniag.sk

Spruce carbon footprint assessment

L. Jeníček[1]

[1]*Department of Mechanical Engineering, Faculty of Engineering, Czech University of Life Sciences Prague, Prague, Czech Republic*

Abstract

This article is talking about carbon footprint of a spruce fuel products, common natural fuel not only for cottagers in Czech Republic. Main concern is taken to the analysis of the regulatory background before the actual tests and chemical analysis can start.

Key words: Carbon footprint, emissions, greenhouse gas, spruce, wooden pellets, woodchip, torificate, renewable energy sources

INTRODUCTION

Regulation 2018/1999 of the European Parliament and of the Council[1] on the governance of the Energy Union and climate action sets, inter alia, a Europe-wide target of reducing greenhouse gas emissions of 43% compared to 2005 and increasing the share of Renewable Energy Sources (RES) in gross final consumption of energy at 32% by 2030.

According to the prepared National Plan[2], the Czech Republic's goal is to reduce greenhouse gas emissions by 30% by 2030 (compared to 2005) and to increase the share of RES in gross energy consumption to 22%.

Following the statistics of Global Carbon Project[3] organization, Czech Republic was on 27th position in global ranking out of all 221 countries with average consumption 10.4mt of CO_2/capita in 2015.

Comparison with the neighbouring countries that are in similar natural conditions gives us a big warning. Slovakian average carbon footprint is 7.0 mt/capita; German 9.1 mt/capita; Austrian 8.2 mt/capita and even Polonia, country well known for consistent usage of coal power plants, 8.8 mt/capita.

MATERIALS AND METHODS

Goal of this paper is to analyse the National and European statistical sources to bring more clarity on the emission sources in Czech Republic and its possible reduction.

As a next step, carbon footprint of different forms of spruce wood used as an energy source will be evaluated. Emissions CO2 will be measured by flue gas analyser GA-60 whose principle is based on the use of electrochemical transducers. The following flue gas components will be analysed: oxygen (O2), carbon monoxide (CO), nitric oxide (NO), nitrogen dioxide (NO2), sulphur dioxide (SO2) and hydrogen chloride (Cl) and from the results Carbon footprint will be calculated for:

- Spruce logs
- Spruce woodchip,
- Spruce pellets (Lyčka, 2011)[4] and
- Spruce pellets combined with torrefacted material in various shares

Results of the analysis will be compared with other researches. See in Table 2 a research analysing the emission of European Spruce (Malaťák, Vaculík, 2008)[5].

Tab. 1 Chemical analysis of European/Norway Spruce - Picea abies

Sample (% of weight)	**Carbon**	**Hydrogen**	**Nitrogen**	**Sulphur**	**Oxygen**	**Chlorine**	**Combustion heat ($MJ.kg^{-1}$)**
Spruce wooden pellets	47.37	6.40	0.19	0.01	36.20	0.04	18.74
Spruce bark pellets	43.70	4.98	0.13	0.04	39.28	0.02	17.48
Brown coal - reference	42.31	4.24	0.58	3.85	7.81	0.076	17.23

Carbon footprint will be calculated using the standard ISO 14067:2018 Greenhouse gases[6].

Carbon footprint results will be compared with national legislative and ongoing subsidies.

RESULTS AND DISCUSSION

Field of energetics, which mainly consists of electricity production and heating has a major impact on CO_2 emission of Czech Republic, therefore also on carbon footprint as can be seen in Fig. 1.

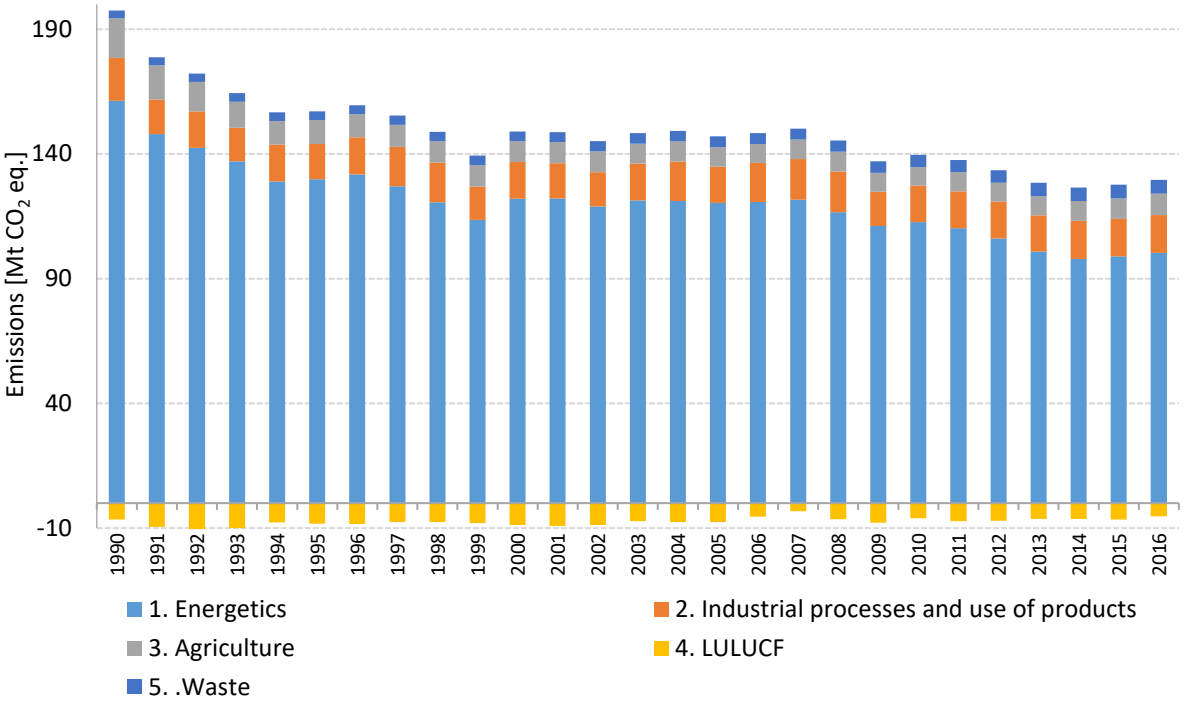

Fig. 1 CO2 emission development in Czech Republic; Source: ČHMÚ

There is a positive development in the field of energetics over time as can be seen in Fig. 2, on the right side. Coal usage has been replaced significantly by natural gas and Renewable Energy Sources (RES) in last three decades. But, to lower the carbon footprint, the transition from coal to more enviromentally friendly sources must be deepen.

Information of who is using which energy sources can be seen on the left side. Renewable Energy Sources are used the most by households, coal by the industry.

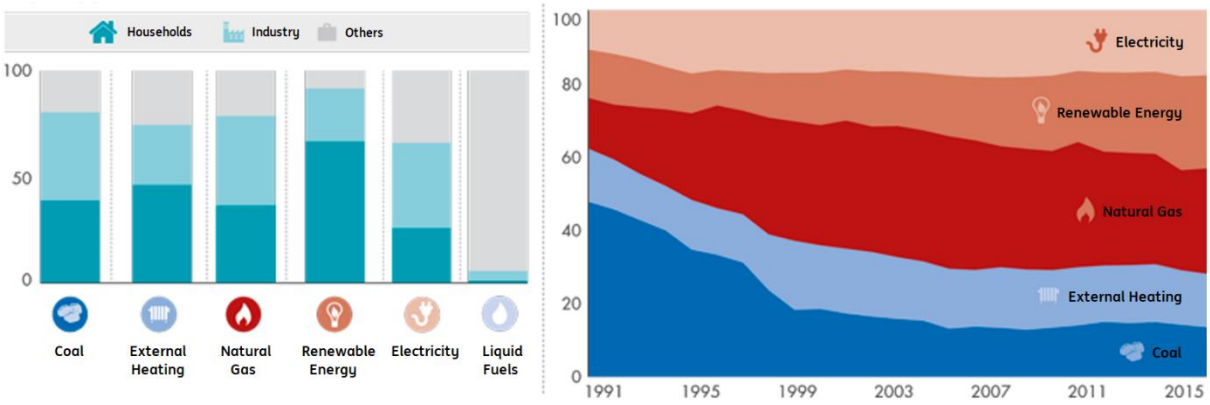

Fig. 2 Distribution of fuel consumption in Czech Republic in 2015; Source: Czech Statistical Office

The disintegration of energy sources is visible on Fig. 3. Coal and RES are used mainly for heating, electricity is shared between heating, boiling, cooking, lightning, cooling and other usage.

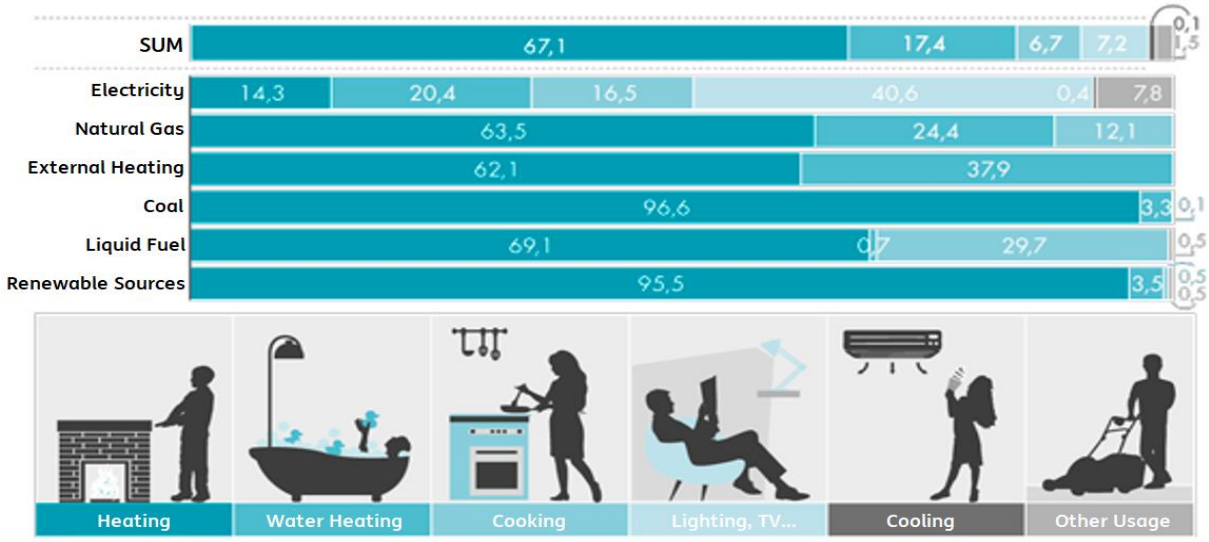

Fig. 3 Energy consumption disintegration; Source: Czech Statistical Office

Information that RES is used mainly for heating in Czech households is useful for the interpretation of the following Table 1. Out of the RES, ca 62 % consist of domestic biomass, represented mainly by wood, wooden chips, wooden pellets and briquets. It is expected that domestic biomass will cover 56 % of RES in 2030. Combining with the information from previous Graph 3 that RES covers 25.3 % of energy sources of households, Domestic biomass can be then interpreted as energy source for 16 % (25.3 x 0.62) of average households.

Tab. 2 RES expected development in the area of heating/cooling (TJ)

RES consumption	2016	2020	2021	2022	2023	2024	2025	2026	2027	2028	2029	2030
Domestic biomass	75 454	74 395	76 198	78 002	79 806	81 610	83 414	85 218	87 022	88 826	90 630	92 434
Non-domestic biomass	26 631	27 561	31 284	31 676	33 614	33 900	34 836	35 097	35 220	35 269	35 318	36 723
Biodegradable municipal waste	2 418	2 690	4 701	5 110	5 600	6 008	6 008	6 008	6 008	6 906	6 906	6 906
Biogas station	7 489	7 595	7 510	7 736	8 146	8 461	8 902	9 571	10 627	11 494	12 371	13 250
Heat pump	4 441	6 621	7 166	7 710	8 255	8 800	9 345	9 890	10 435	10 979	11 524	12 069

Geothermal energy	0,0	310	310	310	310	310	310	960	1 122	1 285	1 447	1 610
Solar panel	787	1 048	1 109	1 169	1 227	1 284	1 339	1 393	1 445	1 498	1 552	1 606
SUM	117 220	120 222	128 281	131 716	136 960	140 376	144 156	148 139	151 882	156 259	159 750	164 599

Source: Ministry of industry and trade Czech Republic[2]

The subsidy program known as „Kotlíkové dotace“ was announced by the Ministry of the Environment of the Czech Republic within the Operational Program Environment 2014–2020. Homeowners can apply for a financial contribution to replace old, non-ecological solid fuel boilers by a new more ecological one.

New boilers are designed to be compliant with Commission Regulation[7] and are mostly powered by wooden pellets/chips, or wooden/coal biogas.

CONCLUSION

Both national and European leaders are trying to lower production of greenhouse gases by implementing new rules and recommendations into legislation in all possible areas. Major producer of greenhouse gases is the field of energetics. This field will be deeply analysed in the next article, focusing on the utilization and carbon footprint of domestic biomass, namely spruce pellets, woodchip etc.

REFERENCES

1. Regulation (EU) 2018/1999 of the European Parliament and of the Council of 11 December 2018 on the Governance of the Energy Union and Climate Action, amending Regulations (EC) No 663/2009 and (EC) No 715/2009 of the European Parliament and of the Council, Directives 94/22/EC, 98/70/EC, 2009/31/EC, 2009/73/EC, 2010/31/EU, 2012/27/EU and 2013/30/EU of the European Parliament and of the Council, Council Directives 2009/119/EC and (EU) 2015/652 and repealing Regulation (EU) No 525/2013 of the European Parliament and of the Council (Text with EEA relevance.), PE/55/2018/REV/1. Available at: http://data.europa.eu/eli/reg/2018/1999/oj
2. Vnitrostátní plán České republiky v oblasti energetiky a klimatu, 2019. Available at: https://www.mpo.cz/cz/energetika/strategicke-a-koncepcni-

dokumenty/verejna-konzultace-k-vnitrostatnimu-planu-ceske-republiky-v-oblasti-energetiky-a-klimatu--250509/

3. Global carbon project. Available at: https://www.globalcarbonproject.org/
4. LYČKA, Zdeněk. Dřevní peleta, aneb, Peleta mýtů zbavená. Krnov: LING Vydavatelství, 2011. ISBN 9788090491403
5. MALAŤÁK, Jan a Petr VACULÍK. Biomasa pro výrobu energie. Praha: Česká zemědělská univerzita v Praze, 2008. ISBN 9788021318106.
6. ISO 14067:2018 Greenhouse gases — Carbon footprint of products — Requirements and guidelines for quantification, 2018.
   Available at: https://www.iso.org/obp/ui/#iso:std:iso:14067:ed-1:v1:en
7. Commission Regulation (EU) 2015/1189 of 28 April 2015 implementing Directive 2009/125/EC of the European Parliament and of the Council with regard to ecodesign requirements for solid fuel boilers.
   Available at: https://op.europa.eu/en/publication-detail/-/publication/8809cda2-2f6e-11e5-9f85-01aa75ed71a1/language-en

Corresponding author:
Ing. Lukáš Jeníček, Department of mechanical engineering, Faculty of Engineering, Czech University of Life Sciences Prague, Kamýcká 129, Praha 6, Prague, 16521, Czech Republic, tel: +420724127798, email: jenicekl@tf.czu.cz

Vegetation indices utilization for poppy seed development monitoring

Z. Jelínek[1], K. Starý[1], J. Kumhálová[1]

[1]Department of Machinery Utilization, Faculty of Engineering, Czech University of Life Sciences Prague, Prague, Czech Republic

Abstract

This article is concentrated on the comparison of various vegetation indices of poppy, planted in conventional system of agriculture. For this study, the Sentinel 2 images with a spatial resolution of 10m/pixel were chosen and processed in GIS software. There were chosen several vegetation indices to compare overall condition, health and development of the poppy plants. The data from Sentinel 2 were chosen from five various terms during the vegetation period. Three vegetation indices were derived from Sentinel 2 satellite images with the utilization of SNAP software: Green ration vegetation index (GRVI), Green normalized difference vegetation index (GNDVI) and Chlorophyll index green (CIG). The results of the comparison proved that the GRVI and CIG indices prove more accurately the real crop condition in compare with the GNDVI, which is more affected by the phenological phases of the poppy seed development.

Key words: poppy seed, vegetation indices, satellite imagery, Sentinel 2A

INTRODUCTION

Remote sensing and crop monitoring is widely used in agriculture for planning the agriculture operations, health and development of crops monitoring and yield prediction. The crop growth monitoring belongs to the most important tasks in agronomy. The results could help to analyse the crop growth process and the conditions (Yang et al., 2015). There are several remote sensing methods, but for agriculture purposes there are three widespread methods: satellite, aerial and ground based. For the remote sensing of the poppy seed field the satellite images were utilized. Satellite methods are able to help with the crop yield estimation, the chlorophyll and nitrogen content estimation, etc. (Vincini et al., 2016). The disadvantage of satellite imagery is its limited spatial resolution in compare with other methods. (Kumhálová et al., 2014)

Poppy seed planting has a long tradition in Czech Republic and the country belongs to one of the most important poppy planter in the world. The poppy was planted on more than 26 000 hectares in 2018. In the previous decade, the poppy was planted on up to 70 000 hectares, but

the low purchase prices for the poppy decreased the planted area on the current situation, which is relatively stable for last 7 years ("Food and Agriculture Organization of the United Nations", 2020), ("Soupis ploch osevů - k 31. 5. 2018", 2018).

Regardless on the sensed object, the main task in the remote sensing is the green object identification. There are several options how to identify greenness in a crop image. The most common method is to use the spectral indices (Guijarro et al., 2011). In the agricultural there are many indices used for the crop analysis, the majority of the indices is used for specific purposes. The indices are based on a color scale where the low and high index values are recognized. The result is, that the sensed area is divided in zones with various colors depending on the index values (McKinnon & Hoff, 2017). For the poppy seed analysis Green ration vegetation index (GRVI), Green normalized difference vegetation index (GNDVI) and Chlorophyll index green (CIG) were chosen. Motohka et al. (2010) conducted a research where the GRVI index was evaluated as a phenological indicator. According to the resulsts, the GRVI index can differentiate between green vegetation, water and soils. They also proved that this index is sensitive to the leaf color change. It determines the index for monitoring phenological changes and indicate plant disturbances. The GNDVI is together with NDVI are well established spectral reflectance indicators of crop environmental stress (Tucker, 1979). According to Gitelson et al. (1996) the GNDVI overcomes the issues of saturation in compare with NDVI at later grow stages. The GNDVI substitutes the red band in the NDVI with the green band and therefore is more useful in later phenological stages when the leaf area is moderately high. This determins the index suitable for measuring within longer vegetation period. The CIG was proposed for the chlorophyll content estimation and it was proved that this vegetation index is a good indicator of canopy chlorophyll content. (Wu et al., 2012)

MATERIALS AND METHODS

Study area

The experiment took part in Lupofyt s.r.o. near Lišany village in Central Bohemia region, Czech Republic (50°9'34.494"N, 13°44'13.616"E). The experimental field has 18.95 ha with the average altitude 349.26 m.

Satellite images processing

For the measurement the datasets from Sentinel 2A were utilized. Sentinel 2A has 13 reflective wavelengths (433 nm to 2190 nm) and it has 20.6° field of view. The satellite senses 290 km swath from the 786 km polar orbit and provides the global coverage every 10 days (Roy et al.,

2017). Satellite images were acquired from the Copernicus Open Access Hubwere processed in SNAP desktop software (Brockmann Consult, SkyWatch). Edited images were then processed in QGIS SW (Free Software Foundation, Inc., Boston, MA, USA). Selected indices (see Table 1) were calculated from the edited satellite image for every data.

Table 1: Selected spectral indices

Spectral Index	Algorithm	References
Green Ration Vegetation Index	$GRVI = \frac{\rho_{green} - \rho_{red}}{\rho_{green} + \rho_{red}}$	(Motohka et al., 2010)
Green normalized difference vegetation index	$GNDVI = \frac{(NIR-GREEN)}{(NIR+GREEN)}$	(Cicek et al., 2010)
Green chlorophyll index	$CIG = \frac{NIR}{GREEN-1}$	(Cao et al., 2015)
Where NIR= Near Infrared Reflectance		

RESULTS AND DISCUSSION

Table 2: Average of selected vegetation indices values of spectral indices GRVI, CIG and GNDVI

Spectral Index	24.05.2019	3.06.2019	8.06.2019	13.06.2019	28.06.2019
Green Ration Vegetation Index	2.16	4.75	3.95	5.25	
Green chlorophyll index	1.16	3.40	4.25	3.40	3.75
Green normalized difference vegetation index	0.36	0.64	0.59	0.66	

Table 2 showed values of average of selected spectral indices GRVI, CIG and GNDVI in year 2019 based on methods of remote sensing. Average vegetation indices values of spectral indices GRVI is 2.16-5.25 and is similar as in spectral indices CIG, there are values 1.16 – 4.25. The highest value is found for GRVI, i.e. 5.25. Spectral indices GNDVI was almost constant at all times with insignificant growth.

Development trend of poppy crop can be seen in the figure 1. Trend of spectral indices GNDVI showed almost constant trend beside spectral indices GRVI and CIG.

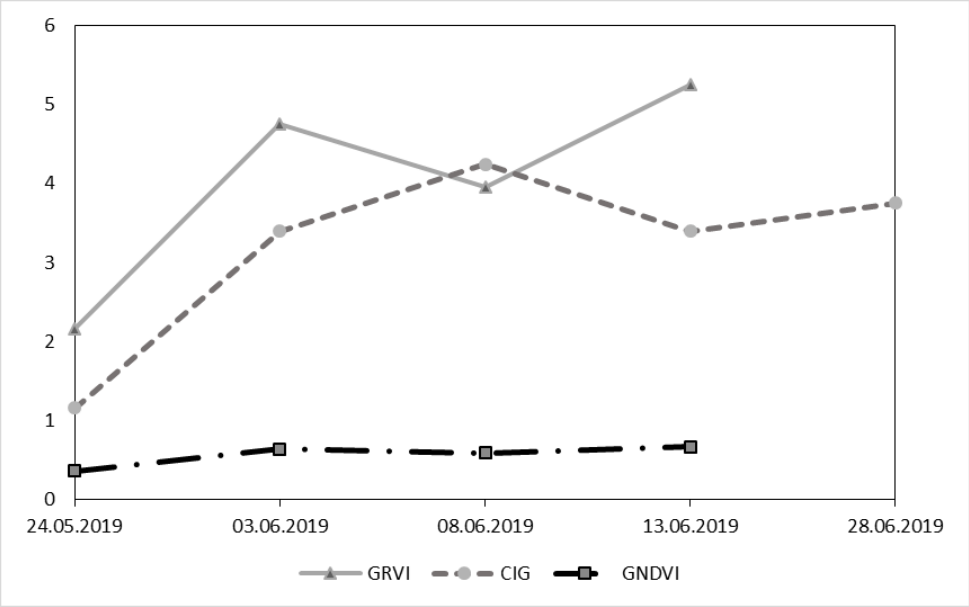

Figure 1: Average vegetation indices values

Table 3: Deviation of selected vegetation indices of spectral indices GRVI, GNDVI and CIG

Spectral Index	24.05.2019	3.06.2019	8.06.2019	13.06.2019	28.06.2019
Green Ration Vegetation Index	0.35	0.98	0.73	1.25	
Green chlorophyll index	0.35	1.03	1.25	1.03	0.98
Green normalized difference vegetation index	0.07	0.07	0.06	0.08	

Table 3 showed values of Deviation of selected vegetation indices of spectral indices GRVI, GNDVI and CIG in year 2019 based on methods of remote sensing. Deviation vegetation indices values of spectral indices GRVI is 0.35-1.25 and is similar as in spectral indices CIG, there are values 0.35 – 1.25. The highest value is found for GRVI, i.e. 1.25 and same value for CIG, i.e. 1.25. Spectral indices GNDVI was almost constant at all times with insignificant growth.

Development trend of poppy crop can be seen on the figure 2. Trend of spectral indices GNDVI showed almost constant trend beside spectral indices GRVI and CIG. Values of spectral indices GNDVI are 0.06 – 0.08.

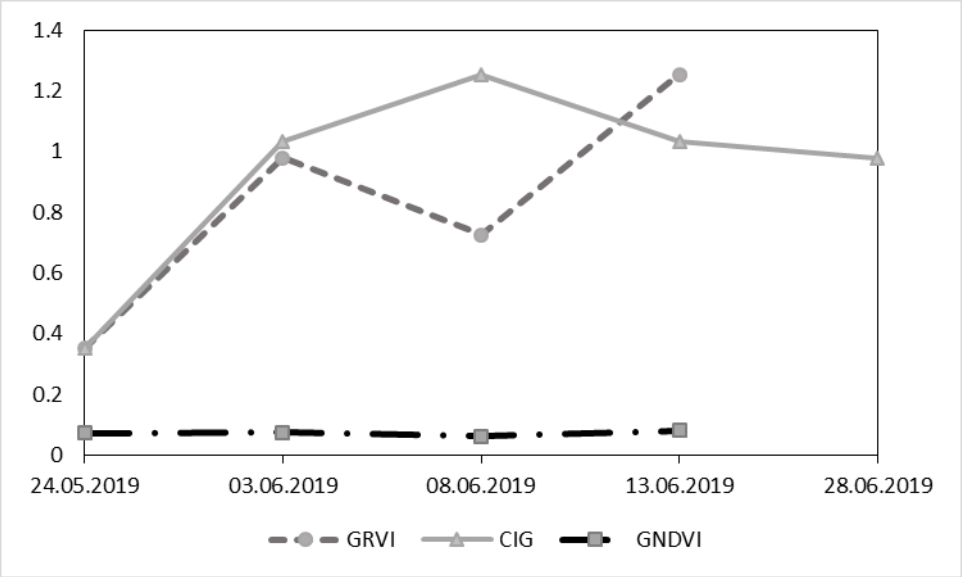

Figure 2: Deviation of selected vegetation indices

The Czech Republic is one of the most important poppy growers in the world. These results showed usability methods of remote sensing for evaluation crop condition, but Domínguez et al. (2017) found, that spectral indices are more accurate for cereals than other crops, also Jelínek et al. (2019) found it, that according to Sentinel 2 image to estimate crop structure from 96% for cereals, specially winter wheat. Our research confirmed usability spectral indices GRVI and CIG for poppy, but spectral indices GNDVI did not prove usability for poppy, because of different plant structure of poppy.

CONCLUSION

The utilization of vegetation indices for poppy seed has its benefits. In this measure three various vegetation indices with the green part of spectrum and wavelength 0.52- 0,60 μm were utilized. The standard deviation and average analysis were used for the process modelling. The results proved that the course of the GRVI and CIG is similar and takes on values 1.10 – 5.30 for the average values and 0.30 – 1.30 for the standard deviation. In compare with these indices, the GNDVI has the values 0.30 – 0.70 for the average and 0.07 – 0.09 for the standard deviation. Vegetation indices GRVI and CIG prove more accurately the real crop condition in compare with the GNDVI, which is more affected by the phenological phases of the poppy seed development.

ACKNOWLEDGEMENTS. This study was supported by Czech University of Life Sciences Prague, when conducted under grant IGA no. 2020:31160/1312/3110. The authors would like to thank to Lupofyt s.r.o. for their time, inputs data and provided experimental field.

REFERENCES

1. Cao, Q., Miao, Y., Feng, G., Gao, X., Li, F., Liu, B., Yue, S., Cheng, S., Ustin, S., & Khosla, R. (2015). Active canopy sensing of winter wheat nitrogen status: An evaluation of two sensor systems. *Computers and Electronics in Agriculture, vol. 112*, 54-67. https://doi.org/10.1016/j.compag.2014.08.012
2. Cicek, H., Sunohara, M., Wilkes, G., McNairn, H., Pick, F., Topp, E., & Lapen, D. (2010). Using vegetation indices from satellite remote sensing to assess corn and soybean response to controlled tile drainage. *Agricultural Water Management, vol. 98*(issue 2), 261-270. https://doi.org/10.1016/j.agwat.2010.08.019
3. Domínguez, J.A., Kumhálová, J., Novák, P. 2017. Assessment of the relationship between spectral indices from satellite remote sensing and winter oilseed rape yield. Agronomy Research, 15(1), 055-068.
4. Food and Agriculture Organization of the United Nations. (2020). http://www.fao.org/faostat/en/#data/QC/visualize
5. Guijarro, M., Pajares, G., Riomoros, I., & Herrera, P. (2011). Automatic segmentation of relevant textures in agricultural images. *Computers and Electronics in Agricilture, 75*(1), 75-83. https://www-sciencedirect-com.infozdroje.czu.cz/science/article/pii/S0168169910001924?via%3Dihub
6. Jelínek, Z., Starý, K., Kumhálová, J. 2019. Assessment of production zones modelling accuracy based on satellite imaging and yield measurement of selected agriculture plot. Agronomy Research 17(2), 447-455.
7. Kumhálová, J., Zemek, F., Novák, P., Brovkina, O., & Mayerová, M. (2014). Use of Landsat images for yield evaluation within a small plot. *Plant, Soil and Environment, vol. 60*(No. 11), 501-506. https://doi.org/10.17221/515/2014-PSE
8. McKinnon, T., & Hoff, P. (2017). Comparing RGB-Based Vegetation Indices with NDVI For Drone Based Agricultural Sensing. In *AgEagle*. agribotix.com/wp-content/uploads/2017/05/Agribotix-VARI-TGI-Study.pdf
9. Motohka, T., Nasahara, K., Oguma, H., & Tsuchida, S. (2010). Applicability of Green-Red Vegetation Index for Remote Sensing of Vegetation Phenology. *Remote Sensing, vol. 2*(issue 10), 2369-2387. https://doi.org/10.3390/rs2102369
10. Roy, D., Li, J., Zhang, H., Yan, L., Huang, H., & Li, Z. (2017). Examination of Sentinel-2A multi-spectral instrument (MSI) reflectance anisotropy and the suitability of a general method to normalize MSI reflectance to nadir BRDF adjusted reflectance. *Remote Sensing of Environment, vol. 199*, 25-38. https://doi.org/10.1016/j.rse.2017.06.019
11. Soupis ploch osevů - k 31. 5. 2018. (2018). In *AGRÁRNÍ KOMORA České republiky*. http://www.akcr.cz/data_ak/18/k/Stat/Osevy180531.pdf
12. Tucker, C. (1979). Red and photographic infrared linear combinations for monitoring vegetation. *Remote Sensing of Environment, vol. 8*(issue 2), 127-150. https://doi.org/10.1016/0034-4257(79)90013-0
13. Vincini, M., Calegari, F., & Casa, R. (2016). Sensitivity of leaf chlorophyll empirical estimators obtained at Sentinel-2 spectral resolution for different canopy structures. *Precision Agriculture, vol. 17*(issue 3), 313-331. https://doi.org/10.1007/s11119-015-9424-7

14. Wu, C., Niu, Z., & Gao, S. (2012). The potential of the satellite derived green chlorophyll index for estimating midday light use efficiency in maize, coniferous forest and grassland. *Ecological Indicators, vol. 14*(issue 1), 66-73. https://doi.org/10.1016/j.ecolind.2011.08.018
15. Yang, W., Wang, S., Zhao, X., Zhang, J., & Feng, J. (2015). Greenness identification based on HSV decision tree. *Information Processing in Agriculture*, *2*(3-4), 149-160.

Corresponding author:

Ing. Zdeněk Jelínek, Department of Machinery Utilization, Faculty of Engineering, Czech University of Life Sciences Prague, Kamýcká 129, Praha 6, Prague, 16521, Czech Republic, tel: +420 773 757 896 , email: zdenek.jelinek@pekass.eu

The Study of Factors Affecting the Efficiency of the Universal Finishing Machine UDS 214

M. Jůza[1], P. Heřmánek[1],

[1]Department of Agricultural Machines, Faculty of Engineering, Czech University of Life Sciences Prague, Prague, Czech Republic

Abstract

The paper deals with the evaluation of the operational performance of the multi-purpose telescopic excavator UDS 214 on the Tatra 815 chassis and its performance parameters. Construction machinery is constantly subjected under ever-increasing demands on the working efficiency, the maintainability, operating costs, and also on the low fuel consumption. Therefore, in order to meet these ever-increasing requirements, it is necessary to use a hydraulic circuit on these machines. Furthermore, this work describes the method of measuring hydraulic circuits on the UDS 214 excavator with two combined gauges, which are able to measure the flow rate, pressure and temperature of the hydraulic oil at a given moment. For each hydraulic circuit of the UDS 214, the hydraulic oil flow values between the pump and the manifold were first measured and then between the manifold and the appliance. The hydraulic circuit can be simply imagined and divided into individual components, which separately affect the energy losses in the flowing hydraulic oil.

Key words: excavator, hydraulic, flow rate, performance

INTRODUCTION

In practice, the working performance of a shovel excavator depends on many factors. Such as the working cycle time, the type and volume of the working shovel, the soil loosening coefficient, the filling factor of the working shovel, the digging depth, the angle of rotation, the method of emptying and also the condition of the cutting edge. It should be noted that the working cycle time affects the excavator performance the most. In the case of shovel excavators, the time required to fill the shovel to the maximum volume, lift the shovel to the discharge height, turn the machine with a full shovel, emptying the shovel to a transport device, turn the machine with an empty shovel, and shift down the shovel to its origin position. (ŠTĚRBA et al., 2013)

The UDS 214 telescopic excavator on a three-axle Tatra 815 chassis is designed for finishing earthworks and, with the use of suitable additional equipment, also for excavation and other earthworks (excavation of foundation trenches, canals, construction and maintenance of utility networks). (JŮZA, 2017)

At present, the UDS 214 telescopic excavator is used for the mining of soil of the I. and II. Classes (ČSN 73 6133, 2010). The excavator is also suitable for dealing with the consequences of emergencies such as floods, landslides and also statically disturbed buildings. The machine can also be equipped with a micro-carriage. It can therefore work in two modes: "work" mode - work activity of the swing body; "drive" mode - allows control of the Tatra 815 car chassis move (for crossings on the construction site) as well as the control the stabilization supports directly from the cab, without the need to start the Tatra 815 chassis engine. (JŮZA, 2017)

Fig. 1 Telescopic excavator UDS 214 on a Tatra 815 chassis during practical testing of working cycle time

MATERIALS AND METHODS

The power unit of the UDS 214 telescopic excavator is an inline four-stroke liquid-cooled four-cylinder John Deere 4045 diesel engine with direct fuel injection, which has the power of 94 kW at 2200 rpm. The engine drives the Bosch Rexroth A8 VO 107 double axial piston pump, which supplies the pressurized hydraulic oil to the hydraulic circuits of the excavator's working movements via a seven-section Bosch Rexroth 7M8 - 22 mono-bloc manifold, allowing the UDS 214 telescopic excavator to perform five basic tool movements:

- extending and retracting the inner telescopic arm,

- raising and lowering the telescopic boom,
- turning the working tool (using the swivel head),
- opening and closing the working tool,
- turning the swing body of the UDS 214 excavator. (JŮZA, 2017)

Fig. 2 Bosch Rexroth A8 VO 107 double axial piston pump (BOSCH REXROTH, 2019)

Because the operator does not use the hydraulic circuit for turning the working tool, which is used only for special operations such as sloping, and this movement is not included in the standard scheme of the excavator work cycle. Therefore, the hydraulic system for turning the working tool was not tested in this study.

The measurement of the hydraulic oil flow rate in the hydraulic circuits of the UDS 214 telescopic excavator was realized in the facility of the cooperating company Vladimír Jůza - Hydraulický servis. The measurement was performed by two combined gauges, which are able to measure the pressure, the flow rate and the temperature of the hydraulic oil at a given moment. The analog meter OTC H50 has been borrowed from the cooperating company, the second one, the digital meter Hydrotechnik GmbH was borrowed from the Department of Agricultural Machinery. Both meters are able to measure the flow rate in the range of 0 – 200 $dm^3 \cdot min^{-1}$, the pressure in the range of 0 – 40 MPa and the temperature in the range of 0 – 120 °C. Both gauges were connected by hydraulic pressure hoses and included into the examined hydraulic circuit during the measurement.

For the each examined hydraulic circuit, measurements were realized firstly between the pump and the manifold and then between the manifold and the appliance. In this case, a linear hydraulic motor or a rotary hydraulic motor is meant as an appliance. (EXNER et al., 1991)

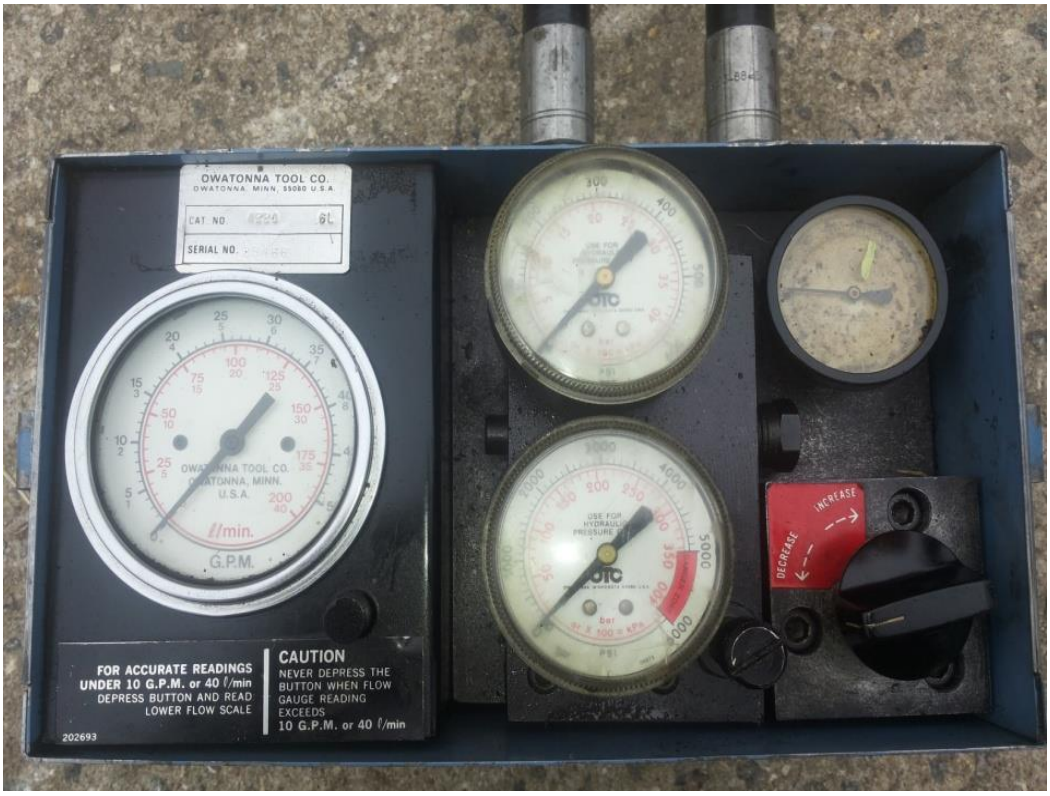

Fig. 3 Combined OTC H50 gauge for measuring pressure, flow rate and temperature

Fig. 4 Connection of the analog meter OTC H50 and the digital meter from Hydrotechnik into the examined hydraulic circuit (measurement at the beginning of the hydraulic circuit)

The given hydraulic circuit in which the measurement took place was loaded by means of a throttle valve, which is a part of the analog meter OTC H50, in such a way that the required maximum pressure is set on this meter up to the setting pressure of the safety valve. The second digital meter from the Hydrotechnik recorded in its memory the measured values of the pressure, the flow rate and the temperature of hydraulic oil in the given hydraulic circuit, where the measurement took place.

Because all hydraulic circuits for controlling the working movements of the UDS 214 are a source of pressurized hydraulic oil from the Bosch Rexroth A8 VO 107 double-acting axial piston pump, the cooperation of three workers was necessary during each measurement. One was sitting in the operator's cab, adjusted the speed of the John Deere 4045 internal combustion engine and set the joystick according to which hydraulic circuit was being tested to tilt the double control axial piston pump. The second one operated the combined analog meter OTC H50 and set the required pressure at which the measurement took place by a throttle valve. The third worker operated the digital combined meter Hydrotechnik, set a time interval on the meter for recording the measured data and wrote the measured data into prepared tables, to back up the measured data for case of failure of the digital combined meter.

RESULTS AND DISCUSSION

The measurement itself was very time consuming, because it was always necessary to disconnect the functional hydraulic circuit and integrate into it the combined meters. Therefore, the substantial losses of excavator hydraulic oil occurred, which then had to be refilled. When everything was ready for testing, the one single measurement took about 2 minutes, the hydraulic oil was heated to temperature of about 60 °C due to the throttling, and then it was necessary to stop testing and let the hydraulic oil cool down. During the testing, the following hydraulic circuits of the UDS 214 telescopic excavator were measured:

- hydraulic circuit for extending and retracting the inner telescopic arm,
- hydraulic circuit for raising and lowering the telescopic boom,
- hydraulic circuit for opening and closing the working tool,
- hydraulic circuit for turning of the UDS 214 excavator swing body.

The overall experiment represents a quite large set of measured data, which will be published in a journal article. Therefore, the only measured values from the hydraulic circuit for the telescopic boom stroke are presented in this paper.

Tab. 1 Measured data for the hydraulic circuit of the telescopic boom stroke (measured on the Bosch Rexroth A8 VO 10 double axial piston pump)

***p* [MPa]**	***Q* [dm^3·min^{-1}]**	***t* [°C]**
0	158	33.6
5	156	35.3
10	153.3	36.7
13	147	38.6
16	131.5	40.4
20	111.7	42
26	80.6	43.5
30	71.3	44.7

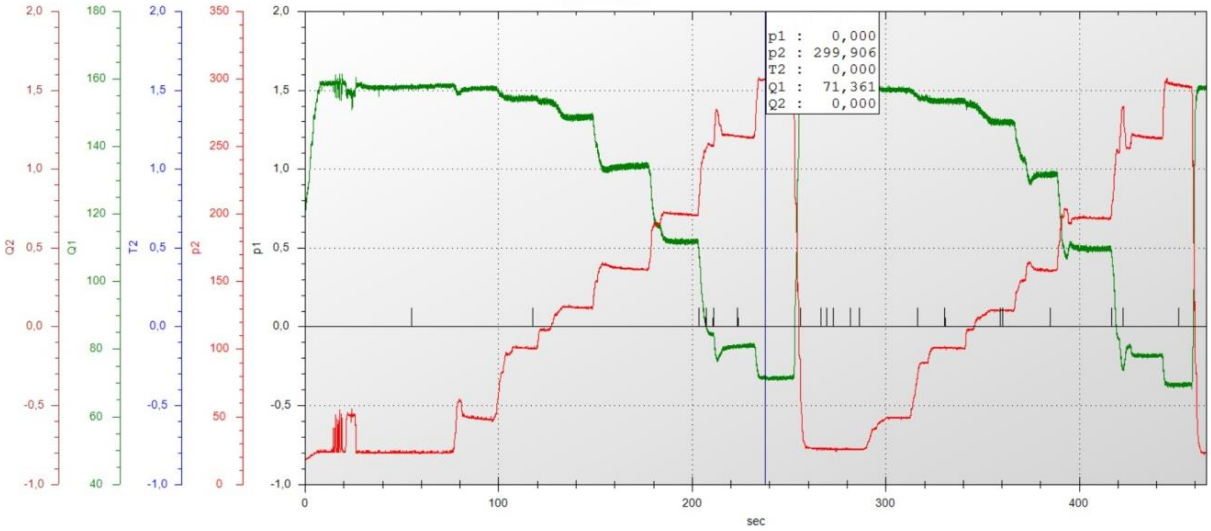

Fig. 5 Time dependency graph of the flow rate and pressure of hydraulic oil in the hydraulic circuit for the telescopic boom stroke (measured on the double axial piston pump Bosch Rexroth A8 VO 10) using the Hydrotechnik software

Tab. 2 Measured data for the hydraulic circuit of the telescopic boom stroke (measured near the input to the pair of linear hydraulic motors)

***p* [MPa]**	***Q* [dm^3·min^{-1}]**	***t* [°C]**
0	149	37.7
5	144	40.4
10	96.3	42.6
13	55	45.2
16	41.5	46.1
20	34.5	47.5
25	11.7	48.7

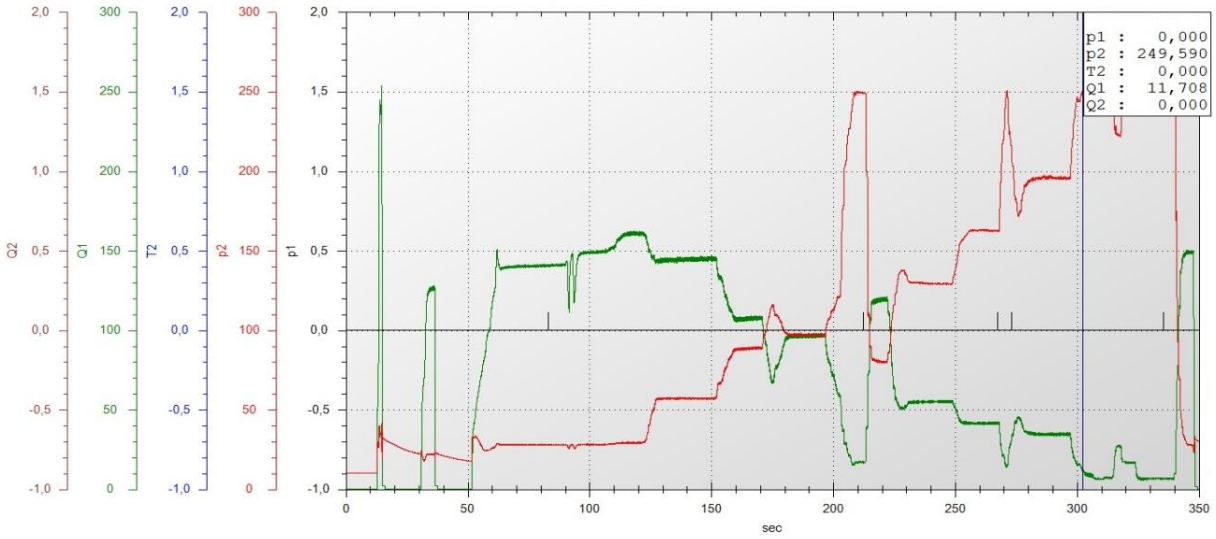

Fig. 6 Time dependency graph of the flow rate and pressure of hydraulic oil in the hydraulic circuit for the telescopic boom stroke (measured near the input to the pair of linear hydraulic motors) using the Hydrotechnik software

From the given measured values in the hydraulic circuit of the telescopic boom stroke, it is seemed that the measured values of the hydraulic oil flow rate when measured at the end of the hydraulic circuit, i.e. before the hydraulic oil enters the appliance, are several times lower than when measured at the beginning of the hydraulic circuit. This is caused by losses in the line, due to local hydraulic resistances and also by hydraulic losses that occur in individual components of the circuit. The quantification of these losses will be described in more detail in a reviewed journal article, which will develop the problem following to this paper.

To evaluate the operating performance of the UDS 214 excavator, it was firstly necessary to measure the average time of the excavator cycle and exactly follow the standard for the Theoretical Work Cycle according to ČSN 27 003 during this measurement:

- the initial position (the shovel is tilted to the maximum tilt angle and is leaned in the middle of the depth range by the teeth or the cutting edge on the opposite side of the mining pit),
- digging and rock picking (the shovel must be filled to the nominal volume),
- raising the shovel to the discharge height (minimum 3.5 m),
- turn of the rotating upper (with a full shovel by 90°),
- rock discharge (at a discharge angle of 45°),
- turn of the rotating upper (back by 90°),
- lowering (setting the shovel to the initial position).

During this practical testing, the average time of the UDS 214 working cycle was ***t*** = 25 seconds and the volume of the working shovel was ***V*** = 0.63 m^3. If we know these two quantities, it is possible to calculate the excavator theoretical performance, as follows.

$$Q_t = \frac{V}{t}\ [m^3 \cdot h^{-1}] \quad (1)$$

$$Q_t = \frac{0.63}{0.006945}$$

$$Q_t = 90.71\ m^3 \cdot\ h^{-1}$$

Then, the operating performance of the excavator $\boldsymbol{Q_p}$ can be calculated according to the formula. The individual coefficients were determined from the tables given for this calculation.

$\boldsymbol{k_p}$ – the shovel filling coefficient according to the rock detachability class (I. and II. Class, i.e. k_p = 0.99)

$\boldsymbol{k_o}$ – the operator qualification coefficient (good operator, i.e. k_o = 1.00)

$\mathbf{k_{ú}}$ – the coefficient of turning angle (90°, i.e. $k_{ú}$ = 1.08)

$\boldsymbol{k_{ol}}$ – the shovel wear coefficient (average wear, i.e. k_{ol} = 0.9)

$\boldsymbol{k_l}$ – the coefficient of the ratio of the shovel volume to the volume of the transport vehicle load space (ratio 6, i.e. k_l = 0.96)

$$Q_p = Q_t \cdot\ k_p \cdot k_o \cdot k_{ú} \cdot k_{ol} \cdot k_l\ [m^3 \cdot h^{-1}] \quad (2)$$

$$Q_p = 90.71 \cdot 0.99 \cdot 1 \cdot 1.08 \cdot 0.9 \cdot 0.96$$

$$Q_p = 83.8\ m^3 \cdot h^{-1}$$

The UDS 214 telescopic excavator has an operating capacity of $\boldsymbol{Q_p}$ = 83.8 m^3·h^{-1} in the original state of the hydraulic system and in the given operational and technical condition.

CONCLUSION

The main purpose of this paper was to evaluate the performance of the UDS 214 excavator on a Tatra 815 chassis in the state before the hydraulic system innovation. The result of the calculation of the operating performance of the machine shows that there is an enough space for innovation of the overall hydraulic circuit of the excavator, which should have a positive effect on increasing the existing performance of the machine. The partial aim of this paper was to measure the flow rates of hydraulic oil in hydraulic circuits of the excavator for controlling the working mechanisms, thanks to which will be better identified weaknesses in the hydraulic system of the machine and propose appropriate adjustments to increase the performance of the UDS 214 telescopic excavator.

REFERENCES

1. ŠTĚRBA, M., ČECH D., VENKRBEC V., MOTYČKA, V.: Design of basic construction machines for earthworks (in Czech). Rail road Magazine, Ostrava, 2013,
2. ČSN 73 6133.: Road earthwork - Design and execution (in Czech). Czech Office for Standards, Metrology and Testing, Prague, 2010,
3. BOSCH REXROTH, SPOL. S R.O.: Axial piston variable double pump A8VO. Bosch Rexroth, spol. s r.o., 2019,
4. JŮZA, M.: Comparison of the energy consumtion of the hydraulic control system of the universal finishing machine UDS 114 (in Czech). Prague, Czech University of Life Sciences Prague, Faculty of Engineering, 2017,
5. EXNER, H., et al.: Basic principles and Components of Fluid Technology. Lohr a. Main, Mannesmann Rexroth AG, 1991, ISBN 3-8023-0266-4

Corresponding author:

Michal Jůza, Department of Agricultural Machines, Faculty of Engineering, Czech University of Life Sciences Prague, Kamýcká 129, Praha 6, Prague, 16521, Czech Republic,
email: juzam@tf.czu.cz

Determining the degradation rate of retroreflective sheeting for traffic signs

M. Khrapova[1], D. Marčev[1], M. Růžička[1]

[1]Department of Vehicles and Ground transport, Faculty of Engineering, Czech University of Life Sciences Prague

Abstract

The article is focused on determining the degradation rate of retroreflective sheeting depending on the conditions of exposure. Ten types of retroreflective sheeting were examined under five different conditions. For one year, the one group of samples was stored in the dark closed box at constant room temperature; the second group was exposed to the natural weathering without solar radiation; the third group was exposed to the accelerated natural weathering including solar radiation, and the fourth group was in-service traffic signs. For all samples, the coefficient of retroreflection was measured by handled retroreflectometer before and after this experiment. Statistical analysis has determined the degree of degradation of retroreflective materials that were exposed to solar radiation. The influence of the material of the sign panel was also tested.

Key words: traffic sign sheeting, reflectivity of sheeting, solar radiation, accelerated natural weathering

INTRODUCTION

Vertical signage is one of the most important parts of the road infrastructure for regulating, warning, and guiding of road users (KOYUNCU et al. 2008), (FEDERAL HIGHWAY ADMINISTRATION, 2009), (BABIĆ et al. 2017). One of the most important challenges of traffic signs is providing drivers important preview time during night-time conditions (EUROPEAN UNION ROAD FEDERATION, 2016) in purpose to increase road safety.

The traffic signs are predefined to play their important role for road users they should meet four basic requirements. According to the International Commission on Illumination there are conspicuity, legibility, comprehensibility and credibility (INTERNATIONAL COMMISSION ON ILLUMINATION, 1988). To ensure compliance traffic signs with these requirements, they must be first and foremost well visible.

The brightness of the traffic sign ensures its visibility. Several studies focused on the relationship between the brightness of the sign and the reaction rate of the driver (KOYUNCU et al. 2008), (SCHNELL et al. 2009). Their results proved that “larger and

brighter signs are more efficient in transferring their message to the driver by reducing information acquisition time (SCHNELL et al. 2009)". The decrease in reaction time means the increase in road safety (UNDERWOOD et al. 2002). This statement is especially valid and important under dark conditions. However, it is not enough to make traffic signs as big as possible and with the highest level of brightness. In most cases, such kind of sign would have an adverse impact on the reaction time of a driver by decreasing the legibility of the sign.

Make a traffic sign retroreflective - is one of the ways how to increase its brightness without significantly increasing the dimensions of the sign. The coefficient of retroreflection R_A is taken as a unit of retroreflectivity for a traffic sign and it describes the amount of light returned at the certain specified entrance and observation angles.

The readability and accuracy of recognition of traffic signs are the key performance indicators of retroreflectivity. From the moment of the first patent for serial production of reflective signs (HELTZER et al. 1940) to the present, a large number of studies have been conducted to determine and identify the degree of influence of various factors on the reflective properties of signs. Aging and materials of the sign are some of them (KHRAPOVA, 2019).

Clearly, the sheeting age is one of the most significant variables affecting sign retroreflective performance (BLACK et al. 1992). However, the degradation rate of different types is not so obvious. The analysis of influence aging on the retroreflective properties is important since this factor is a basement for a minimum of retroreflective standards. The analysis of existing products on the market in the context of retroreflective properties provides guidance to local road agencies regarding the preferred use of retroreflective films.

The variability of existing results obtained by different authors (e.g. (RÉ et al. 2010), (JACKSON et al. 2013), (BABIC et al. 2017)) is so high that it is difficult to draw firm conclusions. According to the authors of this work, such ambiguous conclusions are caused by the fact that the aging of materials is influenced by many factors that should be considered separately in order to determine the impact on the retroreflectivity of each of them.

The aim of this paper is to determine the degradation rate of retroreflective sheeting under different conditions and for two types of material of sign panel. Nowadays in the world, the retroreflective sheeting is attached to Al or FeZn based sign panels. In the Czech Republic the Al sign panels are not commonly used.

MATERIALS AND METHODS

The 10 types of retroreflective sheeting produced by different manufacturers of white, red and yellow-green fluorescent were used in the study. Tab. 1 represents all test samples produced by three manufacturers - Avery Dennison (AD), Oralite (OR) and 3M.

Tab. 1 Test samples according to the class, manufacturer, colour and type. W – white, R – red, F – yellow-green fluorescent; GB – glass bead, M – microprismatic.

Class*	**Manufacturer and serial number**	**Colour**			**Type**
		W	R	F	
RA1	AD 1500	x			**GB**
	OR 5710	x	x		
	3M 3400	x	x		**M**
RA2	3M 3930	x			
RA3	3M 4083		x	x	
	3M 4090	x	x		

* - according to (*ČSN EN 12899-1 Stálé svislé dopravní značení - Část 1: Stálé dopravní značky*, 2003)

The research was divided into two groups in accordance with the studied factor – solar radiation and material of sign panel. In total, 8 groups of samples were formed according to the conditions in which the retroreflective sheetings were studied and the exposure time of samples (Tab.2). All retroreflective sheetings are self-adhesive, the type of adhesive depends on the manufacturer and type of sheeting.

The 20 samples of 10 types of retroreflective sheetings (without any sign panel) were measured by retroflectometer under the laboratory conditions (groups 6 and 8). Then half of samples (group 6) was applied on 1 millimetre thick FeZn panel (group 5), another half (group 8) was applied on 2 millimetres thick Al panel (group 7).

Then group number 5 were installed in the open air (garden) of the Faculty of Engineering of CULS Prague. The desk was inclined at an angle of - 45° in the way, that direct sunlight did not reach the retroreflective surface. These samples were exposed to natural weathering but without direct sun radiation. The samples were exposed to natural weathering for one year.

Another 20 samples of 10 types were applied on FeZn panels. The R_A was measured for all samples. One half of them were putted into the black box in the laboratory (group 4). The samples were not exposed to any meteorological influences or the influence of sunlight.

Tab. 2 The eight experimental groups of samples according to the studied factor, location, time of exposure, the material of sign panel.

Number of group	**1**	**2**	**3**	**4**	**5**	**6**	**7**	**8**
Factor	Solar radiation							
					Material of sign panel			
Location	Test-desk	Test-desk	In-service	Box	Garden	Laboratory	Garden	Laboratory
Number of samples	10							
Time of exposure (months)	22	12			12/-	–	12/-	–
Range of ambient temperature (°C)	–5–35			18–32	–5–35	20–28	–5–35	23–25
Range of relative humidity of air (%)	25–100			45	25–100	45	25–100	45
Orientation to the sun	South			–				
Material of sign panel	FeZn					–	Al	–

Another 10 samples were placed on the test desk that was installed on the roof of the Faculty of Engineering of CULS Prague. It was oriented face to the south and was inclined at an angle of +45° for the accelerated natural weathering. The samples were exposed to natural weathering for one year, then R_A for all samples was measured. The results of measurement formed group number 2. Then these samples were exposed to natural weathering for 10 months more. The data set of R_A after accelerated natural weathering for 22 month formed group number 1.

The group number 3 are 10 in-service traffic signs, located in Prague 6, Horoměřice in the Czech Republic and oriented to the south. Date of manufacture of road signs ranged from 2005 till 2017. Measurements were conducted in October 2018 and October 2019.

The measuring principle was the same for all test samples. The retroreflective sheeting was washed with water and dried before each measurement. The measurement of the coefficient of

retroreflection (R_A) was carried out acccording to the (ČSN EN 12899-1 Stálé Svislé Dopravní Značení - Část 1: Stálé Dopravní Značky, 2003) using handled retroreflectometer Zehnther 6060. The device also provided with information about the average value of three measurements of each sample. The difference between mean values of R_A before and after exposure of each individual sample is degradation rate (hereinafter „DR"). It was used for further analysis.

The „STATISTICA" software was used for all kind of statistical tests. Kolmogorov Smirnov and Shapiro Wilk W test was used to control normality of datasets. The parametric or non parametric test was done based on the results of these tests.

T-test for independent samples was used in order to determine whether there is a statistically significant difference in DR between two unrelated groups. T-test for dependent samples was used to control DR in different conditions but for one sample. The Wilcoxon test was chosen as non parametric test for the case when no normality of the data distribution was not found. The test analyzes if there is a statistically significantly difference in DR between two groups.

For all tests, the null and alternative hypotheses were defined as follows:

H_0: no difference in means of DR between two data sets.

H_1: the average values of DR between two data sets is significantly different.

The null hypothesis for the performed tests can be rejected if the obtained p-value is lower than 0.05.

RESULTS AND DISCUSSION

Kolmogorov Smirnov and Shapiro Wilk W test were done to control normality of measurements inside each group. The DR of each sample in the groups from number 5 till 8 was conformed to the assumptions of normality (Kolmogorov-Smirnov test, $P > 0.2$; Shapiro Wilk test W test, $P > 0.05$). Normality of the data distribution in another groups was not found.

Solar radition (UV radiation)

The series of Wilcoxon tests were carried out for groups from number 1 till numer 5 to find the relation between the amount of sunlight and degradation of materials. The results are representd as p-values in Tab. 3. Group 4 is DR for samples in box, group 5 – in the garden without sunlight, group 2 – on the test desk (accelerated weathering after 12 months), group 3 – in-service signs, group 1 – on the test desk (accelerated weathering after 22 months). The p-values are lower the alpha level for pairs of group 4–2, 4–1, 5–2, 2–3, 3–1. The null hypothsis is rejected for these tests that means there is statistiacly significant diference between pairs of groups.

Tab. 3 The summary of results the Wilcoxon tests represented as p-values for pairs of groups.

Number of test group	**4**	**5**	**2**	**3**	**1**
4		0.114	**0.01**	0.440	**0.025**
5	0.114		**0.005**	0.959	**0.048**
2	**0.01**	**0.005**		**0.036**	0.160
3	0.440	0.959	**0.036**		**0.017**
1	**0.025**	**0.048**	0.160	**0.017**	

From the results presented in Tab. 3, it can be concluded that there is no significant difference in DR of samples that were in the box, samples under natural weathering without sunlight and for in-service signs. Despite the absence of significant difference between the groups, the range of DR values is different.

The box plot of Fig. 1 more clearly demonstrates the range of values in five groups. Group 4 is DR for samples in box, group 5 – in the garden without sunlight, group 2 – on the test desk (accelerated weathering after 12 months), group 3 – in-service signs, group 1 – on the test desk (accelerated weathering after 22 months).

The DR of samples that were in the box is unexpected since presumably the degradation of sheeting after one year should be low – around 1-2%. The DR for glass bead sheeting was the highest – 4%. It was also unexpected that there was no significant difference between samples that were not under direct sunlight and in-service traffic signs. This fact can be explained that the DR of is not a linear function it decreases with time, see (KHRAPOVA et al. 2019). The traffic signs were in service more than 16 months. That is why the degradation rate is in the range from 1% to 9% (Fig. 1).

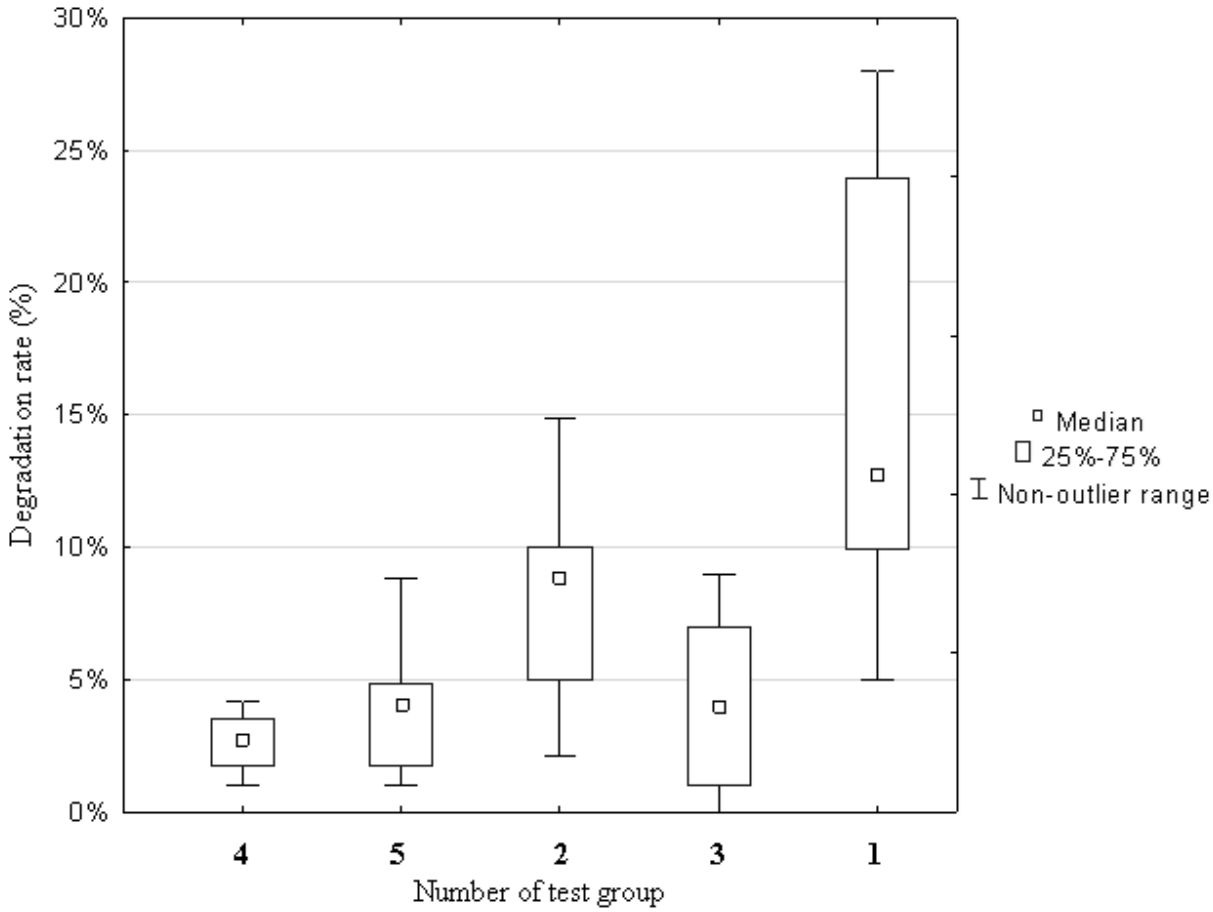

Fig. 1 The box plot of DRs (in %) for test groups 1-5.

The analysis of Tab. 3 shows that the DRs after accelerated natural weathering after 12 months (group 2) and 22 months (group 1) of exposure have significant difference from another gropu because p-values are lower than alpha level. But these two groups do not have difference between each other. Such kind of results show the effectiveness of tilt angle of the test desk and from Fig. 1 is clear that DR in the second year of exposure is higher that in the first 12 months.

Material of sign panel

T-test for dependent samples was done for 10 retroreflective sheetings before their application on FeZn desk (group 6) and after (group 5 before exposure). P-value was 0.104 is the the result of the test. The same test was done for 10 retroreflective sheetings before their application on Al desk (group 8) and after (group 7 before exposure). P-value was 0.129. The results of both tests are higher than alpha value that means the absence of statistical difference between groups. T-test for independent samples was used for pair of group 6 and 7. The degradation rate of each of groupafter one year of exposure in the garden was found. The p-values is 0.048 that is slightly

less that alpha level. The result means small difference in the degradation rate between samples that were applied on FeZn and Al desks after one year of exposure.

The box plot of DRs for these two groups demonstrates the mean value of degradation after one year of exposure in the garden for FeZn panel is 3.2%, for Al panel is 7.0% (Fig. 2). In Fig. 2, group 6 is DR for samples on FeZn panel after year exposure in the garden, group 7 is DR for samples on FeZn panel after year exposure in the garden.

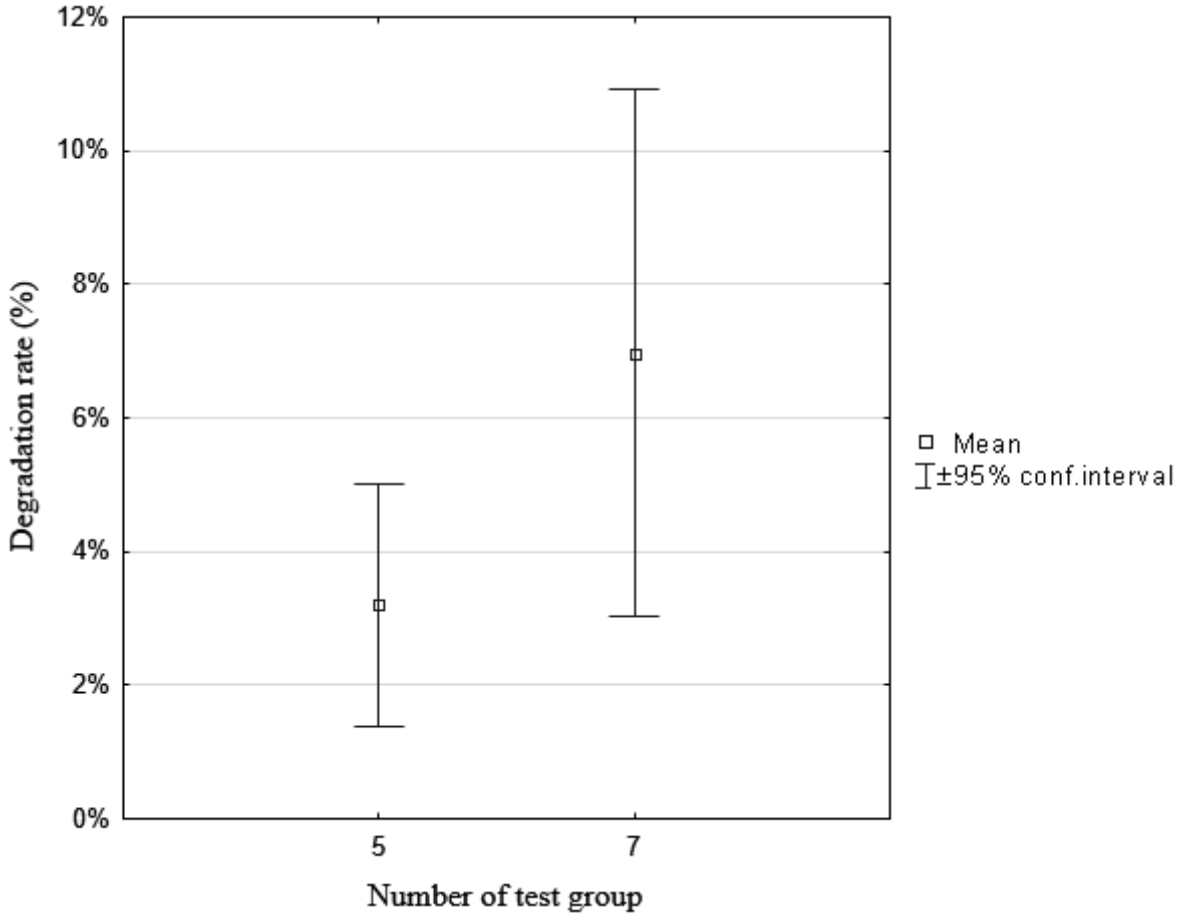

Fig. 2 The box plot of DRs (in %) for test groups 5 and 7.

CONCLUSION

The goal of this paper was to determine the degradation rate of retroreflective sheeting under different conditions and for two types of material of sign panel. The 10 types of retroreflective sheeting produced by different manufacturers of white, red, and yellow-green fluorescent were tested under 5 conditions in the study.

Based on the series of measurements and subsequent statistical analysis, it was found that the degradation rate of retroreflective sheeting even without meteorological influences and without sunlight is quite big 1% to 4% within one year of storage in the box. An unexpected result was

that there was not a significant difference in DR between samples that were in the box, samples under natural weathering without sunlight, and traffic signs that were in service for more than 16 months. Conversely, there is a big difference between these samples and retroreflective sheetings that were exposed to accelerated natural weathering for 12 or 22 months. Such kinds of results can be explained by the fact that DR is not a linear function it decreases with time, the degradation rate after 12 months decreases is around 9%, after 22 months is around 13%. The +45° tilt angle of the samples increases DR almost 2 times during the first year of exposure. The material of the sign panel is also critical for the degradation rate. Nowadays the Al sign panel is not used for traffic signs for economic reasons, but the weathering test shows that the degradation rate of retroreflective sheeting is almost 2 times less when the FeZn sign panel was used.

The results are not enough to conclude if the accelerated weathering is an effective tool for testing retroreflective material but demonstrates a big difference in degradation rate between in-service signs and accelerated weathering. The results of the study can be used as a basis for further researches.

ACKNOWLEDGMENT

The authors gratefully acknowledge that the present research was supported by the Internal Grant of Faculty of Engineering, CULS Prague (grant number IGA 2019: 31150/1312/3107).

REFERENCES

1. Babić, D., Babić, D., Macura, D.: Model for Predicting Traffic Signs Functional Service Life – The Republic of Croatia Case Study. PROMET - Traffic & Transportation, 2017, 29(3): 343.
2. Black, K. L., McGee, H. W., Hussain, S. F.: Implementation Strategies for Sign Retroreflectivity Standards. Transportation Research Board, Virginia, 1992, 43 pp.
3. European Union Road Federation: Improved Signage for Better Roads. An ERF Position Paper towards Improving Traffic Signs in European Roads, 2016.
4. Federal Highway Administration: The Manual on Uniform Traffic Control Devices. Department of Transportation, Washington, 2009, 816 pp.
5. Heltzer, H., Edmund, J.: Light Reflector Sheet., 1940, 9 pp.
6. International Commission on Illumination Roadsigns: CIE Publication No.74, 2004.
7. Khrapova, M.: Determining the Influence of Factors on Retroreflective Properties of Traffic Signs. Agronomy Research, 2019, 17(S1): 1041–1052.

8. Khrapova, M., Hrabánek, L., Marčev, D.: The Degradation Rate of Retroreflective Materials. 7th International Conference on Trends in Agricultural Engineering, 2019, 263–268.
9. Koyuncu, M., Amado, S.: Effects of Stimulus Type, Duration and Location on Priming of Road Signs: Implications for Driving. Transportation Research Part F: Traffic Psychology and Behaviour, 2008, 11(2): 108–125.
10. Schnell, T., Yekhshatyan, L., Daiker, R.: Effect of Luminance and Text Size on Information Acquisition Time from Traffic Signs. Transportation Research Record: Journal of the Transportation Research Board, 2009, 2122: 52–62.
11. Underwood, G., Chapman, P., Bowden, K., Crundall, D.: Visual Search While Driving: Skill and Awareness during Inspection of the Scene. Transportation Research Part F: Traffic Psychology and Behaviour, 2002, 5(2): 87–97.
12. ČSN EN 12899-1 Stálé Svislé Dopravní Značení - Část 1: Stálé Dopravní Značky.

Corresponding author:
Ing. Mariia Khrapova, Department of vehicles and ground transport, Faculty of Engineering, Czech University of Life Sciences Prague, Kamýcká 129, Praha 6, Prague, 16521, Czech Republic, e-mail: khrapova@tf.czu.cz

Digestate application with regard to the reduction of greenhouse gases

J. Korba [1]
[1]*Department of Machinery Utilization, Faculty of Engineering, Czech University of Life Sciences Prague, Prague, Czech Republic*

Abstract

With the simultaneous expansion of biogas plants, a large amount of waste product is generated, namely digestate. This by-product has found application in agriculture as a fertilizer. Like any organic fertilizer, not only when applied to the soil, emissions of gases are released. These are mainly ammonia, nitrous oxide, methane and carbon dioxide. In this article, the data from measurements after application using a two-disc application unit after the second cutting of alfalfa are discussed.

Key words: digestate, greenhouse gases, emission, methane

INTRODUCTION

In today's time of intensive agriculture, when we can grow enough food on a smaller area than before, we have the opportunity to grow plants on the remaining area for other uses. This situation adds to biogas plants, where some surplus agricultural crops can be consumed, but also waste from livestock and food production. Biogas is formed during anaerobic digestion of organic matter in a tank. The resulting gas contains methane, carbon dioxide and other gases. Methane in particular can be used for energy. Biogas production produces a large amount of digestate, which is a waste product of anaerobic digestion. This product is usually used as a liquid organic fertilizer because it contains substances important for plant growth. The disadvantage of this fertilizer is the release of emission gases into the air. (Holm-Nielsen et al. 2009) The digestate contains mainly ammonia, nitrogen in the residual organic matter and is a fertilizer with rapidly releasing nitrogen. The ammonium nitrogen contained in the digestate is easily subject to air losses. Agriculture is one of the biggest air pollutants of this gas. Methods for measuring ammonia emissions in animal production are well developed, but methods for measuring this gas after application are not uniform. (Šimek M, Cooper 2002; Dietrich, M., Fongen, M., & Foereid, B. 2020)

MATERIALS AND METHODS

Alfalfa grows on the experimental plot. The digestate was applied for this measurement after the second mowing (July 29th, 2020), the emissions were measured the following day. The digestate was also applied after the first mowing but no emission measurements were performed. The application was carried out using a self-propelled machine Vredo VT4556 application unit, which consists of two-disc sections forming a V-shaped groove in the turf, into which slurry or digestate is applied. The digestate was applied to four variants and the fifth variant was without application as a control. Applied quantity in variants see Table 1. The monitored elements are N2O, CH4 and NH3. The INOVA instrument was used to measure the emissions of these gases. Due to the dimensions of the device and the battery, it is in the transport vehicle. Special Teflon hoses lead from the probes located at the monitored locations, through which the analyzed air is supplied. In the device, a sample of air in the chamber is exposed to UV rays of a given frequency. Then the molecules of the monitored gas resonate and transform into an oscillating motion of the molecules. No resonance occurs with the other components of the sample. The oscillating motion of the particles is detected by sensitive sensors.

The probes consist of a plastic block that does not have a side on the underside. The probe has two holes. One opening is equipped with a fan with the possibility of speed control, which ensures the exact speed of air flow, see Figure (Fig. 1). Inside is a thermometer that continuously monitors the temperature at which the measurement takes place. Measurements can take place simultaneously on up to five variants. The measuring probes are moved to another location of the variant after one hour, monitoring takes place for approximately three hours. All measured data are recorded in real time and transferable to a PC.

The parameters of the measuring device:
INNOVA 1412 gas analyzer
Basic parameters of the device for ammonia:
Measuring range: 0.2 to 15,000 $mg.m^{-3}$
Operating temperature range: +5 to +40 ° C
Zero-point temperature dependence: 0.02 mg.m-3 / ° C
Zero-point fluctuation: ± 0.2 mg.m-3
Temperature dependence of the control point: 0.3% of the measured value / ° C
Checkpoint fluctuation: ± 2.5% of measured value

Detection limit: of the order of 10-2 ppm at 20 ° C and atm. pressure 101 kPa.

Instrument manufacturer: INNOVA Air Tech Instruments, Denmark.

Fig. 1 Measuring probe

RESULTS AND DISCUSSION

The following table (Tab. 1) describes the application rates after the first mowing, after the second mowing, when the emissions were measured. The average temperatures and humidity at which the measurement took place are given below.

Tab. 1 Applied doses and measurement conditions

Last applied dose (t/ha)	Applied dose (t/ha)	Variant	Average temperature (°C)	Average relative humidity (%)
0	0	7	27.78	65.00
0	50	6	28.77	56.96
0	25	5	29.53	63.45
12.5	12.5	4	29.47	69.47
25	25	3	29.47	69.47

Variant No. 7 was chosen as a control, where digestate was not applied.

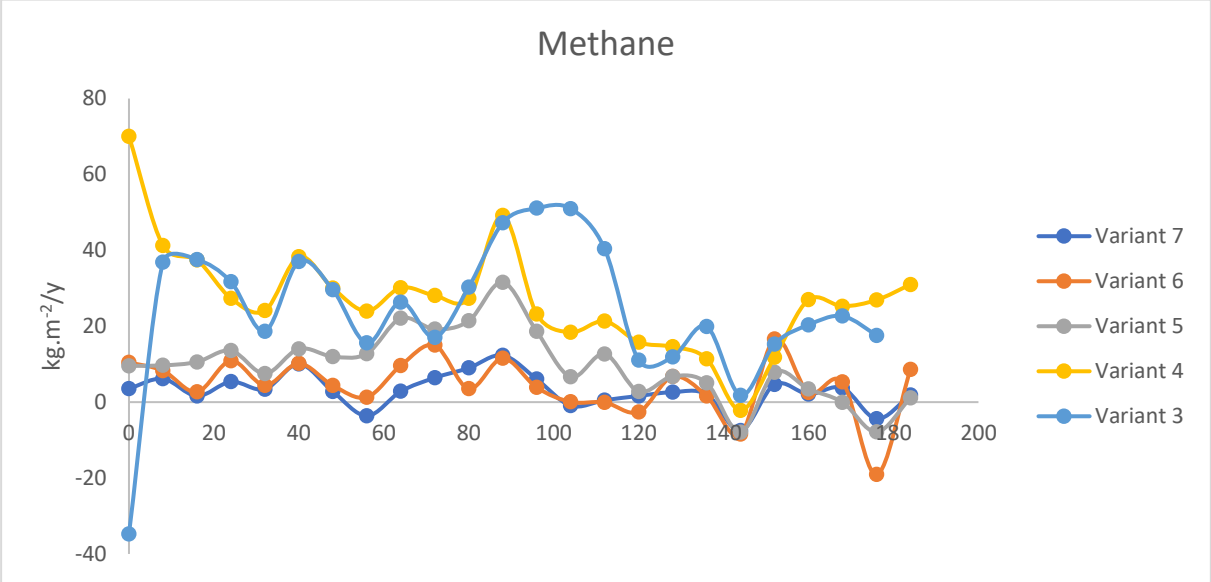

Fig. 2 Course of methane measurement

In the previous figure (Fig. 2), the values of specific emissions are negative in some cases. One of the causes is small measured concentrations, which were at the limit of the measuring range and the fluctuation of the zero point of the instrument. Another influencing factor was a slight variation in the air flow rate in the probe. Furthermore, a slightly rising air temperature may affect the result. During the measurement, there was a temperature rise of less than 5 ° C. The amount of emissions is displayed as a converted value in kilograms from one square meter in one year.

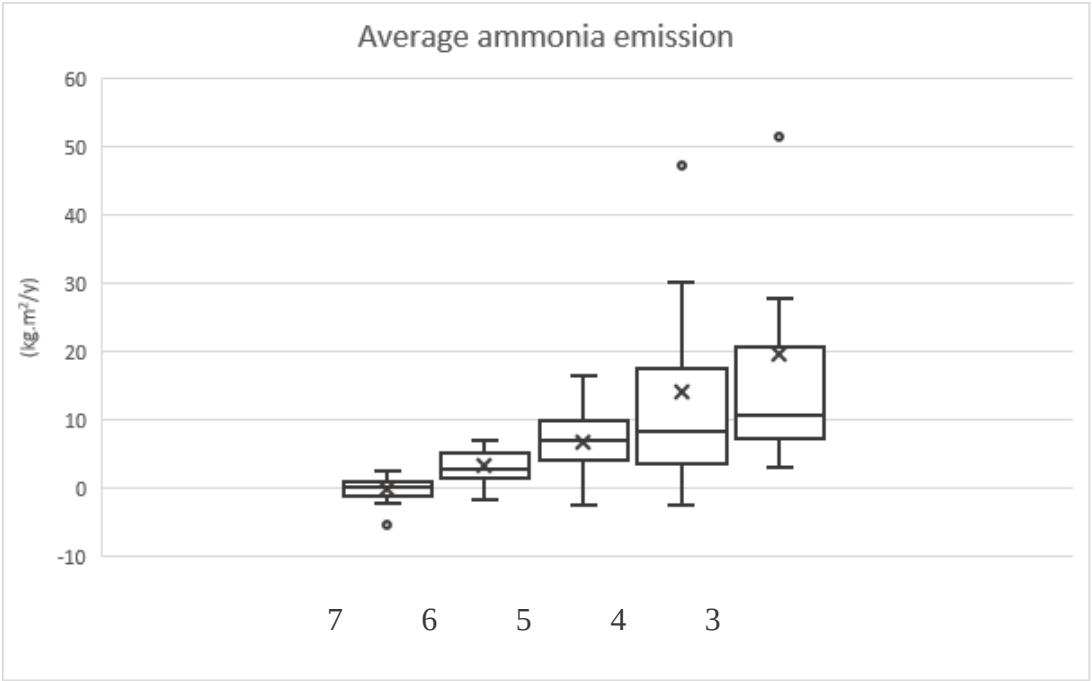

Fig. 3 Average ammonia emission

Explanations for all box charts: (cross - arithmetic diameter, box - 2nd to 3rd quartile, clamp - boundary, ring - remote extreme, comma – median)

Figure (Fig. 3) shows the average ammonia emissions. The lowest measured values were in the control variant. On the contrary, the highest measured values for variants 4 and 3, further for these variants, compared to the others, values with greater variance were measured.

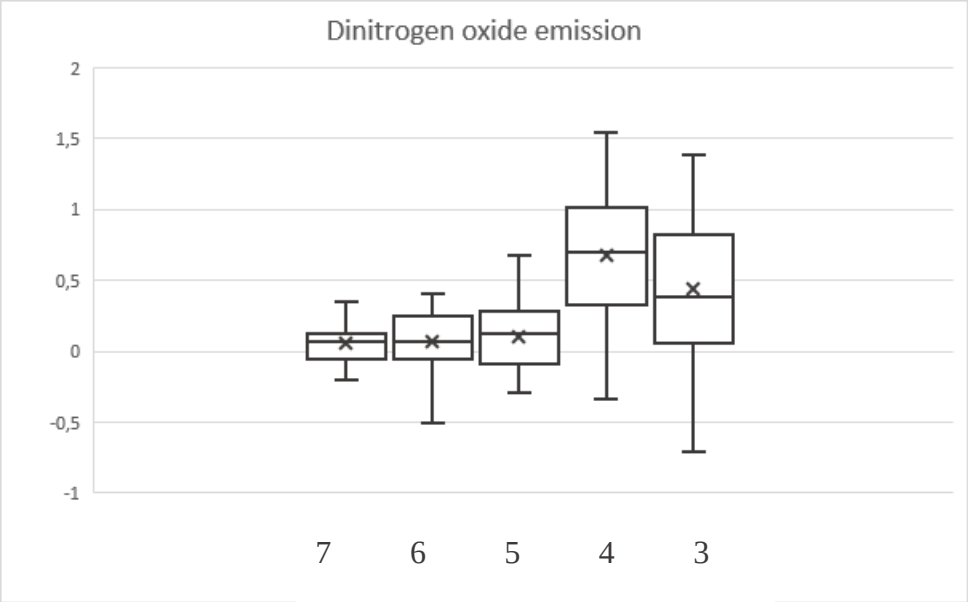

Fig. 4 Average dinitrogen oxide emission

Figure (Fig. 4) shows the average nitrous oxide emissions. For the control variant for the control variant, variants 6 and 5, the emissions are comparable. On the contrary, the values measured for variants 3 and 4 are higher and comparable.

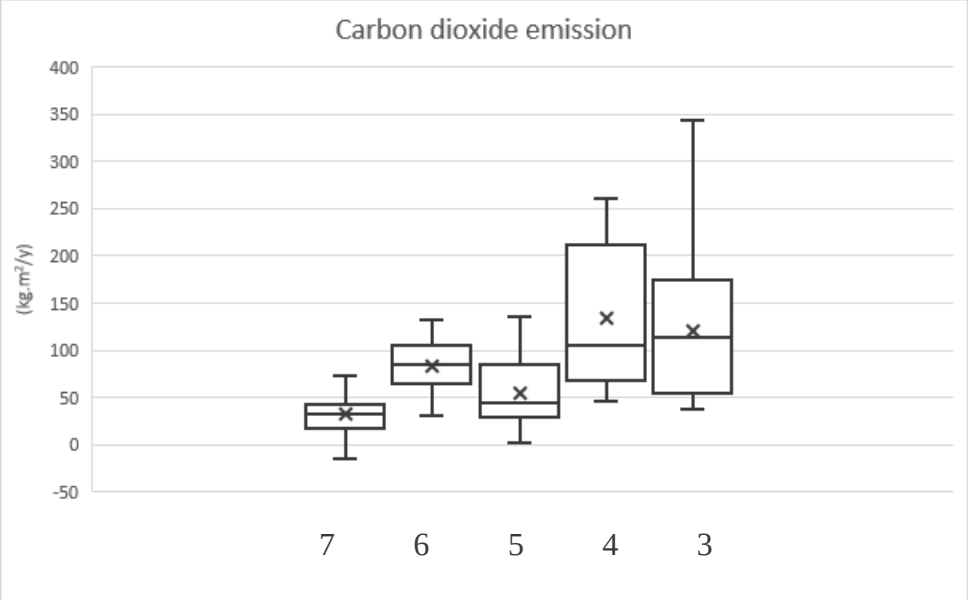

Fig. 5 Average carbon dioxide

Figure (Fig. 5) shows the average carbon dioxide emissions. The lowest emissions were in the control variant. For variants 6 and 5, the emissions are slightly higher than for the control variant with a small variance of values. For variants 4 and 3, the emissions are higher than for the previous two, but the measured data have a larger variance.

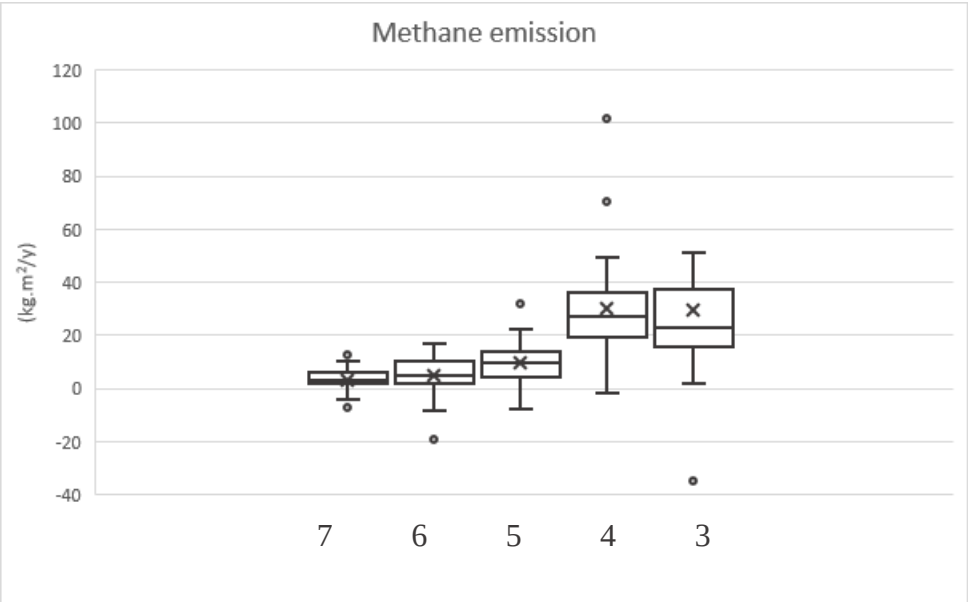

Fig. 6 Average methane emission

Figure (Fig. 6) shows the average methane emissions. For the control variant, variants 6 and 5, there are no significant differences in the measured values. Higher values of methane than in

the previous variants were measured for variants 4 and 3, between which there are no significant differences.

CONCLUSION

From the previous graphs, the result is evident that for variants 3 and 4 the emissions are the highest. For variants 5 and 6, the emissions are similar but lower than for the previous two. In the control variant, the emissions were the lowest or almost zero. This result did not confirm the dependence of the digestate dose on the amount of emissions. The results may be affected by the inhomogeneity of the applied digestate. Its quality cannot be traced back, but in the future, it will be necessary to check the quality of homogenization of digestate in tanks before export to the field, or collection and analysis of the composition of the applied digestate. Furthermore, the previous application of digestate after the first mowing may affect the measurement result. The upper part of the soil could be affected by the previous application, therefore there could be worse seepage into the surface than in variants where the first application did not take place. This hypothesis will need to be verified by future measurements. On the contrary, it is important to perform the measurement at approximately the same temperatures at which the measurement took place. In general, with increasing temperature, the amount of emissions increases.

REFERENCES

1. ŠIMEK M, COOPER JE (2002) The influence of soil pH on denitrification: Progress towards the understanding of this interaction over the last 50 Years. Eur J Soil Sci 53: 345–354.
2. DIETRICH, M., FONGEN, M., & FOEREID, B. (2020). Greenhouse gas emissions from digestate in soil. International Journal of Recycling of Organic Waste in Agriculture, 9(1), 1-19. doi:10.30486/IJROWA.2020.1885341.1005
3. HOLM-NIELSEN JB, AL SEADI T, OLESKOWICZ-POPIEL P (2009) The future of anaerobic digestion and biogas utilization. Bioresour Technol 100 (22): 5478–5484.

Corresponding author:

Ing. Jaroslav Korba, Department of Machinery Utilization, Faculty of Engineering, Czech University of Life Sciences Prague, Kamýcká 129, Praha 6, Prague 16500, Czech Republic, email: jarda.korba@seznam.cz

Comparison of the influence of variable tool geometry during soil cultivation in the soil trough

J. Kuře[1], M. Linda[2], R. Chotěborský[1], M. Hromasová[2]

[1]Department of Material Science and Manufacturing Technology, Faculty of Engineering, Czech University of Life Science Prague

[2]Department of Electrical Engineering and Automation, Faculty of Engineering, Czech University of Life Sciences Prague

Abstract

The paper deals with the comparison of the effect of tillage tools using the soil trough. Individual tillage tools were made of plastic using 3D printing. These models are used to verify the functionality of the tool kinematics and its effect during tillage. Using 3D printing, it is also possible to design new shapes of tillage tools and verify their properties before the final field tests. It is possible to save time and resources before the actual production of inefficient tools. A tillage tool with differently shaped wings was used for testing. The individual parts were printed from PET-G material. Tillage tool assemblies were tested in a soil trough filled with silica sand. The draft force of the tools when passing through sand was compared using a strain gauge between the frame and the traction cable. The process was monitored by two cameras.

Key words: DEM, model, tillage tool, soil trough, 3D printed tool

INTRODUCTION

Development in the agricultural environment and especially in soil processing is still required. Better efficiency of work tools contributes to better tillage, reduces the impact on the environment, speeds up working time and reduces the economic demands on the process (Lovarelli, Bacenetti and Fiala, 2017). Nowadays, there is still a need to improve the efficiency of working with the soil, both to obtain higher yields and to ensure less burden on the environment. One of the aims is to create effective tools. Industry 4.0 also deals with this issue. Research of new components on real prototypes is carried out in the usual way. With the help of modern technologies and mainly thanks to the increasingly available computing power of modern computers, it is possible to simulate this process by mathematical models (Ucgul, Saunders and Fielke, 2018; Mudarisov *et al.*, 2019; Ucgul and Saunders, 2020). However, for proper validation of the models, it is still necessary to verify the results using real tests (Zhang

et al., 2018; Scanlan and Davies, 2019). As agricultural land is becoming increasingly scarce and it is difficult to carry out field tests throughout the year, the alternative is testing by soil troughs. (Ucgul and Saunders, 2020). Using modeling programs, it is possible easily and quickly design the shape of tools. 3D printing can be used for fast production, where nowadays a large number of plastic-based materials with different mechanical properties can be used. (Ge, Wang and Zhou, 2019; Hnízdil, Chotěborský and Kuře, 2020). The model can be verified before testing in simulations. Draft force and soil translocation are primarily determined. This can determine the effect of the proposed tool shape (Sharifat and Kushwaha, 1997; Manuwa, 2013).

The aim of this work is to compare the properties of the proposed shapes of the wings of the tillage tool as it drives through the material. The main aspect for comparison is the draft force of the tillage tool using individual wings. Furthermore, to obtain and define results for comparison in the creation of mathematical models.

MATERIALS AND METHODS

A soil trough was used to make the tests. The trough is used for testing models of agricultural tools with the possibility of variable change of material filling. The dimensions of the trough are: height 500 mm, width 500 mm and length 1500 mm. The soil trough was filled with silica sand fraction 0.1-0.3 mm. The sand was used due to its constant mechanical properties. The subject of interest was the active length. The active length expresses the area, where the tool is already fully recessed. The active length of the trough depends on the tool used, its shape and the length of the engagement. In the case of a tillage tool with variable wings, the active length was 200 mm. The trough diagram including the active length is shown in Figure 1, where F is the measured tool pulling force, d is the tool depth and l_m is the active length.

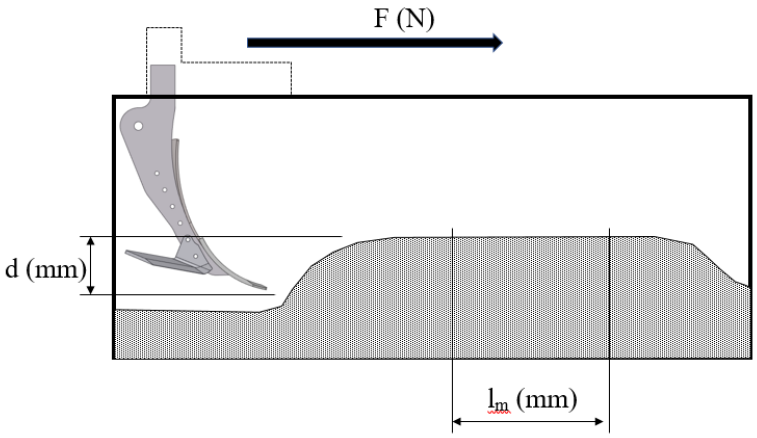

Fig. 1 Schema of soil trough

Two GoPro Hero 8 cameras were used to monitor the progress of the tests. The first camera was placed inside the trough and recorded the movement of the tool in the axis of movement. The second camera was placed outside the trough and captured horizontally the lateral movement of the tool. The force of the drawn tool was measured by a hanging strain gauge. The force was measured in the axis of movement of the tool. The measured strain gauge voltage was amplified and subsequent data were collected using a DAQ card. The evaluation was performed using software on a computer. The conversion characteristic of the strain gauge is given by equation (Eq. 1), where F (N) is the force and u (V) is the amplified voltage from the strain gauge.

$$F = 157.13 \cdot u \qquad (1)$$

The block diagram of the evaluation devices, including the position of the cameras, is shown in Fig. 2.

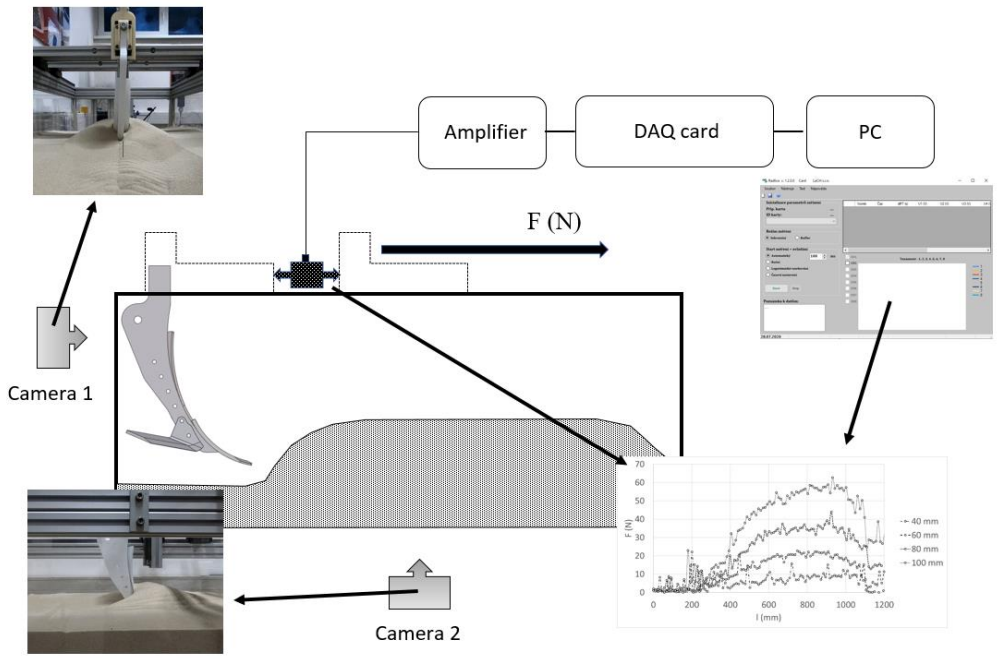

Fig. 2 Schema of soil trough

Various wings shapes have been designed for testing. The wings were gradually tested in the soil trough. In each step, wings of a certain shape were attached to the tillage tool and drives were made. Drives were made for 40, 60, 80 and 100 mm of depth. The driving speed was 100 $mm.s^{-1}$. The proposed wings shapes are shown in Fig. 3.

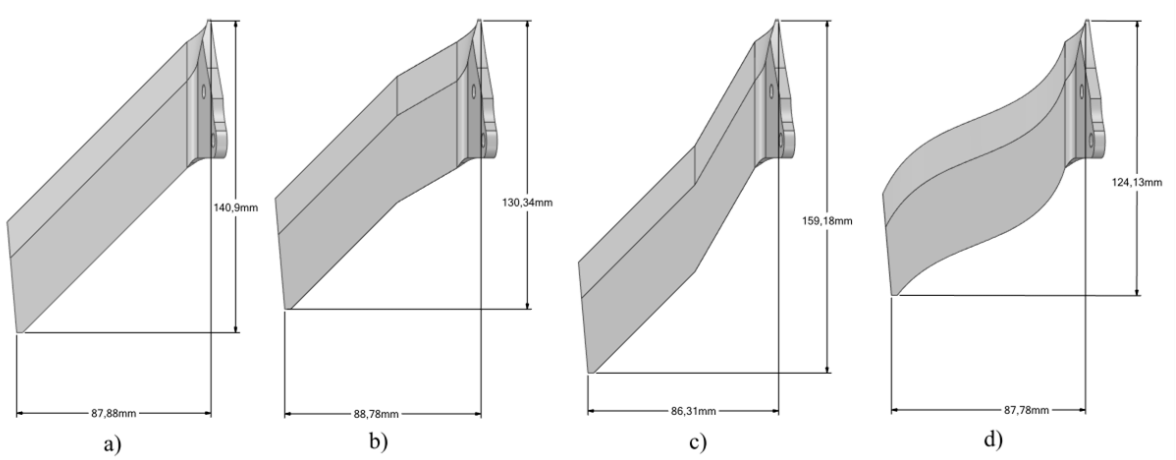

Fig. 3 Schema of wings types: a) type 0 b) type 1 c) type 2 d) type 3

The records from the cameras were evaluated. The angles of wedge of the material created during the drive the tillage tool was determined. These angles correspond to the dynamic behavior of the material and are important for the subsequent comparison of mathematical models in the RockyDEM environment (‘Rocky DEM Particle Simulator’, 2018). The angles of the side wedges were measured from the inside camera and the angles of the front wedges were measured from outside camera (Fig. 4a) and 4 b)).

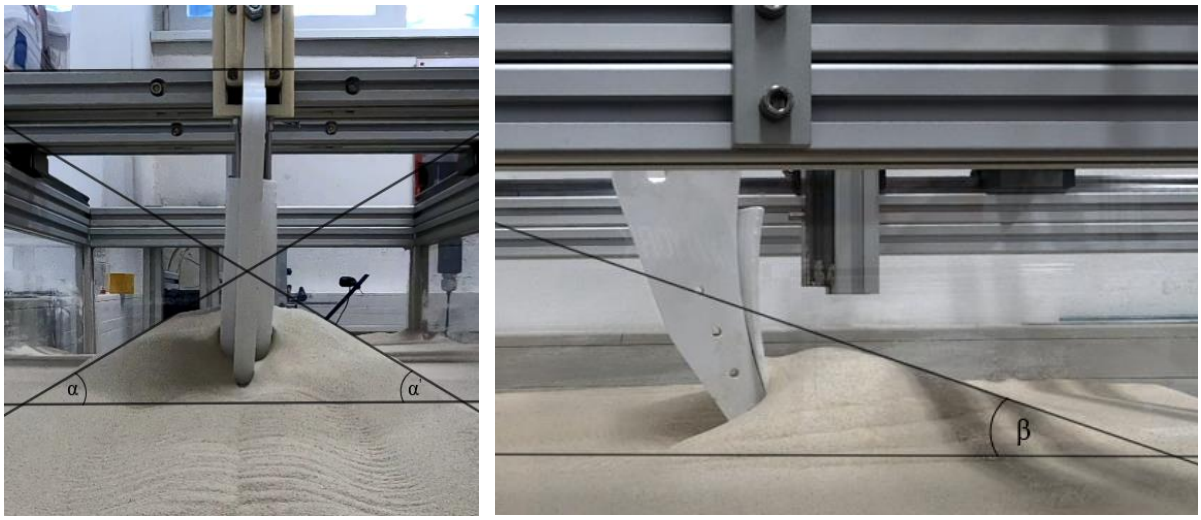

a) b)

Fig. 4 Principle of angle measurement a) Angles of side wedges b) Angle of front wedge

RESULTS AND DISCUSSION

The results of draft force measured by a strain gauge were processed graphically and numerically. The results are in Fig. 5-8. The graphs show the force as a function of the tillage tool depth. The curves show the individual depths d (mm).

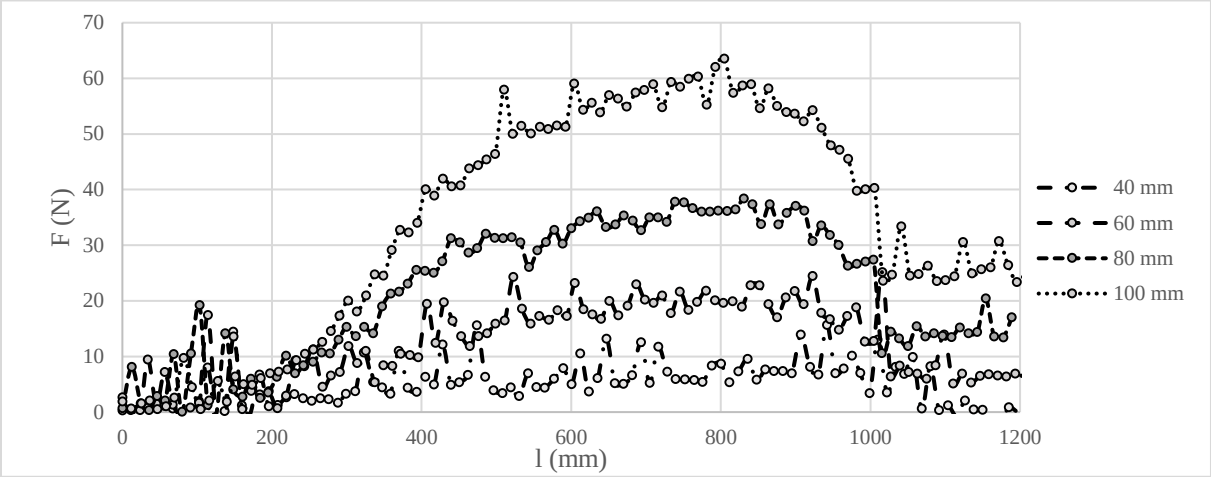

Fig. 5 Measured data of wings type 0

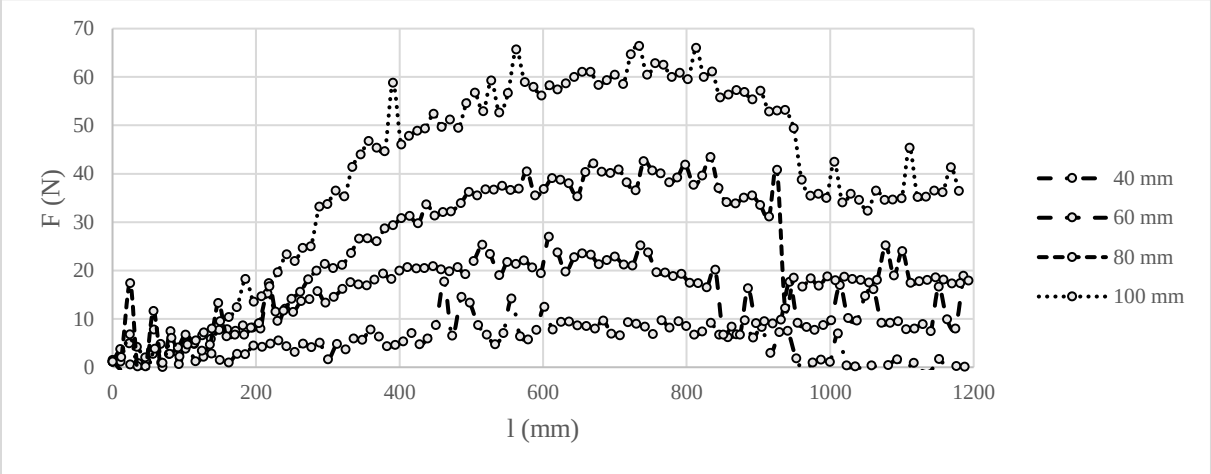

Fig. 6 Measured data of wings type 1

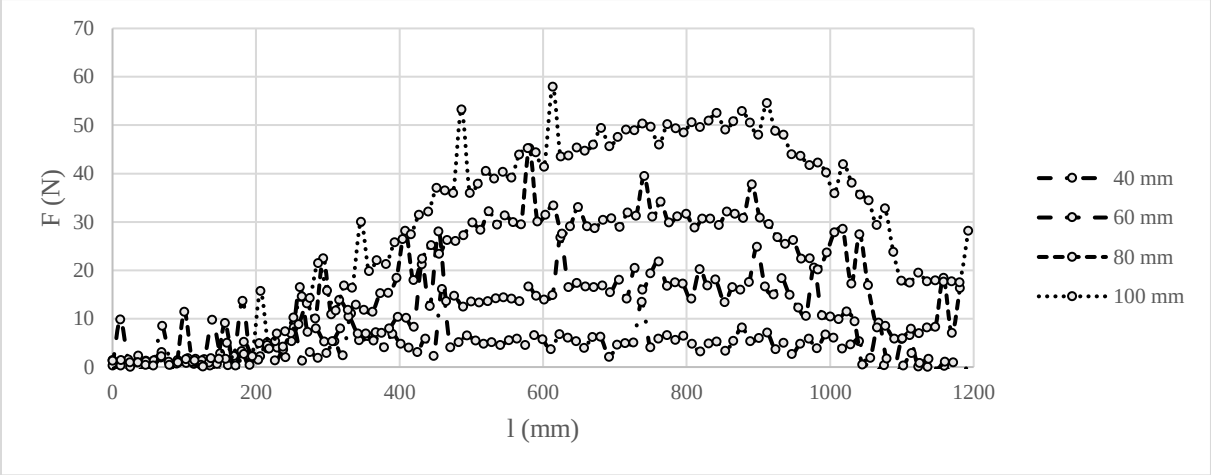

Fig. 7 Measured data of wings type 2

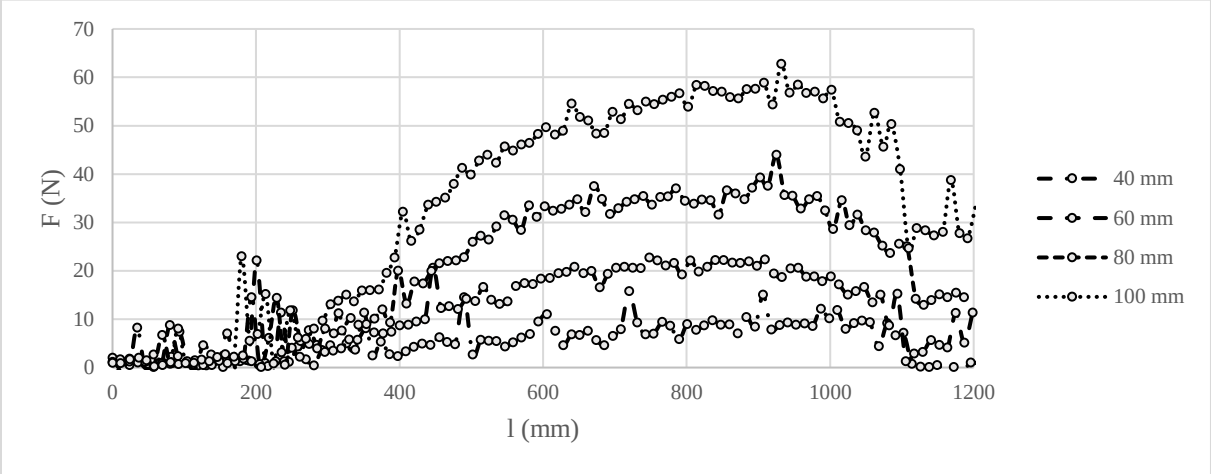

Fig. 8 Measured data of wings type 3

The draft force was evaluated and averaged in the area of the active length. In this area, the draft force reaches its maximum. The measured data are shown in Table 1.

Tab. 1 Measured maximal average force in active length for each type of wings

Depth (mm)	**type 0 F_{ma} (N)**	**type 1 F_{ma} (N)**	**type 2 F_{ma} (N)**	**type 3 F_{ma} (N)**
40	7.334 ± 2.709	8.5187 ± 1.329	5.690 ± 2.192	9.476 ± 1.803
60	19.569 ± 1.851	21.573 ± 2.326	17.164 ± 2.211	20.420 ± 1.442
80	34.846 ± 1.777	39.088 ± 2.049	31.749 ± 2.716	35.663 ± 2.660
100	57.338 ± 2.952	60.184 ± 2.408	49.657 ± 1.624	57.136 ± 1.838

The average maximum forces results were used as a dependence function of depth. These dependencies were expressed by functions. The functions are for wings type 0 (Eq. 2), wings type 1 (Eq. 3), wings type 2 (Eq. 4) and wings type 3 (Eq. 4), where F_{ma} (N) is the average maximum force and d (mm) is the depth of the tillage tool.

$$F_{ma} = 0.002 \cdot d^{2.2305} \quad (2)$$

$$F_{ma} = 0.0033 \cdot d^{2.1383} \quad (3)$$

$$F_{ma} = 0.0005 \cdot d^{2.5713} \quad (4)$$

$$F_{ma} = 0.007 \cdot d^{1.9528} \quad (5)$$

The wedge angles of the filleed material were measured. Angles define the dynamic behavior of the material during its cultivation. GeoGebra software was used to evaluate the wedge angles (‘GeoGebra’, 2019). The results are shown in Table 2.

Tab. 2 Measured angles of filled material for each type of wings

Depth (mm)	**Angle of side wedges (α) (°)**	**Angle of front wedge (β) (°)**
type 0		
80	15.916 ± 0.887	15.749 ± 0.602
60	26.019 ± 0.278	
100	29.392 ± 0.782	
type 1		
80	17.716 ± 0.177	16.109 ± 0.898
60	26.395 ± 0.344	
100	28.404 ± 0.277	
type 2		
80	11.697 ± 0.649	14.791 ± 0.665
60	21.219 ± 0.941	
100	29.155 ± 0.033	
type 3		
80	14.908 ± 0.643	16.008 ± 0.862
60	26.066 ± 0.627	
100	27.183 ± 0.769	

CONCLUSION

It was found that with higher depth and higher draft force, larger deformations occur in 3D printed parts (Hnízdil, Chotěborský and Kuře, 2020). The printed models were embedded to a maximum depth of 100 mm. When comparing the draft forces, it was found that the tillage tool with wings of type 2 has the lowest draft force. From the evaluated functions of the force at depth, it is possible to determine the draft force for individual depth. The evaluated material angles are the initial data for comparing mathematical models for future use.

ACKNOWLEDGEMENTS. Supported by Internal grant 31200/1312/3109 agency of Faculty of Engineering, Czech University of Life Sciences in Prague.

REFERENCES

1. Ge, R., Wang, L. and Zhou, Z. (2019) ‘DEM analysis of compression breakage of 3D printed agglomerates with different structures’, *Powder Technology*. Elsevier B.V., 356, pp. 1045–1058. doi: 10.1016/j.powtec.2019.08.113.
2. ‘GeoGebra’ (2019).
3. Hnízdil, P., Chotěborský, R. and Kuře, J. (2020) ‘Utilization of fused deposition method 3d printing for evaluation of discrete element method simulations’, *Agronomy*

Research. Eesti Pollumajandusulikool, 18(Special Issue 1), pp. 842–851. doi: 10.15159/AR.20.097.

4. Lovarelli, D., Bacenetti, J. and Fiala, M. (2017) 'Effect of local conditions and machinery characteristics on the environmental impacts of primary soil tillage', *Journal of Cleaner Production*. Elsevier Ltd, 140, pp. 479–491. doi: 10.1016/j.jclepro.2016.02.011.
5. Manuwa, S. I. (2013) 'Effect of macro shape tillage tool geometry on draught force and soil translocation', in *American Society of Agricultural and Biological Engineers Annual International Meeting 2013, ASABE 2013*. American Society of Agricultural and Biological Engineers, pp. 758–771.
6. Mudarisov, S. G. *et al.* (2019) 'Modeling the technological process of tillage', *Soil and Tillage Research*. Elsevier, 190, pp. 70–77. doi: 10.1016/j.still.2018.12.004.
7. 'Rocky DEM Particle Simulator' (2018).
8. Scanlan, C. A. and Davies, S. L. (2019) 'Soil mixing and redistribution by strategic deep tillage in a sandy soil', *Soil and Tillage Research*. Elsevier, 185, pp. 139–145. doi: 10.1016/j.still.2018.09.008.
9. Sharifat, K. and Kushwaha, R. L. (1997) 'Soil translocation by tillage tools', *Canadian Agricultural Engineering*, 39(2), pp. 77–84.
10. Ucgul, M. and Saunders, C. (2020) 'Simulation of tillage forces and furrow profile during soil-mouldboard plough interaction using discrete element modelling', *Biosystems Engineering*. Academic Press, 190, pp. 58–70. doi: 10.1016/j.biosystemseng.2019.11.022.
11. Ucgul, M., Saunders, C. and Fielke, J. M. (2018) 'Comparison of the discrete element and finite element methods to model the interaction of soil and tool cutting edge', *Biosystems Engineering*. Academic Press, 169, pp. 199–208. doi: 10.1016/j.biosystemseng.2018.03.003.
12. Zhang, L. *et al.* (2018) 'Coupled Eulerian-Lagrangian finite element method for simulating soil-tool interaction', *Biosystems Engineering*. Academic Press, 175, pp. 96–105. doi: 10.1016/j.biosystemseng.2018.09.003.

Corresponding author:

Ing. Jiří Kuře, Department of Material Science and Manufacturing Technology, Faculty of Engineering, Czech University of Life Science Prague, Kamýcká 129, Praha 6, Prague, 16521, Czech Republic, tel: +420704870131, email: kure@tf.czu.cz

Hands position on the steering wheel in left-hand traffic with regard to the applicability of digital mirror technology

M. Kůrka[1], M. Hruška[1], P. Vaculík[1], T. Benda[2]

[1]Department of Mechanical Engineering, Faculty of Engineering, Czech University of Life Sciences Prague, Prague, Czech Republic

[2]Department of Information Engineering, Faculty of Economics and Management, Czech University of Life Sciences Prague, Prague, Czech Republic

Abstract

This study is concerned with the research of hands position on the steering wheel in drivers when driving and considers the options of placing digital side mirror displays inside a passenger car cabin. In the scope of the research, respondents were asked about their most common hands position on the steering wheel when driving. Regarding the established standard placement of digital side mirrors inside passenger car cabins, it was ascertained that a high percentage of drivers place their hands on the steering wheel when driving in a way that might prevent them from viewing directly the displays of digital side mirrors. This finding may have an impact on traffic safety during driving. The research delineated in this paper is based on a randomly selected sample of drivers who drive in right-hand traffic. The data were collected using electronic questionnaires, featuring an accurately described and visualized situation for a better understanding and presentation of the matter under review. Subsequently, the data were analysed statistically, with the main parameter for identifying dependence being the driver's hands position during driving that prevents a direct view of displays of digital side mirrors. Results of this study may be applied in designing and development of passenger car cabins from the perspective or ergonomy and near-future innovations.

Key words: digital side mirrors, steering wheel, driver, hands position

INTRODUCTION

Observation techniques have been used to date for assessing the safety of passenger car crews, where the observer deals with driver behaviour while driving, e.g. the seat belt use, mobile phone use, seat positioning, etc. Holding the steering wheel correctly is an important aspect of traffic safety (THOMAS & WALTON 2007), (VIANO et al. 1989). Multifunctional steering wheels represent a direct link between driver and machine, and the optimum design of these

elements, coupled with the design of the various armrests, directly affects the overall driver comfort and thus the safety of the vehicle operation (CHANG & CHEN 2016).

A number of researches (HRUŠKA 2018), (SCHMIDT et al. 2014), (WALTON & THOMAS 2005) pay their attention to the ways drivers hold the steering wheel. There is a relatively high consensus among experts on this issue. The most frequently quoted optimum value is according to the analogue clock face, the left hand position on the nine and the right hand on the three, with the driver holding the steering wheel with both hands (HAULT-DUBRULLE et al. 2011), (SCHIRO et al. 2013).

Every year sees new developments in the automotive industry, when innovative technologies stand for the most frequently applied method to attract customers and maintain the market position. Most often, this includes technologies that take account of routine ergonomic standards. The most common reason that lies behind these innovations is to provide the driver and passengers with comfort, to simplify the control features and to ensure a pleasant driving experience and enjoyment. Currently, digital side mirrors (DSM) rank among the most discussed innovations.

Today, it is not unusual to encounter functional prototypes of DSM for testing purposes of this technology, including cars that are commonly available to customers. The German Audi cars manufacturer is seen as an innovation pioneer for DSM, as this technology was used in the series-produced model e-tron. The objective of this technology is to improve aerodynamic effects and to reduce the noise inside the car: properties typically required of electric cars. Another car featuring the DSM technology is Lexus ES 300h 2.5 Takumi. The Japanese company furnished this model with displays fitted in the columns connecting the car roof with the bodywork.

When safety is assessed, sex and age of drivers are other factors to be taken into consideration. Stereotypes in driving, gender-based differences in driving and the effect of drivers' age on traffic safety with conventional side mirrors have already been scrutinized (GRANIÉ & PAPAFAVA 2011), (MOÈ et al. 2015), (SÖLLNER & FLORACK 2019). Areas for further research include differences between hands position in men and women, and the impact of these hands positions on safety, using DSM in Audi e-tron.

The aim of this study is to assess the differences in the approach to the safe holding of the steering wheel of a passenger car in a specifically tested situation, with respect to applicability of digital side mirrors. Another objective pursued by this study is to consider the hypothesis whether there exists a statistically significant difference in the hands positions on the steering wheel in a way preventing a direct view of DSM displays between men and women.

MATERIALS AND METHODS

For the needs of the measurements, a total of 80 participants (40 women and 40 men) from the Czech Republic (Tab. 1). The age of all of the participants ranged from 19 to 64 years (the average age was 30.9). As an essential condition, all of the participants were required to have a driver's license entitling them to drive passenger cars. In addition, all of the research participants were expected to be in good health and have no restrictions on their musculoskeletal system, which could distort the results.

Tab 1. Data regarding the tested persons

	Number	**Age**		
		Average	**Minimum**	**Maximum**
Men	40	29.7	20	52
Women	40	32.2	19	64
Total	80	30.9	19	64

A traffic situation was defined for the purpose of the research, in which the interviewed driver could find himself or herself and describe how he or she held the steering wheel in the given situation. This is a situation in which drivers commonly find themselves when driving. The situation has been thoroughly verbally described and supplemented with an illustrative photo for a better understanding. The tested situation was described as driving on highways or high-speed roads at low intensity traffic exerting no psychological pressure on the driver.

Basic data collection was carried out with the help of electronic questionnaires. As part of the basic information provided in the questionnaire, respondents were advised to devote sufficient time to filling out individual questions and had schemes available to help them better imagine the situation (Fig. 1). Although the questionnaire method may not be as accurate as real-environment testing, given the set objectives and the number of subjects surveyed, testing in a real environment would be virtually impossible in organizational terms.

The questionnaire consisted of nine questions divided into two groups. The first group were questions about age (in years), gender (female, male), and side preference (right-handed, left-handed) of the subject. The height of respondents was not addressed in the present research. In addition, the test subject was interviewed about how long he or she had a driver's licence (in years), how often he or she drove a passenger car (every day, at least once a week, occasionally, exceptionally), with the final data being about the position in which the subject most often sits behind the steering wheel (a choice of three basic positions divided according to the subject's chest distance from the centre of the steering wheel).

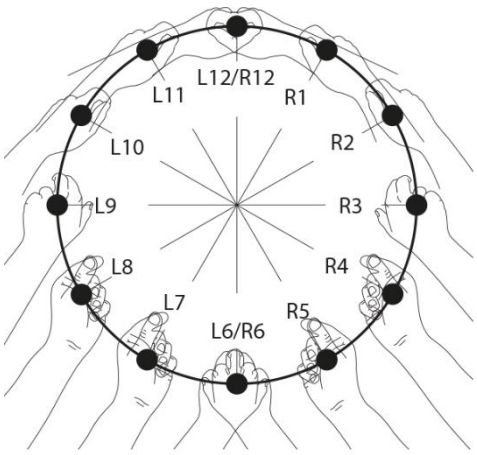

Fig. 1 Scheme of positions of individual grips according to an analogue watch face.

In the second group of questions, the test subject was asked to imagine the traffic situation described above and responsibly state for each of them whether he or she held the steering wheel with one or both hands, and in which position. This was always based on the pre-selected scheme attached to each question (Figure 1), where, according to the watch face, the range of R12-R6 was defined for the right hand, and for the left hand the analogous range of L6-L12. The overlap at 12 and 6 o'clock is selected to enable the side-preference of respondents. The subject was also told to indicate the most prevalent value of the grip on the steering wheel. We dismissed in the first phase extreme values where the test subject crosses the hand and held the steering wheel with, for example, the left-hand on the right, as highly unlikely in view of the objectively high degree of discomfort the driver would experience in such a position. For this reason, we completely discarded these alternatives.

Designers of Audi e-tron 55 quattro placed the DSM display device in the door structure. These displays are optically lower in comparison with conventional side mirrors. Thorough testing of the car revealed that where the driver's left hand is in the positions L9-L10 on the steering wheel, there is a higher risk that the display of the left side mirror is hidden from the driver's view by his hand when driving (Fig. 2). This structural solution presents one possibility of positioning DSM displays in the car cabin. As practice shows, drivers are unwilling to change their routines when driving. Accordingly, to be comfortable, drivers will most often lean with their left hand on the armrest in the door or directly on the edge of the door window (Fig. 3) (PENG et al. 2017), (SMITH et al. 2015).

Fig.2 Hand position L10 (on the left side) and L9 (on the right side) with lean hand on the edge of the door window in Audi e-tron 55 quattro

RESULTS AND DISCUSSION

Table (Tab. 2) illustrates percentage frequencies of the individual hands positions on the steering wheel for the interviewed men. In turn, table (Tab. 3) provides percentage frequencies of the individual hands positions on the steering wheel for the interviewed women. Both tables show that both women and men did not use the positions L6, R12 and R1 during the tested drive. Contrariwise, the positions L9, L10, R2 and R3 were most frequent for both sexes.

Tab. 2 Percentage representation of driver grips in men during tests

Left hand	**L6**	**L7**	**L8**	**L9**	**L10**	**L11**	**L12**	**No hand**	**Σ**
Percentage frequency	0.0 %	7.5 %	7.5 %	30.0 %	30.0 %	7.5 %	2.5 %	15.0 %	100.0 %
Right hand	**R12**	**R1**	**R2**	**R3**	**R4**	**R5**	**R6**	**No hand**	**Σ**
Percentage frequency	0.0 %	0.0 %	20.0 %	15.0 %	10.0 %	5.0 %	2.5 %	47.5 %	100.0 %

Tab. 3 Percentage representation of driver grips in women during tests

Left hand	**L6**	**L7**	**L8**	**L9**	**L10**	**L11**	**L12**	**No hand**	**Σ**
Percentage frequency	0.0 %	7.5 %	10.0 %	27.5 %	42.5 %	2.5 %	5.0 %	5.0 %	100.0 %
Right hand	**R12**	**R1**	**R2**	**R3**	**R4**	**R5**	**R6**	**No hand**	**Σ**
Percentage frequency	0.0 %	0.0 %	22.5 %	15.0 %	15.0 %	7.5 %	5.0 %	35.0 %	100.0 %

The figure (Fig. 3) provides an overview in percentage terms of grips by the left hand for both sexes, with highlighted positions L9 and L10. Apparently, more than 36% of the interviewed drivers, when driving, place their left hand in a position that may prevent a direct view of the left DSM in Audi e-tron. This position is seconded by the position L9, used more than 28 % of the drivers.

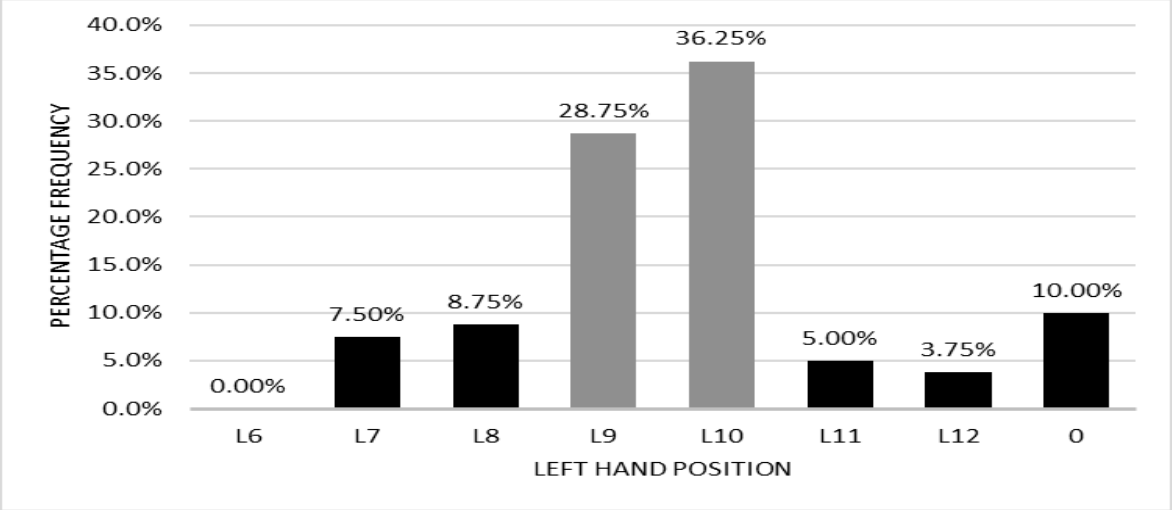

Fig. 3 Grips by the left hand for both sexes

A Pivot Table (Tab. 4) was created to serve the purpose of testing the hypothesis whether there exists a statistically significant difference in the hands positions on the steering wheel in a way that prevents a direct view of DSM displays between men and women. The Pivot Table has one degree of freedom and determines how drivers hold the steering wheel with their left hand during the tested situation, i.e. whether the driver's left hand is in the position L9 or L10 or in another position.

Tab. 4 Relation between men and women for positions L9 and L10

	L9 or L10	**Other position**	**Σ**
Women	28	12	40
Men	24	16	40
Σ	52	28	80

To evaluate the dependency of the hands position on the steering wheel in a tested traffic situation (Tab. 5), the value X^2 (0.8791) was calculated on the level of significance (0.05), lower than the critical value (3.8415), which does not confirm the hypothesis that there exists a statistically significant difference in the hands positions on the steering wheel in a way that prevents a direct view of DSM displays between men and women during driving.

Tab. 5 Statistical results

Degrees of freedom	X^2	Critical value	Significance Level	Degree of dependency
2	0.8791	3.8415	0.05	None

CONCLUSION

In this study, a large amount of valuable primary data was obtained from a group of respondents from the Czech Republic, which may be interesting in terms of possible comparisons with other statistics that could be obtained from respondents with different parameters, or from other countries.

Results of the present research show that 65 % drivers hold the steering wheel in a way that may affect safety when driving in Audi e-tron equipped with DMS technology. The proportion between safety and comfort varies from driver to driver and is individual for everyone. However, as practice shows, drivers are unwilling to change their routines when driving. This fact leads us to believe that a shift from conventional mirrors to DSM will influence the driver's overall wellbeing.

The hypothesis whether there exists a statistically significant difference in the hands positions on the steering wheel in a way that prevents a direct view of DSM displays in Audi e-tron between men and women was not confirmed.

Since Audi e-tron is equipped with DSM displays fitted in the right door in a positional analogous to that in the left door, research into the behaviour and habits of drivers in right-hand traffic might be of certain interest.

Variations of hands positions on the steering wheel in right-hand and left-hand traffic have been researched in plentiful studies (HRUŠKA et al. 2019), (KŮRKA & HRUŠKA 2019).

The results presented in this paper could serve as a basis for future research to further refine the above findings. In addition, the present research may facilitate the design process of DSM systems.

REFERENCES

1. CHANG, Y.-M., CHEN, C.-W.: Kansei assessment of the constituent elements and the overall interrelations in car steering wheel design. *International Journal of Industrial Ergonomics*, *56*, 97–105

2. GRANIÉ, M.-A., PAPAFAVA, E.: Gender stereotypes associated with vehicle driving among French preadolescents and adolescents. *Transportation Research Part F: Traffic Psychology and Behaviour*, *14*, 341–353
3. HAULT-DUBRULLE, A., ROBACHE, F., DRAZETIC, P., GUILLEMOT, H., MORVAN, H.: Determination of pre-impact occupant postures and analysis of consequences on injury outcome - Part II: Biomechanical study. *Accident Analysis and Prevention*, 43(1), 75–81.
4. HRUŠKA, M., VACULÍK, P., KŮRKA, M., HAJLICH, T., BENDA, P.: Holding the wheel in passenger cars in countries with driving on the right and left side depending on the driver's side preference. *Agronomy Research*, 17(4), 1639–1648
5. KŮRKA, M., HRUŠKA, M.: Assessment of the way holding steering wheel in different traffic situations. *International Conference On Trends In Agricultural Engineering*, 7th, 331–336
6. M. HRUŠKA.: Assessment of the actual hand position on the steering wheel for drivers of passenger cars while driving. *Agronomy Research*, 16(4), 1668–1676
7. MOÈ, A., CADINU, M., MAASS, A.: Women drive better if not stereotyped. *Accident Analysis and Prevention*, 85, 199–206
8. PENG, J., WANG, X., DENNINGER, L.: Ranges of the least uncomfortable joint angles for assessing automotive driving posture. *Applied Ergonomics*, 61, 12-21
9. SCHIRO, J., GABRIELLI, F., PUDLO, P., DJEMAI, M., BARBIER, F.: Steering wheel hand position in low-speed maneuvers. *Transportation Research*, 133–145.
10. SCHMIDT, S., SEIBERL, W., SCHWIRTZ, A.: Influence of different shoulder-elbow configurations on steering precision and steering velocity in automotive context. *Applied Ergonomics*, 46(A), 176–183
11. SMITH, J., MANSFIELD, N., GYI, D., PAGETT, M., BATEMAN, B.: Driving performance and driver discomfort in an elevated and standard driving position during a driving simulation. *Applied Ergonomics*, 49, 25–33
12. SÖLLNER, M., FLORACK, A.: Age stereotypes and compliance with feedback in elderly drivers. *Transportation Research Part F: Traffic Psychology and Behaviour*, 67, 66–77
13. THOMAS, J. A., WALTON, D.: Measuring perceived risk: Self-reported and actual hand positions of SUV and car drivers. *Transportation Research Part F: Traffic Psychology and Behaviour*, 10(3), 201–207

14. VIANO, D. C., PATEL, M., CICCONE, M. A.: HUMAN FACTORS-VOLUME 31. Human Factors: *The Journal of the Human Factors and Ergonomics Society*, 31(6), 731–733
15. WALTON, D., & THOMAS, J. A.: Naturalistic observations of driver hand positions. *Transportation Research Part F: Traffic Psychology and Behaviour*, 8(3), 229–238

Corresponding author:

Ing. Martin Kůrka, Department of Technological Equipment of Buildings, Faculty of Engineering, Czech University of Life Sciences Prague, Kamýcká 129, Praha 6, Prague, 16521, Czech Republic, tel: +420728428209, email: kurkam@tf.czu.cz

Analysis of chainsaw chains based on energy intensity

T. Kuvik[1], J. Krilek[1], J. Kováč[1]

[1]*Faculty of Technology, Technical University in Zvolen, Slovakia,*

Abstract

The article is focused on the analysis of available chainsaw chains. The chains were chosen on the basis of the most used types for medium-heavy mining chainsaws. The evaluation was carried out on the basis of energy intensity of individual chainsaw chains. 3 feed speeds, 3 cutting speeds and two wood species (beech and spruce) were chosen for the measurements. Based on the measured data, the results were processed using the STATISTICS program 12.

Key words: Chainsaw chain, energy intensity, catting speed

INTRODUCTION

Nowadays, saw chains (figure 1) with planing tooths are used. A cutter has two plates - the side cutting edge and the top cutting edge. They form a 90-degree angle. The tooth removes a chip of a fixed thickness determined by the difference in height between the depth limiter and the top cutting edge. The peripheral speed of cutter saw chains depends on the type of machine and cutting mechanism 15 to 20 m. s-1 (Kováč and Krilek 2012).

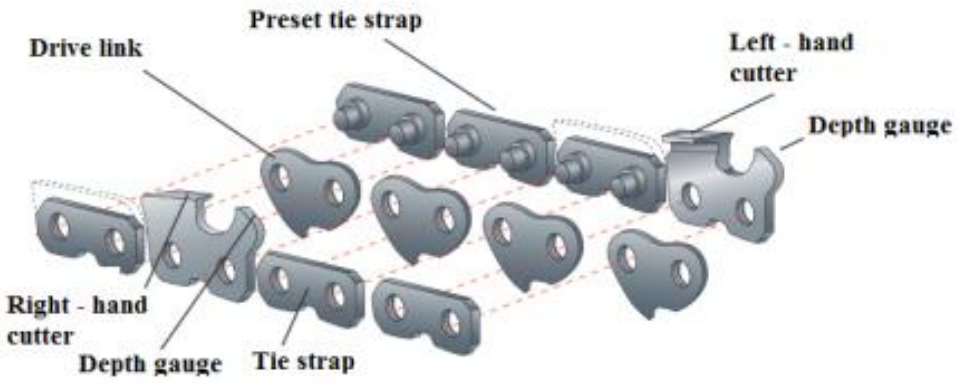

Fig. 1 Parts of a cainsaw chain.

Guide bar

A guide bar is the principal component of a chain saw bearing all external loads affecting the chain cutting mechanism when sawing. Increased attention is paid to the shape of the guide bar which has a great impact on the productivity and safety of the whole mechanism. Guide bars consist of four main parts: a mounting section, a top part, a bottom part and a tip. Most bars vary in size and shape and are adapted to their use (Kováč et al. 2013). The hardness of tree

species affects some extent the process of blunting of a tool, thus causing gradual changes in the intensity of cutting force and the necessary input cutting power.

MATERIALS AND METHODS

The experiment took place in TUZVO workshops with experimental equipment. The cutting mechanisms of the chainsaws were attached using jigs. Using the designed measuring chain, the decrease in cutting speed as well as the magnitude of the torque were monitored.

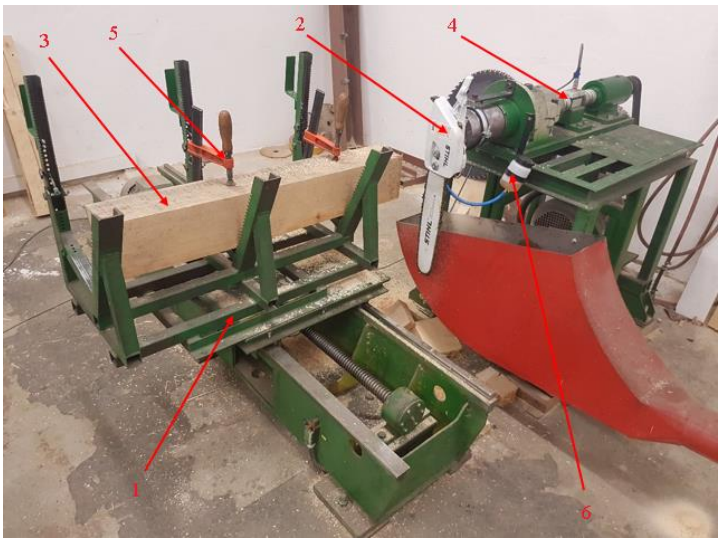

Fig. 2 Experimental device with a jig for holding the cutting mechanism of a STIHL chainsaw 1-sample material, 2 - trolley ensuring movement into the cut, 3 - jig for holding the cutting mechanism of the chainsaw, 4 - tank with oil, 5 - torque and speed sensor HBM T20 WN,

The brands of chainsaws STIHL and HUSQVARNA were chosen for the experiments, they are the most used brands of chainsaws in Slovakia. The types of chainsaws were medium-heavy mining saws STIHL MS 261 and HUSQVARNA XP 550. Chains (Table1) and bars were used types recommended by the manufacturer, also used oils for chain lubrication.

Table 1 Chainsaw chains

Chain	Pitch	Gauge	Length of guide bar (cm)
Husqvarna H21 064E X	*.325*	1.5	38
Oregon 73DP056E	*3/8*	1.5	38
Oregon 21BPX064E	*.325*	1.5	38
Oregon 73LPX	*3/8*	1.5	38
Oregon 73LPX056E	*3/8*	1.5	38
Husqvarna H25 064E X	*.325*	1.5	38

Stihl Oilomatic duro RD3	*.325*	1.6	37
Stihl oilomac RSC	*3/8*	1.6	37
Stihl Oilomatic RMC	*.325*	1.6	37
Stihl Oilomatic RS	*.325*	1.6	37
Stihl oilomatic RSC	*.325*	1.6	37
Husqvarna H42 068E X	*3/8*	1.5	38

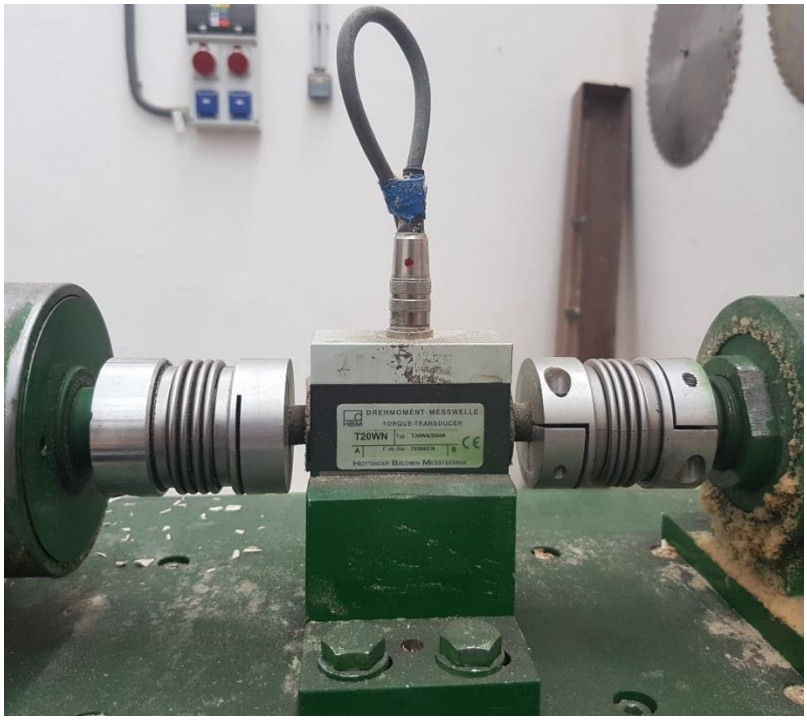

Fig. 3 HBM T20WN torque and speed rate sensor

The HBM T20W strain gauge was used to measure torque and speed (Figure 3). The sensor is protected by two original flexible bellows couplings, which protect the sensor against deviations and throws caused by misalignment of the shafts and limit the transmission of torque to 60 Nm.

Tab. 2 Basic characteristics of the HBM T20WN sensor

Parameter	Unit	Value
Nominal torque	Nm	20
Maximum torque load	Nm	60
Destructive torque load	Nm	108
Nominal sensitivity	V	10
Sensitivity tolerance	%	0.2
Linearity error	%	<±0.1
Relative error related to the change of the output signal	%	<0.05

RESULTS AND DISCUSSION

According to Table 3, the type of chainsaw chain is statistically significant, i.e. it affects the size of the power (Figure 4). The purpose of this analysis is to determine the effect of the chain and its interaction with the remaining factors. As we can see in the table, the two-factor interactions of the chainsaw chain with other factors are significant, as well as the three-factor interactions of the chain - wood - feed speed (Figure 7) and chain - wood - cutting speed (Figure 8). Of the monitored graphs, the most statistically significant influence is wood, feed speed, cutting speed and finally the type of chain.

Tab. 3 Basic table of multifactor analysis of power for chain, wood, feed and cutting speed

	sum of squares	Degree of freedom	Sample of variance	F- test	p – value (sign. level)
Overall average	620771128	1	620771128	155141.0	0.000000
Chain	6400624	11	581875	145.4	0.000000
wood	7847222	1	7847222	1961.2	0.000000
vf	37198762	2	18599381	4648.3	0.000000
vc	8638320	2	4319160	1079.4	0.000000
Chain*Wood	1487938	11	135267	33.8	0.000000
Chain*vf	1283080	22	58322	14.6	0.000000
Wood*vf	818307	2	409153	102.3	0.000000
Chain*vc	826394	22	37563	9.4	0.000000
Wood*vc	15456	2	7728	1.9	0.145456
vf*vc	8770	4	2192	0.5	0.700579
Chain*Wood*vf	341847	22	15538	3.9	0.000000
Chain*Wood* vc	139914	22	6360	1.6	0.041336
Chian*vf*vc	188117	44	4275	1.1	0.354151
Wood*vf*vc	16032	4	4008	1.0	0.405621
Chain*Wood*vf*v c	168463	44	3829	1.0	0.553369
residuum (error)	4321443	1080	4001		

v_c – cutting speed . v_f . feed speed

Figure 4 shows the effect of chain type on the resulting performance. The RD1 chain (Stihl Rapid Duro, with pitch .325) shows an extreme where the average values are much higherthan other chainsaw chains. According to the graph. the most efficient chain is 73 LPX (Oregon, with pitch 3/8)

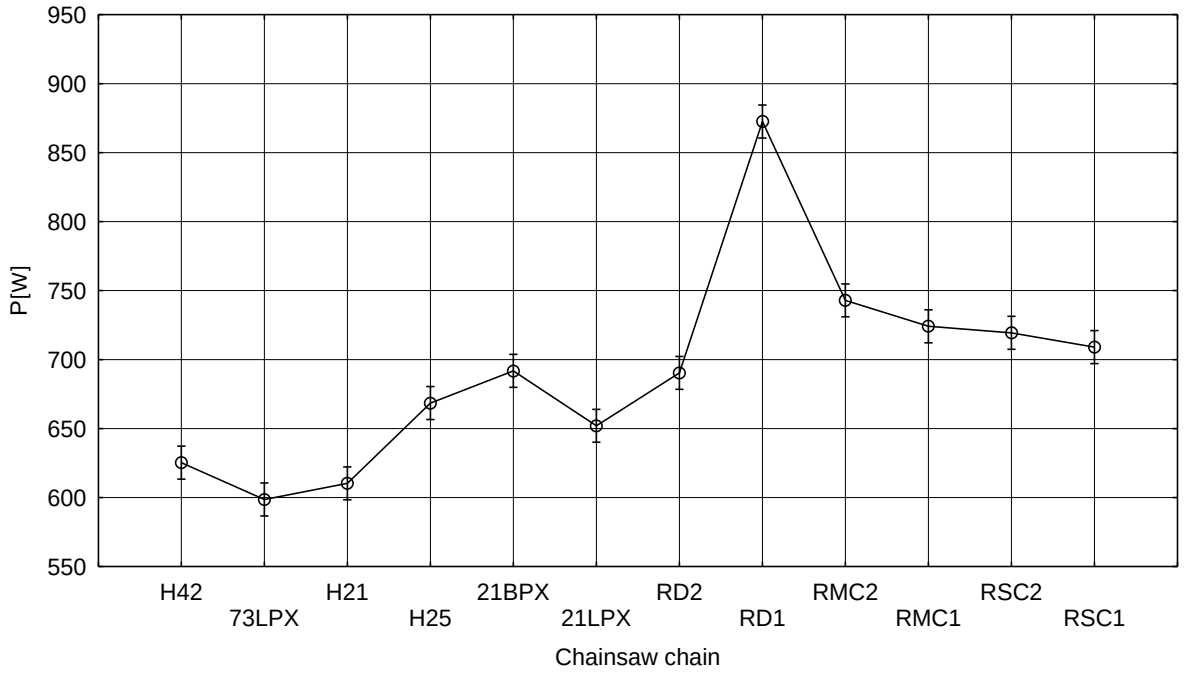

Fig. 4 95% confidence intervals for mean power values depending on the type of chain

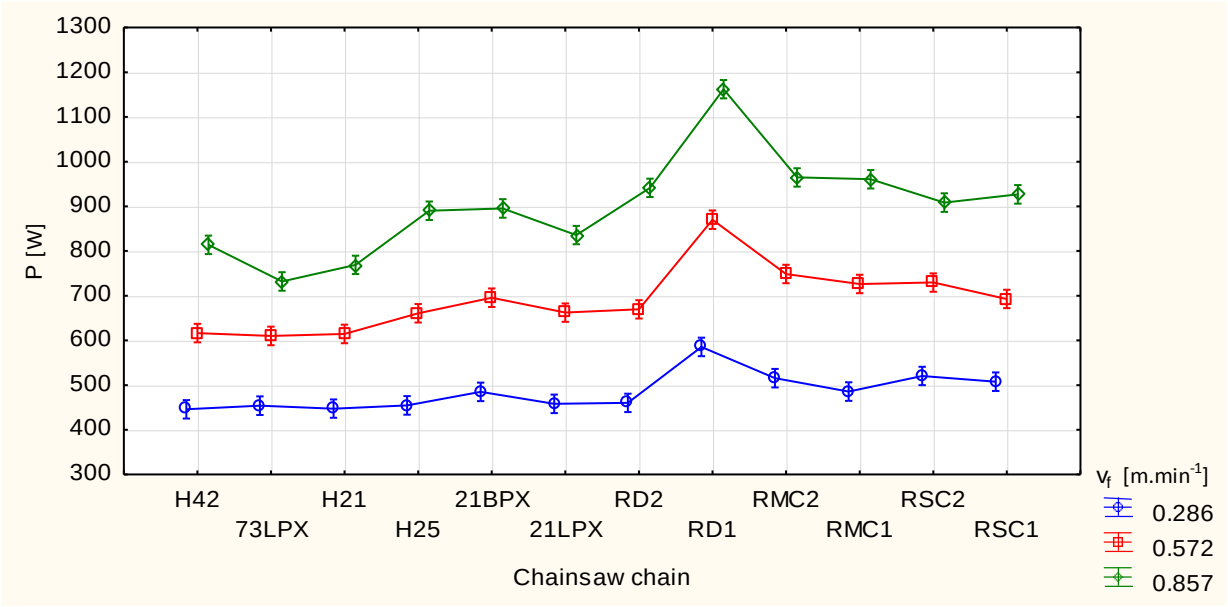

Fig. 5 95% confidence intervals for mean power values depending on chain type and feed speed

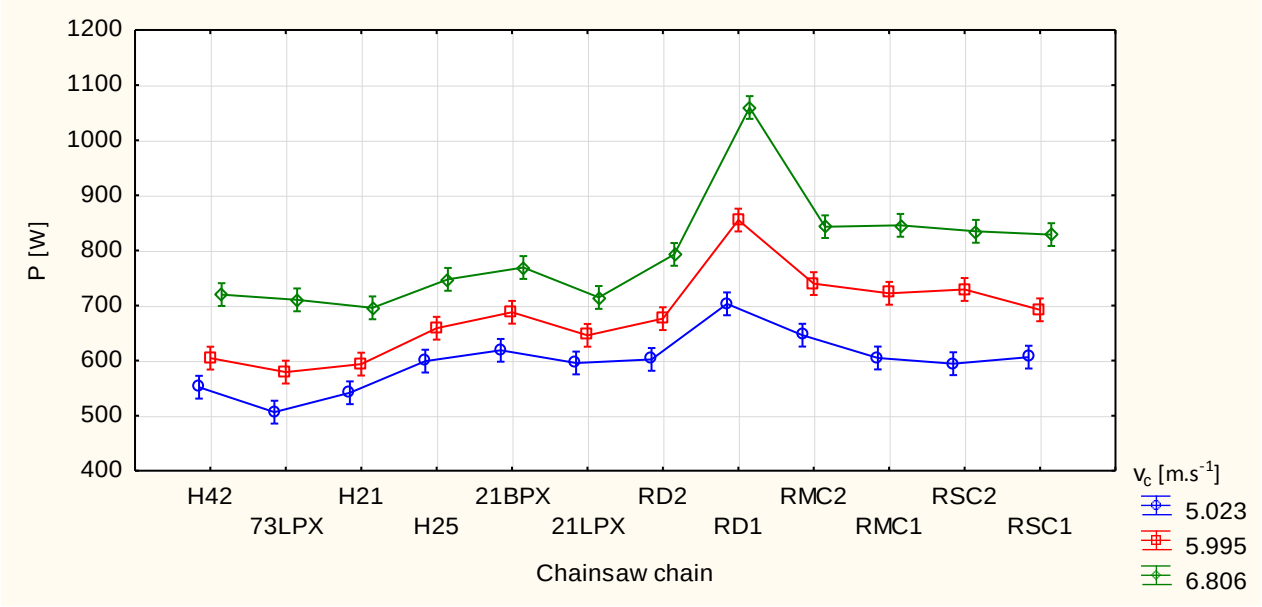

Fig. 6 95% confidence intervals for mean power values depending on chain type and cutting speed

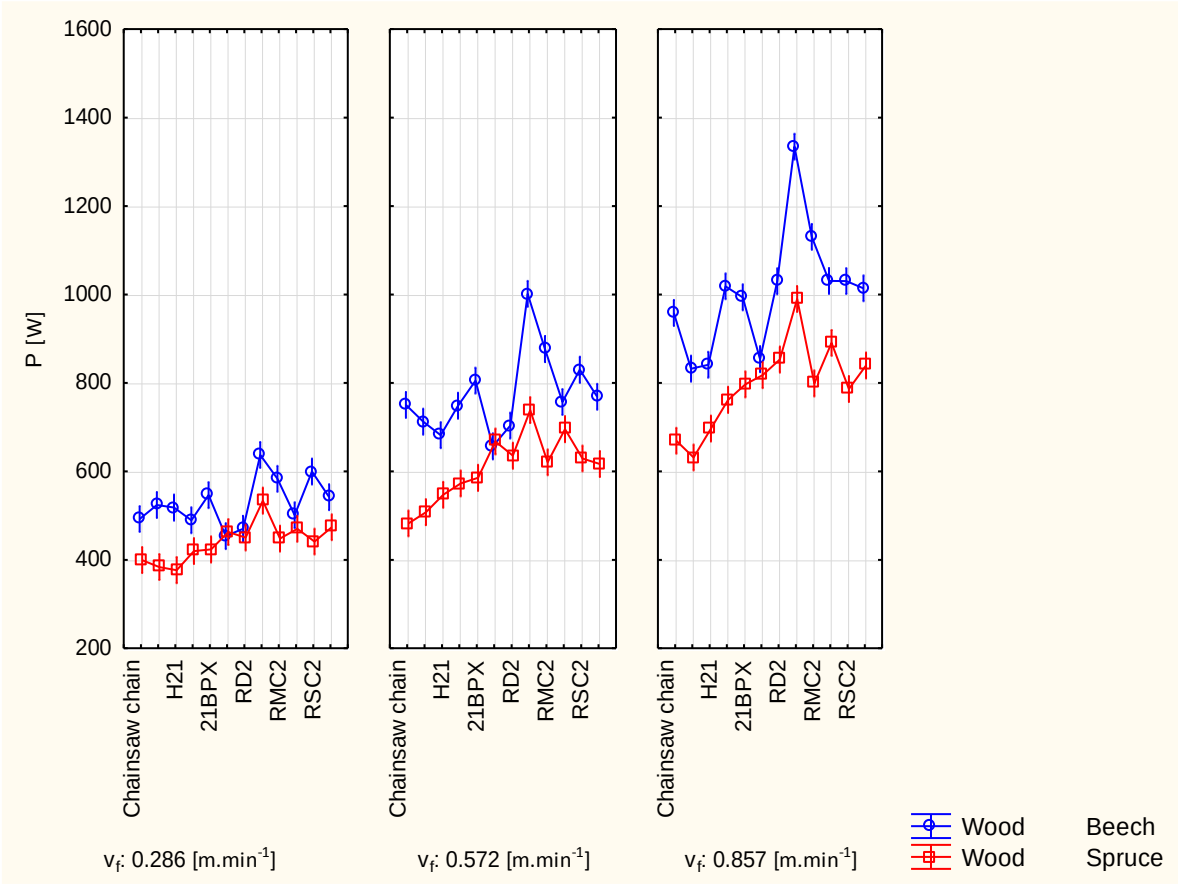

Fig. 7 95% confidence intervals for mean power values depending on the type of chain and sliding speed and wood

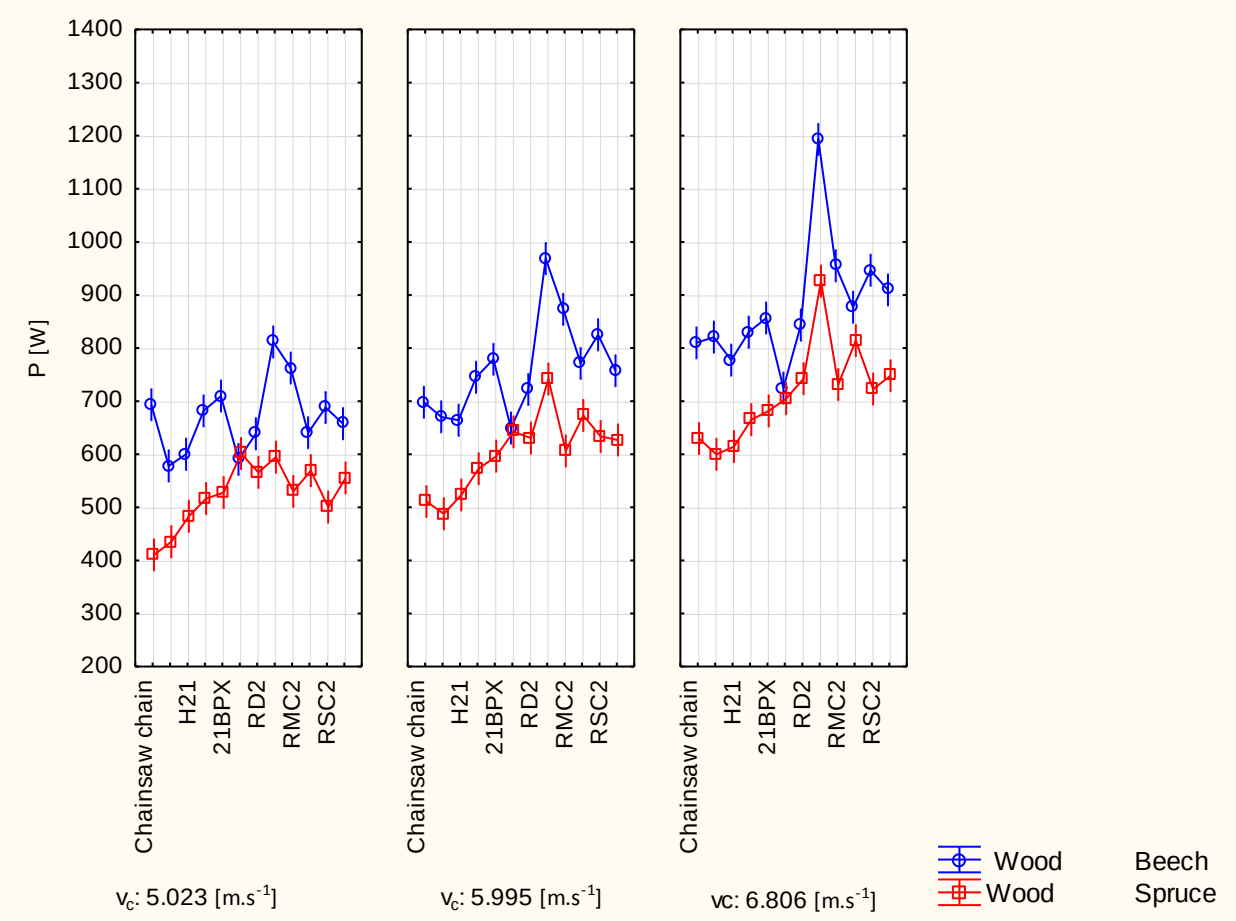

Fig. 8 95% confidence intervals for mean power values depending on chain type and cutting speed

Various methods and devices have been proposed for the research of the cross-cutting process. MACIAK (20015) in his work used a complete chainsaw which was fixed to the table and the workpiece made a feed to the cut. OTTO and PARMIGIANI (2015) used a test apparatus where a guide bar with a saw chain and a sprocket was used. For our experiments. we used the entire cutting mechanism (engine block, oil pump, clutch drum, sprocket, guide bar, chain, tensioning device) which is mounted on the experimental device. We consider the advantage over work where a complete chainsaw is mounted (MACIAK. 2015) that we can precisely set the speed (cutting speed) in our solution. The test apparatus where only the guide bar with the sprocket is mounted (Otto and PARMIGIANI. 2015) is in principle similar to our apparatus. but because we used the whole cutting mechanism, we were able to describe its overall impact on the sawing process.

CONCLUSION

When sawing with a saw chain, the guide bar slides smoothly into the cut. If the chain speed or feed rate is disproportionate, the chain may jam or, in extreme cases, rupture or damage the

cutting mechanism. Therefore, a sufficient speed of the chain must be ensured. which will ensure the cutting speed and thus a smooth movement into the cut. The influence of the chainsaw chain on performance, where the power values were with small differences, just for the Stihl RD chain with a division of .325. there was an extreme in all variations of other parameters and the power jumped high compared to other chains.

The paper was written within the project: *1/0609/20" Research of the cutting tools at the dendromass processing in agricultural and forestry production."*.

REFERENCES

1. KOVÁČ. J.. KRILEK. J.. KUČERA. M.. KOPECKÝ. Z.. HLÁSKOVÁ. L.. 2013: Ergonomic process parameters cutting wood. Mendel University in Brno. 68 pp. 978-80-7375-766-3.
2. KOVÁČ. J.. KUĽKOV. A. 2016. *Rezné mechanizmy s pílovou reťazou ťažobných strojov.*. Zvolen : Technická univerzita vo Zvolene. 2016. kolokvium ku grantovej úlohe č. 1/3534/06.
3. MACIAK. A. 2015. *Impact of the feed force on discontinuity of wood cutting with petrol chainsaw*. 66. Warsaw : Annals of Warsaw University of Life Sciences – SGGW. Agriculture (Agricultural and Forest Engineering). 2015. ISSN 1898-6730.
4. Maciak. Adam; Kubuśka. Magda; Moskalik. Tadeusz. **Forests; Basel** Vol. 9. Iss. 10. (Oct 2018). DOI:10.3390/f9100660
5. OTTO. O .PARMIGIANI. J. 2015.*Velocity. Dpth-of-Cut. and Physical Property Effects on Saw Chain Cutting.*. s.l. : BioResources . 2015. 10(4).. ISSN 1930-2126.
6. SIKLIENKA. M.. KMINIAK. R.. ŠUSTEK. J.. JANKECH. A.. 2017. *Delenie a obrábanie dreva*. Zvolen: Tachnická univerzita vo Zvolene. 2017. ISBN 978-80-228-2845-1
7. ŠTOLLMANN. V.. SLUGEŇ. J.. 2009: Forestry means of mechanization. Technical University in Zvolen. 198 pp. ISBN 978-80-228-2065-3.

Corresponding author:

Ing. Tomáš Kuvik. PhD.. *Faculty of Technology. Technical University in Zvolen. Slovakia.*
t.kuvik14@gmail.com; Tel.: 045/5206550

Changes in Papua's forest: A case study of sago palm area

S. M. A. Letsoin[1,2], D. Herák[2], F. Rahmawan[3], R. Ch. Purwestri[4,5]*

[1]*Department of Mechanical Engineering, Faculty of Engineering, Czech University of Life Sciences Prague, Kamycka 129, 16500 Praha-Suchdol, Czech Republic; Letsoin@tf.czu.cz(S.M.A.L), herak@tf.czu.cz(D.H)*

[2]*University of Musamus, Faculty of Engineering, Merauke Regency, Papua-Indonesia*

[3]*INTSIA Foundation of Papua Province, Furia 3 Number 116 Abepura, Jayapura City 99225 Papua, Indonesia; fajar_rahmawan@yahoo.com(F.R)*

[4]*Faculty of Forestry and Wood Sciences, Czech University of Life Sciences Prague, Kamycka 129, 16500 Praha-Suchdol, Czech Republic purwestri@fld.czu.cz(R.C.P)*

[5]*Institute of Nutritional Sciences, University of Hohenheim, Garbenstrasse 28, 70599 Stuttgart, Germany; rc.purwestri@uni-hohenheim.de(R.C.P)*

Abstract

In Papua Province of Indonesia, forests areas play an important role as a natural habitat of sago palm that grows ecologically in the moist upland rainforest, freshwater, peat lands, swamps or salty areas of tropical lowlands. However, limited studies have examined this palm in one of the Regencies of Papua Province, namely Merauke Regency. In this study, we performed remotely sensed data imagery and supervised classification to evaluate land cover changes from 1990 to 2019. The six classes of the natural forest consists of primary dry land forest, secondary dryland forest, primary mangrove forest, secondary mangrove forest, primary swamp forest and secondary swamp forest; thus fifteen classes of non-forested area. Concerning the sago palm habitat, our study evaluated two different categories (1) based on the land cover scheme from the Ministry of Environment and Forestry and (2) according to peatland land cover ecosystem in Papua. Based on paired samples t-test, the result indicated statistically significant changes specifically at primary dry land, grassland and swamp forest. Twelve from 20 districts of Merauke Regency tend to lose the forecasted natural habitat of sago palm.

Key words: *Merauke Regency, forested area, sagu palm habitat, t-test.*

INTRODUCTION

Sago palm, scientifically known as *Metroxylon sagu Rottb*, is one of the ecological tree species that grows in Indonesia particularly in Papua and West Papua (Karim, A.A.; Tie, A.P.-L.; Manan, D.M.A.; Zaidul, I.S.M., 2008). The palm has tremendous advantages to support the food sector, bioethanol (Jonatan, N.J.; Ekayuliana, A.; Dhiputra, I.M.K.; Nugroho, Y.S, 2017; Thangavelu, S.K.; Rajkumar, T.; Pandi, D.K.; Ahmed, A.S.; Ani, F.N.,2019) as a raw material for agro industry and other aspects of sago (Singhal, R.S.; Kennedy, J.F.; Gopalakrishnan, S.M.;

Kaczmarek, A.; Knill, C.J.; Akmar, P.F., 2008). This palm rises well in freshwater such as in Jayapura and in swamps or salty areas of tropic lowlands for example in Merauke regency. Merauke regency encompasses twenty districts namely Ulilin, Muting, Kaptel, Ngguti, Ilwayab, Tabonji, Waan, Kimaam, Tubang, Okaba, Malind, Kurik, Animha, Elikobel, Jagebob, Tanah miring, Semangga, Sota, Naukenjerai and Merauke. The capital of regency is located in Merauke. This regency has a total area of around 4.851.715 ha and is well known as the regency with the largest area in Papua Province. Merauke regency is also a leader of the top three paddies providers with about 91.47% of paddy production over Papua Province (BPS, 2020). Current satellite imagery has been explored extensively for mapping and monitoring land cover changes, using Landsat (Liping, C.; Yujun, S.; Saeed, S., 2018), Moderate Resolution Imaging Spectroradiometer (MODIS) (Wei, B.; Xie, Y.; Wang, X.; Jiao, J.; He, S.; Bie, Q.; Jia, X.; Xue, X.; Duan, H.,2020) and others openness of data satellite. Furthermore, due to a broad range of suitable spectral bands, very high resolution, and accessibility with various computer-aided software, for instance, System for Automated Geoscientific Analyses (SAGA) (Cando-Jácome, M.; Martínez-Graña, A., 2019) Quantum Geographic Information System (Qgis) (Jakimow, B.; van der Linden, S.; Thiel, F.; Frantz, D.; Hostert, P.,2020), and other platforms such as Google Earth (Stromann, O.; Nascetti, A.; Yousif, O.; Ban, Y.,2019) has been improved the use of remotely sensed data. The long term series of Landsat has been demonstrated successively to monitor land cover changes because of land degradation (Venter, Z.S.; Scott, S.L.; Desmet, P.G.; Hoffman, M.T.,2020) to investigate land cover changes as a result of some variables such as urban expansion (Zhang, Y.; Zhao, H.,2020), and deforestation (Fortin, J.A.; Cardille, J.A.; Perez, E.,2020). It continues to measure forest carbon stock (Ma, W.; Domke, G.M.; Woodall, C.W.; D'Amato, A.W.,2020) biodiversity (Rigge, M.; Homer, C.; Cleeves, L.; Meyer, D.K.; Bunde, B.; Shi, H.; Xian, G.; Schell, S.; Bobo, M.,2020) and other land cover changes. Although some studies have focused on monitoring land cover changes of Indonesia in general, we found studies applying remote sensing to evaluate swamp forest land cover changes and its impact to natural habitat in this location are still unreported (Uda, S.K.; Hein, L.; Sumarga, E.,2017) Therefore this paper aims (1) to achieve the current land cover maps for the Merauke Regency in Papua Province of Indonesia, (2) to evaluate land cover changes. To deal with these objectives, we combined existing land cover maps that we obtained from the Ministry of Environment and Forestry (MoEF), and Landsat imagery to create new land cover maps. Thus we also applied statistical analysis to analyse the significant change of sago palm habitat based on their land cover. Our findings provide current land cover maps and the evaluation of land cover

map changes over time which can be used to support decision making of the local Government for managing and conserving natural resources.

MATERIALS AND METHODS

The study was carried out in Merauke Regency (137°38'52.9692"E - 141°0'13.3233"E and 6°27'50.1456"S - 9°10'1.2253"S; Figure 1), which is located on the Southern part of Papua Province.

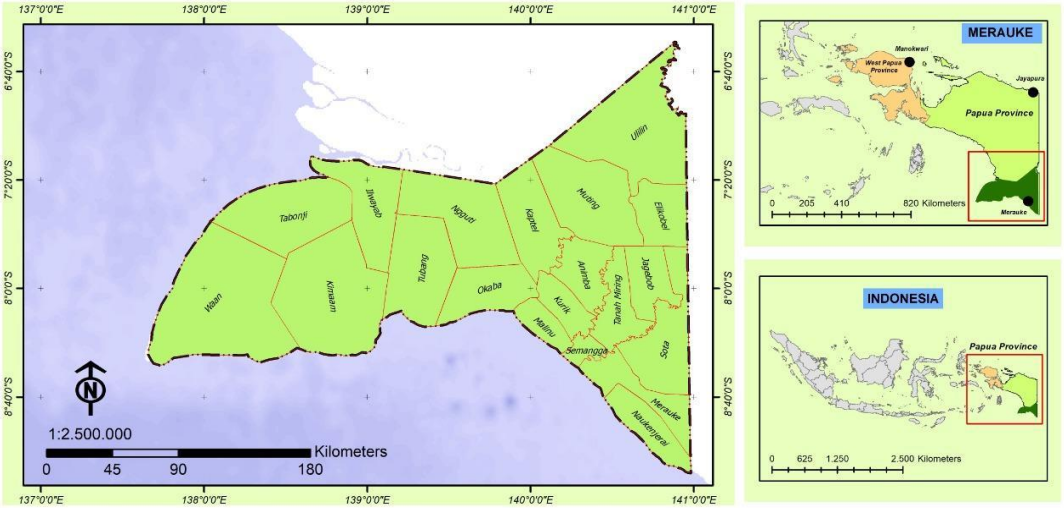

Fig. 1 Geographical position of study area. Study area has boundaries with Mappi and Boven-Digoel Regency at the north, the Arafuru Ocean to the South and West, PNG to the East

The data used in this study consists of two types of data including secondary data and remotely sensed data. Several secondary data such as the type of forest, area of forest by function, were contributed by Government agencies i.e. Plantation and Forestry also Statistics agencies through their catalogues: Papua Province in figure 2020 (Number of catalogue: 1102002.94) (BPS, 2020)**,** and Merauke in figures 2020 (Number of catalogue: 1102002.9401) (BPS, 2020)**.** Existing land cover maps for 1990, 1996, 2003, 2006, 2011, and 2014 were published on webgis.menlhk.go.id. The provincial boundary spatial data were acquired from The Regional Development Planning Agency (BAPPEDA) of Papua Province that we used as supporting data. Land cover classes of Indonesia and the description are referred to The Ministry of Environment and Forestry (MoEF), which includes Standardization Agency of Indonesia (B.S.N.) specifically S.N.I. 8033:2014. The land cover is classified into twenty-three classes that consists of 6 classes of forests, one plantation of the forest, 16 classes of non-forests. To achieve remotely sensed data, we used Landsat multispectral images that since 1972 has provided sensor

Multispectral Scanner Systems (MSS)/Return Beam Vidicon (RBV) (1972/1978), MSS/Thematic Mapper (TM) (1982/1984), Enhanced Thematic Mapper (ETM+) (1993/1999) and Operational Land Imager/Thermal InfraRed Scanner (OLI/TIRS) (2013). In this study we applied Landsat 7 ETM + and Landsat 8 OLI/TIRS (L1T) multispectral images covering the study area. The L-1Terrain (L1T) product will automatically correct their geometrics and radiometric based on inputs from the sensors as well as the Ground Control Point (G.C.P.) and Digital Elevation Models (D.E.M.). We obtained freely for the years 2000, 2009, 2015, 2016, 2017, 2018, and 2019 (E.T.M. + and OLI/TIRS), with 30m of the resolution, 705km of altitude and less than 50% cloud cover. To reduce this cloud cover, we combine multitemporal Landsat images from two seasons of Papua, were appropriately selected from Figure 2. For image classification, firstly the actual land cover maps from MoEF (1990, 1996, 2003, 2006, 2011, 2014, and 2017) were clipped and overlaid on Landsat imagery at the same year. During this process we looked at the entire map and made corrections wherever it was needed. Afterwards, supervised classification was applied (Alonso-Sarria, F.; Valdivieso-Ros, C.; Gomariz-Castillo, F., 2019) training samples were selected by delineating polygons at characteristics sites.

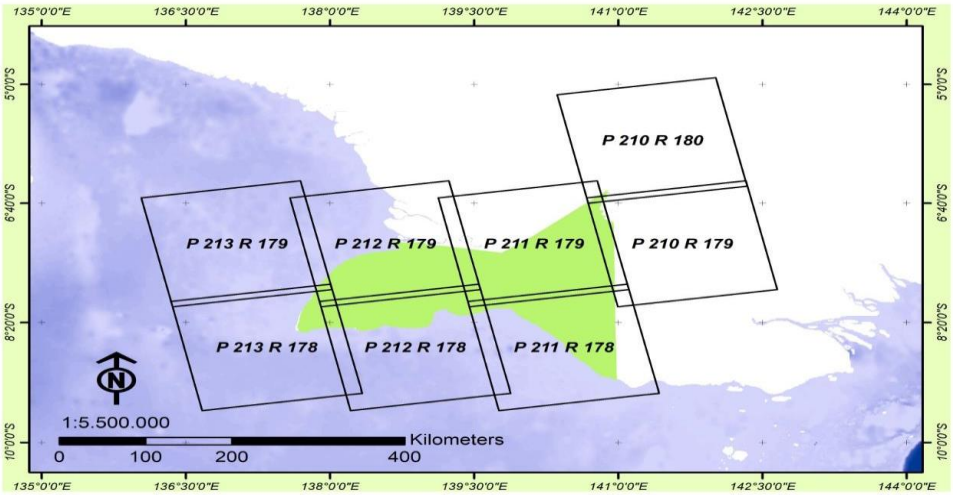

Fig. 2 The study area: Landsat imagery path and row scenes

We chose 15 of each class as the training data; at this procedure, we also compared each class that was collected in the fields by means of G.P.S. The accuracy assessments of the image classification were done as an integral part of the image classification process using QGIS. Next, we developed land cover maps for other years (2000, 2009, 2015, 2016, 2018, 2019) by analysing the supervised classification result and the existing land cover maps. Since the visual interpretation should be more standardised, we complied to the Ministry of Environment and Forestry scheme (MoEF, 2015) which included the Indonesia National Standard (S.N.I.), particularly SNI 8033:2014 that allows us to recognise the image through structure, texture, shape,

pattern and colour; at the same time grants land cover classification in Indonesia. At the final step, we validated the land cover maps by using a geographic browser which is Google Earth Pro (Gilani, H.; Shrestha, H.L.; Murthy, M.S.R.; Phuntso, P.; Pradhan, S.; Bajracharya, B.; Shrestha, B.) that provides higher resolution of satellite imagery. We ensured that checkpoints were spread throughout the study area and expressed all land cover classes; nonetheless these numbers were selected in a different amount due to the possibility of high resolution images. To designate the statistical significance in all analyses, a *p*-value of less than 0.05 was used. Statistical analysis was performed using IBM SPSS statistics version 25 (IBM Corp.,Armonk, NY, USA). In this study a *t*-test was performed to examine the means of land cover for the general characteristics of the site and whether the natural habitat of sago palm has significantly changed over the period of the study or not.

RESULTS AND DISCUSSION

Recent Land cover maps from 1990 to 2019 are presented in Figure 3; we made 13 years of land cover maps in this regency, consisting of land cover maps in 1990,1996,2000, 2003,2006,2009, 2011 and from 2014 to 2019. Twenty-one land cover categories were identified: (1) 6 classes of the natural forest included primary dry land forest, secondary dryland forest, primary mangrove forest, primary swamp forest, secondary mangroves forest, secondary swamp forest; (2) 15 classes of non-forest consisting of swamp shrub, swamp, bush/shrub, estate crop plantation, settlement area, barren land, clouds, grassland, water body, dryland agriculture, shrub mixed dryland, paddy field, fish pond, airport, transmigration area (Figure 3). In 1990, Merauke regency was covered by the natural forest around 2.440.396 ha or approximately 50.3% (figure 4) of the total area of this regency compared to non-forest of about 2.411.319 ha or 49.70% of total area. However in 2019 the Regency was covered by non forested area for about 2.767.158 ha or 57.03% of the entire site.

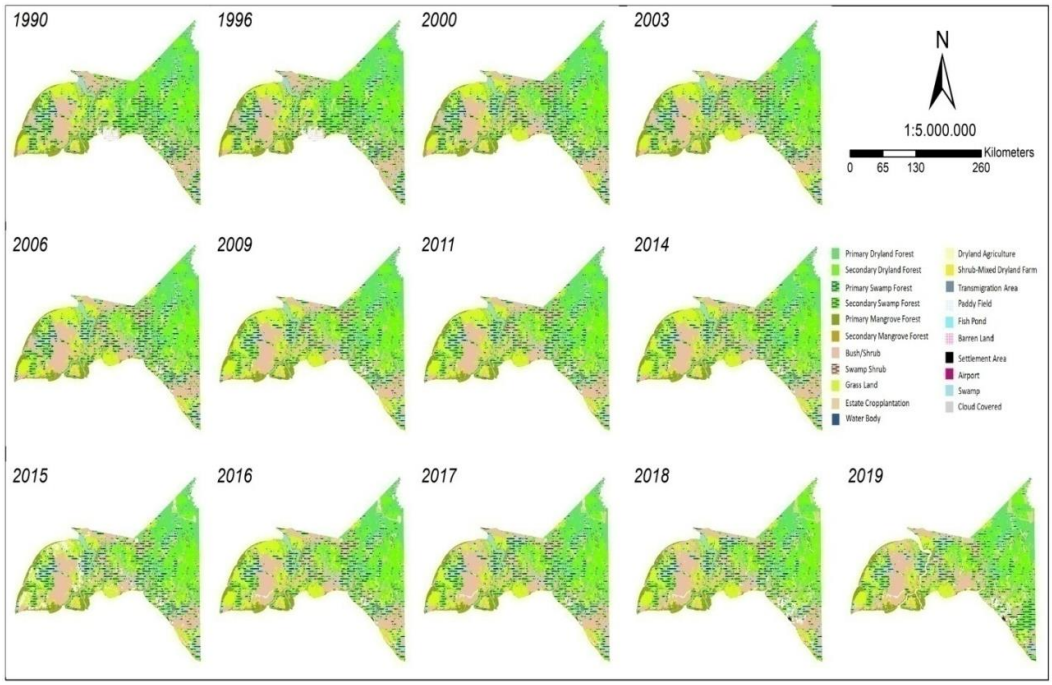

Fig. 3 Merauke Regency land cover maps in 1990, 1996, 2000, 2003, 2006, 2009, 2011 and from 2014 to 2019

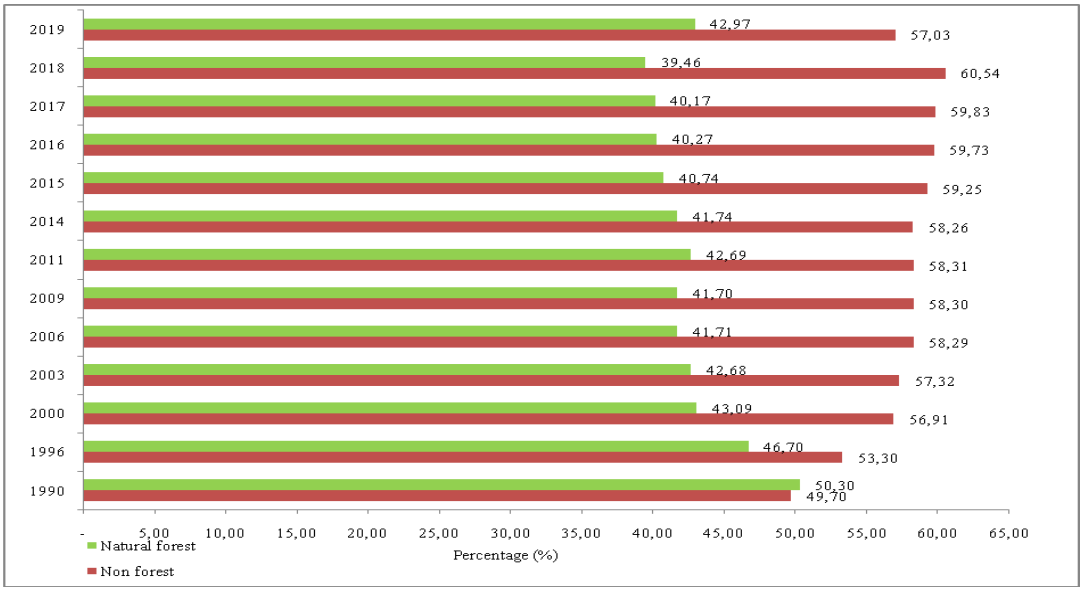

Fig. 4 Percentage of non-forest and natural forest land cover changes during 29-years

We evaluated the natural habitat of sago palm based on the land cover changes of the regency. We used two different categories i.e. (1) based on the Ministry of Environment and Forestry land cover schemes and (2) peatland land cover ecosystem of Papua (Papua Province, 2017). In (MoEF,2015) it predicts two typical habitats of the sago palm namely primary swamp forest and secondary swamp forest. Other natural ecosystems were forecasted i.e. dryland forest, bush/shrub, swamp, swamp shrub, and savanna/grassland (Papua Province, 2017 pp.1-2), the local community usually utilises this peat ecosystem to find fish, or to plant and harvest sago palm (Papua Province, 2017 p.59). Here, we assessed statistically twenty districts of Merauke regency, with N, i.e. primary dry land forest, secondary dryland forest, primary swamp forest, secondary swamp forest, bush/shrub, grassland, swamp shrub, swamp; as shown by table 1 using the paired samples t-test for the year 1990 and 2019. We used this result to examine the significant changes of the various natural sago palm ecosystems in Merauke Regency as well as to support our second aim of this study.

Tab. 1 Land cover changes from the natural habitat of sago (1990 and 2019)

LC	1990	2019	p-value
Primary dryland	34.736,82 ±71.532,46 (0,00 , 315.111,00)	27.686,42 ± 67.227,85(0 , 299.073,00)	0.015
Secondary dryland	31.902,33 ±38.007,26 (1,02 , 118.800,00)	33.604,22 ± 39.934,11(0 , 112.000,00)	0.313
Primary swamp forest	17.126,28 ±23.169,16 (1.276,23 ,107.615)	10.271,99± 8.519,85(531,72 , 24.711,10)	0.107
Secondary swamp forest	26.555,19±24.072,41 (4.668,14, 94.925,10)	18.590,47± 23.439,27(949,07 , 105.92)	0.152
Bush/shrub	3.597,31 ± 6.055,62 (0 ,24.048,80)	8.923,07 ± 16.655,05(0 , 63.317,30)	0.081
Grassland	23.585,31 ± 36.748,43 (0 , 111.643,00)	35.202,67 ± 42.540,96 (0 , 152.745,00)	0.002
Swamp shrub	46.503 ± 52.913,31 (51,08 , 181.539,00)	45.045,15±50.975,60(51,08 , 190.427)	0.723
Swamp	19.197,62 ± 16.473,24 (79,92 , 62.207,50)	25.707,58 ± 17.481,00(34,41, 68.235,40)	0.007

CONCLUSIONS

The study has produced recent land cover maps in MeraukeRegency from 1990 to 2019 using remote sensing techniques and supervised classification. Merauke Land cover consists of twenty one classes which are classified into six classes of natural forest and fifteen classes of non-forested area. Our analysis of land cover map presented the largest declines mostly occurred in natural forest, namely primary dryland forest, secondary dryland forest, primary mangrove, secondary mangrove, primary swamp forest and only secondary swamp forest has slight increased by about +0.03% over time. According to the natural habitat of sago palm, we evaluated eight possible ecosystems namely dryland, bush/shrub, grassland, swamp shrub, swamp, and swamp forest using paired sample t-test. The result indicated statistically significant changes specifically at primary dry land (p-value = 0.015), grassland (p-value = 0.002) and swamp (p-value = 0.007). We also analysed these areas in twenty districts of Merauke Regency.Our findings confirmed that 12 districts from 20 districts of Merauke Regency tend to lose the natural habitat of sago palm, while only 1 district remains unchanged. Nonetheless these particular ecosystems are beneficial to support local community life for example planting and harvesting sago palm. Therefore these outcomes could be integrated within decision makers, stakeholders to evaluate and to establish government development plans.

ACKNOWLEDGMENT

This study is part of on-going research being undertaken for PhD work of the first author. The first author is deeply grateful to Indonesia Endowment Fund for Education (LPDP-Indonesia) for funding and supporting her PhD study. R.C.P is also supported by the grant EVA 4.0 no. CZ.02.1.01/0.0/0.0/16_019/0000803 financed by the OPRDE-Ministry of Education of the Czech Republic.

REFERENCES

1. Alonso-Sarria, F.; Valdivieso-Ros, C.; Gomariz-Castillo, F. Isolation Forests to Evaluate Class Separability and the Representativeness of Training and Validation Areas in Land Cover Classification. *Remote Sensing***2019**, *11*, 3000, doi:10.3390/rs11243000.
2. BPS, Papua Province in Figures 2020. *BPS-Statistics of Papua Province***2020**.
3. BPS, Merauke Regency in Figures 2020. *BPS-Statistics of Merauke Regency* **2020**
4. Cando-Jácome, M.; Martínez-Graña, A. Determination of Primary and Secondary Lahar Flow Paths of the Fuego Volcano (Guatemala) Using Morphometric Parameters. *Remote Sensing***2019**, *11*, 727, doi:10.3390/rs11060727
5. Enping; Yunlin; Hui; Guangxing; Dengkui Improving the Estimation of Forest Carbon Density in Mountainous Regions Using Topographic Correction and Landsat 8 Images. *Remote Sensing***2019**, *11*, 2619, doi:10.3390/rs11222619.
6. Fortin, J.A.; Cardille, J.A.; Perez, E. Multi-sensor detection of forest-cover change across 45 years in Mato Grosso, Brazil. *Remote Sensing of Environment***2020**, *238*, 111266, doi:10.1016/j.rse.2019.111266.
7. Gilani, H.; Shrestha, H.L.; Murthy, M.S.R.; Phuntso, P.; Pradhan, S.; Bajracharya, B.; Shrestha, B. Decadal land cover change dynamics in Bhutan. *Journal of Environmental Management***2015**, *148*, 91–100, doi:10.1016/j.jenvman.2014.02.014.
8. Jonatan, N.J.; Ekayuliana, A.; Dhiputra, I.M.K.; Nugroho, Y.S. The Utilization of Metroxylon Sago (Rottb.) Dregs for Low Bioethanol as Fuel Households Needs in Papua Province Indonesia. *KLS***2017**, *3*, 150, doi:10.18502/kls.v3i5.987.
9. Jakimow, B.; van der Linden, S.; Thiel, F.; Frantz, D.; Hostert, P. Visualizing and labeling dense multi-sensor earth observation time series: The EO Time Series Viewer. *Environmental Modelling & Software***2020**, *125*, 104631, doi:10.1016/j.envsoft.2020.104631.
10. Karim, A.A.; Tie, A.P.-L.; Manan, D.M.A.; Zaidul, I.S.M. Starch from the Sago (*Metroxylonsagu*) Palm TreeProperties, Prospects, and Challenges as a New Industrial Source for Food and Other Uses. *Comprehensive Reviews in Food Science and Food Safety***2008**, *7*, 215–228, doi:10.1111/j.1541-4337.2008.00042.x.
11. Liping, C.; Yujun, S.; Saeed, S. Monitoring and predicting land use and land cover changes using remote sensing and GIS techniques—A case study of a hilly area, Jiangle, China. *PLoS ONE***2018**, *13*, e0200493, doi:10.1371/journal.pone.0200493.
12. Ma, W.; Domke, G.M.; Woodall, C.W.; D'Amato, A.W. Contemporary forest carbon dynamics in the northern U.S. associated with land cover changes. *Ecological Indicators***2020**,

110, 105901, doi:10.1016/j.ecolind.2019.105901.

13. MoEF, National Forest Reference Emission Level for Deforestation and Forest Degradation: In the Context of Decision 1/CP.16 para 70 UNFCCC (Encourages developing country Parties to contribute to mitigation actions in the forest sector), Published by DG-PPI MoEF Indonesia 2015.
14. Papua Province. *RREG Papua Province 2017-2020*, Peatland Restoration Agency, Papua Province. Jakarta, Republic of Indonesia, **2017**; pp. 1-2, p. 59.
15. Rigge, M.; Homer, C.; Cleeves, L.; Meyer, D.K.; Bunde, B.; Shi, H.; Xian, G.; Schell, S.; Bobo, M. Quantifying Western U.S. Rangelands as Fractional Components with Multi-Resolution Remote Sensing and In Situ Data. *Remote Sensing***2020**, *12*, 412, doi:10.3390/rs12030412.
16. Singhal, R.S.; Kennedy, J.F.; Gopalakrishnan, S.M.; Kaczmarek, A.; Knill, C.J.; Akmar, P.F. Industrial production, processing, and utilization of sago palm-derived products. *Carbohydrate Polymers***2008**, *72*, 1–20, doi:10.1016/j.carbpol.2007.07.043.
17. Stromann, O.; Nascetti, A.; Yousif, O.; Ban, Y. Dimensionality Reduction and Feature Selection for Object-Based Land Cover Classification based on Sentinel-1 and Sentinel-2 Time Series Using Google Earth Engine. *Remote Sensing***2019**, *12*, 76, doi:10.3390/rs12010076.
18. Thangavelu, S.K.; Rajkumar, T.; Pandi, D.K.; Ahmed, A.S.; Ani, F.N. Microwave assisted acid hydrolysis for bioethanol fuel production from sago pith waste. *Waste Management***2019**, *86*, 80–86, doi:10.1016/j.wasman.2019.01.035.
19. Uda, S.K.; Hein, L.; Sumarga, E. Towards sustainable management of Indonesian tropical peatlands. *Wetlands Ecol Manage***2017**, *25*, 683–701, doi:10.1007/s11273-017-9544-0.
20. Venter, Z.S.; Scott, S.L.; Desmet, P.G.; Hoffman, M.T. Application of Landsat-derived vegetation trends over South Africa: Potential for monitoring land degradation and restoration. *Ecological Indicators***2020**, *113*, 106206, doi:10.1016/j.ecolind.2020.106206.
21. Wei, B.; Xie, Y.; Wang, X.; Jiao, J.; He, S.; Bie, Q.; Jia, X.; Xue, X.; Duan, H. Land cover mapping based on time- series MODIS- NDVI using a dynamic time warping approach: A casestudy of the agricultural pastoral ecotone of northern China. *Land Degrad Dev***2020**, ldr.3502, doi:10.1002/ldr.3502.
22. Zhang, Y.; Zhao, H. Land–Use and Land-Cover Change Detection Using Dynamic Time Warping–Based Time Series Clustering Method. *Canadian Journal of Remote Sensing***2020**, *46*, 67–83, doi:10.1080/07038992.2020.1740083.

Corresponding author: Sri Murniani Angelina Letsoin, ST., M.Eng., Department of Mechanical Engineering, Faculty of Engineering, Czech University of Life Sciences Prague, Kamýcká 129, Praha 6, Prague, 16521, Czech Republic, phone: +420776569772, e-mail: letsoin@tf.czu.cz

Distance measuring in vineyard row using ultrasonic and optical sensors

D. Marko[1]

[1]*Department of Electrical Engineering, Automation and Informatics, Faculty of Engineering, Slovak University of Agriculture in Nitra*

Abstract

This article deals with measuring the distance in a vineyard row using ultrasonic and optical sensors. Previous research has dealt only with static measurements in which they tested the accuracy and repeatability of measurements and beam angles of sensors on static targets. Their conclusions were that these types of sensors are useful for measuring distance from plants, but their declared measurement parameters are degraded. However, plants, particularly vines are inhomogeneous over their area and to verify the usability of sensors to continuously measure the distance along the entire length of the row in motion, it is necessary to test the sensors dynamically. We tested 3 different sensors – two ultrasonic and one optical without and using smoothing filters. We used a Kalman filter and moving average algorithms. JSN-SR04T-2.0 and VL53L1X sensors with filtering reached 100% of the values in chosen the tolerance of 0.4 m. However, the VL53L1X optical sensor was only usable up to 1.2 m. The last sensor HC-SR04 proved to be the most sensitive to gaps in the vineyard and is therefore the least suitable for this purpose. Sensor JSN-SR04T-2.0 came out as best with data variance 0.0544 m^2 and measuring range 3.2 m.

Key words: distance measuring, vineyard, ultrasonic, laser, sensor, Kalman filter, moving average

INTRODUCTION

With an increasing demand for automation in every sector, including agriculture, there is a need for development and improvement of measurement quality. In the field of mobile robotics, a reliable position data are crucial for correct operation of mobile robots. Distance sensors provide actual position data to the robots. The right sensors have to be chosen for this task.

So far, ultrasonic and optical sensors have been tested for measuring distance from plants only in static conditions. Escolà et al. (2011) carried out static measurements with industrial sensor in apple orchard. The average error was ±5.11 cm. They attributed it to possible interaction between ultrasonic waves and canopy. Most times a single leaf is not enough to generate enough

echo due to its reduced dimensions and/or to its orientation. According to them, to measure a correct distance, the sensor needs to detect a group of leaves approximately placed in the same vertical plane. Gamarra-Diezma et al. (2015) tested more powerful industrial ultrasonic sensor with 28° cone angle, measuring distance from olive trees, in this scenario the cone angle was reduced to 20°. Al Saddik et al. (2018) and Feret et al. (2008) measured optical properties of leaves of different plants including grapevine and found that biggest reflectance from leaves is in the near infrared (NIR) region ranging from 50 to 55 %. This assumes successful function of optical sensors with NIR emitters for this task. However, mobile robots require sensors which are able to deliver reliable distance data and therefore testing of sensors in motion is required. In this article we will be comparing three of commonly available distance sensors – two ultrasonic and one optical. Further, we will utilize smoothing filters to improve the sensors outputs.

MATERIALS AND METHODS

Measurements will be carried out with Arduino Mega 2560 microcontroller which supports communication protocols for each of tested sensors. Obtained sensor data will be sent from the microcontroller to MATLAB for further filtering with chosen smoothing filters algorithms.

Ultrasonic sensors

Main benefits of ultrasonic sensors are unaffected operation by sunlight or dark material. However, acoustically soft materials like cloth can be difficult to detect (Burnett, 2017). There sensors work on principle transmitting series of ultrasonic pulses and detecting their reflection. From elapsed time the distance is calculated.

HC-SR04

HC-SR04 sensor features separate transmitter and receiver. Datasheet recommends to object to be detected should have at least 0.5 m^2 and be as smooth as possible, otherwise, it will affect the results of measuring (Cytron Technologies, 2013). According to Fads to Obsessions (2020) tests the sensor's beam angle is only 20° at 1.2 m distance, so we can expect even more apparent differences between both ultrasonic sensor measurements.

JSN-SR04T-2.0

JSN-SR04T-2.0 sensor has separate closed waterproof cable probe and strong anti-interference (JahanKit Electronic, 2019). Sensor module allows using three different serial communication modes. In testing we will be using mode which sends already calculated distance on request.

Tab. 1 Main parameters of tested sensors from data according to datasheets

Parameter/Sensor	HC-SR04	JSN-SR04T-2.0	VL53L1X
Type	ultrasonic, 40 kHz	ultrasonic, 40 kHz	laser, 940 nm
Power Supply (V DC)	4.5–5.5 V DC	3 – 5.5	2.6 – 3.5
Working Current (mA)	15	<8	max. 18
Ranging Distance (cm)	2–400	20–600	4–400
Distance accuracy (cm)	±0.3	±1	not specified
Resolution (cm)	0.3	0.1	0.1
Beam Angle (°)	<30	75	Programable: 15-27
Communication	Digital pins	Serial 9600 Bd	I^2C

Optical sensors

Optical sensors work on the principle of reflected light waves. Light of certain wavelength is emitted and then reflected from objects to receiver. Since the speed of light is incomparably bigger than sound, optical sensors must be equipped with fast chips to calculate elapsed time and corresponding distance. These sensors are also better at defining edges of an area but at the cost of possible malfunctioning in strong ambient light due to interference (Burnett, 2017).

VL53L1X

VL53L1X is the fastest miniature distance sensor on the market with ranging frequency up to 50 Hz and allows absolute distance measurement for all target colors and surface reflectance (STMicroelectronics, 2018). This sensor uses NIR 940 nm Class1 laser emitter and programable receiver field of view. Another sensor function is measuring ambient light levels in kcps/SPAD (kilo counts per second per Single Photon Avalanche Diode). Boher et al. (2019) have carried out testing of VL53L1X laser diode and Morales (2018) tested beam angle limits. Both found out that maximum beam angle at real conditions is reduced to about 20°.

Kalman filter

Kalman filter (KF) is an algorithm that performs recursive estimation of the state of dynamic system and is also able to estimate unknown state variables (Al Tahtawi, 2018). As distance is proportional to time of one sensing cycle, general KF equations can be reduced to form containing only scalar variables proposed by Al Tahtawi (2018) stated in equations (Eq. 1-5). Equations (Eq. 1-2) calculates the predictions of state $\hat{x}_k^-$ and measurement error covariance matrix P_k^-. Q is process noise covariance matrix. Increasing the value of Q reduces filter robustness.

$$\hat{x}_k^- = \hat{x}_{k-1} \quad (1)$$

$$P_k^- = P_{k-1} + Q \quad (2)$$

Remaining equations (Eq. 3-5) represent correction phase where Kalman gain (K_k), state estimation $\hat{x}_k$ and actual P_k are calculated. Parameter R is measurement noise which is calculated from raw sensor data as variance.

$$K_k = P_k^- (P_k^- + R)^{-1} \quad (3)$$

$$\hat{x}_k = \hat{x}_k^- + K_k(y_k - \hat{x}_k^-) \quad (4)$$

$$P_k = (1 - K_k)P_k^- \quad (5)$$

Moving average

Moving average (MA) is type of smoothing filter calculating output value from average of *n* element subset of input values. Each following output value is calculated by shifting forward the subset – removing the oldest number of the series and adding actual sensor value in the subset. Mathematical formulation of MA is in equation (Eq. 6), where $y_{(i)}$ is filter output value and $x_{(n-k)}$ is filter input value. In real-time filtering MA calculates $y_{(i)}$ from *n* previous *x*.

$$y_{(i)} = \frac{1}{n}\sum_{k=0}^{n-1} x_{(n-k)} \quad (6)$$

RESULTS AND DISCUSSION

The measurements were carried out at height of 1 m in vineyard row section of length *L* of 3 m shown in figure (Fig. 1). Chosen length was sufficient to get relevant results because growth density of vine leaves was variable along it. This tested sensors sensitivity to less dense areas. Basic distance *d* was 1.5 m, but during testing of laser sensor, we found out, that the sensor gives usable results only up to 1.2 m, so for this sensor we used *d* of 1 m.

Fig. 1 Testing vineyard section with marked dimensions

The vine itself has width *w* which had effect on measured data as a signal from sensor can pass through several layers of leaves until it reflects. Therefore, *w* represents the tolerance for measured data. From our measurements of vineyard row width, we opted for tolerance of 0.4 m. Sample time for data collection was 100 ms for all measurements. Values for measurement variance *R* we obtained from static testing of the sensors and are shown in table (Tab. 2).

Ultrasonic sensors result

Obtained data from ultrasonic sensors in figure (Fig. 2) showed how the two sensors differed. We assume measurements with HC-SR04 sensor were inaccurate mostly due to smaller beam angle compared to JSN-SR04T-2.0 sensor. Beam angles from sensor datasheets are in table Tab.1. Smaller the beam angle, the smaller is the diameter of sensed area and thus even small spaces with low growth density were cause for not receiving echo and the sensor evaluated those spaces out of range – 4 m away in the Fig.2.

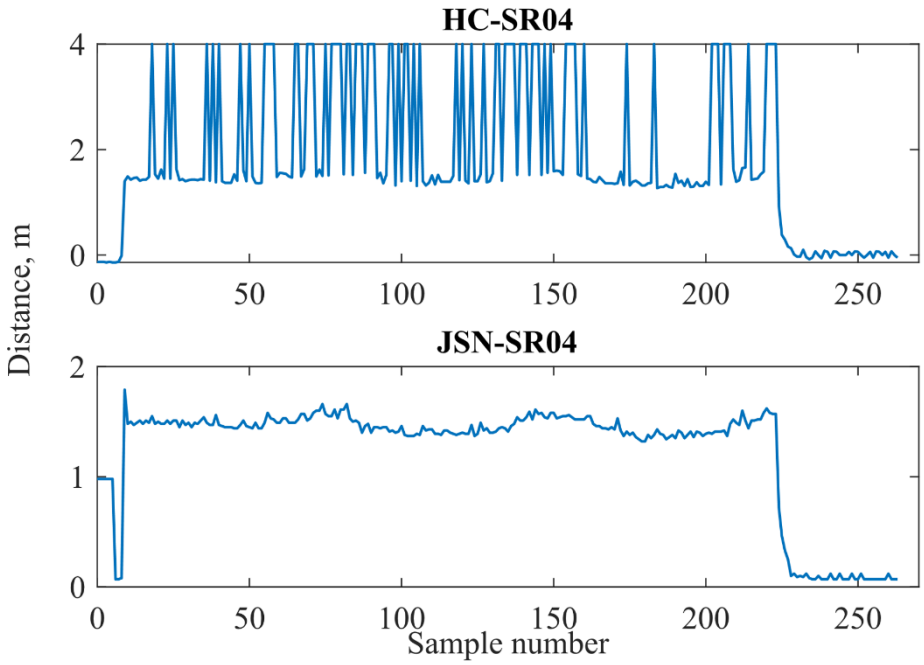

Fig. 2 Measured data from both ultrasonic distance sensors

Maximum sensing distance was 1.8 m, at larger distances the sensor did not give any response. However, ability of measuring distance of smaller areas could be desired in other applications but in our case it was not. On the other hand, JSN-SR04T-2.0 gave us the best results among all tested sensors. With the largest beam angle, it sensed the largest area so the effect of gaps with low or no growth was suppressed. The sensor turned out to be usable up to 3.2 m.

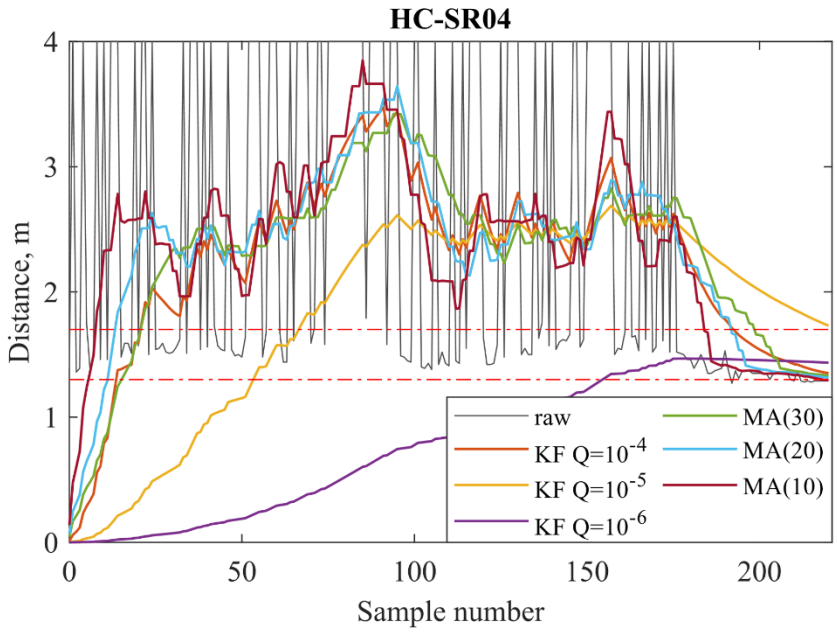

Fig. 3 Filters responses to data from HC-SR04 sensor

To improve the smoothness of raw measured data we implemented proposed KF and MA algorithms with various parameters. Graph (Fig.3) shows response of all six filters to raw data from HC-SR04 sensor. None of the filters was able to deal with big spread of raw data and almost 100 % data were out of tolerance marked with red dash-dotted lines. Using filters with JSN-SR04T-2.0 led to better results as can be seen in graph (Fig. 4). Best results were reached with 10 and 20 element MA and KF with $Q=10^{-5}$. Both moving averages had lower rise time but after settling in the KF was responding faster than the 20 element MA for subtle deviations.

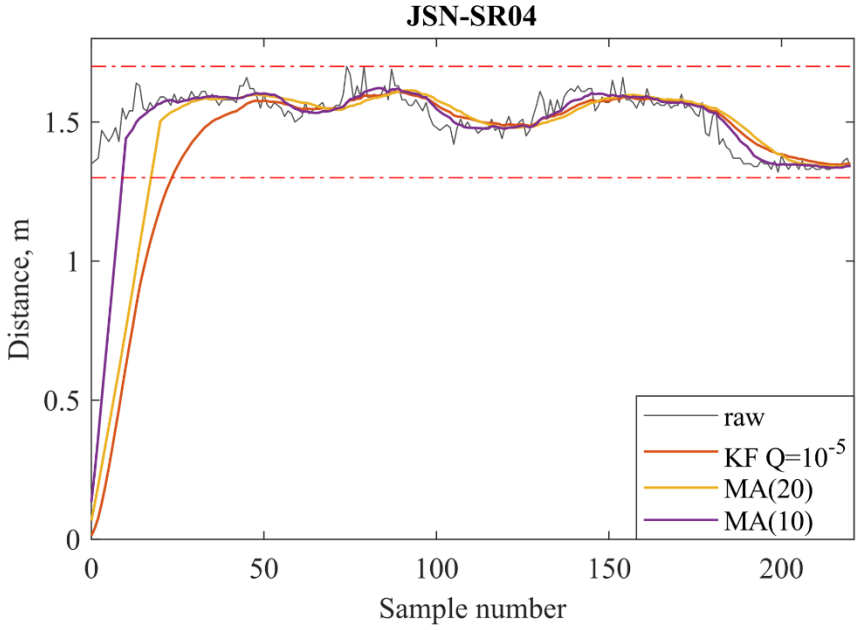

Fig. 4 Best filter responses for JSN-SR04 sensor

VL53L1X laser sensor results

From initial testing of each sensor mode we found out that sensing range was significantly reduced in long and medium modes. This was caused by higher ambient light levels during tests and it confirms information from datasheet. Because of reduced sensor outdoor range during daylight all measurements were performed from distance of 1 m. An average value obtained from sensor was 75 kcps/SPAD which represents illumination of about 1500 lx. In figure (Fig. 5) are shown are measured data with each sensor mode. Same as with ultrasonic sensors we used same filters with the laser sensor.

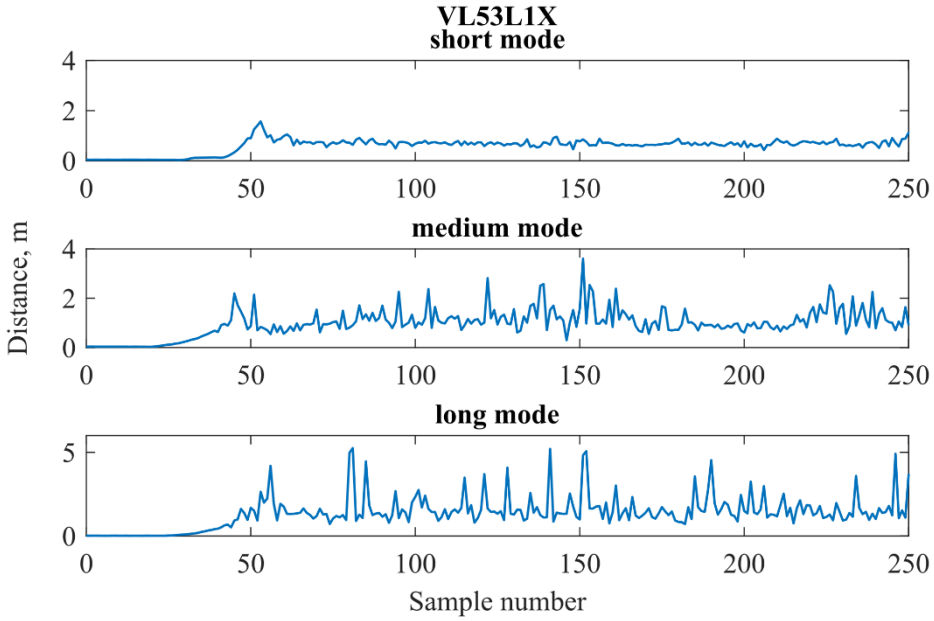

Fig. 5 Measured data with all three modes of VL53L1X sensor

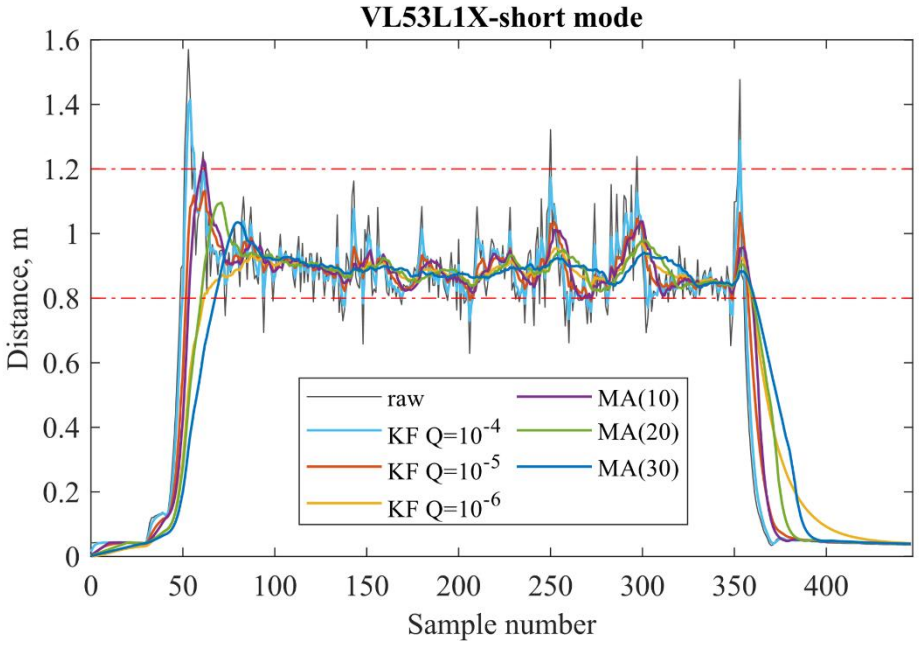

Fig. 6 Filters responses to data from VL53L1X sensor in short mode

The results are shown in graph (Fig. 6). Compared to JSN-SR04 sensor, data from laser sensor were more dispersed but mostly in the tolerance. Best at suppressing the dispersion of data were more robust filters. In graph (Fig. 7) are shown best filters. Same as previously, KF had faster response from the point it settled. Graph (Fig. 8) shows typical responses of used filters. The quickest but also the least robust was KF with $Q=10^{-4}$. Its response was almost immediate. In general, KF had negative logarithmic response curve – the response was faster for smaller distance changes but slower for bigger changes than MA.

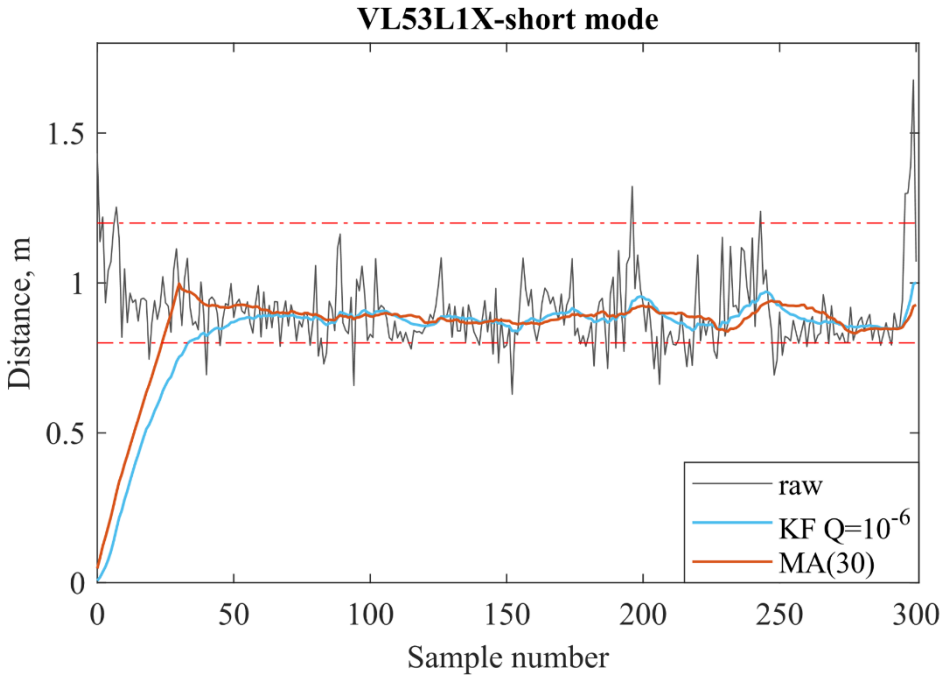

Fig. 7 Best filter responses for VL53L1X sensor

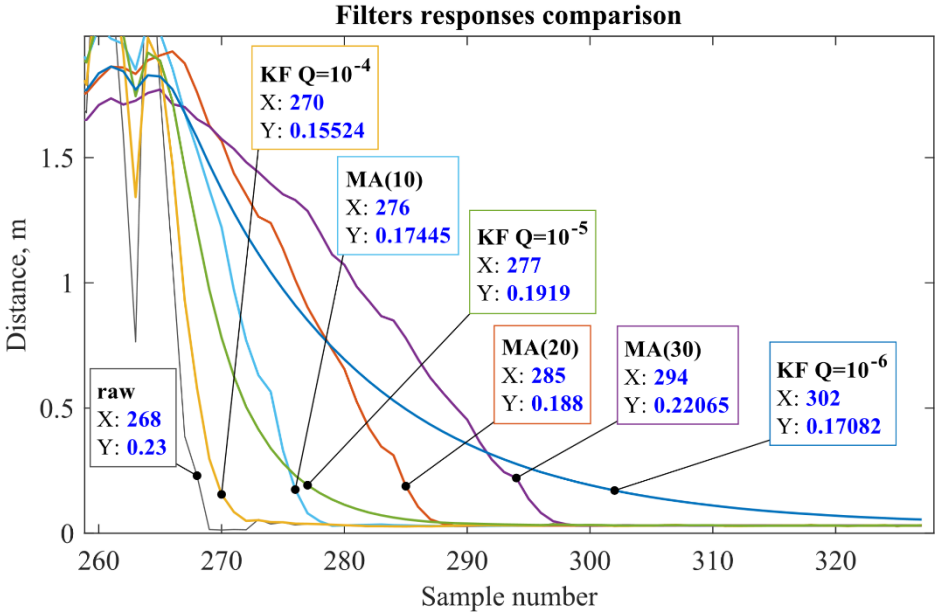

Fig. 8 Response comparison of used smoothing filters

Our obtained results for all sensors are listed in table (Tab. 2). Degree of raw data dispersion and filter smoothing was evaluated using corrected sample standard deviation *s*. For every tested sensor the filters improved *s*. Only with HC-SR04 sensor the filtering reduced amount of data in tolerance to only 0.08 %.

Tab. 2 Comparison of sensors testing results without and with filtering

sensor	**HC-SR04**	**JSN-SR04**	**VL53L1X**
R (m^2)	$1.5 \cdot 10^{-3}$	$1 \cdot 10^{-4}$	$2 \cdot 10^{-5}$
max. distance (m)	1.8	3.2	1.2
data in tolerance %	54.75	99.1	83.72
s (m)	1.1572	0.0943	0.1262
Best filtered results			
filter	MA (30)	KF ($Q=10^{-5}$)	KF ($Q=10^{-6}$)
data in tolerance %	0.08	100	100
s (m)	0.4397	0.0544	0.0401

CONCLUSION

The measurements showed that best results were achieved with JSN-SR04 sensor, mainly due to widest beam angle among all tested sensors. 99.1 % of raw measured data were in chosen tolerance with s=0.0943 m. With filtering we reached s=0.0544 m with 100 % of data in the tolerance. The other ultrasonic sensor HC-SR04 turned out to the least suitable for measuring distance from vineyard rows. This can be attributed to the fact that mentioned sensor has the narrowest beam angle. Filtering improved standard deviation of measured data by more than 60% but simultaneously decreased accuracy to only 0.08% of data in the tolerance. VL53L1X laser sensor showed satisfactory results but only up to 1.2 m. 83.72 % of raw data were in the tolerance with s=0.1262. With filtering 100 % of data were in tolerance with s=0.0301. Results proved suitability of certain sensors for this task. Generally, best results can be obtained with sensors with wider beam angle. In our case it was ultrasonic sensor JSN-SR04 with beam angle of 75°. Furthermore, obtained result will serve for following experiments focused on navigating mobile robot through vineyard rows.

Acknowledgments: This paper was created within the project VEGA no. 1/0720/18 Research of Alternative Navigation Algorithms for the Control of Autonomous Robots in Plant Production.

REFERENCES

1. AL SADDIK, H., LAYBROS, A., BILLIOT, B., COINTAULT, F. 2018. Using Image Texture and Spectral Reflectance Analysis to Detect Yellowness and Esca in Grapevines at Leaf-Level. Remote Sensing. 10. 618. 10.3390/rs10040618.
2. AL TAHTAWI, A.: Kalman Filter Algorithm Design for HC-SR04 Ultrasonic Sensor Data Acquisition System. IJITEE (International Journal of Information Technology and Electrical Engineering). 2018. 2. 10.22146/ijitee.36646.
3. BOHER, P., LEROUX, T. 2019. High Resolution Optical Characterization of NIR Light Sources for 3D Imaging. SID Symposium Digest of Technical Papers, 50. p. 1210-1213. 10.1002/sdtp.13149.
4. BURNETT. R.: Ultrasonic vs Infrared (IR) Sensors – Which is better? [online]. ©2017 [cit. 2020-06-17]. Retrieved from: <https://www.maxbotix.com/articles/ultrasonic-or-infrared-sensors.htm>.
5. Cytron Technologies. Product User's Manual – HC-SR04 Ultrasonic Sensor. [online]. ©2013 [cit. 2020-07-02]. Retrieved from: <http://web.eece.maine.edu/~zhu/book/lab/HC-SR04%20User%20Manual.pdf>.
6. Fads to Obsessions.: HC-SR04 Ultrasonic Ranging. [online]. ©2020 [cit. 2020-07-09]. Retrieved from: <http://www.fadstoobsessions.com/Learning-Electronics/Component-Testing/HC-SR04-Ultrasonic-Ranging.php>.
7. ESCOLÀ, A., PLANAS, S., ROSELL, J. R., POMAR, J., CAMP, F., SOLANELLES, F., GRACIA, F., LLORENS, J., GIL, E. 2011. Performance of an ultrasonic ranging sensor in apple tree canopies. Sensors (Basel, Switzerland), 11(3), p. 2459–2477.
8. FERET, J.-B., FRAN ̧COIS, C., ASNER, G. P., GITELSON, A. A., MARTIN, R. E., BIDEL, L. P., USTIN, S. L., LE MAIRE, G., JACQUEMOUD, S. 2008. PROSPECT-4 and 5: Advances in the leaf optical properties model separating photosynthetic pigments. Remote Sensing of Environment 112 (6), Jun.2008. p. 3030–3043.
9. GAMARRA-DIEZMA, J., MIRANDA-FUENTES, A., LLORENS CALVERAS, J., CUENCA CUENCA, A., BLANCO-ROLDÁN, G., RODRÍGUEZ-LIZANA, A. 2015. Testing Accuracy of Long-Range Ultrasonic Sensors for Olive Tree Canopy Measurements. Sensors. 15. p. 2902-2919. 10.3390/s150202902.
10. JahanKit Electronic. JSN-SR04T-2.0. Datasheet. [online]. ©2019 [cit. 2020-07-02]. Retrieved from: <https://www.makerguides.com/wp-content/uploads/2019/02/JSN-SR04T-Datasheet.pdf>.

11. MORALES, L.: VL53L1x FoV angle limit. [online forum post]. Dec. 2018 [cit. 2020-07-20]. Retrieved from: <https://forum.pololu.com/t/vl53l1x-fov-angle-limit/16307>.
12. STMicroelectronics. VL53L1X Datasheet. [online]. ©2018 [cit. 2020-07-02]. Retrieved from: < https://www.pololu.com/file/0J1506/vl53l1x.pdf>.

Corresponding author:

Ing. Dušan Marko, Department of Electrical Engineering, Automation and informatics, Faculty of Engineering, Slovak University of Agriculture in Nitra, Trieda Andreja Hlinku 2, 949 76 Nitra, Slovak Republic, e-mail: xmarkod@uniag.sk

Evaluation of the effect of crops on erosion parameters in the Central Bohemian Region

A. Melicharová, J. Mašek, P. Novák

Department of Agricultural Machines, Faculty of Engineering, Czech University of Life Sciences Prague, Prague, Czech Republic

Abstract

This paper is focused on evaluation of the effect of some cultivated crops on water erosion parameters (surface runoff, erosive wash). Water erosion is a worldwide problem. In the Czech Republic conditions are at risk by water erosion more than half of the agricultural land. The field trial was based on a site with an average slope of 5.4°. The crops cultivated in the experiment were winter rape, winter wheat, oat, maize, and potatoes. Conventional tillage was used for each of these variants. Black fallow (variant without vegetation) was used as the comparative variant. Using the method of microplots were evaluated by surface runoff and erosive wash during intense rainfalls. The results confirm the risk of wide-row crops cultivation. The erosive wash in maize and potatoes was like the variant without vegetation.

Key words: effect of crops**,** water erosion, surface runoff, erosive wash

INTRODUCTION

Water erosion is a worldwide problem. In the Czech Republic conditions are at risk by water erosion more than half of the agricultural land. The Czech Republic is characterized by a high average gradient of agricultural land. JANEČEK et al. (2005) reports that more than 53 % of area in the Czech Republic is situated on land with an average slope greater than 3º. The high slope of land combined with light soil and expanding wide-row crops (especially maize) increase the risk of water erosion. It is not possible to eliminate the risk of erosion, but it may be reduced.

One of the most important input parameters with a great influence on erosion processes is organic matter (FRANZLUEBBERS, 2002). This effect can take many forms, but the two basic ones are the soil vegetation cover formed by plants and the soil cover formed by organic plant residues (KOVÁŘ et al., 2016). A sufficient vegetation cover affects the course and intensity of erosion processes (HANGEN et al., 2002). Its aim is to protect the soil against the impact of rain drops, to improve soil consolidation through the root system of plants especially in subsurface layers, to increase the infiltration capacity of the soil due to the growth of the root

system and to improve the physical, chemical and biological properties of the soil (ŠAŘEC & NOVÁK, 2017). The roots of some plants can destroy the compacted layer of soil created especially by the technogenic compaction (KROULÍK et al., 2011). The choice of the appropriate crop is the most important issue for each plot. The study by MORGAN et al. (2005) is based on data collected from the authors around the world. Morgan also states that soil losses caused by water erosion can be reduced up to 4.7 times by soil fertilization, by adjusting the microrelief up to 30 times and choosing a suitable crop to 37 times.

The initial hypothesis is based on the assumed reduction of surface runoff and erosive wash in crops that have a higher cover of soil by plant cover at the time of intense rainfall. Furthermore, what is anticipated is higher surface runoff and erosive wash in wide-row crops.

MATERIALS AND METHODS

A field trial was established in the village Nesperská Lhota in the Central Bohemian Region. It was based on light, sandy loam soil at an altitude of 450 m ASL. The average slope of the land is 5.4°.

The field experiment consists of five basic variants and one comparative variant. Each variant has an area of 300 m^2 with dimensions of 6 x 50 m. The long side of each variant is oriented to the slope. Conventional tillage was used for each of these variants.

Variants of the experiment:

1. Winter rape: Conventional tillage. Primary and secondary tillage (a plough and seedbed cultivator) before seeding; seeding on August 17th, 2017.
2. Winter wheat: Conventional tillage. Primary and secondary tillage during autumn, seeding on October 2nd, 2017.
3. Oat: Conventional tillage. Ploughing in autumn; in spring – secondary tillage (using a combinator), seeding on April 6th, 2018.
4. Maize: Conventional tillage. Ploughing in autumn, in spring – secondary tillage and seeding on April 28th, 2018.
5. Potatoes: Conventional tillage. Ploughing in autumn, in spring – preseed preparation using a tine tiller, seeding on 29th April 2018.
6. Black fallow (comparative variant): Conventional tillage (the same as in the case of the previous variants), a non-systemic herbicide (glyphosate) was used to destruct plants.

For each of variants, four runoff microplots were installed after seeding (Fig. 1). The microplots were surrounded by 1.5 mm thick steel sheet. The walls of the microplots were pushed into the

soil to the depth of 0.08 m. The collector is located at the bottom of each microplot. It transports water into a plastic container buried below the catching microplots. The area of each microplots is 0.4 m × 0.4 m.

Fig. 1 Microplot with a plastic container

To measure the volume and intensity of precipitation the weather station Vantage Vue was used. It is located near the experiment site. Measurement of surface runoff followed every time after intense rainfall. Surface runoff was detected by measuring the volume of runoff water, the amount of soil washed by filtering runoff and subsequent soil drying at 105 ºC in the laboratory dryer and weighing the soil on a laboratory scale. The measurement and evaluation method used in the study was published by BAGARELLO & FERRO (2007). The data obtained from the measurements were evaluated in the STATISTICA 12 program. Chart graphs were used to illustrate field trial data. The data were further evaluated by the ANOVA analysis using the Tukey HSD test.

RESULTS AND DISCUSSION

The first soil erosion event was two storms from May 10th and 13th. Total precipitation in this period was 33 mm. The precipitation intensity ranged from 80-100 mm·h^{-1}. The results (Fig. 2 and 3) shows that the lowest surface runoff and erosion wash were in the first three variants. The lowest surface runoff and erosion wash is in winter rape, which is already involved in this period and begins to bloom. On the contrary, the largest surface runoff and erosive wash was expected in the case of the conventional soil cultivation for maize and potatoes (variants 4 and 5). In these variants, the soil is still insufficiently protected by the growth of plants. Variant 6 also showed a high surface runoff and erosion wash. The highest surface runoff was reached

by variant 5 (potatoes), but the erosive wash was a bit lower than the comparative variant (black fallow).

The difference in soil loss weight between rape, wheat and oat variants is below statistical significance. On the contrary, the erosive wash in maize, potatoes, and the comparative variant, is statistically significantly higher than in the first three variants.

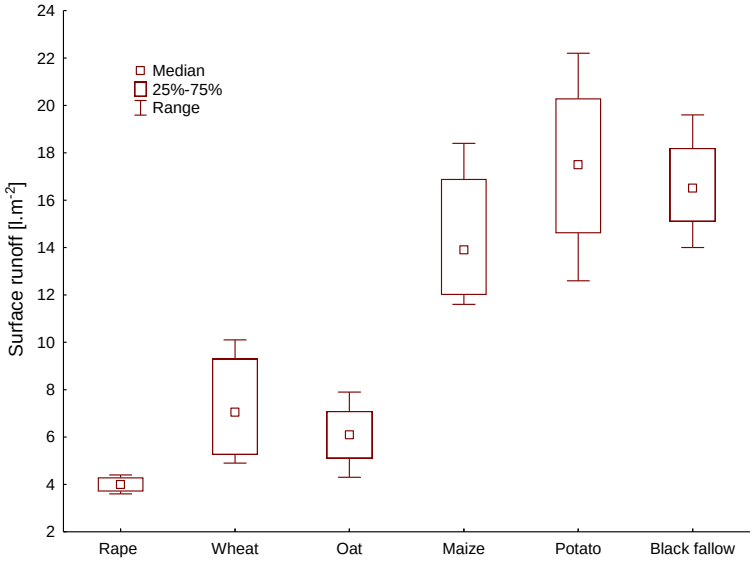

Fig. 2 Surface runoff after two storms in May 2018

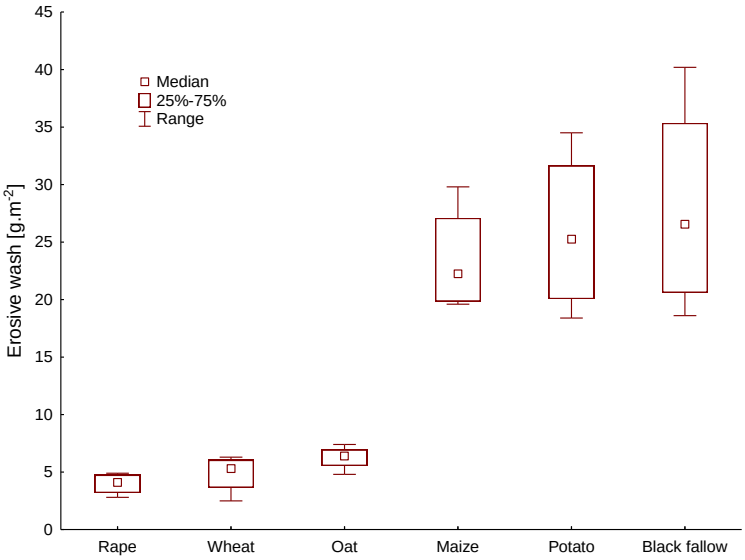

Fig. 3 Erosive wash after two storms in May 2018

Two more significant erosion events occurred during June. The first event occurred between June 10th and 14th, when the rain and two storms with a rainfall of 34 mm were. The precipitation intensity ranged from 80-100 mm·h^{-1}. Fig. 4 and 5 shows that again the lowest surface runoff and erosion wash were recorded in the first three variants. Conversely, the highest surface runoff and erosive wash was measured for variant 5. High values were in the maize variant

whose surface runoff was higher than in the comparative variant, but the erosive wash was smaller than in the potato variant and the comparative one. The surface runoff of the comparative variant was lower than the maize variant and the potatoes, but the erosive wash reached similar values here.

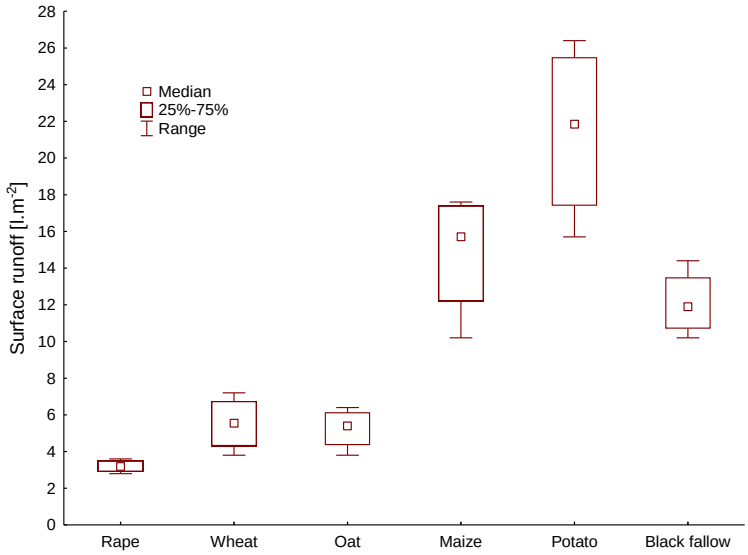

Fig. 4 Surface runoff after two storms in the period 10th to 14th June 2018

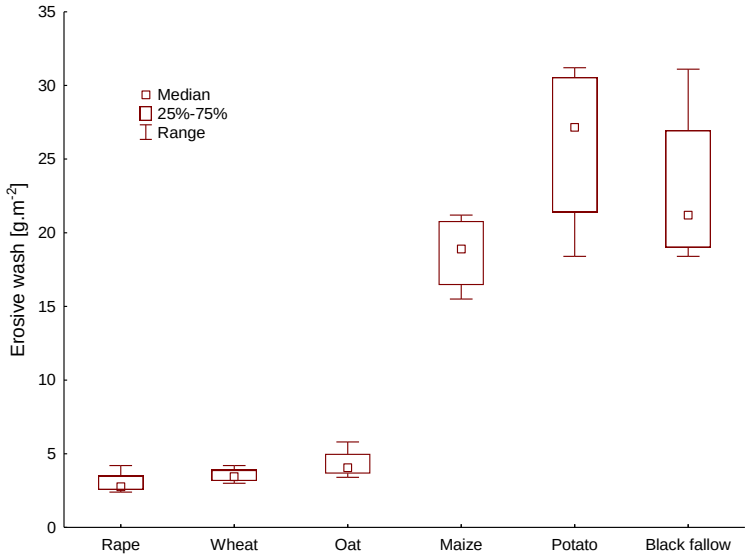

Fig. 5 Erosive wash after two storms in the period 10th to 14th June 2018

The second significant event was occurred between June 26th and 28th. There were two storms with a total precipitation of 44 mm. The intensity of these precipitation reaches up to 200 mm·h^{-1} for a short time. Fig. 6 and 7 shows that the lowest surface runoff and erosive wash were in the first three variants. In these variants the plants are already involved, and the soil is well protected against erosion rainfalls. The lowest surface runoff and erosive wash were in winter rape. On the other hand, the highest surface runoff and erosive wash were achieved by variant

5. Similarly, high values were achieved with the maize and the comparative variants, but erosive wash was lower than in the potato variant.

Again, there is a problem of poorly protected soil by plant residues. Another problem can be seen in wide rows crops production. This measurement reveals the most extreme values of erosive wash measured during the season 2018. The difference in erosive wash between rape, wheat and oat variants is below statistical significance. On the contrary, the soil runoff in the maize, potatoes and the comparative variant is statistically significantly higher than in the first three variants.

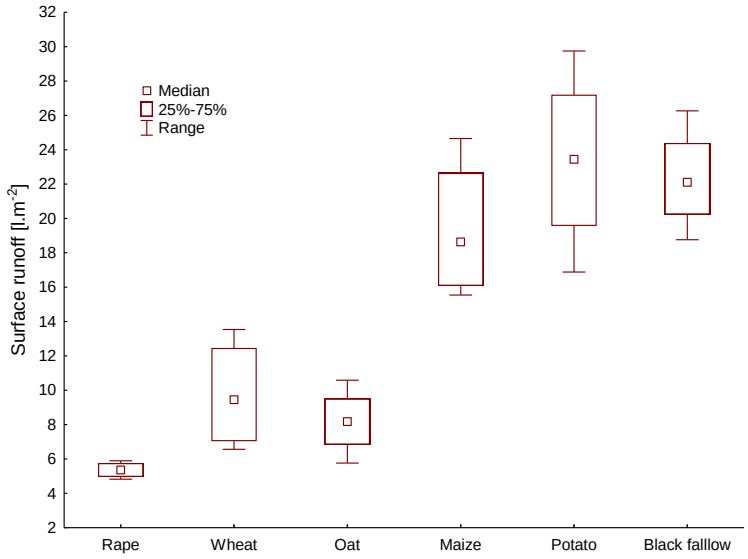

Fig. 6 Surface runoff after two storms in the period 26th to 28th June 2018

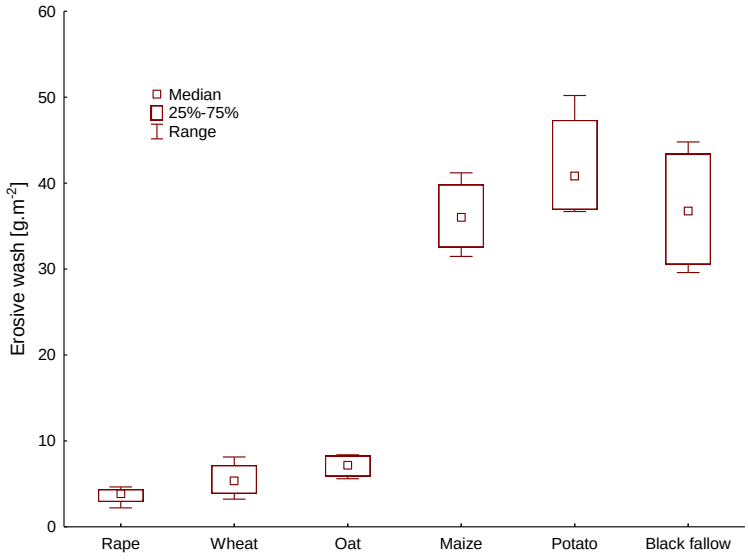

Fig. 7 Erosive wash after two storms in the period 26th to 28th June 2018

Last erosion event occurred on July 6th during a short storm, when the rainfall was 9 mm and the intensity of the rain reached up to 80 mm·h^{-1}. Fig. 8 and 9 shows that the lowest surface

runoff and erosive wash were in variant 1. In the case of wheat and oat, a slightly higher surface runoff was in the case of the rape variant. Higher values of surface runoff were in the potatoes and the comparative variant, where the highest value was reached by the black fallow variant compared with the maize and potatoes variants. The highest values of surface runoff were reached by variant 4 compared with the comparative and potatoes variants.

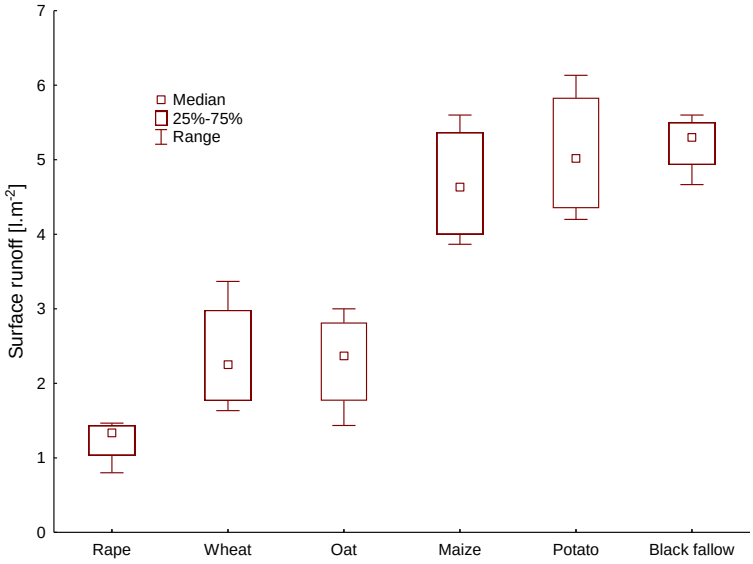

Fig. 8 Surface runoff after a storm on July 6th, 2018

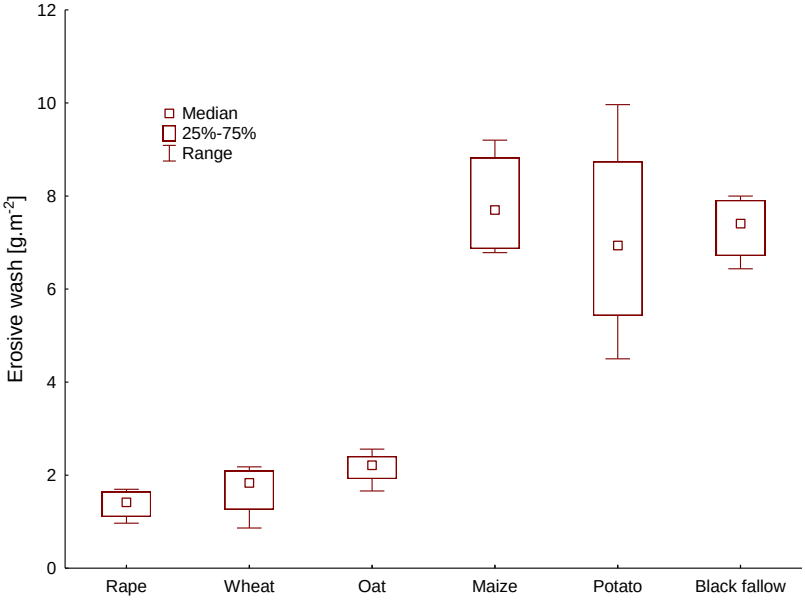

Fig. 9 Erosive wash after a storm on July 6th, 2018

The highest surface runoff and erosive wash were in variants with wide-row crops (maize and potatoes). This has also been confirmed by KARLEN et al. (1994). The soil is not well protected by the associated crop and the large kinetic energy of the falling droplets results in increased surface runoff and consequently erosive wash. The negative aspect for comparative variant

(variant 6) was leaving the soil without any surface coverage by plant residues. In this case as well as in the other cases, there was also an increased surface drainage and consequent soil loss down the slope.

BROWN et al. (1989) measured that for all monitored soil conditions (soil with plants or fallow) the amount of erosion of discrete particles decreased with increasing time since the beginning of the experiments. Generally, freshly treated soil is more inclined to soil erosion than the soil that has undergone several cycles of drying and rewetting.

CONCLUSION

The initial hypothesis has been confirmed by the field experiment. A beneficial effect of vegetation soil cover during erosion precipitation has been demonstrated as a protection of the soil against the large kinetic energy of the falling droplets. It has also been proved that the infiltration of water into the soil has increased, which has led to minimum surface runoff and erosive wash. It has been confirmed that wide-row crops have a higher surface runoff and erosive wash than crops sown in narrow rows. These crops are under risk of creating soil crust, which has a negative effect on the infiltration of water into the soil and the consequent increased surface runoff and erosive wash.

REFERENCES

1. BAGARELLO, V., FERRO, V.: Monitoring plot soil erosion and basin sediment yield at Sparacia experimental area. Changing soil in a changing world: the soils of tomorrow. ESSC, Palermo, 2007, pp. 67-74.
2. BROWN, L. C., FOSTER, G. R. & BEASLEY, D. B.: Rill erosion as affected by incorporated crop residue and seasonal consolidation. ASAE, 1989, 32(6). 1967-1977.
3. FRANZLUEBBERS, A.J.: Water infiltration and soil structure related to organic matter and its stratification with depth. Soil Tillage Res., 2002, 66. 197–205.
4. HANGEN, E., BUCZKO, U., BENS, O., BRUNOTTE, J. & HÜTTL, R.F.: Infiltration patterns into two soils under conventional and conservation tillage. Soil & Tillage res., 2002, 63. 181-186.
5. JANEČEK, M. et al.: Soil erosion protection. Prague: ISV publishing, 2005, 195 p.
6. KARLEN, D.L., WOLLENHAUPT, N.C. & ERBACH, D.C.: Crop residue effects on soil quality following 10-years of no-till corn. Soil Tillage Res., 1994, 31. 149-167.

7. KOVÁŘ, S., KOVAŘÍČEK, P., NOVÁK, P. & KROULÍK, M.: The effect of soil tillage technologies on the surface of the infiltration speed of water into the soil. Agronomy Research, 2016, 14 (2). 434-441.
8. KROULÍK, M., KVÍZ, Z., KUMHÁLA, F., HŮLA, J. & LOCH, T.: Procedures of soil farming allowing reduction of compaction. Precision Agriculture, 2011, 12 (3). 317-333.
9. MORGAN, R. P. C.: Soil erosion and conservation. Third Edition. Blackwell Publishing company, 2005, Malden, USA. 304 pp.
10. ŠAŘEC, P. & NOVÁK, P.: Influence of manure and activators of organic matter biological transformation on selected soil physical properties of Modal luvisol. Agronomy Research, 2017, 15 (2). 565-575.

Corresponding author:

Adéla Melicharová, Department of Agricultural Machines, Faculty of Engineering, Czech University of Life Sciences Prague, Kamýcká 129, Praha 6, Prague, 16521, Czech Republic, email: melicharovaa@tf.czu.cz

Evaluation of the operation of a gas absorption heat pump in partially bivalent mode for the preparation of hot water in an apartment building

P. Míšek[1], R. Adamovský[1], P. Neuberger[1]

[1]Department of Mechanical Engineering, Faculty of Engineering, Czech University of Life Sciences Prague, Prague, Czech Republic

Abstract

This paper focuses on the comparison of gas boiler control strategies with a cascade of sources comprising gas heat pumps and condensing boilers. The paper seeks to determine a suitable control system for preparing household hot water by flow heating in apartment buildings and generally deals with the operation of a gas heat pump in extreme conditions. Five identical boiler rooms with different ways of controlling the cascade of sources will be compared at the same time and in the same place, by comparative measurement. Individual categories will be compared according to the efficiency of gas use, primary energy needs and the share of heat pump heat production in total output will be monitored.

Key words: absorption heat pump, gas utilization efficiency, primary energy, bivalence mode

INTRODUCTION

Current valid European legislation (Fabrizio et al., 2014) places high demands on low energy use in new buildings and reconstructions. For more complex projects, such as apartment buildings, the application of a renewable source may be a suitable solution. With the increasing quality of the insulation properties of building materials, the preparation of domestic hot water (DHW) is becoming an increasingly important component of the energy needs of an apartment building (Delforge et al., 2019). Compared to conventional heating, the domestic hot water system in apartment house has specific requirements on heat pump technology. In the case of heat pump applications, these are the high setpoint temperature, the irregular consumption and the high number of operating hours at partial load of the source. These are extreme conditions from the point of view of most common heat pumps (Staffell, 2012). In such conditions, the pumps achieve significantly worse energy efficiency than in heating mode for central heating systems (HS). The loss of efficiency of heat pumps (HP) at partial load and at high temperatures is also confirmed by Green, (2012) in his study. In addition, as reported (Guo et al., 2018),

conventional pumps are enormously stressed in this mode. This leads to their extreme wear and tear with unsatisfactory operating results.

As stated (Maira et al., 2011) in their study on the long-term operation of heat pumps in Germany, the average heating factor (SCOP) of a compressor heat pump ranges from 2.6 to 5.2. If we consider that the preparation of DHW is an extreme case in terms of application, we can count on the worst case, that is, a value around 2.6. The measurement results for gas heat pumps are given by Ciganda et al. (2015) and have a gas utilization efficiency (GUE) value in the range of 1.17 – 1.61. For the preparation of hot water, a value of about 1.17 can be expected. Wu (2012) is even more critical in his model of absorption pump behavior and estimates a GUE value below 1.1 if the heating medium temperature exceeds 60°C.

Operational analyses performed by Fumagalli et al., 2017 show that the performance and efficiency of heat pump systems are determined not only by the efficiency of the pumps operated, but also by the quality of the heat pump integration in the system. When the heat pump cannot operate in steady state, the efficiency of a heat pump power system can be adversely affected. This is exactly the case in DHW mode. In these cases, Fumagalli recommends not simply verifying the efficiency of the pump itself, but evaluating the entire system. Fumagalli further gives the results of measurements where, at relatively steady operation, the avarage primary energy required (SPER) of the boiler room is 0.76-0.78 and, vice versa, during continuous operation it is 0.58-0.60.

The method of calculating the efficiency of gas use for evaluating heat pump operation and primary energy requirements for the assessment of the system as a whole is given (Wu, 2014) as follows:

$$GUE = \frac{Q_h}{Q_{gas}} = \frac{\Delta Q_h}{\Delta V_{gas,n} * H_{i,n}} \quad [-] \qquad (1)$$

$$PER = \frac{Q_h}{Q_{gas} * f_{gas} + \sum W_{el} * f_{el}} \quad [-] \qquad (2)$$

In equation (1), GUE is defined as the ratio between the heat produced Q_h and the energy Q_{gas} provided by the gas. Also, as a proportion of the produced heat ΔQ_h in the time interval t and the product of the consumed gas volume ΔV_{gas} for the stated time interval t and the calorific value (Loir rating value) $H_{i,n}$ of the gas. The PER in equation (2) is given by the proportion of heat produced Q_h delivered by the primary energy. In this case, the primary energy is the sum of all energy provided by the gas Q_{gas} and the electrical energy W_{el}, weighted according to the

respective primary energy factors for the gas f_{gas} = 1.1 (according to DIN 18599, 2011) and the electrical energy f_{el} = 2.4 (according to DIN 18599, 2011).

If we convert the assumed values of the heat pump heating factor, we obtain PER_{el} = 1.08 for an electric heat pump and PER_{gas} = 1.06 for a gas heat pump. If we take into account that the manufacturers of conventional heating state the efficiency of boilers close to 99%, the question arises whether the application of a conventional source at times of unsuitable operating load will not achieve similar results as with a heat pump, but with minimal wear. However, this consideration only applies to gas boiler rooms. For electric boilers, the results will be significantly worse after conversion to primary energy.

Hypothesis: Can the losses of a gas heat pump resulting from an unsuitable load profile, in this case flow heating domestic hot water system, be so large as to make it more efficient to use a conventional heating source?

MATERIALS AND METHODS

Measurement was conducted in panel block housing units in the Czech Republic. These are blocks of panel construction apartment buildings fitted with identical technology. Figure 1 shows the diagram of the boiler room.

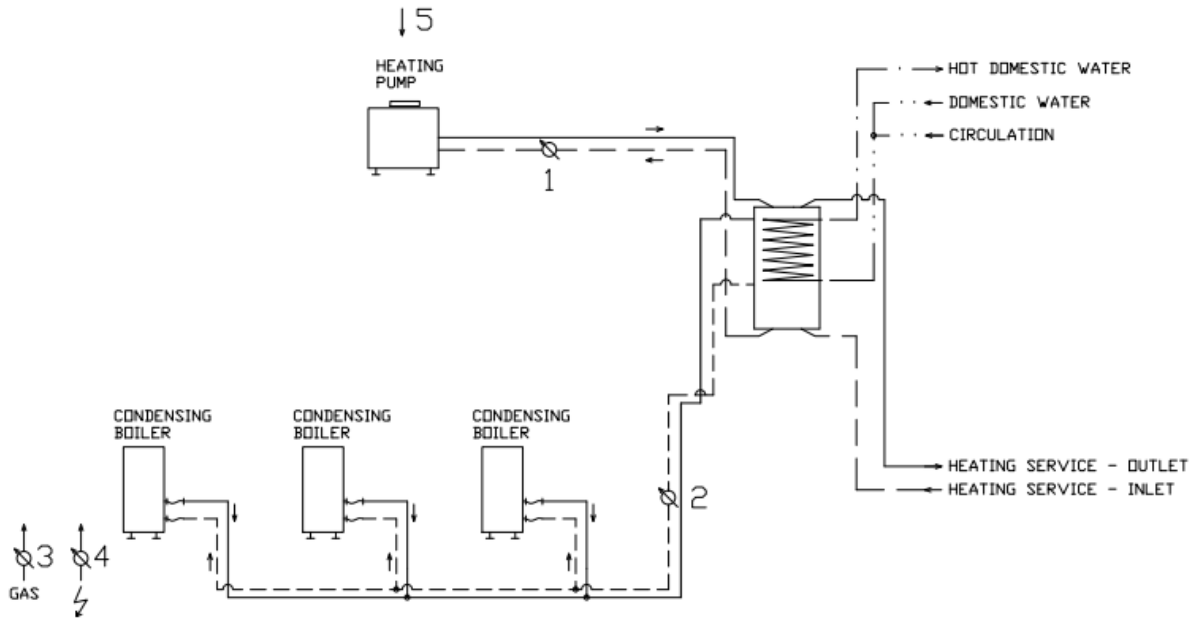

Fig. 1 Diagram of connection of cascading gas sources: 1. Heat pump calorimeter, 2. Boiler calorimeter, 3 Gas meter, 4. Electric meter, 5. Renewable energy

The boiler room is fitted with calibrated billing meters, which are sufficient for measuring energy flows. These were the Elmer membrane gas meter, the three-phase electromechanical

UHER electricity meter and the Sharky ultrasonic calorimeter. Measurement was based on energy balance, i.e. the measurement of input and output energy. The difference between output and input energy is energy supplied from a renewable source. The boiler room was monitored throughout the experiment. The basic parameters of the boiler room are given in table no. 1. The measured heat pump was a Robur GAHP A air absorption gas heat pump. The measured boilers were Robur AY gas condensing boilers.

Tab. 1 Boiler room parameters

Number of apartments	32	-
Heat power	146	kW
Heat pump power (A7/W35)	1 x 41	kW
GUE (A7/W35)	1,64	-
Condensing boiler power	3 x 35	kW
Condensing boiler efficiency	0,99	-
Heat consuption	780	GJ
Hot domestic wate consumption	230	GJ
Tank setpoint	62	°C
Average ambient temperature	19	°C

For the measurement, various cascade switching strategies, were set for individual buildings, which can be briefly described as follows:

- Apartment building no. 1 – normal heat pump operation (default setting)

This is preferably a monovalent operation of the heat pump, which has slow switching times set. This can reduce the impact of cycling losses, but delays the response to changes in the system. In the event of sudden consumption shocks, the boiler may be activated.

- Apartment building no. 2 – operation of heat pump in rapid response to a change in the system

This is preferably a monovalent operation where the heat pump is set to respond rapidly to temperature changes in the system. An advantage is the ensuring of comfort and minimum condensing boiler switching. A disadvantage is the high frequency of activation and short average operation time.

- Apartment building no. 3 – Partially bivalent operation, the heat pump is attenuated for 12 hours daily

The heat pump is only switched on for 12 hours, when peak consumption is expected. This makes it possible to switch the pump on at a time when it will be possible to achieve

smooth operation. In case of unsuitable load profile, it provides heating by condensing boilers.

- Apartment building no. 4 – Partially bivalent operation, the heat pump is attenuated for 16 hours

The cascade operates in the same way as in case no. 3. The heat pump is set for a longer period of attenuation. The precise attenuation setting is described in Table no. 2.

- Apartment building no. 5 – Preferenced bivalent operation

Hot water is preferentially provided by condensing boilers. The heat pump switches on only for the needs of actual securing operations.

Tab. 2 Time of attenuation (economy operation) in individual regimes

Economy modes	Times of attenuation
Economy 12	0-5; 9-11; 13-18
Economy 16	0-7; 10-18; 23-24

RESULTS AND DISCUSSION

Results of the measurements from individual boiler rooms are shown in the following Table no. 3.

Tab. 3 Results of the measurements from individual boiler rooms

5 12.9.2019	TČ	Kotle	Kotelna			Hodnocení kotelny		
Build number	Calorimeter (GJ)	Calorimeter (GJ)	Gas meter (m^3)	Electric meter (kWh)	Calorimeter (GJ)	GUE (-)	SPER (-)	HP Ratio (%)
1	*4.25*	*0.37*	*117.6*	*139.7*	*4.62*	1.14	0.75	0.92
2	*4.52*	*0.07*	*131.4*	*235.1*	*4.59*	1.02	0.61	0.98
3	*2.17*	*3.49*	*164.9*	*89.2*	*5.66*	1	0.74	0.38
4	*1.38*	*2.89*	*125.09*	*86.3*	*4.27*	0.99	0.72	0.32
5	*0.09*	*3.85*	*119.55*	*73.6*	*3.94*	0.96	0.70	0.02

The boiler room that achieved the best gas use efficiency is boiler room no. 1, i.e. a boiler room with a monovalent pump. The boiler room that had the worst GUE value is boiler room 5, i.e. a boiler room with purely bivalent operation of condensing boilers. The GUE value increased with the increasing share of heat pump use in total heat production. The best SPER value was for boiler room number 1, which again used monovalent heat pump operation. The worst value was shown by a boiler room with a cycling pump. This can be explained by the high

consumption of electricity, related to the frequent heat pump operation, and therefore also of all auxiliary equipment. The SPER values are clearly displayed in figure no. 2.

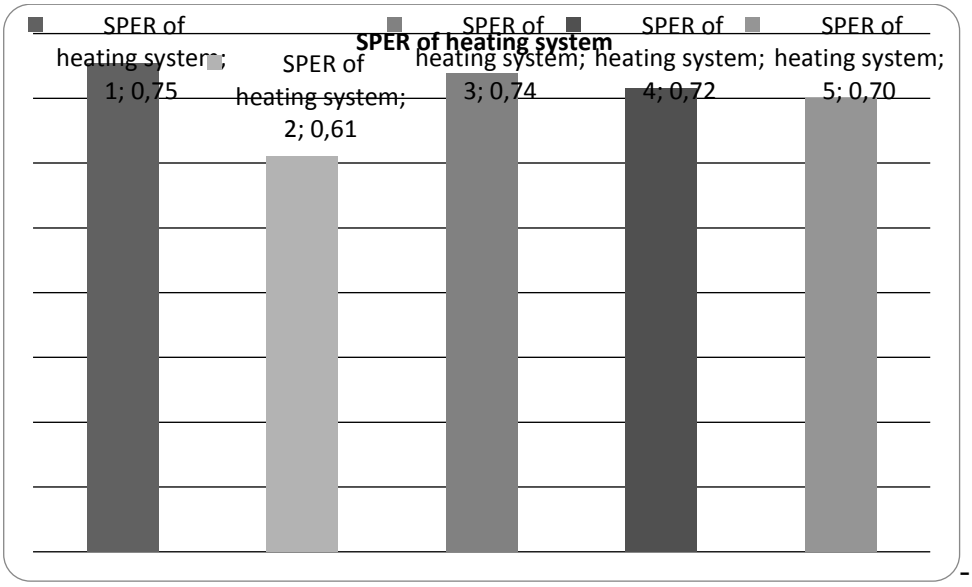

Fig. 2 Primary energy requirement of individual boiler rooms

Boiler rooms with bivalent operation returned very good results regarding the reduction of the operating stress of the heat pump. Boiler room number three has only a one tenth worse SPER value, while reducing the share of the heat pump in heat production by 54%. Boiler room number four has a SPER value three tenths worse, but the share of heat pump heat production decreased by 60%.

CONCLUSION

The results confirm the hypothesis that when using a gas heat pump in a system with an unsuitable load profile, the losses may be so great that it is more efficient to use a conventional heating source. Although the boiler room operating in a partially bivalent mode did not achieve the same result as the boiler room with monovalent operation of the heat pump, the difference was virtually negligible. On the contrary, a boiler room with a deliberately cycling heat pump showed that in the event of a further deterioration of the load profile, operation using conventional sources can be a more efficient solution. The results also show that operation in partially bivalent mode may appear to be a suitable compromise between a system's efficiency and its lifetime.

The measured results do not deviate in any way from the values determined from research in the literature. Comparative measurements, on the other hand, have confirmed that a heat pump that is not properly integrated into the system can have very similar operating values as a conventional heating source. In this case, the system does not make full use of the potential that the heat pump offers, and the only possible way to significantly increase the efficiency of the boiler room without changing the source is to change the technical solution of the boiler room.

REFERENCES

1. FABRIZIO, Enrico, Federico SEGURO a Marco FILIPPI. Integrated HVAC and DHW production systems for Zero Energy Buildings. Renewable and Sustainable Energy Reviews. 2014, 516-527.
2. DELFORGE, Pierre a Lindsay ROBIBINS. HEAT PUMP RETROFIT STRATEGIES FOR MULTIFAMILY BUILDINGS: Energy affordability. New York: Steven Winter Associates, 2019.
3. STAFFELL, Iain, Dan BRETT, Nigel BRANDON a Adam HAWKES. A review of domestic heat pumps. Energy & Enviromental Science. 2012, 5(11). DOI: 10.1039/c2ee22653g. ISSN 1754-5692.
4. GUO, Xiaofeng a Alain GOUMBA. Air source heat pump for domestic hot water supply: Performance comparison between individual and building scale installations. Energy. 2018.
5. GREEN, Robert. TheEffectsofCycling on Heat Pump Performance [online]. EA Technology- DepartmentofEnergy and ClimateChange. Chester, 2012 [cit. 2020-02-11]. Dostupné z: https://assets.publishing.service.gov.uk/government/uploads/system/uploads/attachment_data/file/65695/7389-effects-cycling-heat-pump-performance.pdf
6. MIARA, Marek. Heating Pump Efficiency: Analysis and Evaluationof Heat Pump Efficiency in Real-lifeCondition [online]. Fraunhofer Institute for Solar Energy System.Freiburg, 2011 [cit. 2020-02-11]. Dostupné z: https://wp-monitoring.ise.fraunhofer.de/wp-effizienz//download/final_report_wp_effizienz_en.pdf
7. CIGANDA, José L. C, GRAF, Rupert, KÜHN, Annett, SCHMITH-GEHRKE Paul, ZIEGLER, FelixOperationalexperiences and systém improvementmeasuresforgasabsorptionheat pump systems. 6th IIR Conference: Ammonia and CO2 Refrigeration Technologies, Ohrid, 2015, p. 1-9.
8. WU, Wei, ZHANG, Xiaoling, L, LI, Xiating, T., WANG, Baolong, L, 2012.Comparisons of different working pairs and cycles on the performance of absorptionheat pump for heating and domestic hot water in cold regions. Applied Thermal Engineering. 48, 349-358. ISSN 1359-4311.
9. FUMAGALLI, Marica, SIVIERI, Alessandro, APRILE, Marcello, MOTTA, Mario, ZANCHI, Matteo, 2017. Monitoring ofgasdrivenabsorptionheatpumps and comparingenergyefficiency on primaryenergy. RenewableEnergy. 110, 115-125. ISSN 0960-1481.

10. WU, Wei, WANG Baolong, SHI Wenxing, LI Xianting., 2014b. Anoverviewofammonia-basedabsorptionchillers and heatpumps. Renewable and SustainableEnergyReviews. 31, 681 – 707. ISSN 1364-0321.
11. DIN V 18599-1 2011, Energyefficiencyofbuildings - Calculationofthenet, final and primaryenergydemandforheating, cooling, ventilation, domestic hot water and lighting - Part 1: General balancingprocedures, terms and definitions, zoningandevaluationofenergysources. DIN – German Institute forStandardization.

Pretreatment of the steel surface for powder coating

M. Neškudla[1]

[1]Department of Technological Equipment of Buildings, Czech University of Life Sciences Prague, Prague, Czech Republic

ABSTRACT

This article is about pretreatment of the steel surface for a better adhesion of powder coating. Different level of pretreatment were used and the score of final painted parts were compared each other. The grid method showed that the final outcome is strongly affected by the diverse types of pretreatment methods.

Key words: powder coating, pretreatment, surface, blasting, degreasing, grid method

INTRODUCTION

Electrostatic application of plastics is a widely used surface treatment of parts made of various materials worldwide. This technology is also gradually being introduced in the Czech Republic in the environmentally friendly production of metal parts. Powder coating is mainly used for steel components that are exposed to corrosive or otherwise degrading environments (Frey 2015). Powder coatings are valued not only for their final aesthetic appearance, but also for their protective properties, which increase the life of products, affect their functionality. and extends their applicability up to extreme conditions. (Tulka 2005). The condition for quality surface treatment by electrostatic application of plastic is the correct pre-treatment. Depending on the different shapes of the parts, mechanical or chemical pretreatment is used. Blasting, also known as sandblasting, is a technological surface treatment of materials with a stream of fine particles (Blažek 2009). Chemical pretreatment means degreasing, or phosphating, or chromating.

MATERIALS AND METHODS

In this experiment a steel sheets of 50cm x 50cm were used to find out the affection of different pretreatment methods for the adhesion of painted on the final product. There were 4 different level of pretreatment – without any, mechanical, chemical and mechanical plus chemical.

Mechanical pretreatment

Represented by (Sand) blasting. Blasting is a process during an abrasive or sandblasting material is sprayed against an object under high pressure. With blasting is possible to remove surface impurities such as corrosion, paint etc. and smooth or roughen the surface of the object.

Chemical pretreatment

The surface of metal parts is intentionally provided with an oil layer that has a task of protecting the surface of the parts from environmental influences - corrosion. The protected surface lasts for a very long time in its desirable original form. For the needs of powder coating is however greasy and otherwise soiled surfaces of metal objects clearly unsuitable because powder paint cannot be applied to them.

The technology of degreasing metals consists of heating the cleaned objects to a temperature of around 120° C, when the active vapors of the chemical solvent begin to act on the contaminated surface. The treated surface in this way is completely free of all greasy impurities.

Mechanical and Chemical pretreatment consist of both methods consecutively.

Evaluation

The results were evaluated in comply with ISO 2409 by the grid method. The **grid method** represents a pattern of 6 vertical and 6 horizontal lines with the same proportions created on a surface of the final product was used. The determination of the quality on the scale from 0 to 25 points directly in the accordance with a well cut squares.

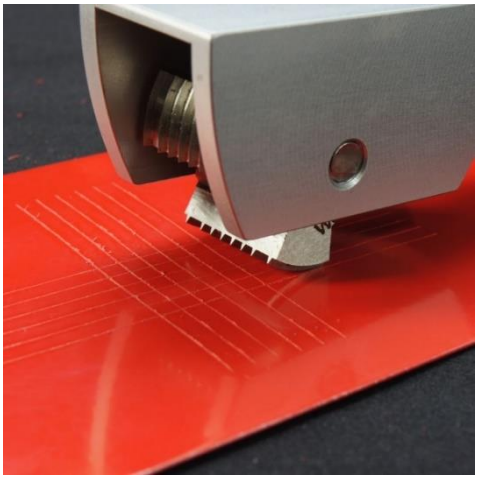

Fig. 1 Source: Proinex

RESULTS AND DISCUSSION

Forty different measurements were carried out to find out the significancy of pretreament to the quality of final product. 10 measurements were carried out without any pretreatment, 10 with blasting only, 10 with degreasing only and 10 with blasting and degreasing subsequently.

Each result was separately evaluated and the points are displayed in the Table Nr 1.

Tab. 1

Number of Measurement	Without pretreatment (Points 0-25)	Blasting (Points 0-25)	Degreasing (Points 0-25)	Blasting + Degreasing (Points 0-25)
1	2	11	20	21
2	6	16	14	22
3	7	14	19	23
4	6	14	21	24
5	3	15	18	22
6	5	15	21	24
7	2	11	16	21
8	5	17	15	21
9	7	12	18	22
10	4	16	18	23
Average	**4.70**	**14.10**	**18.00**	**22.30**
St. Deviation	**1.79**	**2.02**	**2.28**	**1.10**

From the Table Nr. 1 is visible that without any pretreatment the final outcome represented as a specific points per measurement or average is not satisfactory and oscilates at aroud 4.70. After blasting the final average outcome significantly improved to 14.10 points that is however still not acceptable. Measurement after degreasing hit an average of 18. Degreasing is thus better pretreatment activity than blasting but still not good enough to reach a proper level. The last measurements were carried out after blasting and degreasing with all the points exceeding 20 and average of 22.30. Standard deviaton also reached a minimal value of 1.10 that means a highest stability from all measurements. There is a need to improve also other parameters on non-prepayment level to reach an average above 24.

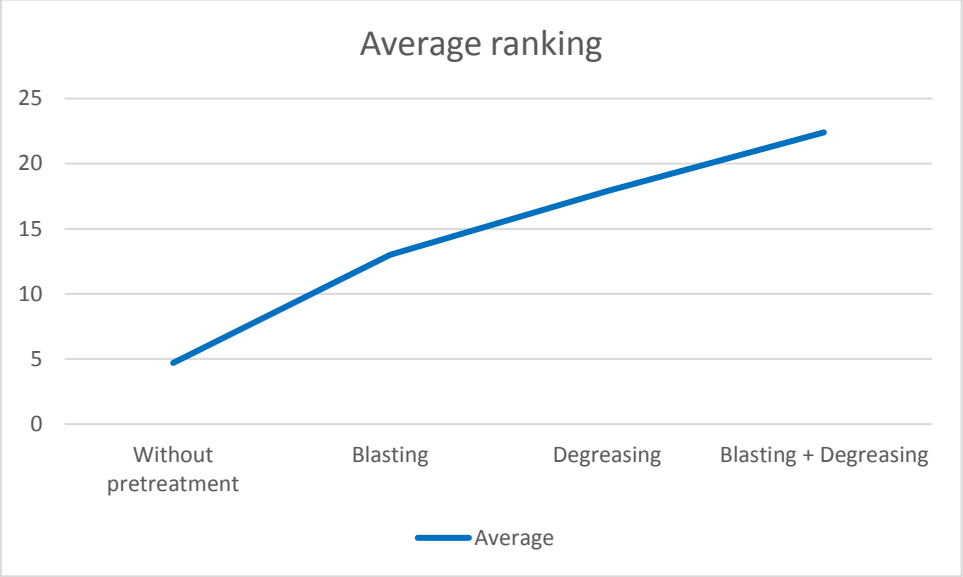

Fig. 2 The acquired points and ascending curve with more advance pretreatment

Tab. 2

SWOT Analysis of pretreatment of the steel surface for powder coating	
Strengths	**Weaknesses**
• Solid proof of pretreatment effect with measurable figures	• Time and cash consuming
Opportunities	**Threats**
• Possibility to find out a better way to make the pretreatment.	• Inaccurate level set of other parameters with inconclusive effect of pretreatment methods

CONCLUSION

There is a strong connectivity between the pretreatment and the quality of the final painted product. Mechanical pretreatment only is far better that nothing and slightly worse than the chemical one. Combination of mechanical and chemical pretreatment showed the best option and secured almost flawless results.

REFERENCES

1. Blažek, Jaroslav. Optimalizace teploty vytvrzování při práškovém lakování. Brno:Vysoké učení technické v Brně, Fakulta strojního inženýrství, 2009.68 s, 4 přílohy
2. Frey, Hartmut a Hamid R Khan. Handbook of thin-film technology. Berlin:Springer, 2015, xiiii, 379 stran: ilustrace. ISBN 978-3-642-05429-7

3. Tulka, Jaromír. Povrchové úpravy materiálů. Vyd. 1 Brno: Vysoké učení technické v Brně, Fakulta chemická, 2005, 135 s ISBN 80-2141-3062-1

Corresponding author:

Ing. Michal Neškudla, Department of Technological Equimpent of Buildings, Faculty of Engineering, Czech University of Life Sciences Prague, Kamýcká 129, Praha 6, Prague, 16521, Czech Republic, email: neskudla@tf.czu.cz

Distribution grid stability

T. Petrík[1], I. Uhlíř[1]

[1]Department of Physic, Faculty of Engineering, Czech University of Life Sciences Prague, Prague, Czech Republic

Abstract

In this paper an influence of network frequency oscillations on exciting of hunting synchronous machines coupled with masses of great moments of inertia is shown. It solves the maximum permissible value of a moment of inertia on the shaft of a synchronous machine in respect to an oscillation of network frequency.

Key words: Network frequency oscillations, mechanical, electromechanical system, inertial masses

INTRODUCTION

The idea of a network voltage having a coherent sinusoidal course of a constant frequency holds restrictedly only. Precision measurements establish oscillations of a network frequency and instantaneous phase of power net voltage. A network frequency oscillation has a random noise course because it is only the response of an energy system to a casually changing daily consumed energy diagram /1/.

The phenomenon of network oscillations may be described in terms of statistic dynamics using the power spectral density S_ω (Ω) of a power net angular frequency fluctuation. An example of this function characterizing the frequency spectrum of network frequency deviations shows Fig. 1.

A spectrum of network frequency deviations has two components:

— a slow component for $\Omega < 2\ s^{-1}$ determined by properties of regulation of rotation in power plants as well as of superior central frequency regulation,

— a fast component for $\Omega > 2\ s^{-1}$ determined by an elasticity of the supply system in case of power changes. A fast component originates from magnitude and phase changes of instant

voltage decreases on line and transformer impedances in a network due to fast load changes of a network.

If a synchronous machine driving inertial masses is connected to a network, the mechanical movement of a machine shaft must follow frequency and therefore even phase changes of a network. A shaft follows the instantaneous network voltage phase with an angle deviation, which produces a load angle β of a synchronous machine. The instantaneous power consumed or supplied by a machine to a network depends on a magnitude and an orientation of the load angle β. The greater the inertial masses on the shaft in comparison to the size of a synchronous machine, the greater the dynamic deviation of the following fast network phase changes and thus even oscillations of a load angle /5/.

Since an electromechanical system — synchronous machine and inertial masses — is very little dumped, the oscillations of a load angle, excited by network frequency fluctuations, have a harmonic swinging character and are accompanied with an undesirable overflow of energy between a network and inertial masses on a shaft.

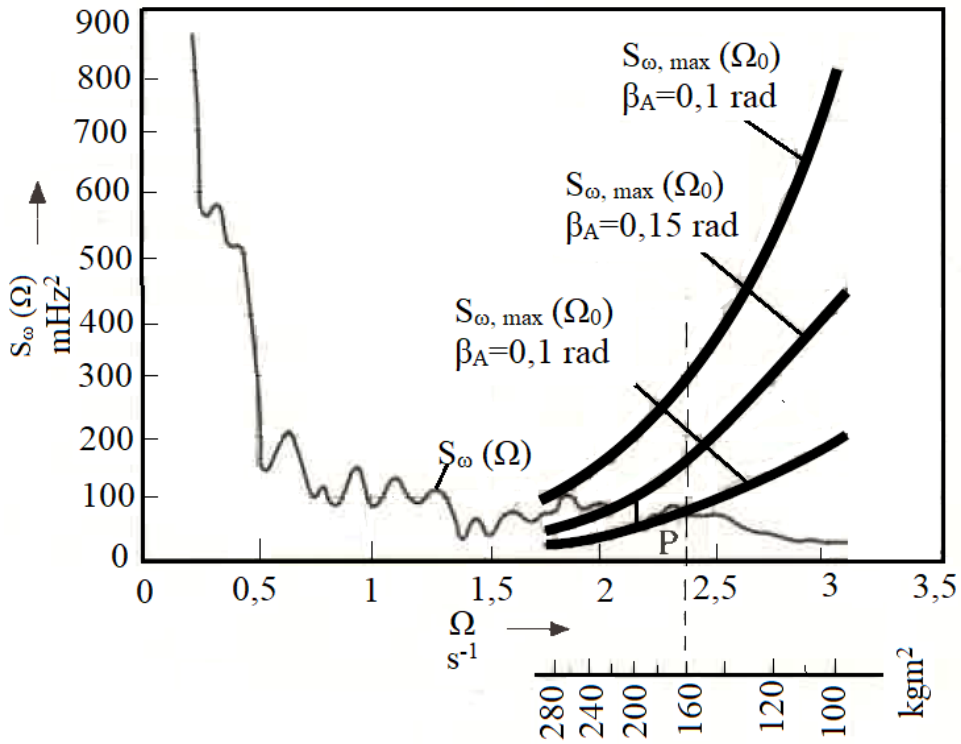

Fig. 1 Fluctuation spectrum of the network angular frequency $S_\omega(\Omega)$

MATERIALS AND METHODS

Description of a modeled System

The electromechanical swinging system created by a rigidity of a synchronous machine magnetic field, its damping effects and a moment of inertia, connected with a shaft, is presented in Fig. 2. The system from Fig. 2 is described by the differential equation

$$I\ddot{\beta} + B\dot{\beta} + k\beta = \frac{I}{P_d}\dot{\omega} \quad (1)$$

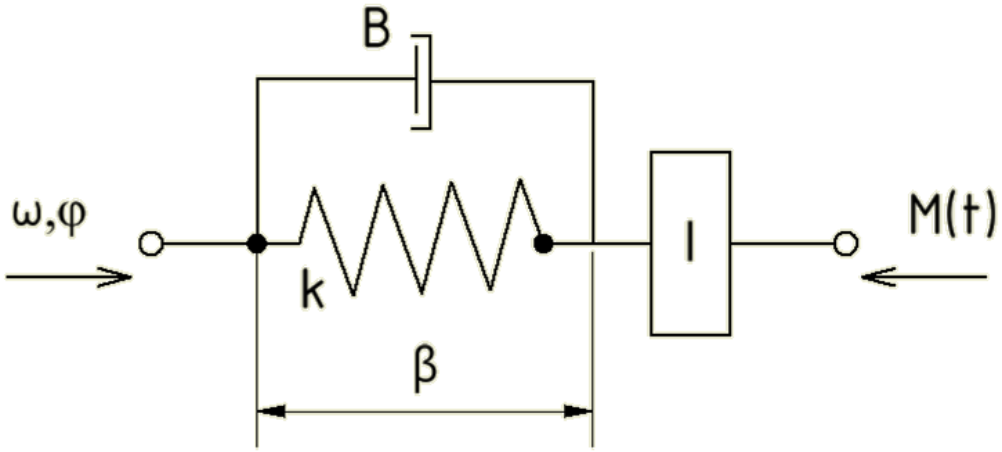

Fig.2 Electromechanical vibrating set of the synchronous machine

With:

β	load angle of a synchronous machine
ω	network frequency [s^{-1}],
I	overall moment of inertia connected to a shaft [$kg \cdot m^2$],
B	torsion damping constant [N·m·s],
k	torsion rigidity of a synchronous machine [N·m],
P_d	number of pole pairs of a synchronous machine.

The precision of the system is described by eq. (1) in Laplace's transformation /2, 3/:

$$G(p) = \frac{pI}{P_d(p^2I + pB + k)} \quad (2)$$

The power spectral density of a load angle fluctuation is

$$S_\beta(\Omega) = \lim_{n\to\infty}\left(G(p)\right)^2 S_\omega(\Omega) \quad (3)$$

with

$S_\beta(\Omega)$ power spectral density of a load angle fluctuation,

$S_\omega(\Omega)$ power spectral density of a fluctuation of angular frequency fluctuations [s^{-2}],

$$S_\beta(\Omega) = \frac{\Omega^2 I^2 S_\omega(\Omega)}{P_d[(k-\Omega^2 I)^2+\Omega^2 B^2]} \quad (4)$$

The natural frequency of the system is Ω_0:

$$\Omega_0 = \sqrt{\frac{k}{I}} \quad (5)$$

The coefficient of a relative system damping

$$a = \frac{B}{2\sqrt{kI}} \quad (6)$$

is very low for most synchronous machines, being usually a < 0.1; in this case the resonance is very selective, the system almost only transmits the natural frequency. A system response almost has a sinusoidal course of a load density swinging with an amplitude β_A. From eq. (4) results for $\Omega = \Omega_0$:

$$S_\beta(\Omega_0) = \beta_A^2 = \frac{I^2}{P_d^2 B^2} = S_\omega(\Omega_0). \quad (7)$$

RESULTS AND DISCUSSION

If the response of a load angle swinging has to have an amplitude A as the maximum, the power spectral density of the network angle frequency must not be greater than $S_{\omega,max}$ (Ω_0)

$$S_{\omega,max}(\Omega_0) = \frac{P_d^2 B^2}{I^2}\beta_A^2 \quad (8)$$

with

$S_{\omega,max}$ (Ω_0) upper limit of the power spectral density of a power net angle frequency [s^{-2}].

Substituting in eq. (8) the variable Ω_0 from eq. (5) instead of the parameter I, it follows:

$$S_{\omega,max}(\Omega_0) = \frac{P_d^2 B^2}{k^2} \beta_A^2 \Omega_0^4 . \quad (9)$$

Now the maximum size of a flying wheel is determined for which the amplitude of the load angle swinging does not exceed the given value β_A.

Courses are drawn $S_{\omega,max}$ (Ω_0) according to eq. (9) for the chosen β_A (e. g. 0.1 rad ... 0.15 rad ... 0.2 rad) into Fig. 1. These courses constitute the upper limits of power spectral densities of the network angle frequency fluctuations $S_{\omega,max}$ (Ω_0) for the permitted β_A. The courses of the upper limits are fitted with a scaled I according to eq. (5):

$$I = k/\Omega_0^2 \quad (10)$$

The maximum value of the moment of inertia placed on the shaft of a synchronous machine is given by the first intersection point (from the right) of the function $S_{\omega,max}$ (Ω_0) for the permissible maximum of the load angle oscillation amplitude β_A with the course S_ω (Ω) a measured in the network section at the considered time.

Practical Verifying

The synchronous machine MEZ- A 225 MO 4 with parameters:

S = 50 kVA
n= 1 500 min^{-1}
k= 1 140 N·m
B = 14 N·m·s

was chosen as an example. Under permissible load angle oscillation amplitude β_A= 0.1 rad (equal to the overflow of active power P = 20 kW) the intersection point P presents the maximum value I=160 kg·m^2.

Fig. 3 gives the evidence of a conformity of the calculated value J = 160 kg·m^2 of an average amplitude with the real recording of network frequency fluctuation and corresponding response of the load angle /4/.

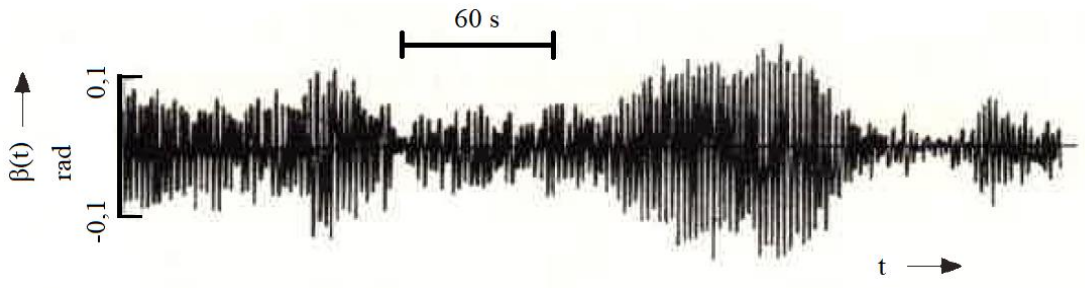

Fig. 3 Time behavior of the network frequency

CONCLUSION

Network frequency variation causes a load angle swinging with the synchronous machines of the network. Network frequency variation spectrum shape has the effect, that with the growing inertia moment on the shaft of the synchronous machine also the swinging amplitude is growing. For safe swinging amplitude a maximum inertia moment value has been determined which enables the machine to be driven. This limitation should be respected both in drives with tens and hundreds of kW as well as in drives with small synchronous machines and stepping motors, where large inert masses have to be driven.

REFERENCES

1. Amin W.T., Montoya O.D., Garrido V.M., Gil-González W., Garces A.: Voltage and Frequency Regulation on Isolated AC Three-phase Microgrids via s-DERs. In Proceeding soft 2019 IEEE Green Technologies Conference (GreenTech), Lafayette, LA, USA, 3–6 April 2019; pp. 1–6.
2. Han J.; Liu Z., Liang N., Song Q., Li P.: An Autonomous Power Frequency Control Strategy Based on Load Virtual Synchronous Generator. Processes 2020, 8, 433, doi:10.3390/pr8040433.
3. Haque M.E., Negnevitsky M., Muttaqi K. M.: A Novel Control Strategy for a Variable Speed Wind Turbine With a Permanent-Magnet Synchronous Generator. IEEE Trans. Ind. Appl. 2010, 46, 331–339, doi:10.1109/TIA.2009.2036550.
4. Uhlir I.: Pendeln unerwilnscht. Elektrotech. 72 (1990) no. 10, pp. 32-35
5. F. M. Serra, Fernandez M.L. 1, Montoya O. D., Gil-Gonzalez W. J., Hernandez J. C.: Nonlinear Voltage Control for Three-Phase DC-AC Converters in Hybrid Systems: An Application of the PI-PBC Method. Electronics 2020, 9, 847

Comparison of operating parameters of hybrid vehicles in urban and extra urban traffic

Š. Pícha[1], V. Hartová[1]

[1]Department of Vehicles and Ground Transport, Faculty of Engineering, Czech University of Life Sciences Prague, Prague, Czech Republic

Abstract

The development of hybrid vehicles combining an electric and a conventional internal combustion engine is one way of reducing greenhouse gas emissions, costs and other undesirable transport products. This article is focused on the analysis of operating parameters of hybrid vehicles. The aim of the work was to compare the parameters given by the manufacturer and the real values measured in tested vehicle in operation and to evaluate the obtained results. Information about the vehicle, the specific test route, measurement methodology, instruments used in measuring and evaluation equipment are provided.

Key words: hybrid vehicle, vehicle range, fuel consumption

INTRODUCTION

Undoubtedly, the main drivers of the development of hybrid vehicles are fuel consumption - closely related to operating economy, emissions production, driving characteristics, operational safety and others. Oil and oil product prices are a source of pressure on the of new technologies development (*Oil prices historical chart | GlobalPetrolPrices.com*, 2015). Fuel consumption itself (usually converted to 100 km) is another important factor. In the 1970s and mid-1980s, there was an increase in fuel consumption, caused by parallel increase in engine power and vehicle weight. For almost two decades until 2004, innovations were made in automotive technology to support vehicle attributes such as weight, power and other attributes, but it was not accompanied by activities reducing fuel consumption or CO_2 emissions. This was enabled in part by relatively stable oil prices and also later by gradual technical improvements (*EPA fuel economy report finds weight and power leveling off, footprint stable - Green Car Congress*, 2018; *Fact #630: July 5, 2010 Fuel Economy vs. Weight and Performance | Department of Energy*, 2010). Internal combustion engines are currently very technologically advanced, but they have number of shortcommings and therefore it is important to look for a suitablealternatives. The biggest problem is the ever-decreasing reserves of fossil fuels, which

are estimated to be depleted by about the middle of the 21st century (National Geographic, 2018).

At the same time, the issue of internal combustion engine emissions is being addressed. With regard to the previously mentioned factors, optimal alternative solution to the situation is being sought. There are number of options, from alternative fuels to electrification of vehicle propulsion. Electrification can take place either in full or only partially using electricity. An example could be operating the vehicle in cities only on electric propulsion, i.e. with zero current emissions or to extend the range or to improve the acceleration of the vehicle (Emadi, 2015). This document compares the values given by the vehicle manufacturer with the values measured on the experimental route with the test vehicle.

MATERIALS AND METHODS

The following parameters of a hybrid vehicle are specified.

- Created test route
- Determining the conditions of individual rides
- Used measuring instruments, equipment and vehicles
- Processing of measured data

The whole measurement was divided into three basic types of traffic - urban, extra-urban and highway. The individual sections are marked by color. The individual tracks were gone in both directions to provide more valid measured data. The route was created according to the assumption on which the driver and vehicle occur in practice most often. The entire route is placed in the territory of the Capital City of Prague and the close vicinity.

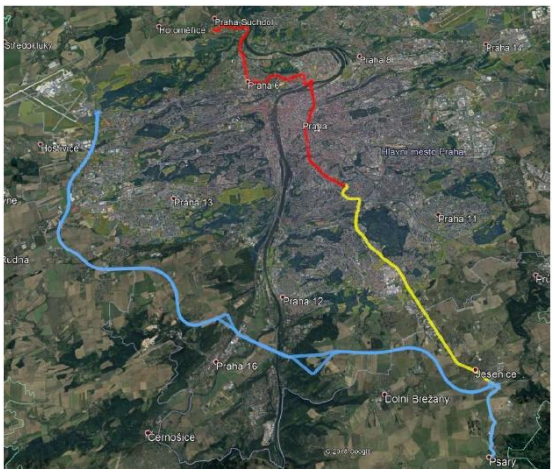

Fig. 1 Testing routes

The section marked in red characterizes city traffic with a maximum speed of 50 $km.h^{-1}$. The next part of the test route is marked in yellow and characterizes the suburban operation with a

maximum permitted speed of 80 km.h^{-1}. The highway section is marked in blue. The outside temperature during the measurement was in the range of 4 - 7 ° C. The measurement itself took place between 10 am and 2 pm, outside rush hours.

The driving mode: The "Normal" was set for the whole measurement period. During the measurement 3 people with an experienced driver were present in the vehicle.

For the measurement itself, the VMK emission analyzer was placed. It was the portable 5-component fuel gas analyzer measuring the instantaneous values of emissions of carbon oxides (CO, CO_2), unburned hydrocarbons (HC), nitrogen oxides (NOX) and oxygen (O_2)(*Emise | Katedra vozidel a pozemní dopravy*, n.d.). To determine the exact position of the vehicle, Garmin GPS 18x (5 Hz) GPS receiver was used, which was placed on the roof of the vehicle and recorded each second. The GPS receiver and the emission analyzer were interconnected.

The actual vehicle speed, rotation per minute of engine and intake air volume were recorded using a multi-brand OBD (On Board Unit) program by Bosch. The current data were received via an on-line laptop and OBD socket.

The tested car was Toyota RAV4 SUV (4th generation); year of manufacture2018.

This is car was equipped by with an e-CVT (Continuously Variable Transmission) automatic transmission and all-wheel drive (AWD). The vehicle parameters are listed in the table (Tab. 1).

Tab. 1 Technical parameters of the measured vehicle

Parameter	Value
Cylinder volume [cm3]	2 494
Fuel [-]	BA
Maximum performance [kW]	114
Rotation per minute at max power [min^{-1}]	5 700
Highest speed [km/h]	180
Operating weight [kg]	1 765

The driving was fitted by several modes, with regard to eco-driving or dynamic, on the contrary – the "Normal" set is default, next modes were "EV, Power and Eco". Normal is common mode that is preset and does not require activation each time the car is started - the optimal combination of both types of the engines. When using the Eco mode, both drives are optimally used to achieve minimum emission production. At the same time, it is characterized by more frequent use of the electric motor while driving. EV mode allows vehicles to be operated as pure electric. Power mode is characterized by the more dynamic transmission settings and overall car behavior (*Toyota RAV4 Comfort SUV 5dv. | Skutečné SUV*, n.d.).

It was necessary to synchronize uploading of the measurement data. Each second of the measurement specific data were collected including the vehicle position, traveled distance instantaneous engine and car speed, instantaneous battery condition and emission values.

The start and end seconds of the measurement are included in the measurement time. Average values parameters are calculated using the arithmetic mean function.

CO, CO_2, NO and HC emissions: these data are expressed by the sum of all the route individual substances divided by the path of the section in km.

The calculation of actual fuel consumption is performed according to the methodology published by the US Environmental Protection Agency (EPA). The formula for calculating actual consumption is available on the web: (*Spočítejte si, kolik emisí CO_2 vyprodukuje Vaše auto | ekoblog.cz*, n.d.)

RESULTS AND DISCUSSION

The table shows the measured and recalculated data.

Tab. 2 Overview of measured operating parameters - U – urban, SU – suburban, H - highway

Parameter	U - 1	U - 2	SU - 1	SU - 2	H - 1	H - 2	Units
Time of testing	1728	1742	1832	1458	1424	1425	s
Distance	15711.4	15629.3	16000.9	15639.3	32681.8	32635.9	m
Average speed	32.73	32.3	31.44	38.62	82.62	82.45	$km.h^{-1}$
Highest speed	75	68	80	77	116	118	$km.h^{-1}$
Operating time of the combustion engine	622	596	693	490	1197	1183	s
Combustion engine idle time	1106	1146	1139	968	227	242	s
Average combustion rotation per minute of engine	1444.77	1525.59	1470.75	1459.67	1874.68	1736.79	min^{-1}
The highest rotation per minute of engine	3738.5	3799	2973	2099	4261	4058	min^{-1}
Number of engines starts	42	31	35	26	11	6	-
Average operating time of an internal combustion engine per 1 start	14.81	19.23	19.8	18.85	108.82	197.17	s
Average battery charge status	53.3	55	54.8	52.8	53.3	57.7	%
The highest battery level achieved	65.9	63.1	62	59.6	67.1	63.9	%
The lowest battery level reached	49.2	44.7	43.9	48.2	52.5	53.7	%

The first parameter is the driving time. In the first and last three measurements, the passage of the selected route was almost identical. The difference in time between the individual runs is negligible in terms of comparing operating parameters. The lengths of the test routes are almost identical for urban and extra-urban routes similarly the time taken to travel correlated to traffic

density during the measurements. It is obvious that the average speed in the second measurement of the suburban part is 38.62 $km.h^{-1}$. Which is approximately 6 km/h higher compared to urban and second extra-urban route. In the case of the motorway road, the operating average speeds and distances were almost identical, namely 82.62 $km.h^{-1}$ and 82.45 $km.h^{-1}$.

An interesting indicator is the time of operation and inactivity of the internal combustion engine during the test. In the case of the urban and extra-urban part, the significant share of electricity use is in the range of 490 - 693 seconds out of the total time of 1458 - 1832 seconds. This means that the internal combustion engine was running approximately 34% of the total time. On the contrary, in the case of motorway traffic, there is a significant predominance of the use of an internal combustion engine as the main source of vehicle propulsion, namely 81% of the total driving time. It is not very clear from the measured data when the vehicle uses an electric motor, but it can be estimated that activation occurs at speeds higher than 80 km/h and, conversely, deactivation occurs when the speed drops below 70 km/h. However, the main factor in switching an internal combustion engine in this case is the condition of the battery. If acceleration is required for at least 3 seconds, the internal combustion engine is switched on and, on the contrary, it is switched off while maintaining a constant speed or when the vehicle decelerates for 1 - 3 seconds.

Another parameter is the number of engines starts. The measured data show the dependence among the average speed of the vehicle, but also the maximum speed achieved, the number of starts and the time of the engine started. During city traffic, several dozen engine starts were recorede (up to 42). Comparing, when the vehicle was operating on the highway, there were 6 and 11 engine starts. The internal combustion engine is significantly more heavily loaded due to frequent sweeping. This fact has already been mentioned in connection with the Start-stop system, where dry friction of the engine can occur causing damage. Furthermore, when the crankshaft which secondarily drives another device such as an oil pump stops, reduction in oil pressure can enhance the motor damage. When the engine is switched on, the unit sets a slightly richer mixture - this increases the emission of harmful substances at a given moment and dilutes the oil in petrol engines.

The last tested parameter is the battery charge status. On average, the values were maintained around 50 %. The lowest achieved level was 43.9 % and the highest achieved state 67.1 %. According to the manufacturer, the operating range of the battery charge should be maintained at 20-80 % (*Toyota RAV4 Comfort SUV 5dv.* | *Skutečné SUV*, n.d.).

Performed study showed that the SOC (State Of Charge) of a battery does not actually fall below 39-40 % (also for Toyota vehicles). The average SOC of the battery ranged from around 55 to 56 % (Pitanuwat & Sripakagorn, 2015).

From the point of view of vehicle emission production, the measured data are shown in the following tables. An interesting data is the average consumption displayed and actually measured by diagnostics.

Tab. 3 Consumption and emissions of harmful substances – U – urban, SU – suburban, H - highway

Parameter	U - 1	U - 2	SU - 1	SU - 2	H -1	H - 2	Units
Average fuel consumption displayed	6.2	6.5	6.8	4.8	7.3	7.3	l.100 km^{-1}
Average actual fuel consumption	8.1	8.7	9	6.3	10.8	9.3	l.100 km^{-1}
CO	0.2102	0.0609	0.1037	0.0208	0.0175	0.0243	g.km^{-1}
CO_2	190.4035	202.6267	211.2256	146.2152	252.6872	217.1936	g.km^{-1}
NOX	0.0017	0.0011	0.0013	-0.0003	0.0011	0.0007	g.km^{-1}
HC	0.023	0.0212	0.0058	0.0099	0.0276	0.0176	g.km^{-1}

In the table (Tab. 3), it can be seen, that the real consumption is 1.5 - 2 l.100 km^{-1} higher than it is displayed on on-board instruments. the greatest difference occurred during motorway traffic namely 3.5 l.100 km^{-1}.

According to the values specified by the manufacturer, the consumption should reach a maximum of 6.2 l.100 km^{-1} and the average consumption should be 5.0 - 5.8 l.100 km^{-1} (*Toyota RAV4 Comfort SUV 5dv. | Skutečné SUV*, n.d.). Urban and extra-urban traffic differed from this value in several cases. However, higher values were measured in two cases, namely 6.5 l.100 km^{-1} in urban traffic and 6.8 l.100 km^{-1} in extra-urban traffic. In one case, significantly lower consumption was measured, namely 4.8 l.100 km^{-1} in extra-urban traffic. Consumption of 7.3 l.100 km^{-1} was measured on the motorway part of the test route, mainly due to the use of an internal combustion engine for most of the journey.

The manufacturer also states an average CO_2 emission range of 117 - 131 g. km^{-1} (*Toyota RAV4 Comfort SUV 5dv. | Skutečné SUV*, n.d.). How it can be seen in the table (Tab. 3) non of the CO_2 emissions measured reach the interval given by the manufacturer. Average value found out for the whole measurement- 203 g. km^{-1}, differs approximately by 55 % from the values given by the manufacturer. Data are not provided by the manufacturer for other measured emission values (CO, HC and NOX). However, the values were almost the same throughout the measurement. In one case, a negative value was measured, which is most likely due to an

emission analyzer error. However, this fact does not affect the overall comparison of NOX emissions. The table also shows a certain dependence between CO_2 and CO emissions, namely their increasing and decreasing concentration. This can serve accuracy of of the WLTP (Worldwide Harmonized Light-Duty Vehicles Test Procedure) methodology. According to the standards for this methodology, the driver's weight (75 kg) is also included in the operating weight, and an additional 200 kg of load is added to this. Conversely, with the NEDC (New European Driving Cycle) methodology, only the operating weight without the driver's weight is taken into account and 100 kg of load has been added to it.(*Emission Test Cycles: WLTC*, n.d.; *Nový homologační emisní test WLTP: Opravdu znamená konec lhaní? | auto.cz*, n.d.) It does not agree too match much when compared to the experimentally measured data. The weight limit in the case of this measurement was not exceeded, when there were 3 people in the vehicle, an emission analyzer and minor essentials. Therefore, it is possible to exclude the effect of weight on the increased production of CO_2 emissions.

CONCLUSION

The internal combustion engine was in operation approximately 34 % of the total time in the urban and extra-urban part of the test route. On the other hand, it was in operation approximately 81% of the total time on the motorway part of the testing route.

Using of the internal combustion engine was more frequent during urban and extra-urban traffic than in the case of on the motorway driving. In the urban and extra-urban part of the route, there were 26 - 42 starts of the combustion engine, while in motorway traffic there were substantionaly less actions - 6 and 11.

Fuel consumption declared by vehicle manufacturer differed from the measured values approximately by 1.5 - 2 l / 100 km. In motorway traffic, the difference was even greater - 3.5 l / 100 km.

During the entire measurement period, the average found out CO_2 emissions were 203 g. km^{-1}, that was the really significant difference comparing with the manufacturer´s declarated values - approximately 55 %. However, other measured produced emissions, such as CO, HC, NOX, (not specified by the manufacturer), displayed stabile values and did not differ significantly during the experiments.

ACKNOWLEDGEMENT

I would like to thank to Ing. Jana Stočesová for assistance in collecting and processing measured data.

REFERENCES

1. Emadi, A. (2015). *Advanced electric drive vehicles*. Boca Raton: CRC Press.
2. *Emise | Katedra vozidel a pozemní dopravy*. (n.d.). Retrieved July 27, 2020, from https://katedry.czu.cz/kvpd/merici-vybaveni/emise
3. *Emission Test Cycles: WLTC*. (n.d.). Retrieved July 29, 2020, from https://dieselnet.com/standards/cycles/wltp.php
4. *EPA fuel economy report finds weight and power leveling off, footprint stable - Green Car Congress*. (2018). Green Car Congress. https://www.greencarcongress.com/2018/01/20180116-epa.html
5. *Fact #630: July 5, 2010 Fuel Economy vs. Weight and Performance | Department of Energy*. (2010). https://www.energy.gov/eere/vehicles/fact-630-july-5-2010-fuel-economy-vs-weight-and-performance
6. National Geographic. (2018). *Kdy dojde ropa a co se stane? V optimistické verzi za 60 let. A v pesimistické.. - National Geographic*. https://www.national-geographic.cz/clanky/kdy-dojde-ropa-v-optimisticke-verzi-za-60-let-a-v-pesimisticke.html
7. *Nový homologační emisní test WLTP: Opravdu znamená konec lhaní? | auto.cz*. (n.d.). Retrieved July 29, 2020, from https://www.auto.cz/novy-homologacni-emisni-test-wltp-opravdu-znamena-konec-lhani-110305
8. *Oil prices historical chart | GlobalPetrolPrices.com*. (2015). https://www.globalpetrolprices.com/articles/28/
9. Pitanuwat, S., & Sripakagorn, A. (2015). An Investigation of Fuel Economy Potential of Hybrid Vehicles under Real-World Driving Conditions in Bangkok. *Energy Procedia*, *79*, 1046–1053. https://doi.org/10.1016/j.egypro.2015.11.607
10. *Spočítejte si, kolik emisí CO2 vyprodukuje Vaše auto | ekoblog.cz*. (n.d.). Retrieved July 27, 2020, from http://www.ekoblog.cz/?q=emise
11. *Toyota RAV4 Comfort SUV 5dv. | Skutečné SUV*. (n.d.). Retrieved July 27, 2020, from https://www.toyota.cz/new-cars/rav4/#/ajax/%2Fnew-cars%2Febrochure-hybrid.json

Corresponding author:

Ing. Štěpán Pícha, Department of Vehicles and Ground Transport, Faculty of Engineering, Czech University of Life Sciences Prague, Kamýcká 129, Praha 6, Prague, 16521, Czech Republic, email: pichas@tf.czu.cz

Accumulation of solar energy

J. Šafránková[1], M. Daneček[1], V. Beránek[2], V. Poulek[1], M. Libra[1]

[1]*Department of Physics, Faculty of Engineering, Czech University of Life Sciences Prague, Prague, Czech Republic*

[2]*Solarmonitoring, Ltd., Prague, Czech Republic*

Abstract

New glass/polysiloxane/glass laminate PV panel with integrated lithium battery was developed. Design of the new compact unit with integrated battery in new cooling box is described in the article. It can be suitable for BIPV applications like for instance emergency power supply. Temperature of lithium accumulators integrated with PV panels for period of one year was evaluated. Even at high ambient temperature +40°C the temperature increase of lithium accumulators was at maximum +13°C during 8 A (0.2 C) charging/discharging cycles. As the operating temperature of lithium accumulators is limited to +65°C, it should work well in regions with ambient temperatures up to +50°C.

Key words: Photovoltaics, PV panel, battery

INTRODUCTION

There were few studies [1,2] concerning the PV panels integrated with lithium accumulators. Main problems in these studies were: a) non compact design (lithium accumulators did not fit into the PV panel frame) and b) temperature control of lithium accumulators integrated with PV panels. Failure in thermal control could lead to thermal runaway which is very dangerous for humans and electric system. Several types of thermal management system have neen introduced by researches such as in [3,4] which investigated the system using air, liquid, boiling, heat pipe and solid-liquid phase change to control the heat. Most of the previous research was focused on electric vehicles, however the research on PV panel/accumulator integrated system is also available from [1,5].

MATERIALS AND METHODS

The PV panel with integrated lithium accumulators was placed at the flat roof faced south with tilt angle 30° (see Fig. 1). A glass/glass PV panel 260 W with polysiloxane encapsulant [6] sized 1650x990x40 mm was integrated with 6 Lithium accumulators (pouch) NCM type, 40

A.h capacity sized 210x188x8 mm. Two 3 mm hardened glass sheets of the PV panel have 1 mm polysiloxane gel layer in between. Monocrystalline solar cells are embedded in the gel. There is 54 solar cells sized 156x156mm with thickness 180 microns. The solar cells layout is 6x9.

Fig. 1 PV panel with integrated Lithium accumulator

The accumulators were fixed by silicone adhesive to aluminium cooling profile box. The cover of the cooling box (Fig.2) is polished to reflect thermal radiation from the PV panel rear side. It is thermally insulated from the cooling case. There is just 3 mm gap between the cooling box cover and the rear side of the PV panel. So the hot air can flow there using chimney effect. Standard thermocouples were used to measure temperatures. Flir IR camera was used for cross check. The flat accumulators were arranged “parallel” way with respect to the cooling profile. The accumulators were charged by the PV panel and discharged by the EA-EL 3160-60 digital load apparatus. The discharge current was fixed at 8 A (0.2 capacity). The temperature of the aluminium case, the PV panel laminate and the accumulator pouch were measured using thermocouples for period of one year. The ambient temperature and intensity of solar radiation was measured by the professional meteorological station.

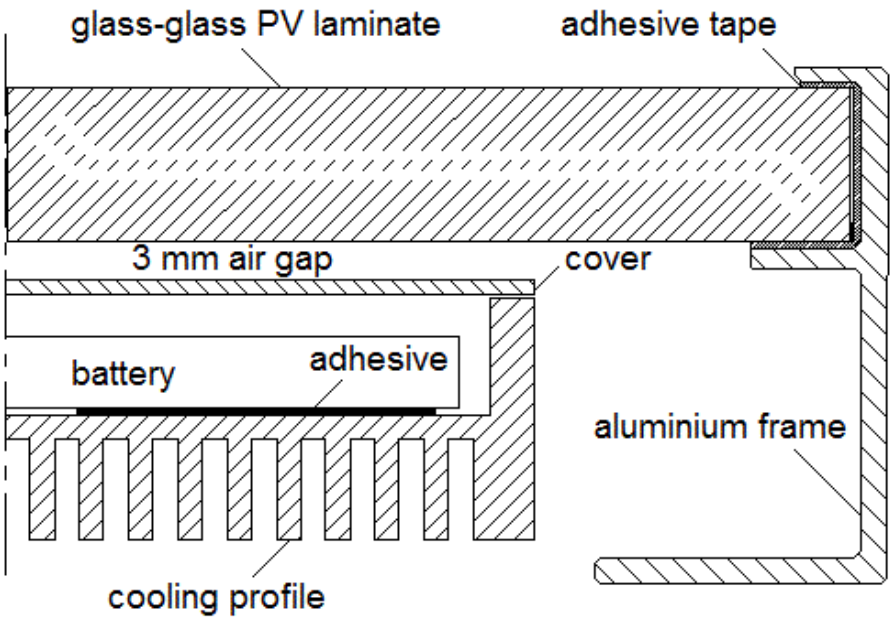

Fig. 2 Lithium accumulator integrated with PV panel - scheme

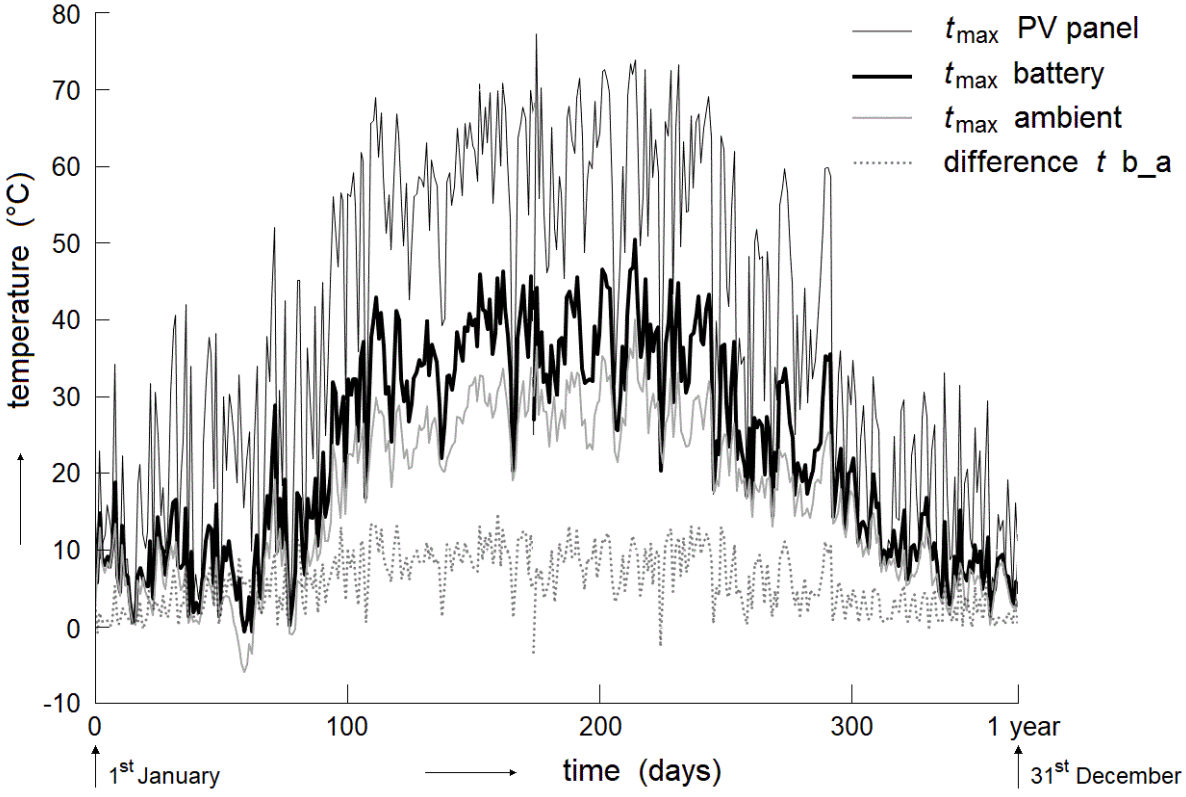

Fig. 3 PV panel, Li-ion battery, air maximum temperature and battery-air temperature difference

RESULTS AND DISCUSSION

Main results are presented by Fig. 3. It indicates that max. increase of accumulator temperature over ambient temperature was 13 K. It is in good accordance with theoretical calculation and with short time laboratory test [1]. So unlike the previous designs, in the new design the lithium accumulators in cooling box fit well into PV panel frame. The new compact design is very important for real outdoor application of PV panels with integrated lithium accumulators worldwide.

CONCLUSION

New glass/polysiloxane/glass PV panel with integrated lithium accumulators was successfully tested. During the experiment, the temperature of lithium accumulators integrated with usual size PV panel was kept 13 K only above ambient temperature during one year period at real outdoor conditions. It is very important for real outdoor applications of PV panels integrated with Lithium accumulators especially in tropical countries with ambient temperatures up to +50°C. As the operating temperature of lithium accumulators is limited to +65°C, it should work well in regions with ambient temperatures up to +50°C. It is very important for commercial applications of lithium accumulators integrated with PV panels in tropical countries. Some results were published in [7] as well.

REFERENCES

1. VEGA-GARITA, V, RAMIREZ-ELIZONDO, L, BAUER, P.: Physical integration of a photovoltaic-accumulator system: A thermal analysis. Applied Energy, 2017, 208: 446-455.
2. NARAYAN N, PAPAKOSTA, T, VEGA-GARITA, V, QIN, Z, POPOVIC-GERBER, J, BAUER, P, ZEMAN, M.: Estimating battery lifetimes in Solar Home System design using a practical modelling methodology. Applied Energy, 2018, 228: 1629-1639.
3. MALIK, M, DINCER, I, ROSEN, M, FOWLER, M.: Experimental investigation of a new passive thermal management system for a lithium accumulator pack using phase change composite material. Electrochimica Acta, 2017, 257: 345-355.
4. PANCHAL, S, DINCER I, AGELIN-CHAAB, M, FRASER, R, FOWLER, M.: Experimental and theoretical investigation of temperature distributions in a prismatic lithium-ion accumulator. International Journal of Thermal Sciences, 2016, 99: 204-212.

5. GRZESIAK, W, MACKOW, P, MAJ, T, POLAK, A.: Klugmann-Radziemska E, Zawora S, Grzesiak P. Innovative system for energy collection and management integrated within a photovoltaic module. Solar Energy, 2016, 132: 442-452.
6. POULEK, V., STREBKOV, D.S., PERSIC, I.S., LIBRA, M.: Towards 50 years lifetime of PV panels laminated with silicone gel technology. Solar Energy, 2012, 86(10): 3103–3108.
7. POULEK, V., DANG, M.Q., LIBRA, M., BERÁNEK, V., ŠAFRÁNKOVÁ, J.: PV Panel with Integrated Lithium Accumulators for BAPV Applications - One Year Thermal Evaluation. IEEE Journal of Photovoltaics, 2020, 10(1): 150-152.

Corresponding author:

Ing. Jan Šafránková, Department of Physics, Faculty of Engineering, Czech University of Life Sciences Prague, Kamýcká 129, Praha 6, Prague, 16500, Czech Republic, email: janicka.safrankova@gmail.com

Utilization of pyrolysis technology in Thuja occidentalis processing waste

T. Saller[1], D. Herák[1], L. Sedláček[1], P. Hrabě[2], Č. Mizera[1]

[1]Department of Mechanical Engineering, Faculty of engineering, Czech University of Life Sciences Prague, 165 21 Prague 6 – Suchdol, Czech Republic.
[2]Department of Material Science and Manufacturing Technology, Faculty of engineering, Czech University of Life Sciences Prague, 165 21 Prague 6 – Suchdol, Czech Republic.

Abstract

The article is focused on utilization of pyrolysis technology in thuja occidentalis processing waste. Pyrolysis technology in this case is interesting because it can transform the thuja waste into the useful product. This product can be used as a fuel in internal combustion engines. Czech University of Life Science has built a laboratory pyrolysis unit for this special purpose. On this unit is tested the efficiency of the process and the whole process itself. Real-time pressure and temperature are the most important factors of the process and have the main impact on quality and quantity of the final product.

Key words: pyrolysis, thuja waste, pyrolysis unit, waste processing, alternative fuels

INTRODUCTION

By the thuja waste is meant all waste from the gardening processes as leaves, branches or wood itself.

Pyrolysis is physicochemical action that affects material inside a high-temperature reactor. The temperatures range is from 300 °C to 1200 °C. The most important thing for pyrolysis process is no oxygen present during the reaction (Jilková et al., 2012). Utilization of pyrolysis technology for waste processing instead of standard burning limits negative effects on environment and is more economical due to production of a useful fuel. Products of the process are pyrolysis gas, pyrolysis oil and carbon. All products can be further used (Zafar, 2008).

Pyrolysis gas can be used as a fuel for electricity generation (via internal combustion engine or a gas turbine) and/or for methane or hydrogen separation (Biogreen, 2019).

Pyrolysis oil can is a source of bio-molecules, fuel for further refining, food aromas (liquid smoke), pesticides and plant enhancers (wood vinegar) (Biogreen, 2019).

Pyrolysis carbon can be used as tires filler (Continental Carbon, 2014) or as an input for developing activated carbon (Indayaningsih et al., 2017)

This research is focused on processing of thuja waste and pursues the pyrolysis oil as a final product. Eny Kusrini conducted a similar research, where he examined pyrolysis oil based on input materials. Inputs were various ratios of oil palm empty shells and polyethylene (Kusrini et al., 2018). Sabar Pangihutan Simanungkalit examined the influence of polyethylene terephthalate (PET) as an input for pyrolysis of oil palm empty shells. He concluded that PET increases the pyrolysis oil production (Simanungkalit et al., 2018; Williams et al., 2003).

The aim of this article is to provide a method, how to process the thuja waste by pyrolysis technology.

MATERIALS AND METHODS

There was developed a laboratory pyrolysis unit (Fig. 1) for the purpose of using biomass as an input for the reaction. As a fuel is used waste from the northern white-cedar (Thuja occidentalis) as leaves and chopped branches with size no longer than 30 mm and diameter no wider than 5 mm. The waste was naturally dried before used as an input for pyrolysis reaction.

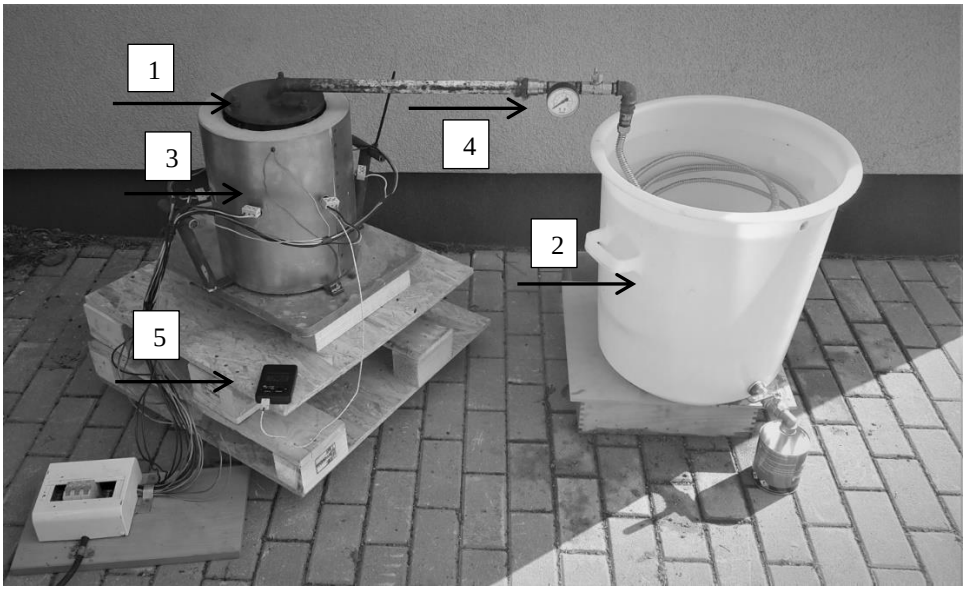

Fig 1. Pyrolysis unit

The unit itself consists of reactor (1), cooler (2), heating shield (3), pressure guide (4), temperature meter (5) and it is powered by electricity. Heating system itself can be adjusted to three different stages, based on the necessary heating speed.

On the pyrolysis unit is possible to measure real-time pressure inside the reactor and temperature between the reactor and the heating shield. Maximal temperature during the tests reached to 814 °C, maximal tested pressure was 300 kPa.

Each measurement was filled in tables. Weight of inputs was measured before each process and the final weight was measured too.

RESULTS AND DISCUSSION

Tab.1 shows the main results as starting and ending weight, consumption of electricity or the oil gain.

Tab. 1 Results of pyrolysis of dried and natural thuja

Results		
-	Natural thuja	Dried thuja
Starting weight [kg]	2.419	1.48
Ending weight [kg]	1.14	1.05
Weight of oil [kg]	1.063	0.307
Consumption of electricity [kWh]	12	6.62
Time [min]	170	100
Oil gain [%]	43.9	20.8
Electricity consumption per 1 kg of oil [kWh]	11.29	21.55

The results of measurement and the course of reaction are shown in the Fig. 2, resp. Fig. 3. The pyrolysis unit starts to produce the pyrolysis oil around 550 °C. The oil is produced up to 700 °C when the pressure drops.

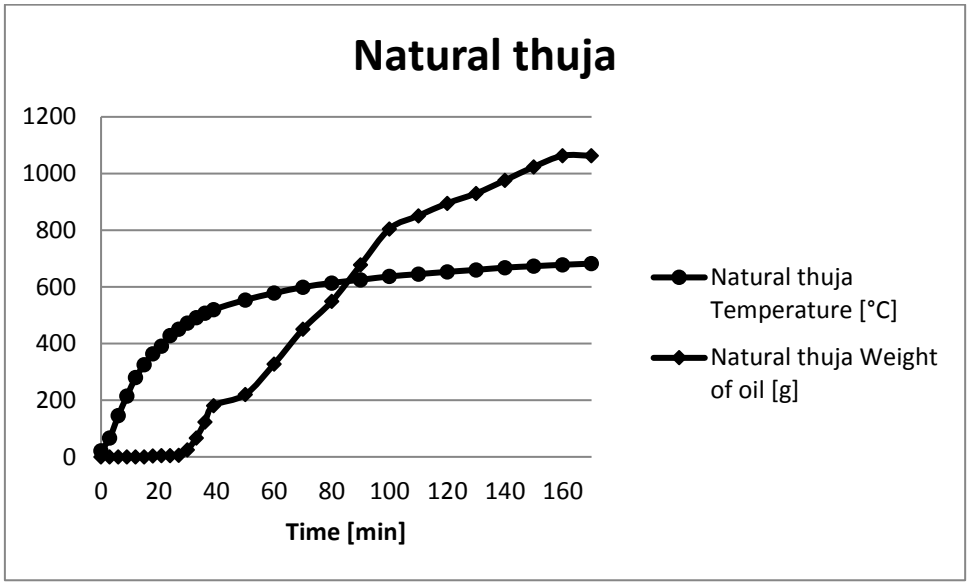

Fig. 2 Course of natural thuja pyrolysis

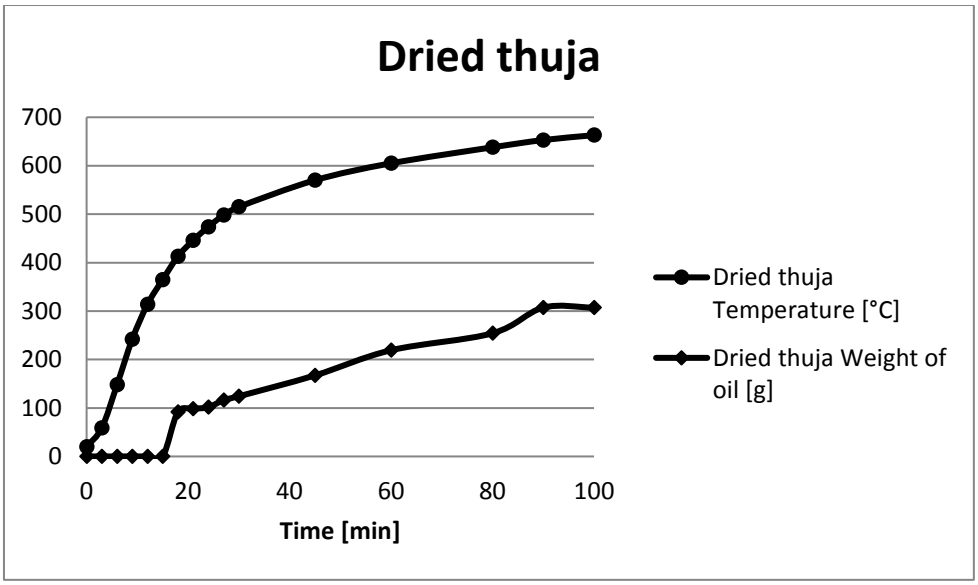

Fig. 3 Course of dried thuja pyrolysis

250 ml (287,5 g) of pyrolysis oil was produced in 80 minutes from 1030 g, which is 27,9 %. Kusrini produced 3.48 g of pyrolysis oil from 20 g of EFB (main agricultural waste of the palm industry). It could be transferred as 179 g from 1030 g of input, which is 17.4 % (Kusrini et al., 2018).

He produced 3.27 g of pyrolysis oil from 20 g of mass while contained 90 % of EFB and 10 % of HDPE (high-density polyethylene), which is 16.35 % and only 1.35 g of pyrolysis oil from 20 g of mass while contained 25 % of EFB and 75 % of HDPE, which is 6.75 % (Kusrini et al., 2018).

This leads to the conclusion, that pure bio waste in pyrolysis process can be transformed into pyrolysis oil in higher amount than while HDPE is added. On the other hand plastic waste may improve calorific value of the oil by up to 37 % because of content of the carbon (Simanungkalit et al., 2018).

CONCLUSIONS

The pyrolysis process on the newly developed unit is fully operational and we were able to gather reliable data.

307 g resp. 1063 g of pyrolysis oil was produced out of 1480 g resp. 2419 g of thuja bio waste. The whole procedure took 100 minutes resp. 170 min.

For future work is recommended to measure different moisture and density of the input material and to perform at least 5 measurements in each heating stage.

It is also recommended to analyze the pyrolysis oil and to compare its composition during the different stages of heating.

REFERENCES

1. Biomass Wastes from Palm Oil Mills. BioEnergy Consult [online]. 2018, December 28, 2018 [cit. 2019-08-04]. Dostupné z: https://www.bioenergyconsult.com/palm-biomass/

2. Jílková, L., Ciahotný, K., & Černýb, R. (2012). TECHNOLOGIE PRO PYROLÝZU PALIV A ODPADŮ. VŠCHT. 2012 Dostupné také z: paliva.vscht.cz/download.php?id=76

3. ZAFAR, Salmar. BIOMASS PYROLYSIS. Altenergymag [online]. 2009, 02/01/09 [cit. 2019-08-04]. Dostupné z: https://www.altenergymag.com/article/2009/02/biomass-pyrolysis/502/

4. Biogreen. : Pyrolysis oil: compounds for green chemistry [online]. 2019 [cit. 2019-08-05]. Dostupné z: http://www.biogreen-energy.com/pyrolysis-oil/

5. Tire Rubber Carbon Blacks. Continental Carbon [online]. 2014 [cit. 2019-08-05]. Dostupné z: http://www.continentalcarbon.com/rubber-carbon-black-tire-grades.asp

6. INDAYANINGSIH, N, F DESTYORINI, R I PURAWIARDI, D R INSIYANDA a H WIDODO, 2017. Production of activated carbon by using pyrolysis process in an ammonia atmosphere. *Journal of Physics: Conference Series* [online]. **817**, 012006. ISSN 1742-6588. Dostupné z: doi:10.1088/1742-6596/817/1/012006

7. KUSRINI, Eny, Dijan SUPRAMONO, Volkan DEGIRMENCI, Saeful PRANATA, Aji Agraning BAWONO a Nasir ANI, 2018. Improving the Quality of Pyrolysis Oil from Co-firing High-density Polyethylene Plastic Waste and Palm Empty Fruit Bunches. International Journal of Technology [online]. 9(7), 1498. ISSN 2087-2100. Dostupné z: doi:10.14716/ijtech.v9i7.2531

8. SIMANUNGKALIT, Sabar Pangihutan, Dieni MANSUR a Muhammad Arifuddin FITRIADY, 2018. Effect of plastic blends on slow pyrolysis of oil palm empty fruit bunch. In: AIP Conference Proceedings [online]. s. 20002 [vid. 2019-02-27]. ISBN 9780735417441. Dostupné z: doi:10.1063/1.5064289

9. WILLIAMS, Paul T a Anton R REED, 2003. Pre-formed activated carbon matting derived from the pyrolysis of biomass natural fibre textile waste. Journal of Analytical and Applied Pyrolysis [online]. **70**(2), 563–577. ISSN 01652370. Dostupné z: doi:10.1016/S0165-2370(03)00026-3

Corresponding author:
Ing. Tomáš Saller, Department of Mechanical Engineering, Faculty of engineering, Czech University of Life Sciences Prague, 165 21 Prague 6 – Suchdol, Czech Republic,
e-mail: saller@tf.czu.cz

Study of tribology wear properties of polymers fabricated by Additive manufacturing (3D printing).

R. Sangam[1], A. Zdeněk[1]

[1]Department of Mechanical Engineering, Faculty of Engineering, Czech University of Life Sciences, Prague, Czech Republic

Abstract

This paper deals with the study of wear properties of the polymers that are the most commonly used in rapid prototyping technologies. Sample parts are manufactured with additive manufacturing (AM) technology. First sample is acrylonitrile butadiene styrene (ABS) with blue filament and second is polylactic acid (PLA) with grey filament manufactured (3D printed) by fused deposition modeling (FDM) technology. Both the samples were tested on reichert friction and wear tester machine with rigidly-mounting test sample roller, which presses against a revolving friction wheel by means of a weighted lever. Water is used as lubricant for first 2 trials and second trial is dry contact without lubrication. ABS and PLA polymers are thermoplastics and wear of the samples was estimated after the experiments. Analysis of the experiment data has shown that printer settings has significantly influence not only on the strength and stiffness of the parts, but also on the quality of the surface that affects the tribological properties of the samples. The results of this study shows tribological wear properties of ABS and PLA.

Keywords: Additive manufacturing, Fused deposition modelling, WEAR, Tribology Properties, 3D Printing, Polymers, Aerospace.

INTRODUCTION

Additive manufacturing (AM) technology is currently one of the most developing technology for industries, enabling the growth of practical use of several composite materials. 3D printing is expected to be one of the key developmental technologies that will shape the new approach to manufacturing. This article focused mainly on study of tribology properties of polymers like ABS and PLA manufactured (3D printed) by fused deposition modeling (FDM) technology. Thermoplastics ABS (Sun, Rizvi, Bellehumeur, & Gu, 2008; Tran, Ngo, Ghazlan, & Hui, 2017) and polylactic acid (PLA) (Tymrak, Kreiger, & Pearce, 2014), are commonly used due to their low melting temperature as well as their diversity and ease of adoption to different 3D printing

processes. The capability of employing 3D printing of polymers and composites has been explored for several years in many industrial applications, such as the aerospace, architectural, toy fabrication and medical fields.

Tribology deals with the relative motion of surfaces. It involves friction, wear of materials, scratching and rubbing. A more precise definition describes tribology as a science and technology of surfaces that are in contact and relative motion, as well as supporting activities that should reduce costs resulting from friction and wear (Bhushan, 2013). Polymers can be picked as a solution in specific applications of machine construction because of their strength, chemical resistance, and self-lubricating ability (Zsidai et al., 2002). It has been noticed from the literature that widespread interest in plastics has raised in the mid-twentieth century due to the features of their structure, specific mechanical behaviour, and the signifi cant possibility to change the polymer properties. Consequently, extensive studies over many years have developed in the field of modern engineering in which the plastics can be applied as tribological materials.

However, it is apparent to recognise from the literature that there is a lack of research that deals with the tribological characteristics of the 3D printed structure. Therefore, it appears essential to study the tribology of 3D printed polymers in order to grasp the influence of 3D printed structures and surfaces on the tribology behaviours of polymers.

In the present research, 3D printed polymer specimens are produced by the fused deposition modelling (FDM) technology. The wear properties of 3D printed polymer samples are considered as the fundamental tribological features. As experimental conditions for the 3D printing, different materials (ABS and PLA) and colours (blue and grey) of polymer in different printing machines in order to estimate the wear properties of samples.

MATERIALS AND METHODS

Material used are ABS and PLA. For the purposes of the experiment 2 rollers were printed by fused deposition modeling (FDM) on Pursa i3 3D printer and second sample ABS was printed on Ender printer. Test rollers have size dimension of diameter D = 12 mm and length l = 18 mm. Slip rings (Refer Fig.3) were also produced with same material as rollers.

Discription of the samples:

- Sample 1:Refer Fig. 1, material produced by Fused deposition modeling (FDM) on Pursa i3 3D printer

Fig. 1 ABS material

- Sample 2: Refer ***Fig. 2,*** material produced by Fused deposition modeling (FDM) on Ender 3D printer

Fig. 2 PLA material

Fig. 3 Slip rings

Further, the rollers were subjected to hardness test and method used is Shore A hardness Scale and resulting hardness value is 83 A for ABS and 80 A for PLA.

Roughness parameters were measured using a portable profilometer Mitutoyo Surftest 301. Border wavelength cut-off was set at 0.8 mm. Around 10 different locations were measured.

The test parameters of the surface roughness were Ra and Rz parameter. For ABS Ra varies between 9.3 μm to 12.13 μm, however PLA surface quality is different due to different printing paramenters and machine which range from 3.9 μm to 6.04 μm.

Reichert test M2 was used in order to assess intensity of wear (Fig. 4). This method is widely used for testing the efficiency of additives in lubricating oils with regard to friction coefficient and wear (Aleš, Pavlu, Hromasová, & Svobodová, 2019). With this friction-testing machine, a tightly fixed test roller is pressed by means of a lever system on a rotating slip ring wheel, which is immersed to its lower third in the test lubricant. The driving motor and slip ring wheel rotate together at the same speed. With regard to the number of revolutions per minute, it has to be insured that the lubricant flowing into the contact point (friction wear point) between test roller and test ring is always sufficient. After testing, abrasive areas (elliptic wear scars) appear on the test roller. The dimensions of these wear scars depend on the load-carrying capacity of the test lubricant. The sharply limited abrasive area allows a precise measurement, which favours the exact determination of the load-carrying capacity of the test lubricant. The higher the load carrying capacity the smaller the wear scar is after a certain running time or precise distance (e.g. 100 m of the peripheral distance of slip ring wheel).

$$\boldsymbol{A = \pi \cdot \frac{l}{2} \cdot \frac{d}{2} = 0,785 \cdot l \cdot d}\ [mm^2], \tag{1}$$

Where:
A…elliptical wear area [mm^2]
l… length of elliptical wear area [mm]
d …width of elliptical wear area [mm]

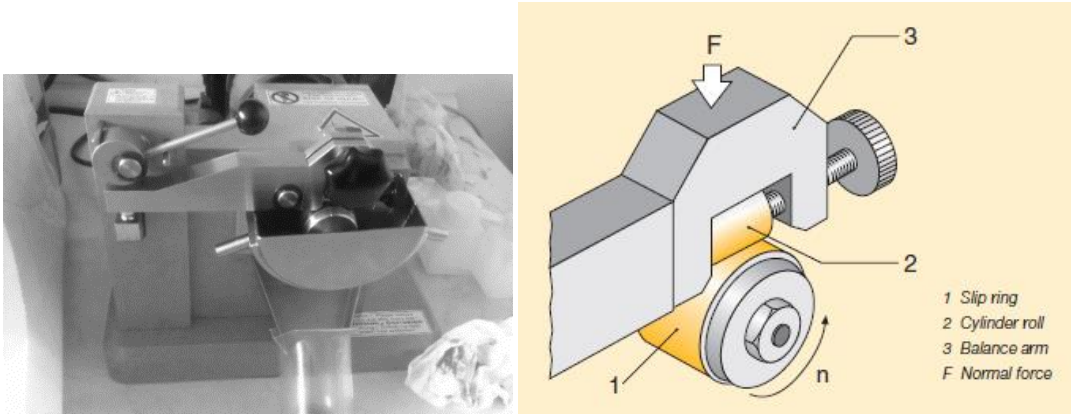

Fig. 4 Reichert Friction and Wear Tester

Range and measurement accuracy are determined by the used measuring device of length l and width d of el-liptical wear area A, which evaluates load carrying capacity of lubricating film.

Each test roller was used four times in order to create elliptical wear area. Water is used as lubricant for creation of each elliptical wear area.

Measured elliptical wear area of dry run samples and with lubrication on each sample are compared to study the wear properties of the materials.

RESULTS AND DISCUSSION

Both sample surface was evaluated by scanning electron microscopy (SEM) after Reichert Friction test and wear test. Fig. 5 and 6 shows the surface of PLA (sample 2) and Fig. 8, 9 shows the surface of ABS (sample 1) after the wear test. From the pictures, there is visible even worn area. Refer Fig. 7 and Fig. 10 showing surface after wear test without any lubrication and the surface is uneven compared to surface with lubrication a significant plastic deformation of worn surface ends is also visible. By subsequent dividing of these particles the representation of large particles in lubricant increases. This state is undesirable for practical application. From pictures its clearly visible that along with strength and stiffness of the parts quality of the surface and lubrication affects the tribological properties.

From the experiment results it is obvious that the elliptical wear area A increased when samples tested without lubrication.

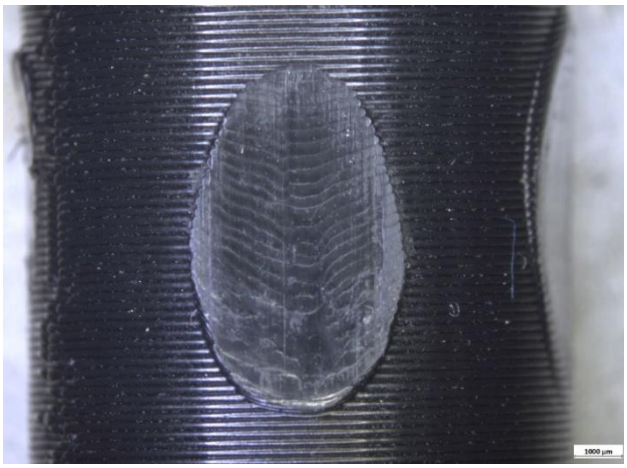

(1000 µm)

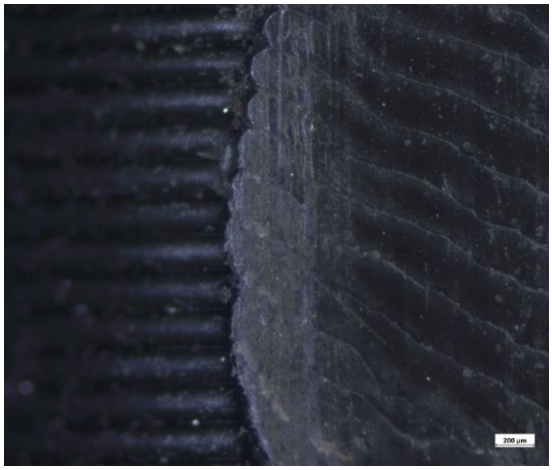

(200 µm)

Fig. 5 and Fig. 6 Elliptical wear area after Reichert Friction and Wear test with lubricant

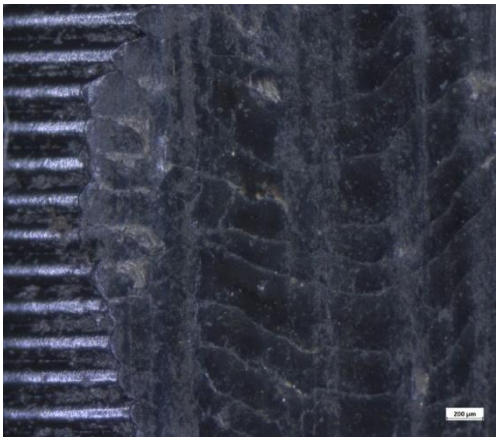

(200 µm)

Fig. 7 Elliptical wear area after Reichert Friction and Wear test without lubricant

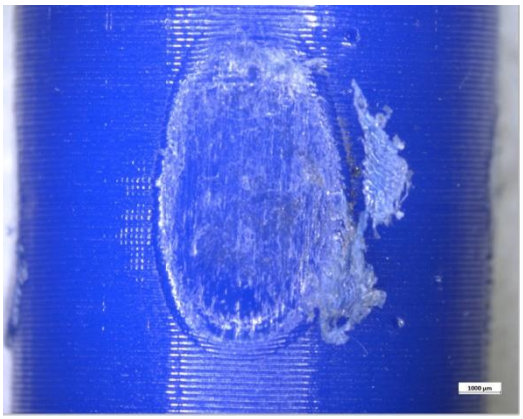

(1000 µm)

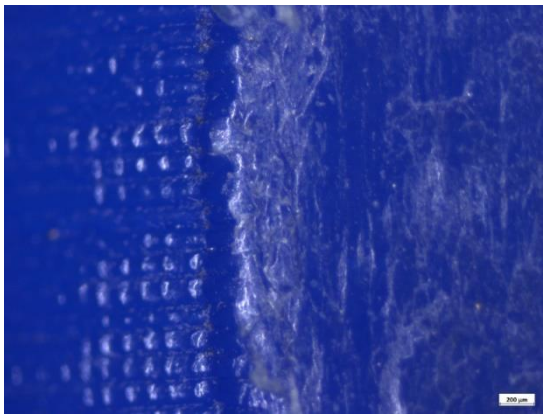

(200 µm)

Fig. 8 and Fig. 9 Elliptical wear area after Reichert Friction and Wear test with lubricant

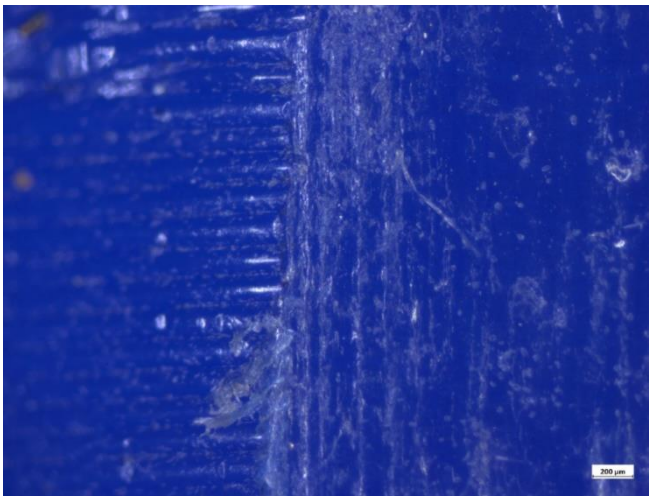

(200 µm)

Fig. 10 Elliptical wear area after Reichert Friction and Wear test without lubricant

In terms of the influence of variation of experiment on elliptical wear area A, the results (Ref. Table 1) of ANOVA F-test are as follows:

Tab. 1 ANOVA F-test

F-Test Two-Sample for Variances		
	Without Lubrication	*With Lubrication*
Mean	0.281815	0.111371875
Variance	0.004154281	0.000676243
Observations	4	4
df	3	3
F	6.143179877	
P(F<=f) one-tail	0.085089047	
F Critical one-tail	9.276628153	

Results from the Anova F test shows f-value is lower than F critical value, so H_0 the null hypothesis is accepted.

Below Fig. 11 and Fig.12 shows chart of measured wear values. These values indicate that the largest elliptical wear area is at the sample 1. Conversely, the smallest elliptical wear area was measured in sample 2, refer Fig. 13 and Fig.14 charts. From these measured values it is possible to conclude that sample 2 is the best in case of resisting to specified load. It is necessary to note that the sample 2 was printed with same parameters. It can be assumed that the surface roughness contributed to the erasure lubricating process and thus to decreasing intensity of wear.

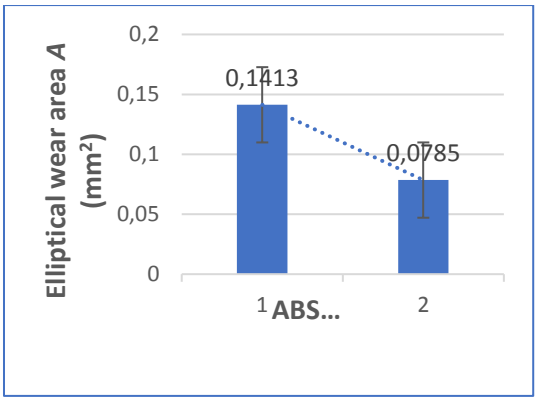

Fig. 11 Tested with Lubrication

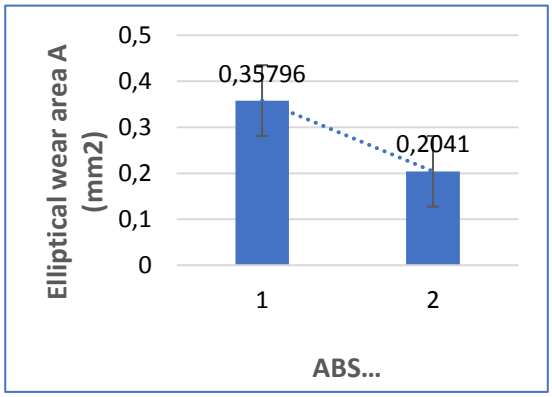

Fig. 12 Tested without Lubrication

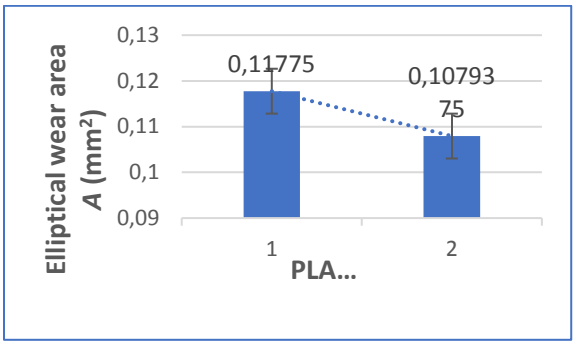

Fig. 13 Tested with Lubrication

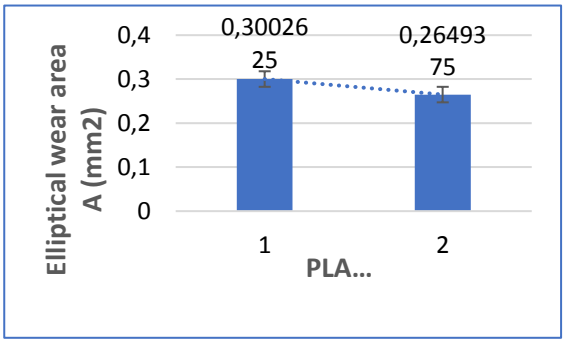

Fig. 14 Tested without Lubrication

CONCLUSION

This research aims to obtain tribological properties of different 3D printable filaments, including the determination and examination of wear values. In the light of these findings, it is concluded with a statement on the effect of the 3D printing parameters on the tribological property. Based on the experiments carried out on the printed polymers pairs used in this investigation, the following can be drawn:

– The research allows to measure the difference between wear areas of varour polymers, so it is suitable for comparative tests of this type.

– Both ABS and PLA materials are considered to be variations in the properties of the raw materials.

– The 3D printing with the similar print parameters settings tested showed some discrepancies, but they did not show a clear tendency to draw a conclusion.

This experiment examined the variations in mechanical properties of 3D printed material due to a variety of factors like strength, stiffness, surface roughness, hardness, durability and flexibility. It is clear that further study of the trends proposed by this study is necessary due to the limited number and limited quality of samples are used to provide these results. There are so many factors that need to be analyzed when it comes to predicting the strength of 3D printed parts. As 3D printing becomes more mainstream, companies will want to know how to maximize the strength and durability of the products they print.

The research on this topic can be further developed in many ways. It would be worthwhile to carry out further research on different properties of the polymer workpieces. It would also be an impressive area to perform a comparative examination of other material properties while looking for technological differences. Research could be extended to include mechanical tests (e.g., tensile strength) and material science measurements (e.g., hardness).

Further study is necessary with Reichert test to be performed considering varying load cases, different material pairs of polymers, different material pairs of metallic printed samples and also using various lubrication oils.

REFERENCES

1. Aleš, Z., Pavlu, J., Hromasová, M., & Svobodová, J. (2019). Tribological properties of brass surfaces machined by abrasive - Free ultrasonic finishing process. *Manufacturing Technology*. https://doi.org/10.21062/ujep/235.2019/a/1213-2489/mt/19/1/3
2. Bhushan, B. (2013). Principles and Applications of Tribology, Second Edition. In *Principles and Applications of Tribology, Second Edition*. https://doi.org/10.1002/9781118403020
3. Sun, Q., Rizvi, G. M., Bellehumeur, C. T., & Gu, P. (2008). Effect of processing conditions on the bonding quality of FDM polymer filaments. *Rapid Prototyping Journal*. https://doi.org/10.1108/13552540810862028
4. Tran, P., Ngo, T. D., Ghazlan, A., & Hui, D. (2017). Bimaterial 3D printing and numerical analysis of bio-inspired composite structures under in-plane and transverse loadings. *Composites Part B: Engineering*. https://doi.org/10.1016/j.compositesb.2016.09.083
5. Tymrak, B. M., Kreiger, M., & Pearce, J. M. (2014). Mechanical properties of components fabricated with open-source 3-D printers under realistic environmental conditions. *Materials and Design*. https://doi.org/10.1016/j.matdes.2014.02.038
6. Zsidai, L., De Baets, P., Samyn, P., Kalacska, G., Van Peteghem, A. P., & Van Parys, F. (2002). The tribological behaviour of engineering plastics during sliding friction investigated with small-scale specimens. *Wear*. https://doi.org/10.1016/S0043-1648(02)00149-7

Utilization of Remote Sensing for Palm Oil Monitoring in Conditions of Indonesia

A. Sembiring[1]

[1]Department of Mechanical Engineering, Faculty of Engineering, Czech University of Life Sciences Prague, Prague, Czech Republic

Abstract

Currently, Indonesia stands as the biggest producer of palm oil in the world. More than 40 million tons of its production in 2018 had fulfilled both domestic as well as global demand for various palm oil based products. However, due to the many environmental as well as social destruction associated with palm oil production in the country, many problems needed to be addressed including yield gap among agricultural practice of smallholder farmers. In order to assist this effort, accurate data and information is needed. This research aims to exemplify the capability of satellite image gained from publicly available sources to give an overview on productivity of smallholder farmers. By using the computation of three different vegetation indices, productivity of plantations in 5 different sub-districts in RIAU province is discussed. Given the wide spectrum of smallholder farmer's characteristics, many factors need to be taken into account in analyzing the data obtained.

Key words: Palm Oil, Remote Sensing, Smallholder Farmers

INTRODUCTION

Currently, Indonesia is the largest palm oil producer in the world. Indonesia's palm oil production had reached more than 40 million tons in 2018 (Direktorat Jenderal Perkebunan, 2019). This production had used a land area of more than 14 million hectares that spread across 25 provinces in Indonesia from Sumatra to Papua (Badan Pusat Statistik, 2018). Due to the wide distribution of oil palm agricultural locations, there has also been a wide variety of agricultural practices among independent smallholders.

There were many research have been done to classify characteristics of agricultural practices among smallholder farmers. These classifications were mainly based on ecological, demographical, and socio-cultural conditions. At the moment, smallholder farmer's production practice still demanded various improvements. Among the independent smallholder farmers, land expansion is still an option to increase production meanwhile the use of existing land is still 50% of its optimal (Euler, Hoffmann, Fathoni, & Schwarze, 2016). This has resulted in

various environmental and socio-cultural problems. For this reason, various approaches need to be taken to support improvements among independent smallholders. Given the wide variety of agricultural practices among independent smallholders as well as ecological conditions of plantations, a body of research suggested the need for more targeted and measured approach. For this reason, a monitoring technique to assist farmers and other stakeholders is needed and remote sensing technology can be useful.

At the moment there are many publicly available satellite data that are accessible to farmers to gain data and information. Through spectral and texture analysis, vegetation conditions can be classified and treatment can be applied. In palm oil agriculture, remote sensing has been used for many purposes such as age and yield estimation, pest and disease detection, and tree counting (Chong, Kanniah, Pohl, & Tan, 2017).

By using publicly available satellite data, this study aims to provide an overview of the different vegetation conditions of oil palm plantations in several locations in Indonesia

MATERIALS AND METHODS

Study Area

Using Google Earth Pro we identified area of palm oil plantation in Rokan Hulu and Rokan Hilir. Rokan Hulu and Rokan Hilir are two districts in RIAU province, location of. We then used Geographic information system (GIS) software to capture the targeted area we wanted and selected the period 1 July to 31 July 2019. From the images showed we selected areas with the minimum percentage of cloud to get the best view of the plantation area. We then selected image taken from 13 July 2019 with 0,1% and randomly drew polygons on 5 different areas. Selected areas are illustrated in Figure 1.

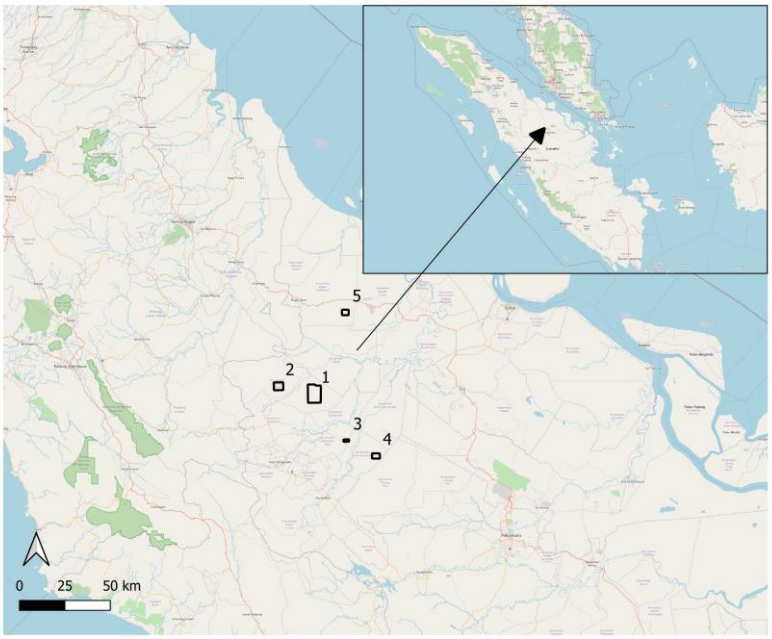

Fig. 1 Sample areas

Data Processing

Three Vegetation indices are used. These indices are Normalized Difference Vegetation Index (NDVI), Green Normalized Difference Vegetation Index (GNDVI), and Normalized Difference Water Index (NDWI).

NDVI relates near-infrared and red bands and has a positive correlation with biomass content (Alvino, Aleman, Filgueiras, Althoff, & da Cunha, 2020). The index ranges from −1.0 to 1.0, that indicates greenness or high chlorophyll content as it approaches 1.0 (Candiago, Remondino, De Giglio, Dubbini, & Gatelli, 2015). Moreover, photoactive pigments in plants can be distinguished by GNDVI (Alvino, 2020). GNDVI ranges from 0 to 1.0, which indicates strong nitrogen status and other stress factors as it approaches 1.0.

NDWI demonstrate the ability to monitor changes in vegetation water content, and thus can be used to improve irrigation and crop monitoring (Alvino et al., 2020). NDWI ranges between -1 and +1, depending on crop water content, vegetation species, ground cover, and bottom effect. A high NDWI, green color, corresponds to high water content in vegetation and wider vegetation cover, whereas negative NDWI, red color, corresponds to low vegetation biomass and more exposed soil, as crops in central pivots are subjected to irrigation management (Alvino et al., 2020)

Tab. 1 The considered Vegetation Indices

Index	Sentinel-2 Formulation
NDVI	(B8 - B4)/(B8 + B4)
GNDVI	(B8 - B3)(B8+B3)
NDWI	(B2 - B4)/(B2+B4)

Statistical Analysis

For each area, basic statistics of indices values, *i.e.*, Mean ($\overline{x}$) and Standard Deviation (σx), were calculated (Table 2). The mean values of the vegetation indices were used to define plant condition profiles of each sample areas and standard deviation values were used to analyze data variability (Junges, Fontana, Anzanello, and Bremm, 2017).

RESULTS AND DISCUSSION

The mean NDVI values of study area 1, 2, 3, 4, and 5 and its deviation are presented to show variation of greenness of the area. The highest NDVI value (0.90) occurred in sample areas 3, 4, and 5 whilst lowest NDVI value (0.09) occurred in sample area 1. According to Candiago et al (2015) higher NDVI value indicates higher productivity and biomass content of vegetation.

Tab. 2 Mean, Standard Deviation, Minimum, and Maximum of sample areas 1, 2, 3, 4, 5

NDVI				
Area	**Mean**	**Standard Deviation**	**Minimum**	**Maximum**
1	0.83	0.04	0.09	0.89
2	0.82	0.05	0.12	0.88
3	0.82	0.06	0.25	0.90
4	0.84	0.07	0.19	0.90
5	0.84	0.05	0.24	0.90
GNDVI				
Area	**Mean**	**Standard Deviation**	**Minimum**	**Maximum**
1	0.74	0.03	0.14	0.81
2	0.71	0.04	0.15	0.78
3	0.74	0.04	0.26	0.80
4	0.76	0.05	0.23	0.82
5	0.75	0.04	0.33	0.80
NDWI				
Area	**Mean**	**Standard Deviation**	**Minimum**	**Maximum**
1	0.64	0.05	-0.23	0.74
2	0.63	0.06	-0.13	1.00
3	0.62	0.05	0.26	0.72
4	0.65	0.06	0.22	0.73
5	0.67	0.06	0.18	0.75

The GNDVI mean and standard deviation obtained showed similar values to NDVI. Slight differences occurred on the highest mean value (0.76) in sample area 4 which corresponded to the highest NDVI mean value, however, on the same NDVI mean value of sample area 5 GNDVI mean value was lower. Maximum GNDVI value can be found in sample area 4 whilst minimum GNDVI value can be found in sample area 2. Overall, wider range of GNDVI value can be found in area 1 and smaller range of GNDVI value can be found in area 5.

Meanwhile, NDWI value showed main differences in comparison with the two other indices. Maximum NDWI value can be found in sample area 2 which obtained the lowest maximum GNDVI and NDVI values. Widest range of NDWI value can be found in sample area 2 with value -0.13 to 1.00.

CONCLUSION

This research has shown the capability of satellite image to give an overview on the differences of productivity among smallholder farmers. The three vegetation indices can be a tool to obtain data and information regarding plant condition that can be useful as a base for efforts on improvement. Given the wide variability of smallholder farmer's agricultural practice, many factors need to be taken into account. Data and information gain from satellite images to increase productivity should also be improved and adjusted according to the specific needs and challenges of smallholder farmer's agricultural practices.

REFERENCES

1. Alvino, F.C.G., Aleman, C.C., Filgueiras, R., Althoff, D., & Da Cunha, F. F. (2020). Vegetation Indices for Irrigated Corn Monitoring. *Engenharia Agricola*, *40*(3), 322 - 333. doi: http://dx.doi.org/10.1590/1809-4430-Eng.Agric.v40n3p322-333/2020

2. Badan Pusat Statistik. (2018). *Statistik kelapa sawit Indonesia.* Jakarta, Indonesia: Badan Pusat Statistik

3. Candiago, S., Remondino, F., De Giglio, M., Dubbini, M., & Gatelli, M. (2015). Evaluating Multispectral Images and Vegetation Indices for Precision Farming Applications from UAV Images. *Remote Sensing. 7*, 4026-4047. doi:10.3390/rs70404026

4. Chong, K. L., Kanniah, K. D., Pohl, C., & Tan, K. P. (2017). A review of remote sensing applications for oil palm studies. *Geo-spatial Information Science, 20*(2), 184-200, doi: 10.1080/10095020.2017.1337317

5. Direktorat Jenderal Perkebunan. (2019). Statistik perkebunan Indonesia 2017-2019. Jakarta, Indonesia: Direktorat Jenderal Perkebunan

6. Euler, M., Hoffmann, M., Fathoni, Z., & Schwarze, S. (2016). Exploring yield gaps in smallholder oil palm production systems in eastern Sumatra, Indonesia. *Agricultural systems, 146*, 111-119. doi: 10.1016/j.agsy.2016.04.007

7. Junges, A. H., Fontana, D. C., Anzanello, R., & Bremm, C. (2017). Normalized difference vegetation index obtained by ground-based remote sensing to characterize vine cycle in Rio Grande do Sul, Brazil. *Ciência e Agrotecnologia, 41*(5), 543-553, doi: http://dx.doi.org/10.1590/1413-70542017415049016

Comparison of tracking properties using multiple GNSS systems

A. Sirotek[1], J. Hart[2]

[1]*Department of Technological Equipment of Buildings, Faculty of Engineering, Czech University of Life Sciences Prague*

[2]*Department of Vehicles and Ground Transport, Faculty of Engineering, Czech University of Life Sciences Prague*

Abstract

This article deals with the use of multiple GNSS (Global Navigation Satellite System) systems in receivers. Using multiple GNSS systems can improve tracking properties. In particular, it will improve reliability, consistency and accuracy. The improvement will be reflected mainly in conditions of poor signal reception. It can be used in agriculture, forestry, logging and guarding of machines. For this reason, Multi GNSS receivers have been tested in well-defined environments. This allows us to judge the benefits of integrating multiple GNSS systems in receivers.

Key words: Multi-GNSS, tracking, low cost receivers

INTRODUCTION

Nowadays, it is possible to determine the position and parameters of movement of people, animals and things using GNSS. American GPS began to be widely used after the year 2000, when the use of Selective Availability was discontinued. In addition to the longest used American GPS, other systems from other countries are now in operation. Using Russian GLONASS, you can determine your location anywhere on Earth. Development began in 1796 and the system has been fully operational since 2011. But fewer devices use GLONASS system. The civilian equivalent of the American GPS is the European system Galileo. The project was launched in 1999. The system has been fully operational since 2019 and the complete system with 24 satellites is expected by the end of 2020. As a result, devices using other systems are appearing on the market. However, many devices still use a single GPS system. The question is whether and what is the benefit of integrating multiple GNSS systems in receivers. The accuracy and availability of satellite information is affected by a number of factors. The availability of information from satellites is primarily affected by the environment in which the

receiver is located. The receivers are not able to pick up the signal in dense vegetation, underground buildings and other places without a direct view of the sky. The integration of multiple GNSS systems can improve the reliability of the receivers. We assume the lowest reliability for a receiver using only GPS, greater reliability for a receiver using GPS and GLONASS at the same time, and the best properties can be expected for a receiver using GPS GLONASS and Galileo at the same time.

MATERIALS AND METHODS

Receivers using GPS, GLONASS and Galileo systems were used. The device used code measurements to determine its location. The code measurement principle use the distance between the receiver and the transmitter to determine the position (Kaplan, 2017). This method is used in most ordinary GPS receivers (Bensky, 2016). The accuracy displayed by the equipment is an estimate of accuracy in meters, called medium position error. The magnitude of the medium positional error is affected by the number of received signals, the location of the transmitters and the strength of the received signal and the constellation of satellites (Bhatta, 2011). This is why the accuracy and reliability of the location depends on the view of the sky (Ge, 2017). Measurements took place in Central Bohemia Region in Czech Republic. Territory with coordinates 50 ° 3′0 ″ N, 14 ° 42′36 ″ E. The measurement took place during the day and on weekdays in 2020.

Navigation equipment model M1805D1SG was used. It is a mobile low-cost receiver with localization via A-GPS, GLONASS and Galileo. It has a CPU 8 × Cortex-A53 Qualcomm Snapdragon 625 2 GHz, chipset Qualcomm Snapdragon 625 MSM8953, a Li-Ion battery with a capacity of 4000 mAh, for long life and works on the Android 10 platform.

The measurement was always performed using three devices simultaneously. At the same time and same location, was determined at the geographical location. The first device determined the position only by GPS, the second one by GPS and GLONASS simultaneously, the third one by GPS GLONASS and Galileo simultaneously. SBAS (Satellite Based Augmentation Systems) and GBAS (Ground Based Augmentation Systems) were not used. The measurement took place in defined environments:

- Forest

It is densely wooded environment in which trees hinder the view of the sky. Conifers and deciduous trees are higher than 5 m. We can assume a weaker GNSS signal.

- Open landscape

This is an environment with an excellent view of the sky. Conditions for receiving GPS signals are ideal.

- City

The city environment consists of dense building clusters where houses are over six meters high and the view of the sky is worsened. It is possible to assume a lower visibility of GPS satellites. The receivers were outside the buildings when measured.

RESULTS AND DISCUSSION

The results of GPS-only tracking are shown in Table 1. It can be seen that the accuracy decreases in the city and in the forest, where there is no good view of the sky.

Tab. 1 GPS-only measurement

Environment	**Average accuracy (m)**	**Number of measurements**
Forest	6.6	500
Open landscape	5.2	500
City	13.4	500

The results of GPS + GLONASS tracking are shown in Table 2. It is obvious that in ideal conditions for signal reception there is no difference, the improvement occurred in an environment of worse signal reception.

Tab. 2 GPS + GLONASS measurement

Environment	**Average accuracy (m)**	**Number of measurements**
Forest	6.2	500
Open landscape	5.2	500
City	10	500

The results of GPS + GLONASS + Galileo tracking are shown in Table 3. Again, in an environment with ideal reception conditions, there is no difference. In the forest and in the city, the accuracy of tracking has again improved, as confirms Cole (2020).

Tab. 3 GPS + GLONASS + Galileo measurement

Environment	**Average accuracy (m)**	**Number of measurements**
Forest	5.4	500
Open landscape	5.2	500
City	6.3	500

Tracking using GPS-only code measurement for the civil sector is a relatively accurate method. However, only in ideal conditions it achieves an accuracy of about 5 m, in an environment with a poor view of the sky, the accuracy and reliability deteriorates significantly. Surprisingly good results were obtained when positioning with two or three GNSS systems together, as confirmed by the author Kiliszek (2020). Compared to GPS-only, the results were always better or the same.

CONCLUSION

GNSS locators operating only in ideal conditions for signal reception with a perfect view of the sky can use only one GNSS system. They will achieve good results assuming that the receiver will not occur in a degraded environment and it is not an emergency system and there is no need for high reliability. When using multiple GNSS systems, the improvement did not show in an ideal environment, the average accuracy was the same. Surprisingly good results were in an environment of poor signal reception. The integration of multiple systems GNSS is ideal for emergency systems, for systems where failure will endanger property or lives, and for autonomous systems without human control, as confirmed by the author Elghamrawy (2020). The integration of multiple systems in receivers appears to be very beneficial, reliable, affordable and does not have to significantly increase the weight and energy consumption of the device. It is therefore desirable that the integration of multiple GNSS systems be used by multiple receivers in future.

REFERENCES

1. KAPLAN, E.D., HEGARTY, C.J. (2017) Understanding GPS/GNSS: Principles and Applications. Artech House: Boston, MA, USA
2. BENSKY, A. 2016. Wireless positioning technologies and applications. London. Artech House, London. 401pp.
3. BHATTA, B. 2011 Global navigation satellite systems: insights into GPS, GLONASS, Galileo, Compass, and others. Hyderabad, India: BS Publications, 438pp.
4. GE, X.; GU R.; LANG Y.; DING Y. 2017. Design of Handheld Positioning Tracker Based on GPS/GSM.3rd IEEE Information Technology and Mechatronics Engineering Conference (ITOEC). IEEE 345 E 47TH ST NEW YORK, Chongqing, pp. 868-871
5. Cole, B., Awange, J., Saleem, A,. Environmental spatial data within dense tree cover: exploiting multi-frequency GNSS signals to improve positional accuracy, International Journal of Environmental Science and Technology, 2020, 17: 2697-2706
6. KILISZEK, D., KROSZCZYŃSKI, K. Performance of the precise point positioning method along with the development of GPS, GLONASS and Galileo systems, Journal of the International Measurement Confederation, 2020, 164: 108009
7. ELGHAMRAWY, H., KARAIM, M., TAMAZIN, M., NOURELDIN, A, Experimental evaluation of the impact of different types of jamming signals on commercial GNSS receivers, Applied Sciences, 2020, 10: 4240

Corresponding author:

Ing. Antonín Sirotek, Department of Technological Equipment of Buildings, Faculty of Engineering, Czech University of Life Sciences Prague, Kamýcká 129, Praha 6, Prague, 16521, Czech Republic, e-mail: siroteka@tf.czu.cz

Influence of change of construction parameters of working tools on quality tillage

J. Šmíd[1], J. Vomáčka[1] J. Mašek[1]
[1]Department of Agricultural machines, Faculty of Engineering, Czech University of Life Sciences Prague, Prague, Czech Republic

Abstract

This article is focused on working tools, which can be used for combinator, not only for preparing soil in small depth after primary soil tillage. Purpose of this work is suggesting a useful machine which will obtain usability in conservation tillage.

Key words: soil, combinator, tools, soil tillage

INTRODUCTION

Soil tillage and especially the choice of technological line for its preparation is a difficult task within the company, especially nowadays. When deciding on the composition of machines, especially in soil preparation, there are a number of issues, whether precipitation fluctuations, legislative restrictions in the field of chemical plant protection, which has a significant decision-making role in the final choice of the chosen technology. *(Hůla, Procházková a kol., 2008).*

This article focuses on the innovation of an agricultural machine for pre-sowing soil preparation, the subsequent innovation of which can be used to process the soil profile, especially by conservation tillage where they are only to reduce the number of crossings, but especially to leave the remains of bioamide and intermediate crop on the surface, or at male depths. The aim of my work is to oversize the combiner, especially the machine frame, including working tools and fuses. In the article we deal with the secondary tillage of a combined machine, which is arranged according to individual working sections. The amount of plant residues by the selected method is evaluated here. Subsequently, the machine will be conceptually designed so that, depending on the working speed and depth of processing, there will be a minimum coverage of plant residues or a set limit value.

MATERIALS AND METHODS

For the measurement itself, basic method were selected to evaluate the condition of the land before and after tillage. For tillage was select a combinator, which is shown: fig. 1. Tillage and plant residues

Fig. 1 Operating mode of the machine

were measurements in locality Stolany altitude of 420 m a.s.l. Combinator contains six working sections with individual working tools. Front section has double rows of plate tools. Support points are front pipe roller and rear crosskill roller. Working speed, which was used was about 8 $km.h^{-1}$. Working depth was approximatelly. The overall weight of machine is 2 800 kg. Setting depth of Duck foot which are connect with tines is mechanically. Used tractor Case IH 285 MX. The main goal was to determine the amount of plant residues by one crossing the machine in the field. The measurement took place in March as a preparation of a field for sowing corn. First, it is necessary to take a photo of the surface of the plot. The important thing is to take a photo outside the direct radiation of the sun, because the shadows distort the results. Creating photos was Canon EOS 77D. Picture is shown (2).

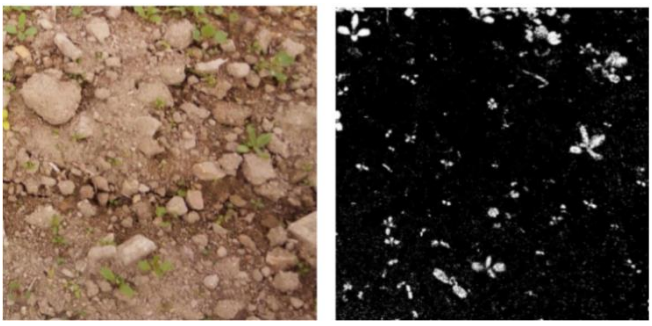

Fig. 2 Soil cover with plant residuas

The photos taken in this way and their evaluation serves the initial data, which are a priority for further research, especially Soil Tillage Minimalization. The photos created in this way were transferred to the computer for further processing after measurement. Here the photos created were edited using color correction tools and color replacement tools edited to photos images consisting only of black and white color, where in the space of the bare surface of the soil is located black and white are marked plant remains. Then, thanks to the histogram function, we found the percentage of black and white color in the image. These black and white representation values correspond to the percentages of land covered with plant residues and the percentage of bare soil. Data were processed by the programmes MS Excel and Statistica.

RESULTS AND DISCUSSION

Tab. 1 Graph of the representation of plant residues

		Coverage by plant residues (%)	
		Before tillage	After tillage
Number of measurements	1	5	0.3
	2	9.6	0.6
	3	7.1	1.7
	4	12	1
	5	6.9	0.5
Average		8.12	0.82

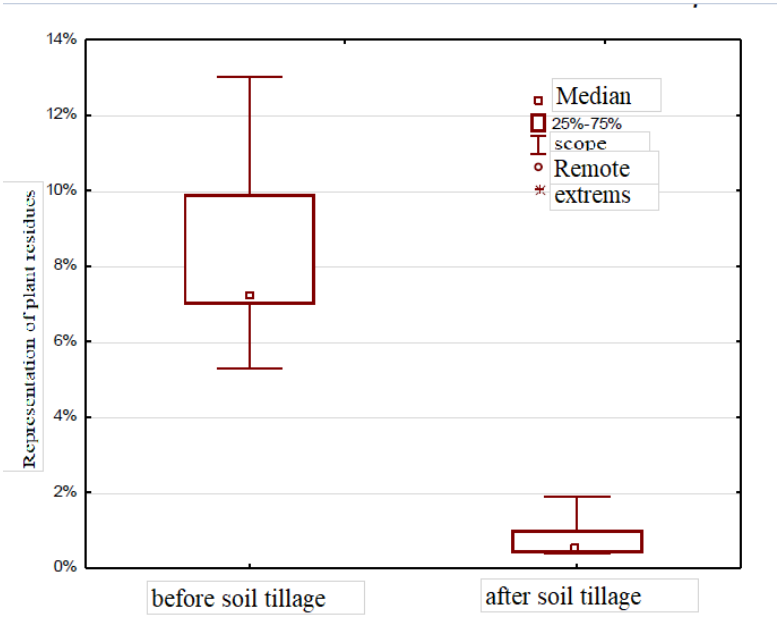

Fig. 3 Default graph

The measurement results recorded in Table 1 clearly indicate that: the vast majority of plant residues on the soil surface were incorporated. Using the analysis, according to Tukey, we see

a clear statistical difference between the incorporation of post-harvest residues before and after crossing.

CONCLUSION

The measurement results recorded in Table 1 clearly indicate that: the vast majority of plant residues on the soil surface were incorporated. Using the analysis, according to Tukey, we see a clear statistical difference between the incorporation of post-harvest residues before and after crossing.

REFERENCES

1. Wei, M., Zhu, L., Luo, F., Zhang, J. W., Dong, X. W., & Jen, T. C. (2019). Share-soil interaction load and wear at various tillage conditions of a horizontally reversible plough. *Computers and Electronics in Agriculture*, *162*, 21-30.
2. Zeng, Z., & Chen, Y. (2018). The performance of a fluted coulter for vertical tillage as affected by working speed. *Soil and Tillage Research*, *175*, 112-118.
3. Hůla, J., & Procházková, B. (2008). *Minimalizace zpracování půdy*. Profi Press, 248p.
4. El Titi, A. (2002). *Soil tillage in agroecosystems*. CRC Press, 367 p.
5. Usaborisut, P., & Prasertkan, K. (2018). Performance of combined tillage tool operating under four different linkage configurations. *Soil and Tillage Research*, *183*, 109-114.
6. Cardei, P., Vladutoiu, L. C., Gheorghe, G., Fechete, T. L. V., & Chisiu, G. (2018, January). Multidisciplinary Investigations Regarding the Wear of Machine Tools Operating Into the Soil. In *IOP Conference Series: Materials Science and Engineering* (Vol. 295, No. 1, p. 012007). IOP Publishing.
7. Askari, M., Shahgholi, G., & Abbaspour-Gilandeh, Y. (2019). New wings on the interaction between conventional subsoiler and paraplow tines with the soil: effects on the draft and the properties of soil. *Archives of Agronomy and Soil Science*, *65*(1), 88-100.
8. Lisowski, A., Klonowski, J., Green, O., Świętochowski, A., Sypuła, M., Strużyk, A., ... & Mieszkalski, L. (2016). Duckfoot tools connected with flexible and stiff tines: Three components of resistances and soil disturbance. *Soil and Tillage Research*, *158*, 76-90.
9. MAŠEK, J.; NOVÁK, P.; CHOLENSKÝ, J. Vliv technologie zpracování půdy na její vlastnosti. *Agrjournal*. 5.4.2015. [cit. 18.11.2017] Dostupné z: https://www.agrojournal.cz/clanky/vliv-technologie-zpracovani-pudy-na-jeji-vlastnosti-43
10. SOMMER, C.; ZACH, M. *Langfristige Sicherung der Bodenfruchtbarkeit durch konservierende/schonende Bodenbearbeitung.* Feldwirtschaft, 1990, 342 s.

Corresponding author:

Ing. Josef Šmíd, Department of Agricultural machines, Faculty of Engineering, Czech University of Life Sciences Prague, Kamýcká 129, Praha 6, Prague, 16521, Czech Republic, tel: +420 775 216 009, email:smidj@tf.czu.cz

Fuzzy control application system of moving object with different dynamic libraries

R. Srnánek[1], D. Horňák[1], V. Cviklovič[1], D. Hrubý[1]
[1]Department of Electrical Engineering, Automation and Informatics, Faculty of Engineering, Slovak University of Agriculture in Nitra, Tr. A. Hlinku 2, 949 76, Nitra, Slovakia

Abstract
In the last time technology was focusing on size and speed of parts. Usually we can talk about size of mechanical parts but also about size of virtual parts like algorithms and programs. When we can simplify program part then we can store more data into memory and use it for other variations of our program or for other purpose. On the other hand, we still need some precision. For better efficiency we can use one of the non-conventional algorithms which are also used more often in normal population and not only in research centers If we want to replace our conventional system with Fuzzy system, we can expect better efficiency and secure the same terms and states of our program. We compared these different algorithms in this work. Because in this time, native support is not for fuzzy system we are using dynamic libraries for testing. The purpose of this work is to find how to make algorithm for path finding to run over most area of the and labyrinth correctly set up fuzzy system for mobile robot. We compared solutions and options that we have with each solution that we suggest.

Key words: C#, artificial intelligence, mobile robots, controlling movement in 2D, .NET, dll

INTRODUCTION
In the last decades started trend to use more often non-conventional algorithms for programing. The reason is we can make better algorithms with more efficiency and they also can use smaller space in storage memory. We chose C# language for testing which is most used in technical sphere. The language was developed in 2000 as part of .NET standard core by Microsoft. It's used wildly in all kinds of technical areas and it can be extended by dynamic libraries (dll) or Application programming interface (api). These methods are giving us a huge potential to use it everywhere in technical area, because there is huge development support. We can also develop in this language database programs, web applications and pages, web services, mobile software and Windows form applications. Syntax of this language is similar to C and it's possible to move it in between C++. The code is divided into classes and there is no need to use

any sort of a translation language. Most types in the language correspond to the valuable types implemented in the Common Language Infrastructure layer.

The fuzzy system was developed by the American mathematician of Russian origin prof. Lotfi A. Zadeh in year 1973 for the need to define mathematical vague and unclear values which are called fuzzy values. He determined theory of fuzzy logic and how could be achieved system limited with non-crispy values but values in range. The typical examples are like tall man, hot water and fast car.

In the last conference ICYS 2019 we presented work where we compared computing time. We compared dll in testing computing fuzzy system which haves two inputs and give us one output. We want to continue in this development and apply it on the moving simulation of object which can be presented as mobile robot. We want to control it by fuzzy system instead of conventional programing methods.

MATERIALS AND METHODS

Mathematic of movement in 2 dimensions can be presented by multiple points on the radius which are relative to middle point. In our case we don´t include dynamics of mobile robots. Usually there is used slow speed robot and we can ignore dynamics. In this article we are working with single point, which represents middle point of moving robot.

To move testing robot, we use easy mathematic equations which are showed like computing coordinates (Eq. 1) and (Eq. 2). There is negative increase because in the Microsoft Visual two-dimension topologies for object elements are negative directions up and left.

$$x_1 = x_0 + (-5 \cdot \cos(\theta)) \quad (1)$$

$$y_1 = y_0 + (-5 \cdot \sin(\theta)) \quad (2)$$

Where: x_0, y_0 old coordinates,

x_1, y_0 new coordinates,

θ angle of rotation.

Angle of absolute coordinates can be computing also like proportion of *y* and *x* coordinates or also sin and cos θ.

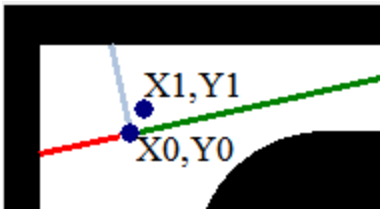

Fig. 1 Old and new position

The easiest way to imagine fuzzy system is by extending logical binary operators with fuzzy sets which are vague. Every set has degree of belonging to this set and it is named as fuzzy membership function. Values are not like in classic binaries 0 or 1, but there is a range between for example 0 and 1. It is not clear sets. These are distinguished by the fact that the characteristic function characterizes the degree to which the element belongs in the set, as opposed to the classical logical approach, which characterizes only the values. It is necessary to use linguistic variables which values will interpret fuzzy sets. A set of such values is referred to as a set of terms, and they are defined as a universal set. Linguistic variables are not expressed quantitatively in units of measurement. Therefore, it is difficult to decide which variable element it belongs to. For every term is characteristic function called the function of belonging $m_S(t)$. *Fuzzyfication* is process of assigning values of the input variables to the sets by using functions. There are multiple affiliation functions, but basic and most used are:

- Λ - function (triangle function),
- L - function,
- Π - function (trapezoidal function)
- Γ - function,
- S – function,
- Z – function (Modrlák, 2004).

Interference rulse are base of determines of rules for fuzzy control inference that describes the behavior of the management system. It is jurisdiction interference system which determines the degree of each rule. Usually there are very often used this type:

- min- at which the resulting degree of jurisdiction is trimmed by the lowest degree of affiliation of inputs (fuzzy set penetration)
- max- at which the resulting function of affiliation is created by adding the maximum values of the function of the conclusions of the points by point (unification of fuzzy sets).

There are a lot of methods of interfering with rules evaluation. The control of logical is most often expressed by like conditionals programing. Expressed by statement IF- THEN how it is showed under in statement (Eq. 3).

$$\text{If STATEMENT1}_{(\text{antecedent})} \text{ then STATEMENT2}_{(\text{consequent})} \quad (3)$$

There are two parts antecedent and consequent. Antecedent has parts which are connected by logical operators. There can by also used negation of these operators. It is called decision rules. Consequent respond to a change in the quantities decaled in antecedent. The affiliation of the input value is determined in a consistent level by which it cuts the output values. Implication of interference rule is performed in the fuzzification process. The most used is Mamdani implementation and Sugeno. But there are many ways how to calculate defuzzification´s system. For better understand there are a few differences. (L.A.Zadeh, 1965).

Tab. 1 Comparing Mamdani and Sugeno output

	Mamdani	**Sugeno**
Output Membership Function	Is intuitive.	It is most linear or constant, like PID control.
Mathematical Rules	Have only classic rules.	Have much more mathematics rules.
Adjustable Parameters	Are well-suited to human input.	There are more adjustable parameters.

As we can see in the table (Tab. 1) the most significant difference is that Sugeno method has linear function output which is constants. And uses weighted average to compute the crisps output. But Mamdani´s implication it has output value with outputs fuzzy sets. There are examples for better understanding. Mamdani is first (Eq. 4) and next statement (Eq. 5) is Sugeno.

$$IF\ A\ is\ X1\ and\ B\ is\ X2\ then\ C\ is\ X3 \quad (4)$$

$$IF\ A\ is\ X1\ and\ B\ is\ X2\ then\ C = AX1 + BX2 + C \quad (5)$$

The assignment of output linguistic variables by the inferior mechanism to the sharp values of the action variable called defuzzification. It is done within the permissible range of affiliation functions. At the end the result of fuzzy control is trimming of the function of jurisdiction by decision rules for individual terms of output variables.

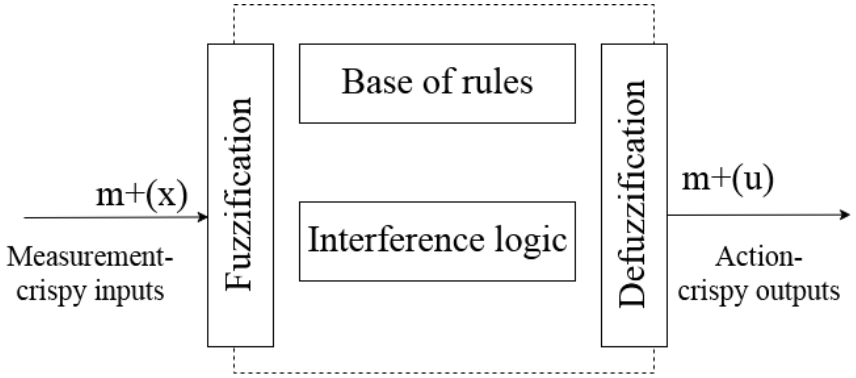

Fig. 2 Diagram of fuzzy System

The most used methods for defuzzification are surface and an acceptable solution. And these methods are modified. Output for each methods are for sure different and for this there is necessary to choose right one for our application (L.A.Zadeh, 1965).

RESULTS AND DISCUSSION

Fuzzy framework FLS is developed on the .NET core platform. It is without description of components but is very simple to use and to understand. It can be used correctly because we also found a lot of libraries which are not specified in description how they are computing fuzzy output and how to correctly make fuzzy system with them. And for this reason, we can´t use them for our experiment. This library is very simple in declaring all fuzzy components. And we can´t change settings. Supports continuous and discrete settings. Any fuzzy sets can be used if they can be described by a polynomial function group. Standard C # operators can be used to create relationships and implications. Defuzzification the relationship to a sharp value is done directly using the C # method. It is supported for graphs, relationships and hierarchy in the tree view. There are Center of Gravity and Middle of Maximum methods for defuzzification. Multiple classes are predefined and can be used to declare membership functions. These are the most used types: trapezoidal, triangular, bell, singleton, Z, Composite, and Gausses. Implications for interference rules are Sugeno and Mamdani.

```
FLS.LinguisticVariable lvright = new FLS.LinguisticVariable("lvright");

var near = lvright.MembershipFunctions.AddTrapezoid("near", -45, 5, 15, 60);
var medium = lvright.MembershipFunctions.AddTrapezoid("medium", 15, 30, 60, 80);
var far = lvright.MembershipFunctions.AddTrapezoid("far", 60, 80, 120, 120);
```

Fig. 3 Example of declaring linguistic variables of membership functions

Very easy with declaring linguistic variables, how we can see on the figure (Fig. 3), *lvright* with linguistic name. Subsequently there are assigned a membership functions where they will set what type of its values have. With using *IFuzzyEngine* class we can set a fuzzy set and processing system is created on a sharp fuzzy output. The interference rules are assigned to system. They are using by declared names in parentheses. For making rules, there are typical connectors: and, not. Variables values must be written in parentheses and joined together to form rules by using a dot and interference tag. On the end, all the rules are assigned to a fuzzy system called *fuzzyEngine*. Result is invoked after writing to the output variable and calling the defuzzification function.

AForge.NET is library for artificial intelligence and image processing. It is open source library. The part for Fuzzy system consists of classes to perform fuzzy sets and linguistic variables using interference rules. Type for defuzzification is Center of Gravity. But you can create new class for other new method. The result of defuzzification system is determined as the coordinate of the center of gravity of the area formed after the unification of the areas that arise by limiting the functions of the output terms with non- zero values. Membership function which are available are trapezoid, singleton and piecewise. Piecewise linear function is a function in which a set or array of points is specified on the x-axis that creates a bounded area. Singleton function is single point. Implication of interference rule is implied by Mamdani´s implication for this library.

```
IS.NewRule( "Rule 7", "IF RightDistance IS Far AND LeftDistance IS Far AND FrontalDistance IS Near THEN Angle IS Positive" );
```

Fig. 4 Example declaring new rule in AForge

For someone can by advantage function for evaluating of rules. Every rule can be evaluated for verifying fuzzy rule. It means that if these rules are used to calculate the result. There are serves

the rule class. Each new rule must be assigned to the rule database or to the interference system. It is declared by name and word in string format. *FuzzySet* class declares the linguistic name and the corresponding function with values. Each function is then added to the linguistic variable. When we create linguistic variable, we must also create a database of interference system. Consequently, you only need to set a linguistic variable that serves as an input and enter a value into it.

At last conference we used MATLAB COMPILER which is extension of MATLAB. This extension can transform MATLAB projects into .dll, but after several tests and many trials we decided not use it, because our program was busy, and it can´t worked correctly.

Programing for simulation which we used was inspired by one of testing program for fuzzy library. We made similar program for testing and comparing dynamic libraries and algorithms. The point on the figure (Fig. 5) represents mobile robots' middle point which is moving in two-dimension labyrinth. The light blue line is measuring distance from obstacle in front of him and red represent left side and green right side. The dashed line is traveled track path.

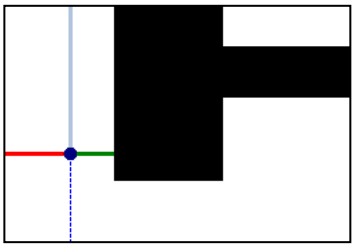

Fig. 5 Preview of simulation of mobile robot in program

We drew map with curved and sharp edges. There are wider and thinner corridors along the path and we also tried to make some local minimums where the robot could be trapped. This planned map we can see on figure 6.

We used simple fuzzy system to compare libraries, for testing and for better understanding on how to build fuzzy system to control a mobile robot in future works and in real condition. The fuzzy system consists of three inputs and one output. The inputs are distances from the obstacle in front, right and left side of mobile robot. The code was launched for 30 *s.* After this time, we analyzed traveled path of the vehicle.

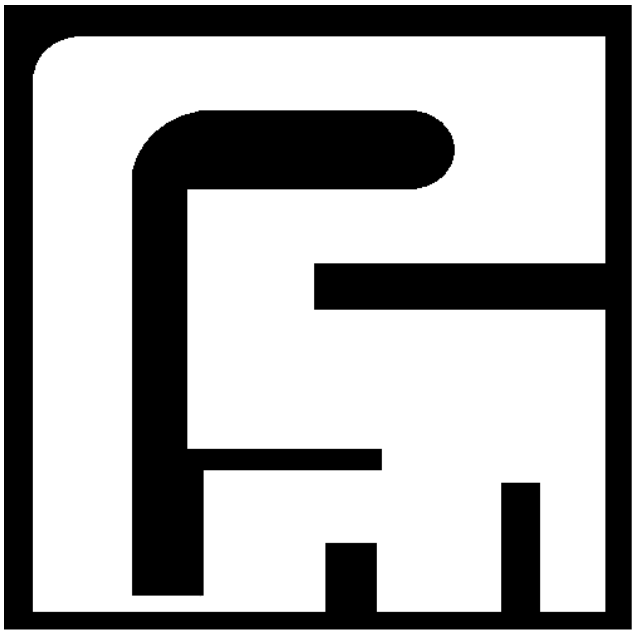

Fig. 6 Map of labyrinth

Rule 1: IF Frontal Distance IS Far THEN Angle IS Zero
Rule 2: IF Frontal Distance IS Far AND Right Distance IS Far AND Left Distance IS Far THEN Angle IS Zero.
Rule 3: IF Right Distance IS Near AND Left Distance IS Not Near THEN Angle IS Little Negative.
Rule 4: IF Right Distance IS Not Near AND Left Distance IS Near THEN Angle IS Little Positive").
Rule 5: IF Right Distance IS Far AND Frontal Distance IS Near THEN Angle IS Positive.
Rule 6: IF Left Distance IS Far AND Frontal Distance IS Near THEN Angle IS Negative.
Rule 7: IF Right Distance IS Far AND Left Distance IS Far AND Frontal Distance IS Near THEN Angle IS Positive

Fig. 7 Fuzzy rules

The fuzzy system has 3 fuzzy sets, each of them was trapezoidal function. They are:

- near {0, 5, 15, 20},
- medium {15, 30, 60, 80},
- far {60, 80, 120,120}.

For output was angle fuzzy set and has 5 fuzzy sets:

- negative { -40, -35, -25, -20},

- little negative {-25, -20, -10, -5},
- zero {-10, 5, 5, 10},
- little positive {5, 10, 20, 25},
- positive {20, 25, 35, 40}.

For getting output we have 5 interference rules which used centroid defuzzification and Mamdani ´s implication. We wanted to set up this setting for both algorithms, but it is hard to tell if they are 100% alike.

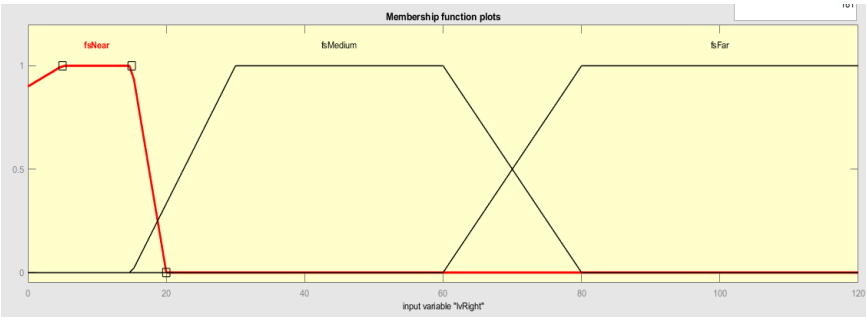

Fig. 8 Membership input function in plot

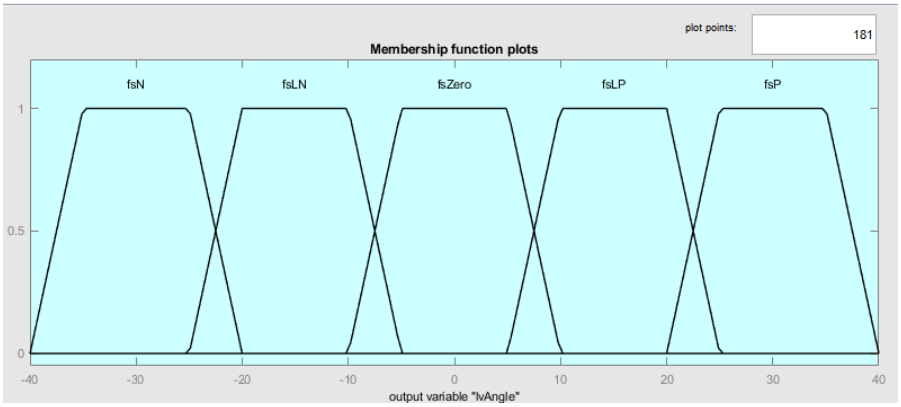

Fig. 9 Membership function for output

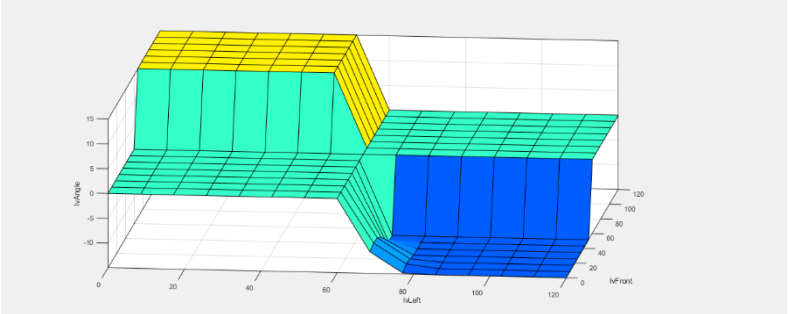

Fig. 10 Output surface for the fuzzy inference system

For comparing fuzzy system with conventional solution, we have made decision algorithms with conditional formatting IF- THEN. There are 8 states like 7 rules in fuzzy system, and one state is for option when it does not match any state. We can see on this solution is path very

straight and it is very similar to BUG algorithms. It looks like typical path for robot which use three sensors and follow the obstacle like we know from our previous experiences.

```
void iffuzzy(double distanceF, double distanceR, double distanceL)
{
    if (distanceF >= 60) { ans = 0; }//R1
    else if ((distanceF >= 60) && (distanceR >= 60) && (distanceL >= 60)) { ans = 0; }//R2
    else if (distanceR <= 60 && distanceR >= 0 && distanceL <= 80 && distanceL >= 15) { ans = -12.5; }//R3
    else if (distanceR <= 80 && distanceR >= 15 && distanceL <= 60 && distanceL >= 0) { ans = 12.5; }//R4
    else if (distanceL >= 60 && distanceF <= 15 && distanceF >= 0) { ans = -30; }//R6
    else if (distanceR >= 60 && distanceF <= 15 && distanceF >= 0) { ans = 30; }//R5
    else if ( distanceR >= 60 && distanceL >= 60 && distanceF <= 0 && distanceF >= 15) { ans = 30;  }//R7
    else { ans = 0; }
```

Fig. 11 Declaring conventional system for controlling

Fuzzy system which was performed may be for first look like chaotic path. But how we know there is controlled driving, which was made correctly, and it reach most places of all labyrinth. There are some places where mobile robot was a little bit too close to the wall. We are sure there should be more testing and there can be modification in fuzzy sets or maybe adding fuzzy sets.

How we can see at the comparison, the path for mobile robot is smoother and we also tracked the length of traveled path which is in pixel points. It is almost same but in the real-world fuzzy system would be more efficient and can avoid more intricate obstacles. Also, we can see the fuzzy algorithm was faster because it made longer path. We can see the convictional system was stuck in the loop.

How we can see on the bottom figure (Fig.12), we also tried more starting positions for robot path. First row is from left bottom start position. The second is right bottom side and last two are from right upside and left upside.

Our map has little corridors and didn´t reach most of all labyrinth. We should set new labyrinth, or we can change fuzzy membership functions limits for better ones. From path distance we cannot say which algorithm is more efficient. All of the algorithms reached almost every area of the labyrinth.

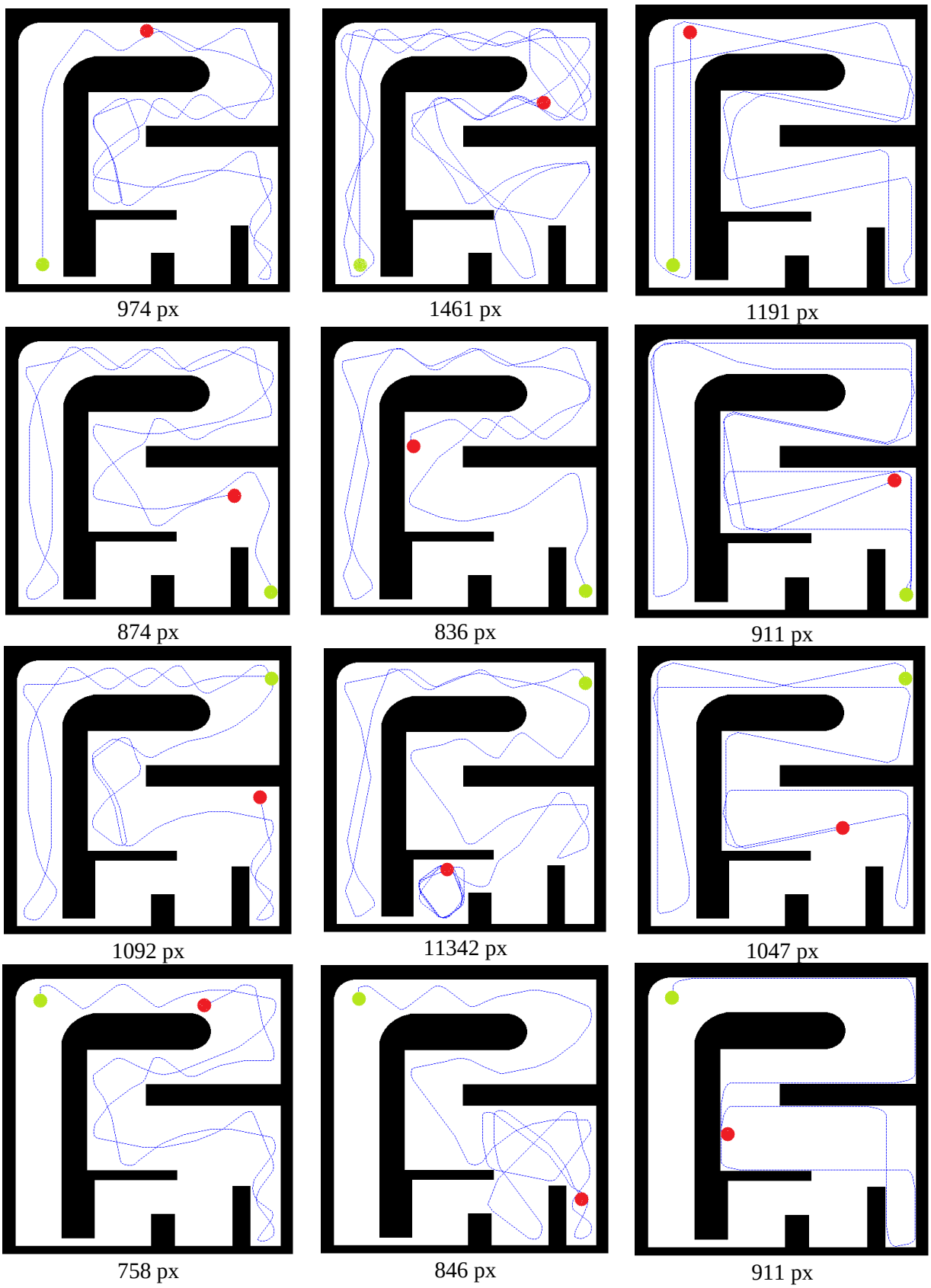

Fig. 12 Comparing solution for AForge (left column), FLS library (middle column) and conventional system (right column). Number below screenshot is distance of path. For each row is different starting position.

When we look at the outputs from our libraries and if we compare them, we can see the difference from each library and we also can´t tell if the fuzzy control is more effective than conventional If-Then. There are results which show us the solution was not a shortened path. When we made some earliest attempts, we can´t see this system is not bad for this solution. After then we can tell for each dynamic library there are different solutions under the same conditions.

CONCLUSION

We made many tests with many variations of fuzzy settings. The setting depends on a specific application like anywhere else. But we can see the fuzzy control system reacts dynamically to obstacles and crispy step changes like conventional conditional statement IF-Then. As find Patrik Kósa and collective (2019) in article, *"The continuous increase in the number of inference rules increases the quality of control and also the complexity of the system and, it is, therefore, important to determine an optimal number of inference rules in order to ensure an optimal control quality together with the smallest possible complexity of the fuzzy controller."*
We must find suitable number of rules for our mobile robot control and set right membership functions. Because Razif Rashid (2010) with collective presented the results there is no benefit with more membership functions. The times to reach the target points were longer than with more membership function. "*It is shown that fuzzy logic controller with input membership of three provides better performance compared with five and seven membership functions."*
We achieved that fuzzy dynamic libraries can control mobile robots in simulation, and we want to continue with testing in real application. Libraries have enough potential to build fuzzy system and use it for almost all main elements for building this system. For MATLAB compiler there must be done thorough research and some testing on how to effectively implement it into the code.
Conventional IF-THEN system can be used for some exact state system. It means for some setting system or like adjustment states in exact conditions. Or maybe in positioning or ride backwards, positioning from one state to other, etc. If we have not exactly sharp corner area can used fuzzy system for better controlling also can be better to react in dynamic environment. In our future work we want aim for targeting this aspect of fuzzy rules and membership functions for good driving and achieve good controlling with minimum senseless fuzzy membership function. The aim for building good fuzzy system is targeting the good value of membership function and not giving more membership or fuzzy rules.

ACKNOWLEDGMENTS

This paper was created within the project VEGA no. 1/0720/18 Research of Alternative Navigation Algorithms for the Control of Autonomous Robots in Plant Production.

REFERENCES

1. AMRICH, M. – HRUBÝ, D. 2006. Simulation and design of fuzzy control algorithms. In International Professional Seminar Topical Questions of Instruction of Electrical Engineering Subjects at Faculties with Non-electrical Orientation“ SEKEL ´06. September 12 – 14, 2006, Vrátna, Slovakia. s. 29-33. ISBN 80-8070-584-4.(In Slovakia: Možnosti simulácie a návrhu fuzzy riadiacich algoritmov)
2. CVIKLOVIČ, V. – OLEJÁR, M. – HRUBÝ, D. – LUKÁČ, O.: 2013. Odometry in navigation of autonomous mobile robots. (Monograph). Nitra: SPU, 2013, 94s. (In Slovakia: Odometria v navigácií autonómnych mobilných robotov.)
3. CVIKLOVIČ, V. - OLEJÁR, M. - HRUBÝ, D. - PALKOVÁ, Z. - LUKÁČ, O. - HLAVÁČ, P. 2016. Navigation algorithm using fuzzy control method in mobile robotics. In Acta technologica agriculturae. ISSN 1335-2555, 2016, vol. 19, no. 1, s. 19-23. Available on:<http://www.degruyter.com/dg/viewjournalissue.articlelist.resultlinks.fullcontentlink:pdfeventlink/$002fj$002fata.2016.19.issue-1$002fata-2016-0004$002fata-2016-0004.pdf?t:ac=j$002fata.2016.19.issue-1$002fissue-files$002fata.2016.19.issue-1.xml>.
4. Kósa, P. Olejár, M. Palková, Z. Hrubý, D. Cviklovič, V. Harničárová, M. Valíček, J. (2019). The effect of the number of inference rules of a fuzzy controller on the quality of control of a mobile robot. MATEC Web of Conferences. 299. 05002.
5. L.A. Zadeh. Fuzzy sets, Information and Control, Volume 8, Issue 3,1965, Pages 338-353, ISSN 0019-9958, https://doi.org/10.1016/S0019-9958(65)90241-X. (http://www.sciencedirect.com/science/article/pii/S001999586590241X)
6. LUKÁČ, O. – BRACHTÝR, B. – HRUBÝ, D. 2001. Utilization of Matlab for modeling of dynamic systems. In: SEKEL 2001, medzinárodný odborný seminár. Zvolen: Technická univerzita, 12. - 14. 9. 2001, s. 80-83. ISBN80-228-1001-0. (In Slovakia: Využitie programu Matlab na modelovanie dynamických systémov.)

7. MODRLÁK, O. 2004. Fuzzy control and regulation, Technická univerzita v Liberci, 2004, Available on: https://www.kirp.chtf.stuba.sk/~bakosova/wwwRTP/tar2fuz.pdf (In Czech: Fuzzy řízení a regulace)
8. OLEJÁR, M. Implementation Possibilities of Control Surfaces of Fuzzy Controller to Central Control System of the Mobile. 2017. Habilitation thesis. Slovak university of agriculture (Nitra, Slovakia), Faculty of engineering, Department of Electrical Engineering, Automation and Informatics. Robot (Možnosti implementácie riadiacich plôch fuzzy regulátora do centrálneho riadiaceho systému mobilného robota).
9. Rashid, R. Elamvazuthi, I. Mumtaj, B. Arrofiq, M. (2010) Fuzzy-based Navigation and Control of a Non-Holonomic Mobile Robot In JOURNAL OF COMPUTING. ISSN 2151-9617. vol 2 Available on:< https://arxiv.org/ftp/arxiv/papers/1003/1003.4081.pdf>
10. TÓTH, L. - HRUBÝ, D. - OLEJÁR, M. - CVIKLOVIČ, V. 2013. Key point following control algorithm design for the mobile robot. In Trends in agricultural engineering 2013. 1st ed. 725

Corresponding author:

Ing. Rastislav Srnánek, Department of Electrical Engineering, Automation and Informatics, Faculty of Engineering, Slovak University of Agriculture in Nitra, Tr. A. Hlinku 2, 949 76, Nitra, Slovakia, mob: +421908448897, email: xsrnanek@uniag.sk

Modelling of soil organic carbon in a long-term experiment Trutnov: climate scenarios with shifted precipitation, temperature and CO_2 concentration

M. Stehlík[1,2], M. Madaras[2] , M. Kroulík[1]

[1)]Department of Agricultural Machines, Czech University of Life Sciences, Prague, Czech Republic

[2)] Division of Crop Management Systems, Crop Research Institute, Prague, Czech Republic

Abstract

Different climate scenarios can cause a change in soil conditions. For the simulation of this change, the process-based cropping systems EPIC model was used. The model outputs were compared with fertilization treatments in a long–term field trial. The results show that the model responds well to the changing climate conditions. Organic fertilization was found as an important factor stabilizing the level of soil organic carbon in tested scenarios.

Key words: SOC, fertilization, soil quality, simulation, sustainable agriculture, retention

INTRODUCTION

The soil quality is mostly indicated by soil organic carbon (SOC) content. Higher content of SOC is connected with organic fertilization and has positive influence on yield and soil properties (LIPAVSKÝ et al., 2008; STEHLÍKOVÁ et al., 2016; STEHLÍK et al., 2019). Various models such as CENTURY and ROTHC, are used to predict SOC content. Complex process-based cropping systems models can be used as a tool to search for and valuate possible strategies in order to model the reality and future scenarios in agriculture (BALKOVIČ and SOBOCKÁ, 2006; BARANČÍKOVÁ, 2007; BALKOVIČ et al., 2013). The EPIC model (GERIK, et. al, 2015) includes the CENTURY model and it was also used to predict the dynamics of SOC (CAUSARANO et al., 2007). Simulation models are a good tool to predict the consequences of climate change in agriculture. Climate change, which manifests itself in changing temperatures and precipitation, is being predicted in various scenarios of CO_2 concentrations (IPCC, 2014). These scenarios and their possible impacts in the Czech Republic are simulated and visualized in detail on the www.klimatickazmena.cz (CZECH GLOBE) webpage. The aim of our study was to show how the validated EPIC model responds to changed climate parameters and various scenarios.

MATERIALS AND METHODS

Long-term experiment

The research has been based on the data gathered through a long-term field experiment, that was carried out near the town of Trutnov (430 m a.s.l., annual mean temperature 7.5 °C, annual mean precipitation 750 mm, 50°33'44"N, 15°53'25"E). This field experiment was carried out in the years 1965-2009. Its aim was to compare the effect of organic fertilization with treatments on crop yields and soil fertility: farmyard manure (FYM); cereal straw supplemented with mineral N; no fertilization. FYM was applied before potato season in every 4^{th} year starting from 1965, at the rate of 30 t/ha. Straw was applied in the same years, after the harvest of cereals (rate of straw 6 t/ha after wheat, rate of straw 4.5 t/ha after barley). Mineral N fertilizer was added at the rate of 1 kg N per 100 kg straw. The straw was harvested in all treatments and taken away and in the treatment based on straw, straw was re-implement in rate 4.5 or 6 t/ha.

The eight-year crop rotation consisted of cereals (50%), potato (25%), and a fodder crop (clover; 25%). Conventional soil cultivation was maintained, including ploughing to the depth of 25–30 cm. SOC content was about 1.15% by weight at the beginning of the experiment.

The soil was a silty loam Cambisol (29% of sand, 62% of silt), with the initial SOC of 1.15% by weight in the layer 0-30cm and 0.2% by weight in the layer under 30cm in 1965. Mean C inputs at the FYM and Straw plots were similar.

In this study, data from non-fertilized treatment (Cont), only mineral fertilization (NPK), straw with mineral fertilization (Straw+N+NPK) and manure with mineral fertilization (FYM+NPK) were used. Soil organic carbon (SOC) content was sampled in the plow layer of 15cm depth during this experiment (1965-2009).

Scenarios

The EPIC model was used for local implementation, which was pre-set, calibrated and validated for the conditions of the Trutnov experiment (MADARAS et al., 2017). The model operated with the daily climate data (1965-2009) consisted of the daily precipitation, maximal and minimal daily temperatures and solar radiation.

Thirty scenarios were created, which transformed original data towards lower/higher precipitation, higher temperature and higher atmospheric CO_2 concentration. Daily air temperature was increased by +1°C and +2°C, precipitation was also modified at a daily basis in order to reach an increase of +10% / +30% and decrease -10% / -30% (Tab. 1).

Soil organic carbon (SOC), in this long-term experiment, was simulated at 350 ppm CO_2, corresponding to the simulated period 1965-2009. The rise of CO_2 concentration is expected and it can reach the climate scenarios from 420 ppm to 540 ppm in 40 years (STEIN, 2020). Actually, the value of CO_2 concentration is 417 ppm for May 2020. (STEIN, 2020). Therefore, CO_2 concentration was set to 420 ppm (RCP 2.6), 540 ppm (RCP 4.5) and 670 ppm (RCP 6.0) in our model runs (IPCC, 2014).

The simulated SOC was represented by the EPIC output variable OCPD (organic carbon in a plow depth of 15 cm).

Scenarios were simulated with and without water erosion (EROSION, NO EROSION) as an important factor of soil conservation. The period of simulation was 45 years, matching the duration of the long-term experiment.

Tab.1: Precipitation in the used climate scenarios

PREC	**mm/year**	**Count of years**	**Annual PREC**	**Min PREC mm**	**Max_PREC mm**
OBSERVED (1965-2009)	> 830mm	12	755	574	976
OBSERVED (1965-2009)	< 680mm	13	755	574	976
OBSERVED (1965-2009)	In 680-830mm	20	755	574	976
SCENARIOS_-30%	< 680mm	44	530	402	683
SCENARIOS_-10%	< 680mm	22	680	516	878
SCENARIOS_+10%	> 830mm	24	830	631	1073
SCENARIOS_+30%	> 830mm	36	980	746	1268

RESULTS AND DISCUSSION

The simulated SOC content with the CO_2 concentration of 350 ppm corresponded well to the observed values from the data set gained through the experimental period (Tab. 2). The increase in SOC at the non-fertilized treatment (Cont) was negligible compared to the fertilized treatments. The system was saturated in SOC at Cont at 540 ppm already, while at fertilized treatments the saturation occurred in higher concentration (Fig. 1). The simulation of higher CO_2 concentration led to an increase in SOC also in the study of CHENG and JOHNSON (1998). The growth stimulus due to the elevated CO_2 may offset potentially negative yield impacts of temperature increase by +2°C and soil degradation in most of Europe (BALKOVIČ et al., 2018).

Tab. 2 Comparison of SOC in simulated (CO_2 concentration in 350 ppm used in the EPIC model) and observed values in the data set 1965-2009

	Year	**1972**		**1998**		**2004**	
	Variant	**Simul**	**Observ**	**Simul**	**Observ**	**Simul**	**Observ**
SOC (%)	Cont	1.19	1.23	1.1	1.07	1.13	1.085
	NPK	1.23	1.17	1.17	1.305	1.205	1.215
	Straw+N+NPK	1.28	1.32	1.33	1.37	1.346	1.36
	FYM+NPK	1.28	1.27	1.34	1.405	1.368	1.29

	Year	**1972**		**1998**		**2004**	
	Variant	**Simul**	**Observ**	**Simul**	**Observ**	**Simul**	**Observ**
SOC (t/ha)	Cont	26.78	27.68	24.75	24.08	25.43	24.41
	NPK	27.68	26.33	26.33	29.36	27.11	27.34
	Straw+N+NPK	28.80	29.70	29.93	30.83	30.29	30.60
	FYM+NPK	28.80	28.58	30.15	31.61	30.78	29.03

* Initial SOC content for all treatments at the beginning of the trial (1965)- 26.5 t/ha (1.15 %)

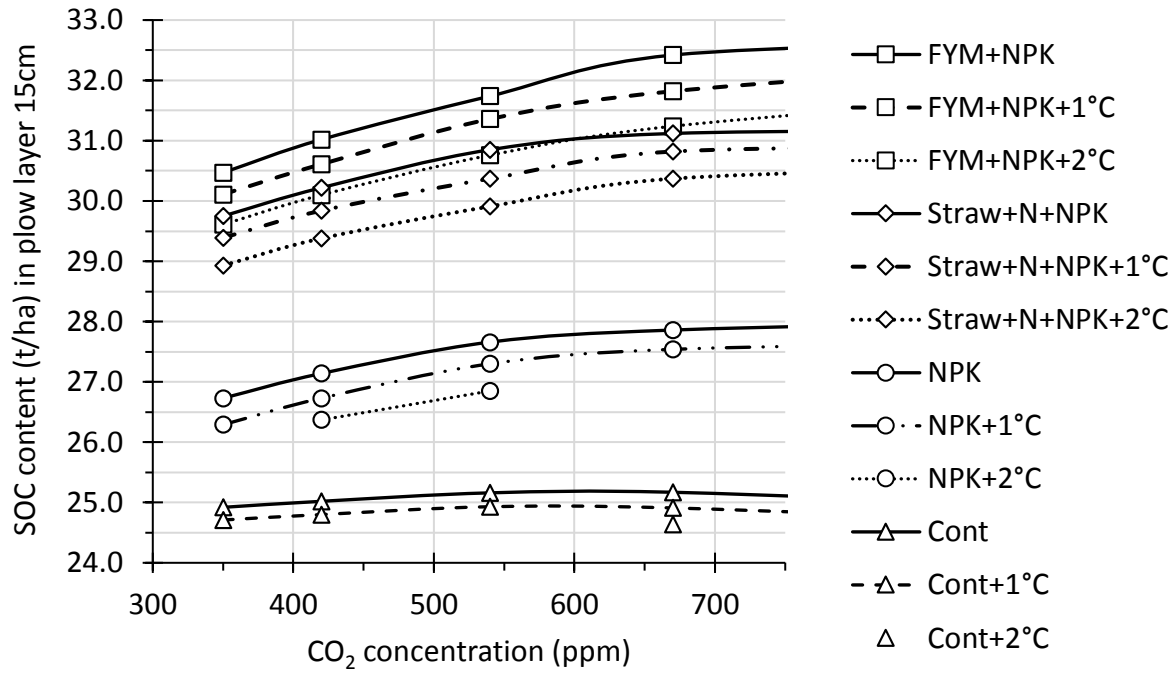

Fig. 1 The progress of simulated SOC content in different CO_2 concentrations and treatments of the field trial after 45 years of simulation (initial SOC content 26.5 t/ha)

Tab. 3 Influence of water erosion elimination and difference in precipitation on the SOC content after 45 years of simulation

	CO_2 Concentration/variant	**+/- Difference in sum of precipitation**				
EROSION	**350 ppm**	**-30%**	**-10%**	**0**	**+10%**	**+30%**
	Cont	25.3	25.0	24.9	24.8	24.8
	NPK	27.4	26.9	26.7	26.6	26.4
	Straw+N+NPK	30.8	30.1	29.8	29.5	29.0
	FYM+NPK	31.7	30.9	30.5	30.2	29.6
NO EROSION	Cont	26.7	26.6	26.5	26.4	26.2
	NPK	29.4	29.1	29.0	28.8	28.5
	Straw+N+NPK	34.0	33.5	33.1	32.9	32.4
	FYM+NPK	34.8	34.2	33.9	33.6	33.1
EROSION	**420 ppm**					
	Cont	25.3	25.0	25.0	24.8	24.8
	NPK	27.8	26.9	27.1	26.6	26.4
	Straw+N+NPK	31.3	30.1	30.2	29.5	29.0
	FYM+NPK	32.2	30.9	31.0	30.2	29.6
NO EROSION	Cont	26.9	26.7	26.6	26.5	26.3
	NPK	30.0	29.6	29.6	29.4	29.1
	Straw+N+NPK	34.6	34.0	33.7	33.4	32.9
	FYM+NPK	35.5	35.0	34.6	34.4	33.8
EROSION	**420 ppm +1°C**					
	Cont	25.3	24.9	24.8	24.7	24.7
	NPK	27.4	26.9	26.7	26.6	26.4
	Straw+N+NPK	30.8	30.2	29.8	29.6	29.0
	FYM+NPK	31.7	30.9	30.6	30.3	29.7
NO EROSION	Cont	26.9	26.5	26.4	26.3	26.1
	NPK	29.5	29.2	29.0	28.9	28.6
	Straw+N+NPK	34.0	33.5	33.2	33.0	32.5
	FYM+NPK	34.8	34.3	34.0	33.7	33.3

*Initial SOC content for all treatments at the beginning of the trial (1965)- 26.5 t/ha (1.15%)

The SOC content decreased with rising temperature, resulting in higher mineralization of organic matter confirmed in EPIC simulations (Fig. 1). This corresponds with the results of KIRSCHBAUM (1995).

Simulations in the EPIC model showed a slight change in the SOC content influenced by change in precipitation (Tab. 3). Precipitation had obviously an impact on the microbial activity and the intensity of decomposition (EVANS and WALLENSTEIN, 2012; MARTINY et al., 2017).

Elimination of water erosion affected the SOC content more, as the erosion factor had three times higher significance than the precipitation factor (Tab. 3). Elimination of erosion led to the compensation of decline in the SOC content at Cont. The SOC content was at the same rate as in the starting year of simulation in the treatment without fertilization and without elimination of erosion. Fertilization is usually used to achieve higher yield and better soil quality; however, erosion can contribute to stopping the SOC growth in NPK treatment (Fig. 2, Fig. 3). Erosion factor had the potential to reduce the SOC content up to 10-12% in all treatments. Water erosion inhibited the SOC increase to such a degree that the SOC content in NPK treatment was similar to the treatment without fertilization and without water erosion (Tab. 2). Study of ONTL and SCHULTE (2012) remarks erosion as an important factor influencing SOC.

The SOC content in NPK treatment was about 11-15% lower than at the treatments with organic fertilization apart from erosion. The total SOC was about 1.5 t/ha higher in the treatments with organic fertilization after 10 years simulation; about 2 t/ha higher after 20 years simulation, and 3-3.5 t/ha higher after 45 years of simulation (Fig. 2). This growth raised up to 4 t/ha with higher CO_2 concentration after 45 years at FYM variant (Fig. 3). Elimination of water erosion in simulations can cause the increase in the SOC content up to 6-7 t/ha, i.e. 25% of the initial SOC. Positive effects of organic fertilization on the climate adaption had impact on improving the better soil properties (STEHLÍK et al., 2019), lower surface runoff (KOVAŘÍČEK et al., 2019) and higher water retention (STEHLÍK et al., 2016). Preservation of soil organic carbon seems to become a problem in future, because of the lack of livestock. Straw application and implementation of the intercrops in the crop rotation could contribute to the SOC conservation.

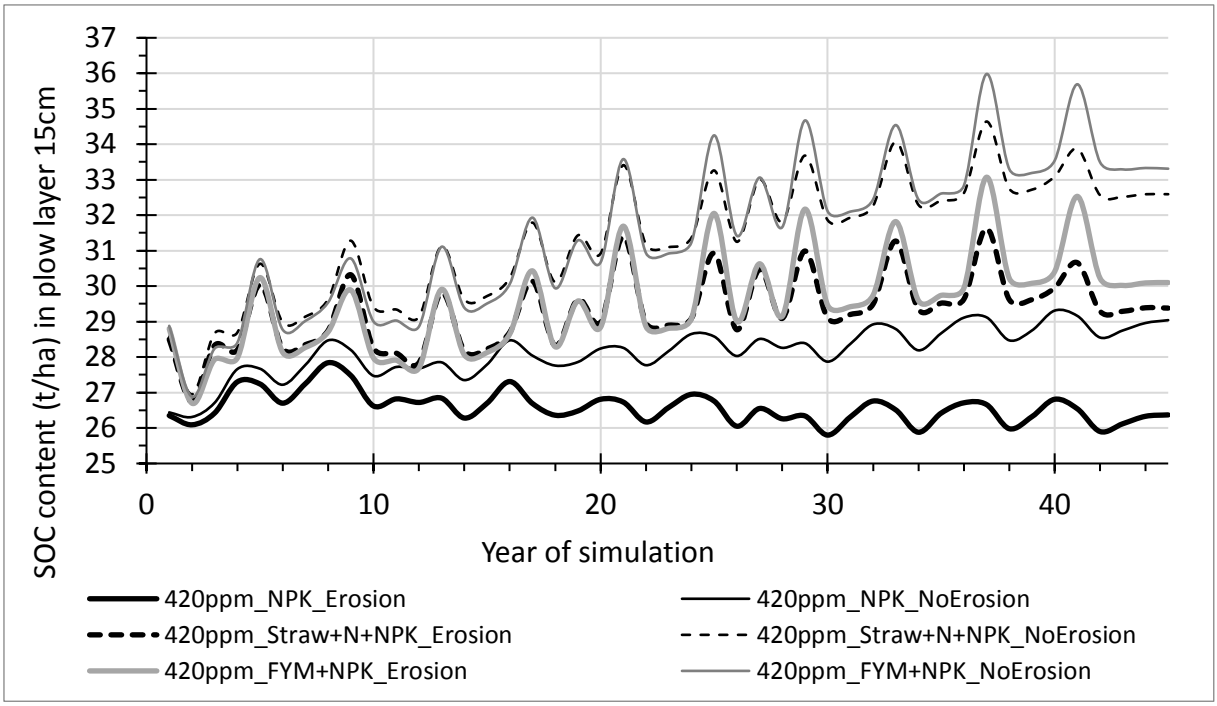

Fig. 2: The SOC content in the completed simulation (45 years) of the field variants in the CO_2 concentration 420ppm +2°C

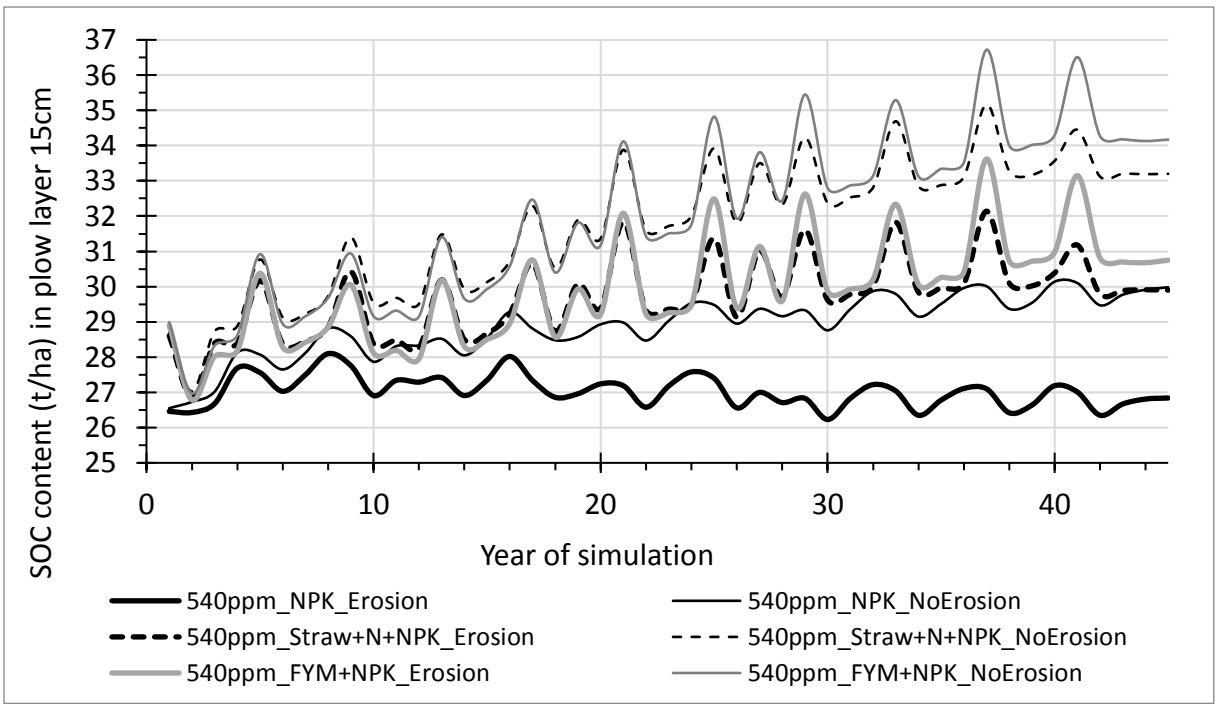

Fig. 3: The SOC content in the completed simulation (45 years) of the field variants in the CO_2 concentration 540ppm +2°C

CONCLUSION

Climate change with raising temperature and precipitation oscillations represents a significant threat for agriculture. It will become more difficult to maintain the crop production and soil quality in such a changing climate. Soil organic carbon is one of important factors in order to secure the soil quality. The EPIC model enables to simulate the soil organic carbon levels under various climate scenarios and types of fertilization. Simulations under various scenarios confirmed the rise of SOC with elevated CO_2 concentration, but also the drop of SOC with higher temperature. Change in precipitations had no significant impact on the SOC content. On the contrary, the elimination of erosion and long-term organic fertilization combined with mineral fertilization raised the SOC substantially. Sufficiency of the soil organic carbon provides higher water retention and it is one of methods which might help to ensure sustainable agriculture in the time of climate change. The EPIC model proved to be a useful tool to forecast SOC and other factors.

ACKNOWLEDGEMENTS

This study was supported by the Ministry of Agriculture of the Czech Republic, projects Nos. MZE-RO0418 and QK1810186.

REFERENCES

1. BALKOVIČ, J., SKALSKÝ, R., FOLBERTH, C., KHABAROV, N., SCHMID, E., MADARAS, M., OBERSTEINER, M. and VELDE, M. VAN DER: Impacts and Uncertainties of +2°C of Climate Change and Soil Degradation on European Crop Calorie Supply. Earth's Future, 2018, 6: 373–395
2. BALKOVIČ, J. and SOBOCKÁ, J.: Soil carbon storage modeling in chernozem at predicted climate change. Bioclimatilogy and water in the land, 2006, 11–14
3. BALKOVIČ, J., VELDE, M. VAN DER, SCHMID, E., SKALSKÝ, R., KHABAROV, N., OBERSTEINER, M., STÜRMER, B. and XIONG, W.: Pan-European crop modelling with EPIC: Implementation, up-scaling and regional crop yield validation. Agricultural Systems, 2013, 120: 61–75
4. BARANČÍKOVÁ, G.: Influence of climate parameters on modelling of the soil organic carbon stock by ROTHC model. STŘELCOVÁ, K., ŠKVARENINA, J., BLAŽENEC, M. (eds.): Bioclimatilogy and natural hazards, 2007, 6 pp

5. CAUSARANO, H.J., SHAW, J.N., FRANZLUEBBERS, A.J., REEVES, D.W., RAPER, R.L., BALKCOM, K.S., NORFLEET, M.L. and IZAURRALDE, R.C.: Simulating Field-Scale Soil Organic Carbon Dynamics Using EPIC. Soil Sci Soc Am J, 2007, 71: 1174–1185
6. GERIK, T., WILLIAMS, J., DAGITZ, S., MAGRE, M., MEINARDUS, A., STEGLICH, E. and TAYLOR, R.: Environmental policy integrated climate model, Temple, 2015, 102 pp
7. CHENG, W. and JOHNSON, D.W.: Elevated CO 2 , rhizosphere processes, and soil organic matter decomposition. Plant Soil, 1998, 202: 167–174
8. CZECH GLOBE. Klimatická změna. https://www.klimatickazmena.cz/en/.
9. EVANS, S.E. and WALLENSTEIN, M.D.: Soil microbial community response to drying and rewetting stress: Does historical precipitation regime matter? Biogeochemistry, 2012, 109: 101–116
10. IPCC.: Climate Change 2014: Synthesis Report. doi:10.1016/S0022-0248(00)00575-3, 2014
11. KIRSCHBAUM, M.U.F.: The temperature dependence of soil organic matter decomposition, and the effect of global warming on soil organic c storage. Soil Biol Biochem, 1995, 27: 753–760
12. KOVAŘÍČEK, P., HŮLA, J., HÁJEK, D. and VLÁŠKOVÁ, M.: Surface water runoff during rainfall after compost incorporation into soil. HERÁK, D. (ed.): Trends in Agricultural Engineering 2019, 2019, 287–292
13. LIPAVSKÝ, J., KUBÁT, J. and ZOBAČ, J.: Long-term effects of straw and farmyard manure on crop yields and soil properties. Archives of Agronomy and Soil Science, 2008, 54: 369–379
14. MADARAS, M., BALKOVIČ, J. and SKALSKÝ, R.: EPIC model based search of agronomic strategies for increasing SOC (case study), 2017
15. MARTINY, J.B.H., MARTINY, A.C., WEIHE, C., LU, Y., BERLEMONT, R., BRODIE, E.L., GOULDEN, M.L., TRESEDER, K.K. and ALLISON, S.D.: Microbial legacies alter decomposition in response to simulated global change. The ISME Journal, 2017, 11: 490–499
16. ONTL, T.A. and SCHULTE, L.A.: Soil Carbon Storage | Learn Science at Scitable. Nature Education Knowledge, 2012, 3: 10 pp

17. STEHLÍK, M., CZAKO, A., MAYEROVÁ, M. and MADARAS, M.: Influence of organic and inorganic fertilization on soil properties and water infiltration. Agronomy Research, 2019, 17: 1769–1778
18. STEHLÍK, M., KOVAŘÍČEK, P., VLÁŠKOVÁ, M. and RENČIUKOVÁ, V.: Influence of compost on water retention in conventional farming with ploughing. Úroda, 2016, 12: 425–428 (in Czech)
19. STEHLÍKOVÁ, I., MADARAS, M., LIPAVSKÝ, J. and ŠIMON, T.: Study on some soil quality changes obtained from long-term experiments. Plant, Soil Environment, 2016, 62: 74–79
20. STEIN, T.: Rise of carbon dioxide unabated. https://research.noaa.gov/article/ArtMID/587/ArticleID/2636; accessed: 04/06/2020

Corresponding author:
Mgr. Martin Stehlík, Department of mechanical engineering, Faculty of Engineering, Czech University of Life Sciences Prague, Kamýcká 129, Praha 6, Prague, 16521, Czech Republic, email: martinstehlik@seznam.cz

Driving parameters of the selected electric vehicle

V. Štekerová[1], M. Kotek[1]

[1]*Department of Vehicles and Ground Transport, Faculty of Engineering, Czech University of Life Sciences Prague, Prague, Czech Republic*

Abstract

This article is focused on the selected electric vehicle and its driving parameters. The selected electric vehicle was Fiat 500e. The electric vehicle was driven in sections that allowed monitoring of values for evaluation and comparison of operating parameters, battery discharge characteristics and energy consumption. The chosen test route was 30 km. First 15 km of the route led around the city (urban) and 15 km outside the city (suburban). Also, the specific conditions under which the test runs took place, such as outside temperature, geographic terrain or traffic conditions along the route were also monitored. This paper presents the results of conducted test drives. The obtained data were evaluated and conclusions were drawn. The article also shows average charging current during recuperation. The results show that the electric vehicle is suitable for urban traffic, where its operation can reduce local emissions from traffic.

Key words: electromobility, electric drive, transport, consumption of electricity, driving patterns

INTRODUCTION

Many industries currently deal with electromobility. However, the automotive industry invests the most money in electromobility. Although the electric car has a so-called exhaust elsewhere, its local emissions are zero. That is why electromobility is positively received mainly in areas of large cities, where the emphasis is on reducing local emissions, mainly from transport (May, 2017). Thanks to the current political pressure, car manufacturers are now also moving towards the development and production of electric cars. This pressure is mainly due to the considerable demands placed on ecological CO_2 regulations. The current EU Regulation 443/2009 established emission performance standards for newly manufactured passenger cars as a part of the Community's integrated approach to reducing CO_2 emissions. The emission limits set for new vehicles are 130 g CO_2 per km. By 2020, emission limit will be reduced down to 95g CO_2 per km. If this limit is exceeded, manufacturers will face financial penalties (European

Commission, 2010). Electric vehicles are not responsible for direct greenhouse gas emissions, but for indirect emissions from the production and operation of these vehicles. The carbon footprint of electric cars thus depends primarily on the energy mix, which is currently dependent on the production of electricity (Ehrenberger et al., 2020; Kromer & Heywood, 2007). The disadvantages of electric vehicles are their range, charging time and costs, which make them less comfortable in today's world. EVs are more expensive than conventional motor vehicles (Coffman et al., 2017). Because of range Tamor et al. (2013) concluded that PHEVs may be more acceptable than BEVs. Due to enhnaced charging infrastrucute range is no longer such a big problem today. Due to enhnaced charging infrastrucute range is no longer such a big problem today. However charging time still stays problematic and charging involves a number of technological obstacles that need to be addressed. The biggest challenge at present seems to be the traction battery, which affects key vehicle features such as range, power, weight and vehicle charge level. Electric car batteries are an expensive item, which causes not only a high purchase price of the electric car, but also high operating costs associated with battery replacement. The purchase price is the main reason why customers have not yet found their way to electric cars (Kaya et al., 2016). Tran et al. (2013) stated in his article that according to empirical review, first owners was heterogeneous motivated by financial benefits, environmental appeal, new technology, and vehicle reliability. The aim of this article is to analyze the driving parameters of a selected electric vehicle.

MATERIALS AND METHODS

The measurement of operating parameters and characteristics of the battery took place on a pre-selected route in Prague. The electric vehicle was a fully electric Fiat 500e. The measurement was performed using TEXA diagnostic equipment. During the measurement, the vehicle communicated with the electric drive control unit, which constantly measured the battery voltage and current, the speed of the electric motor and the speed of the car. These values were continuously recorded and stored by the system. Furthermore, the car was equipped with GPS 18x USB navigation units with a frequency of 1 Hz for immediate mapping of the vehicle's position.

Fiat 500e

The Fiat 500e is a fully electric car from the Italian manufacturer FIAT. The electric version of the model is based on the current form of the conventional Fiat 500. Its first generation began production in 1957. The Fiat 500e is a small passenger car that is very popular among people.

Thanks to its dimensions and driving parameters, the modernized electric version of the car is an ideal car for city traffic. It has an electric motor with a torque of 200 Nm. From zero to one hundred kilometers per hour, The fiat 500e can accelerate from 0 to 100 in 9.2 s. The top speed of the vehicle is 142 $km.h^{-1}$. In winter, its range is up to 140 km thanks to smart solutions such as heat pum saving up to 60 % energy. In summer, its range can be up to 200 km on a single charge and thus allows trouble-free operation, especially in the city. The design of the Fiat 500e is shown in Fig. 1.

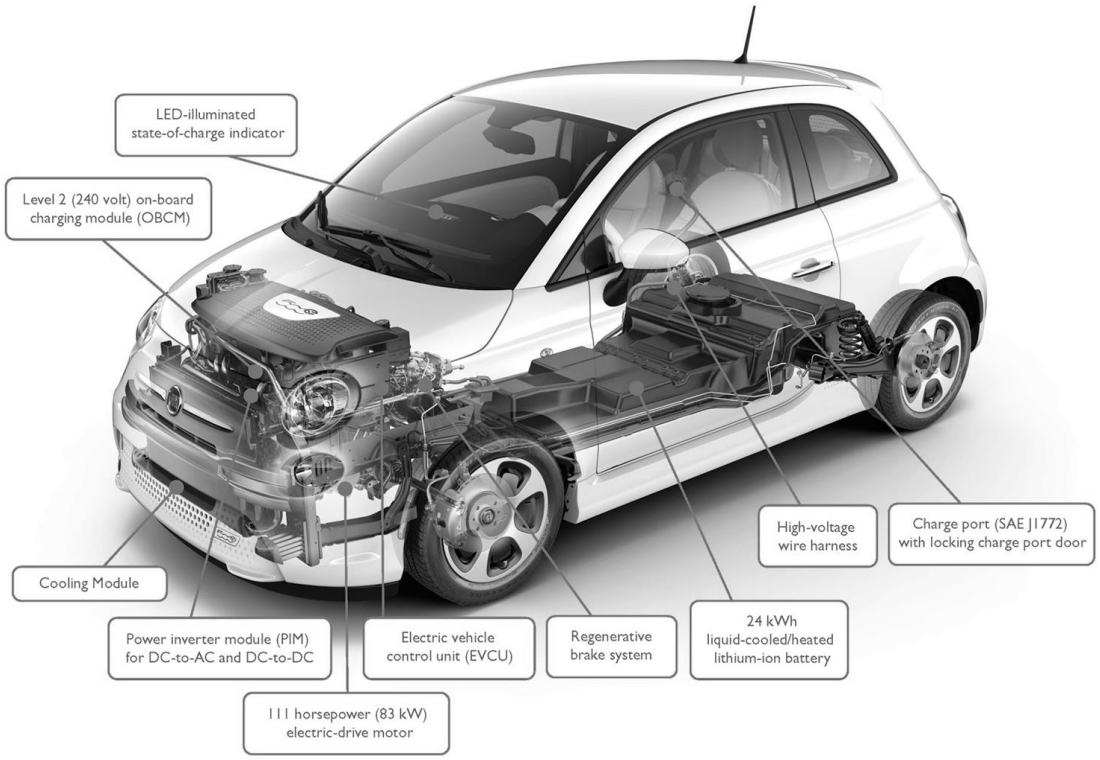

Fig. 1 Electric vehicle - Fiat 500e

The following table 1 shows the operating parameters of the electric vehicle Fiat 500e.

Tab. 1 Fiat 500e operating parameters

MOTOR		**VEHICLE**	
Design	Synchronous DC motor with permanent magnets	**Weight**	1352 kg
Power	83 kW	**Year of manufacture**	2015
Maximum torque	200 N/m		
Drive	Electric		

BATTERY		**DRIVING ABILITIES**	
Type	li-ion 364 V	**Top speed**	142 km·h^{-1}
Capacity	24 kWh	**Acceleration 0-100 km·h-1**	9.1 s
Number of cells	97	**Energy consumption**	18 kWh·100 km^{-1}
Weigth	260 kg	**Range**	140 km

TEXA

The Texa diagnostic (Fig. 1) unit is designed for monitoring and evaluating measured values from the motor in real time. Only passenger cars with an OBD diagnostic socket (since 2001, all petrol cars have had it and since 2003 all diesel cars) can be diagnosed. The OBD diagnostic adapter is firmly attached to the device. The IDC3 and IDC3 Pocket software only makes vehicles equipped with an OBD socket available. The device is therefore connected to the vehicle's diagnostic socket and uses Bluetooth to communicate between the vehicle and the display unit (PC or PDA). Thanks to continuous measurement, it is possible to monitor the characteristics of the engine while driving.

Fig. 1 TEXA diagnostic

Measurement

The driving routes were designed to include two different types of sections. Both routes are shown in Fig. 2. The first section is 15 km long and leads from the Czech University of Life

Sciences (CULS) to the Budějovická metro station, where there is a fast charging station for electric cars. The driving routes were designed to include two different types of sections.

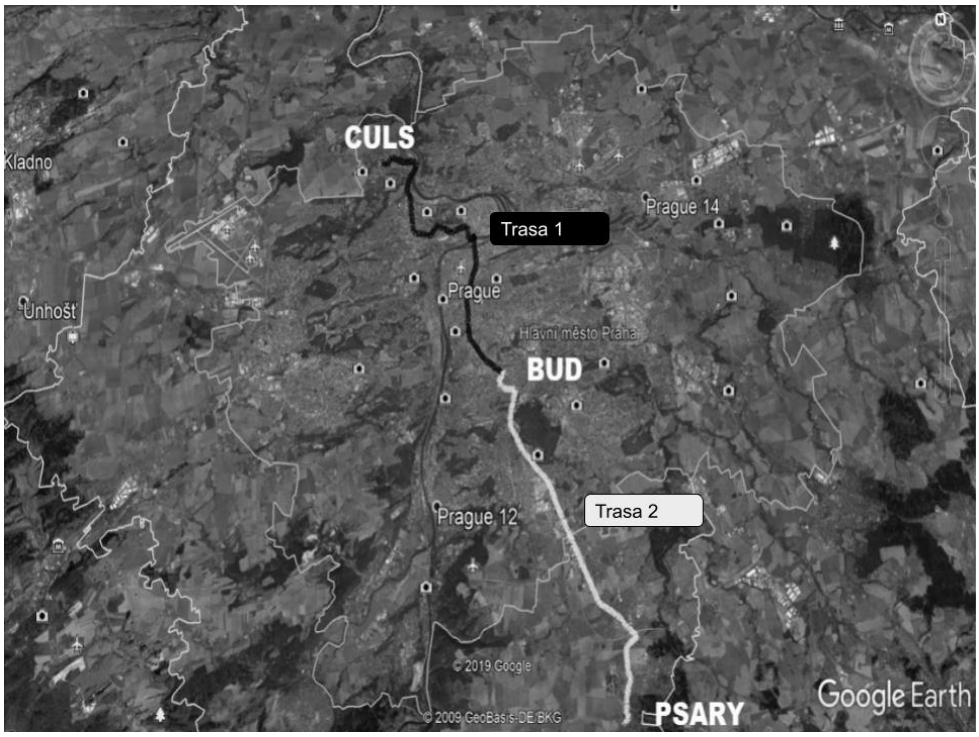

Fig. 2 Test drive map

The second section was also 15 km long and represents extra-urban traffic conditions. The route leads from the end of the first section, ie from the metro station Budějovická (BUD), to Psáry (PSARY), which is located south of the capital city of Prague.

RESULTS AND DISCUSSION

Table 2 shows the resulting values from the measurement of operating parameters. The table shows that the average speed in the city was lower than when driving suburban. This difference can be explained by the driving style, which differs mainly due to the frequent stopping in city traffic. City traffic corresponds to higher electricity consumption.

Tab. 2 Measured values of test drives

	Vehicle	**Fiat 500e**	
	Route	**Urban**	**Suburban**
Driving time	min	33.45	33.86
Length of the ride	km	14.97	15.82

Average speed	km.h-1	27.0	29.50
Power consumption	kWh·100 km^{-1}	13.80	13.33
Total energy	kWh	2.07	2.11
Total average energy	kW	3.72	3.72

The 2017 International Energy Agency (IEA) data showed that the energy use in transport significantly increased in 1971 from 23 % of total final consumption to 29 % in 2015. Fiat 500e had an average consumption of 13.8 kWh per 100 km in the city (urban) and 13,33 kWh per 100 km outside the city (suburban). Both achieved consumption on both routes were lower compared to values stated by manufacturer (18 kWh·100 km^{-1}). The amount of carbon dioxide produced by vehicle is calculated by dividing the average electricity consumption per 100 km by the CO_2 production per kWh. The quantity is given in grams. The weight of CO_2 per 1 kWh depends on the current composition of the country's energy mix. The energy mix of the state is influenced by the composition of power plant types, such as combustion power plants, nuclear power plants, wind and solar power plants. This mix then fundamentally changes the weight of CO_2. These data are essential for presenting how environmentally friendly electric cars are. Tab. 3 shows the CO_2 production per 1 km, which was calculated with different input parameters from 27.01.2020 and 27.06.2020.

Tab. 3 CO_2 production per 1 km

		27.1.2020		**27.6.2020**	
		Urban	**Suburban**	**Urban**	**Suburban**
Amount	g CO_2/ kWh	502	502	336	336
Power consumption	kWh·100 km^{-1}	13.80	13.33	13.80	13.33
CO_2 production	g CO_2 /1 km	69.28	66.92	46.37	44.79

The amount of grams of CO_2 per 1 km in this case is mainly affected by the season. Both values are recorded at 6 p.m. By January, the sun had set at this time, so solar power plants could not produce emission-free solar energy. At the end of june, the sun went down later and solar power

plants can produce emission-free energy. Solar energy is an important part of the energy mix. From this easy calculation, it can be concluded that the operation of an electric vehicle in the summer months is certainly more environmentally friendly.

Figure 3 and 4 show the electric current levels of both routes. The main monitored parametr was the changing level of the battery discharge current which depends heavily on the way of operation, altitute profile of the route and driving speed of the vehicle. Negative current values indicate consumed current, positive values indicate recuperation energy.

The graph 1 shows that the average current consumption was 18.9 A. The maximum current reached 152.5 A, which was consumed by the electric car during the first climb in Suchdol.

The average recuperation current reached 16.3 A. The maximum measured value of the recuperation current was 82.8 A.

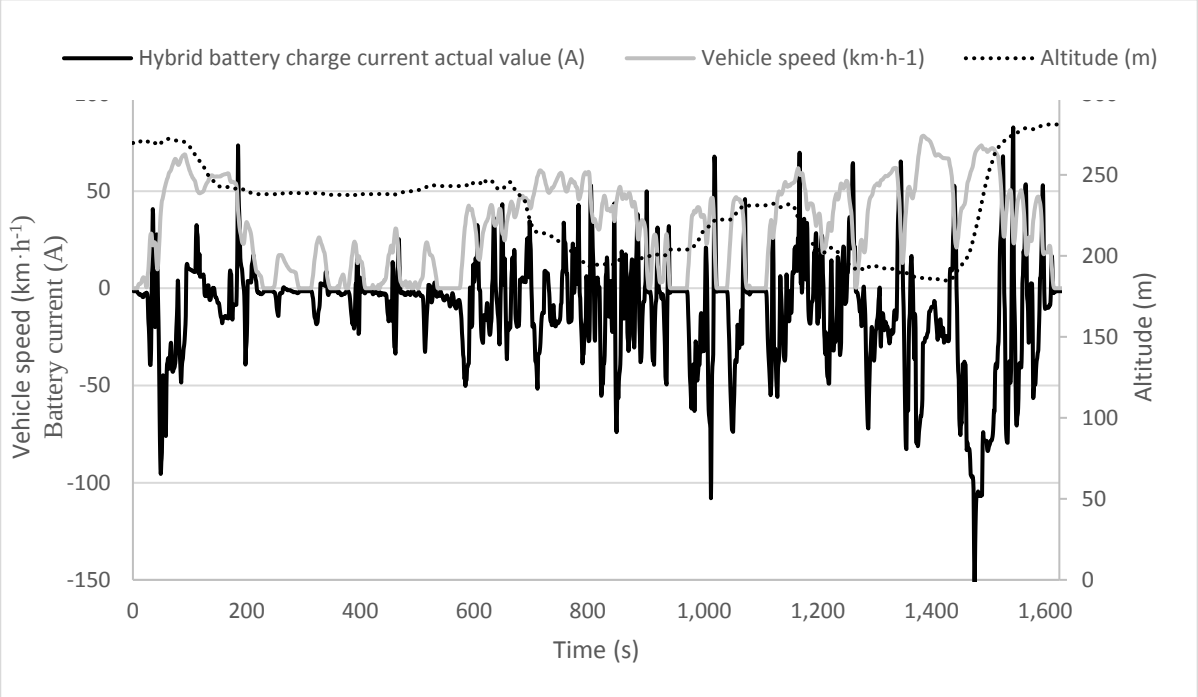

Fig. 3 Characteristics of the Fiat 500e in the suburban section

Figure 4 shows that the Fiat 500e reached an average consumption of 20.35 A. The maximum electric current in urban traffic was 77.9 A. The average charging current during recuperation was 14.27 A. At the moment of generating current by recuperation the highest current value was 69 A.

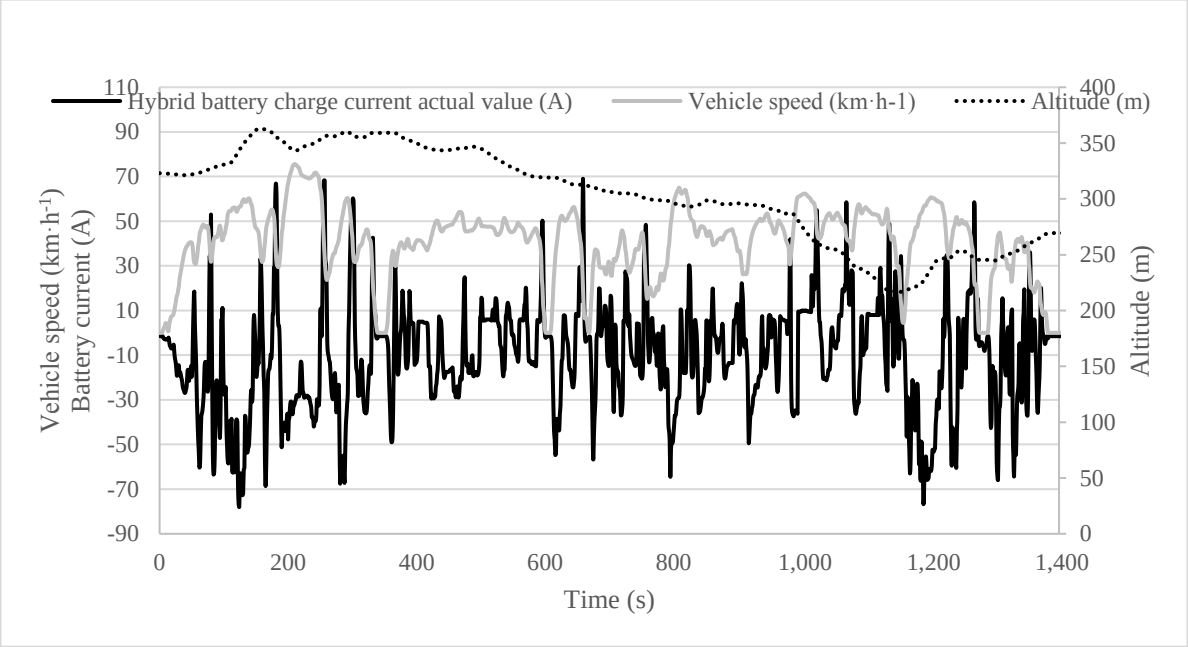

Figure 4 Characteristics of the Fiat 500e in the urban section

The results of the measurements showed that the current consumption from the traction battery increases significantly in urban traffic, due to driving in congestion, stopping at traffic lights and more frequent need for acceleration. It is obvious that dimensions and weight plays a crucial role in the degree of current discharge. Emissions generated indirectly by electric cars also corresponded to these values. Zhang et al. (2020) deals in detail with the analysis of the energy consumption of an electric vehicle thanks to real-world driving data. Both sections experienced recuperation, which helped recharge the battery, especially when driving downhill. When driving from a higher altitude, it was enough to sufficiently charge the batteries and thus be able to effectively extend the range of the vehicle. In urban traffic, recuperation for recharging was not as efficient. But it helped with braking, which is more common in urban traffic. The results therefore indicate that small electric vehicles are clearly suitable for urban traffic.

CONCLUSION

The measurements determined the values of discharge currents of accumulators in urban and non-urban traffic, which showed the effect of acceleration and recuperation on energy consumption. Recuperation has thus proved to be an effective mean of recharging the battery, especially when descending from a higher altitude, when it was able to charge the battery efficiently.

Electricity consumption is affected by driving style, geography and, among other things, by weather, which affects the need for air conditioning or heating. The use of an electric vehicles

is always influenced by the vehicle user. The measurement shows the suitability of Fiat 500e for city traffic. The measurement also shows that real consumption reached lower values than stated by the manufacturer (13,8 kWh·100 km^{-1} in the city (urban) instead of 18 kWh·100 km^{-1}), which is mainly caused by the defensive driving style.

EVs do not produce local harmful emissions. However it should be noted that it generates indirect emissions depending on how electricity is produced (energy mix), and it is also necessary take into consideration the entire life cycle of an electric vehicle from production to disposal, when additional emissions are produced. The production of harmful emissions from EV is strongly dependent on the electricity source, the type of power plant and its primary energy source. In conclusion, it must be said that after the analysis of the recorded data from the electrical map, the operation of the electric car is significantly more environmentally friendly in the summer months, when the composition of the energy mix is more favorable.

REFERENCES

1. Coffman, M., Bernstein, P., & Wee, S. (2017). Electric vehicles revisited: a review of factors that affect adoption. *Transport Reviews*, *37*(1), 79–93. https://doi.org/10.1080/01441647.2016.1217282
2. Ehrenberger, S. I., Konrad, M., & Philipps, F. (2020). Pollutant emissions analysis of three plug-in hybrid electric vehicles using different modes of operation and driving conditions. *Atmospheric Environment*, *234*, 117612. https://doi.org/10.1016/j.atmosenv.2020.117612
3. Evropská komise. (2010). *ZPRÁVA KOMISE EVROPSKÉMU PARLAMENTU A RADĚ: POKROK PŘI DOSAHOVÁNÍ CÍLŮ KJÓTSKÉHO PROTOKOLU*. https://eur-lex.europa.eu/legal-content/CS/TXT/PDF/?uri=CELEX:52010DC0569&from=CS
4. Kaya, S., Kilic, N., Kocak, T., & Gungor, C. (2016). A battery-friendly data acquisition model for vehicular speed estimation. *Computers and Electrical Engineering*, *50*, 79–90. https://doi.org/10.1016/j.compeleceng.2016.01.017
5. Kromer, M. A., & Heywood, J. B. (2007). *Electric Powertrains: Opportunities and Challenges in the U.S. Light-Duty Vehicle Fleet*.
6. May, N. (2017). Local environmental impact assessment as decision support for the introduction of electromobility in urban public transport systems. *Transportation Research Part D: Transport and Environment*, *64*(July 2017), 192–203. https://doi.org/10.1016/j.trd.2017.07.010

7. Tamor, M. A., Gearhart, C., & Soto, C. (2013). A statistical approach to estimating acceptance of electric vehicles and electrification of personal transportation. *Transportation Research Part C: Emerging Technologies*, *26*, 125–134. https://doi.org/10.1016/j.trc.2012.07.007

8. Tran, M., Banister, D., Bishop, J. D. K., & McCulloch, M. D. (2013). Simulating early adoption of alternative fuel vehicles for sustainability. *Technological Forecasting and Social Change*, *80*(5), 865–875. https://doi.org/10.1016/j.techfore.2012.09.009

9. Zhang, J., Wang, Z., Liu, P., & Zhang, Z. (2020). Energy consumption analysis and prediction of electric vehicles based on real-world driving data. *Applied Energy*, *275*, 115408. https://doi.org/10.1016/j.apenergy.2020.115408

Corresponding author:

Ing. Martin Kotek, Ph.D., Department of Vehicles and Ground Transport, Faculty of Engineering, Czech University of Life Sciences Prague, Kamýcká 129, Praha 6, Prague, 16521, Czech Republic, tel: +420224383181, email: kotek@oikt.czu.cz

Comparison of thermal features of vehicle exteriors

D. Švorc[1], M. Růžička[1]

[1]Department of Vehicles and Ground Transport, Faculty of Engineering, Czech University of Life Sciences Prague, Prague, Czech Republic

Abstract

The main aim of this paper is to compare the thermal features of electric and conventional (equipped with combustion engines) vehicle exteriors. The thermal cameras can complement or substitute visible spectrum video cameras and other conventional sensors and provide rich classification data linked with vehicle type recognition. The thermal images, obtained through an infrared thermography camera, were evaluated. The important differences between thermal features of these types of vehicle exteriors were found out. The results confirmed the hypothesis that it is possible to use an infrared thermography for vehicle drive categorization, collection of traffic data and eventually for traffic management, Smart city implementation and telematics systems in the towns in future as well.

Key words: Thermal analysis, Vehicle classification, Electric vehicles, Thermal imaging, Detection of electric vehicles

INTRODUCTION

According to TRB [1] more than one billion motorized vehicles were driven on the earth in year 2009 and in the next two decades, vehicle ownership was expected to double worldwide. This fact causes and will cause many problems such as a traffic congestions and growing number of traffic accidents, air pollution by pumping extraordinary quantities of greenhouse gases into the atmosphere, draining the world's conventional petroleum supplies etc. Electromobility is considered to be one of the way how to reduce carbon gas emissions and dependence on petroleum and it is gaining popularity in the present society due to reason of energy consumption reduction [2]. In order to avoid problems of growing motorization and urban growth, it is necessary to set up traffic rules correctly and to regulate traffic accordingly. All types of transportation data is necessary to collect in traffic planning, management and transport safety [3]. Historically, traffic data acquisition has been limited to manual methods or induction loop collection at defined positions [4]. Moreover, it is necessary to monitor traffic

flow in such a way that traffic control can be adapted in real time. Therefore, it is essential to implement Intelligent Transport Systems (ITS) [5].

In near future and even actual ITS applications are required to categorize vehicle type according their emissions standards or type of engine unit for toll way, emission zones, emergency systems, safety etc.

Due to lower accuracy occurring under bad weather conditions, e.g. fog, snow or heavy rain; it is necessary to replace or complement conventional methods using visual cameras with infrared cameras [6]. Infrared images of vehicles are expected to provide continuous and independent detection of vehicles on the conditions in their surroundings [6].

In this paper, we propose novel method of detection of full electric vehicles (FEV). We use advantages of an infrared camera to measure thermal patterns of the vehicle exteriors (grille area and front side) to establish the criteria for recognition of the battery electric vehicles in traffic flow

MATERIALS AND METHODS

The text of the article [7] shows up the possibilities of classification of the vehicle based on their temperature pattern. The authors focus on the different thermal features of various vehicle categories and distinguish between them by statistical analysis of their thermal images, with the detection area is the entire image of a given height and width. They take into account only that part of the temperature histogram that was statistically evaluated as a representative part for the vehicle category. Author [7] uses the windshield and its surroundings as a detection area. However, this method proved to be less accurate under winter conditions due to similar windshield temperatures and ambient temperatures [8]. Authors [9] used both visual and thermal video for detection and use the grille areas and headlight as the detection area. Every single car generates heat during drive [7]. Even the car equipped with an electric engine generates heat, but when it is compared with conventional vehicles, it is significantly less heat. The heat is emitted to the body of the vehicle and it is easily visible on the front mask and side of the vehicle.

Vehicles use cooling systems with coolant for the purpose of engine cooling. One of the parts of the cooling system is a radiator that absorbs heat from the coolant transported from the engine and due to it its body is heated. It means that temperature is partly proportional to engine load and his temperature. This property is possible to use and target detection to the grille area. Running engine warms its own body as well as other auxiliary parts of engine and emits this heat to neighbouring parts as mask, hood and side of the vehicle.

Other parts that do not come directly into contact with the heat from the engine are significantly colder and this is used in this research using the differences between the drive installation of the electric vehicle and the vehicle with internal combustion engine.

The preliminary measurements confirmed the assumption of physical differences in the operation of these drives. The electric motor and the components required for its operation only heat up to a level that is much lower in comparison with the internal combustion engine. We use this temperature difference to detect electric vehicles.

The area of the radiator grille and the area of the right fender above the front wheel, which we have identified as the region of interest from the thermal camera images, were selected as the detection areas.

The optimal conditions of measurement were set up; the suitable engine laboratory equipped with a dynamometer for vehicle test bench was selected. The laboratory enabled to drive a car and warm it up to operational temperature together with stationery position and stabile indoor temperature in vehicle surroundings. The temperature was set up in the laboratory to the usual temperature as occur in summer season in the Czech Republic.

Vehicles were selected for a purpose of good comparison. They were equipped with the same body for an electric and combustion engine models. Selected models were WV eGolf and WV Golf 1.5 TSI.

The measurement under laboratory conditions forewent a prepared works in an outdoor environment. Measurement was performed at the vehicle in a stationary position as well on slowly moving vehicle to test usage of thermocamera and vehicle recognition (electric vehicle and vehicle equipped with combustion engine). The usage of special thermocamera to measure the temperature of train wagon wheels etc. is apparent in [10]. Measurement will be further tested with the potential of verification during higher vehicle velocities. Vehicles were tested with the use camera FLIR E5 [11] according to following process:

<u>Positions of thermal camera for measurement:</u>

1. thermal image of mask of the vehicle
2. thermal image of side of the vehicle in area of front fender
3. thermal image of side of the vehicle in high of floor of the vehicle.

<u>Time interval of measurement:</u>

1. measuring after 15 minutes at constant vehicular speed 60 $km.h^{-1}$ – laboratory measurement
2. measuring after 30 minutes of driving in city traffic.

Setting the parameters of the thermal camera:

1. colour scale and MSX mode
2. emissivity 0.95
3. ambient temperatures 18 °C, 6 °C, 4 °C.

RESULTS AND DISCUSSION

The results of measurement shows a significant difference when they are compared. The temperature patterns of electrical and combustion propulsion of vehicles are evidently different. During measuring under laboratory conditions and controlled ambient temperature, the biggest difference in the detected emitted temperatures was up to several tens of degrees Celsius. Tables that are part of thermogram pictures (below) show the highest reached temperature (Max) in the detection window (frame) and average temperature from all detection area. The results of electric vehicle see Fig. 1a), b) are:

a) Mildly temperature affected body of a vehicle in detection area Bx1 and the warmest source of the heat is mainly radiator and its grille, potentially brakes from side.

b) Created second measured area Bx2 see Fig. 1b) due to reason of the existence of passive radar, which is independently heated and would distort the measurement itself.

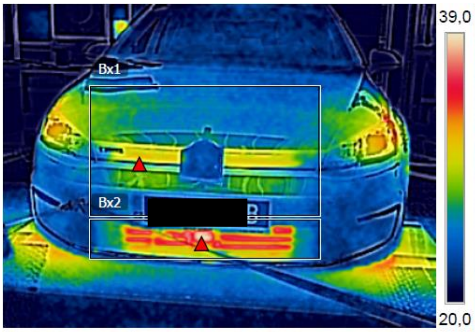

Measurements		
Bx1	Max	25,0 °C
	Average	21,6 °C
Bx2	Max	38,7 °C
	Average	24,1 °C

Parameters	
Emissivity	0.95
Refl. temp.	18 °C

a)

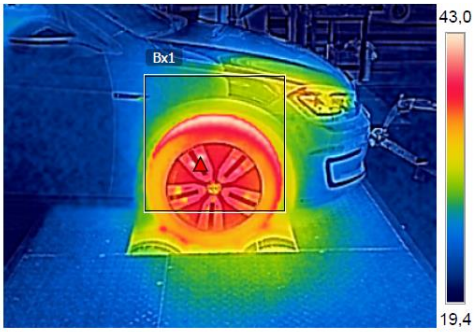

Measurements		
Bx1	Max	43,0 °C

Parameters	
Emissivity	0.95
Refl. temp.	18 °C

b)

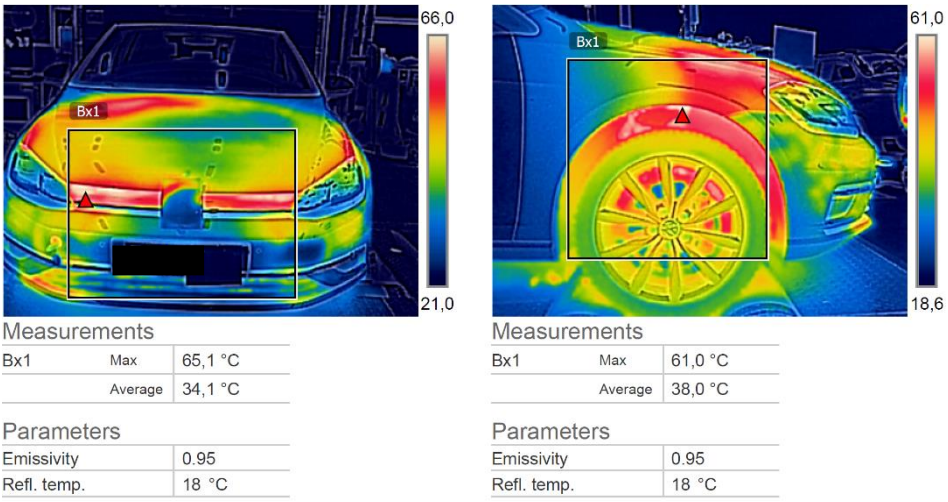

c) d)

Fig. 1 Example of laboratory measurement of vehicles; a) electric vehicle's front, b) electric vehicle's side, c) front of vehicle with combustion engine and d) side of vehicle with combustion engine

Fig. 1c) of combustion vehicle thermogram shows considerably affected area of the mask of vehicle, primarily grille area and vehicle hood. Temperatures are about 40 °C higher in comparison with the electric vehicle, respectively average temperature of detection area is more than 10 °C higher by the same vehicular speed, time of drive and same setting of measuring parameters of a thermal camera. This temperature gap confirms results of measurement carried out from the side of vehicle. The electric vehicle had warmed tires see Fig. 1 b) and the surrounding area of wheel arch and fender is slightly warmed in comparison with combustion engine see Fig. 1 d) where, in addition to warm tires, the wheel arch and front fender area are more affected by higher temperature.

In the case of outdoor measurements, the situation is similar, as can be seen on Fig. 2 a) - d). The components of the electric vehicle that are warmed up while drive, remain at a temperature several degrees higher than the ambient temperature (around 5 °C at the time of measurement of the electric vehicle). The internal combustion engine is heated to a temperature of two tens of degrees from atmospheric ambient temperature (at the time of measurement -1 °C). These measurements show that, despite of negative temperatures, there is still a difference in vehicles' thermograms and exists the possibility of finding appreciable differences between them.

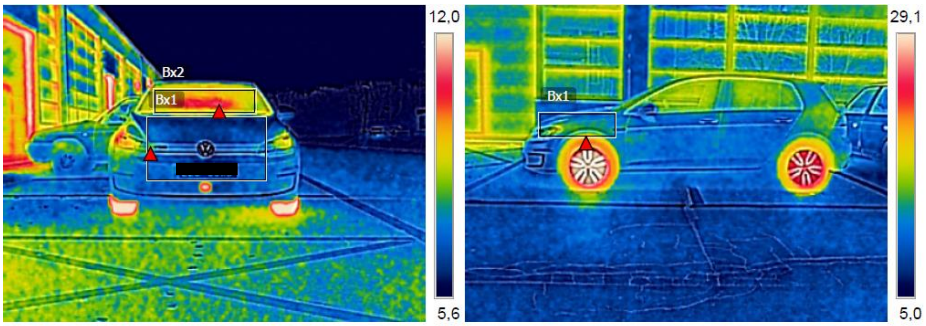

Measurements		
Bx1	Max	7,3 °C
	Average	6,5 °C
Bx2	Max	10,5 °C
	Average	8,4 °C

Parameters	
Emissivity	0.95
Refl. temp.	6 °C

a)

Measurements		
Bx1	Max	11,3 °C
	Average	7,6 °C

Parameters	
Emissivity	0.95
Refl. temp.	6 °C

b)

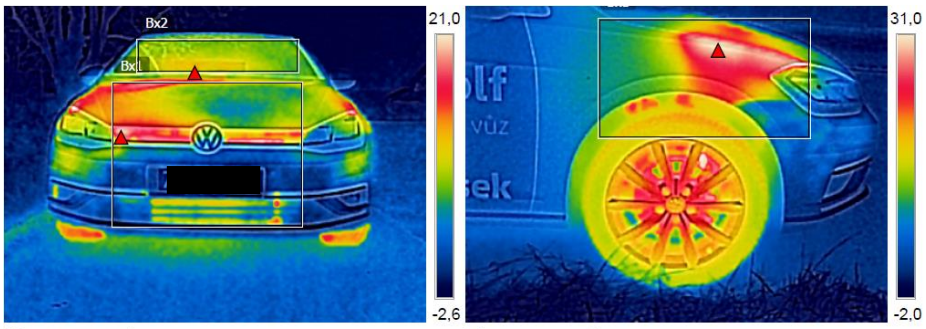

Measurements		
Bx1	Max	20,3 °C
	Average	1,3 °C
Bx2	Max	4,5 °C
	Average	1,7 °C

Parameters	
Emissivity	0.95
Refl. temp.	4 °C

c)

Measurements		
Bx1	Max	31,0 °C
	Average	11,5 °C

Parameters	
Emissivity	0.95
Refl. temp.	4 °C

d)

Fig. 2 Example of outside measurement of vehicles; a) electric vehicle's front, b) electric vehicle's side, c) front of vehicle with combustion engine and b) side of vehicle with combustion engine

Temperature scales of Fig. 2 a) - d) show, that it is evidently to recognize whether combustion engine works or not in the case of PHEV. This information is very important in the first few kilometres of drive, where engine is not warmed up to operational temperature, yet is possible to clearly seen the differences. Even with respect to area of vehicle body measurement, as FEV and PHEV are heated in different locations of the vehicle exterior.

The graphs (see on Fig. 3 a),b)) are appreciable difference in intensities of particular temperatures and in different shape of thermal histogram. Histogram of electric vehicles becomes semi-Gauss curve; therefore, histogram of conventional vehicle has larger number of temperature intensities and his graphical distribution is different from Gaussian curve. The obtained knowledge proves and confirms another hypotheses i.e. recognition of different drive

aggregates and detection of electric vehicles based on their thermal pattern in pattern matching is possible.

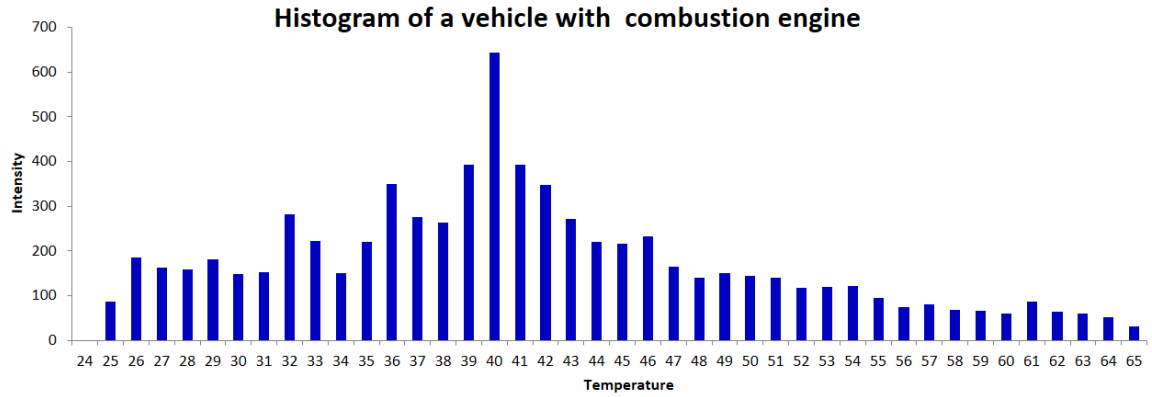

a)

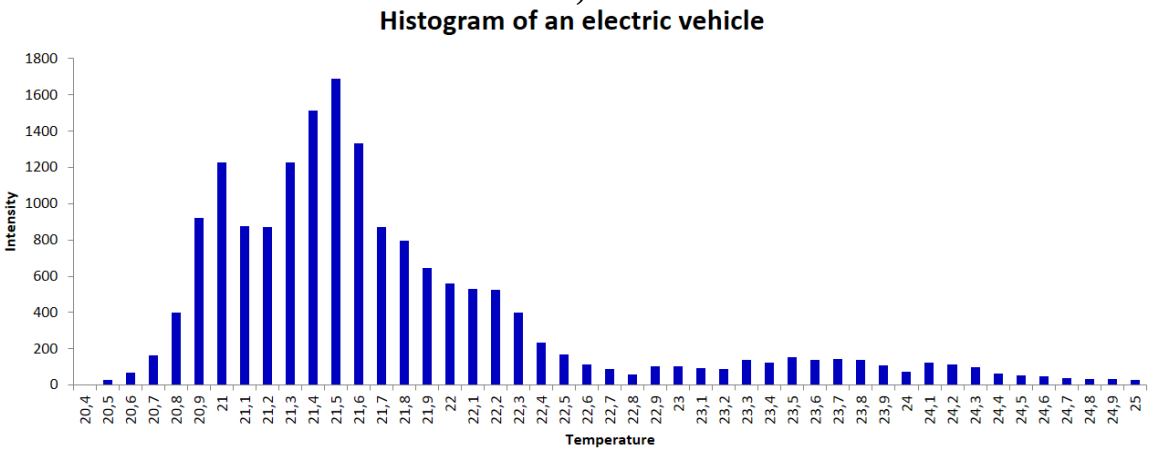

b)

Fig. 3 Intensities on a vehicles thermal image; a) histogram of a vehicle with combustion engine and b) histogram of an electric vehicle

For vehicle classification is also necessary to take into account that vehicles have different bodies, based on aerodynamics, size of engine, purpose of usage, driver's view etc. Hence, it is necessary the size of detection window of front part and side of vehicle set on proper size that can fulfil all vehicles' category (personal car, van, truck). Due to learned pattern of semi-Gauss curve and pattern matching then will be filtered out the surroundings of the image not corresponding to the specified detection conditions, as was similarly solved for differentiation of various types of convectional vehicles in the reference [7].

It is considered realistic to use different thermal signature patterns of electric vehicles and internal combustion engines for their detection and classification.

The reliable thermal detection requires keeping of several rules. It is also necessary to provide side detection of the vehicles, as the confirmation of front images of these vehicles; since following vehicles may partially dim and reduce detection accuracy.

The measurements also confirmed the correct positioning of the detection surfaces and the most temperature - affected parts of the car body. It is therefore necessary to verify these detection areas on several vehicle models and to measure them under real traffic conditions.

CONCLUSION

Proposed approach shows possible way of reliable detection of electric vehicles for recognition conventional and even PHEV vehicles with internal combustion engine and FEV, because it is not ever possible yet to find out required data from a licence plate and vehicle register. Another usage of detection is offered and reliability is around 90 % under different weather conditions like hot weather and temperatures below 0 °C. The application of reliable detection of electric vehicles is possible consider to use for vehicle priority systems at intersection with traffic lights, suitable activation for parking and smog situations, but especially for using toll systems. The proposed detection can support a development of electromobility in cities as well. Another use of detection based on thermal camera images is obvious in Smart cities, where it is possible precisely detect number of passengers in vehicles, detect potential accidents and overheating of particular vehicle parts and prevent fire beforehand, because these problems will be substantial for electric vehicles. The use of thermal detection can be useful for tunnel technologies but even for control of some diagnostic systems and prediction of state. It is possible to see, results of experiments are very interesting with potential high use of these technologies for electromobility, transportation, diagnostic, even for the usage in Smart applications, their usability check and other improvements.

REFERENCES

[1] D. Sperling and D. Gordon, “Two billion cars transforming a culture,” *TR News*, no. 259, pp. 3–9, 2008.

[2] C. Li, H. Guo, W. Wang, and X. Jiang, “Stabilization Analysis of Mixed Traffic Flow with Electric Vehicles Based on the Modified Multiple Velocity Difference Model,” in *Lecture Notes in Electrical Engineering*, 2019, pp. 251–261.

[3] K. Robert, “Night-Time Traffic Surveillance: A Robust Framework for Multi-vehicle Detection, Classification and Tracking,” in *2009 Sixth IEEE International Conference on Advanced Video and Signal Based Surveillance*, 2009, pp. 1–6.

[4] S. J. Bahler, J. M. Kranig, and E. D. Minge, “Field Test of Nonintrusive Traffic Detection Technologies,” *Transp. Res. Rec. J. Transp. Res. Board*, vol. 1643, no. 1, pp. 161–170, Jan. 1998.

[5] D. Ni, “Determining Traffic-Flow Characteristics by Definition for Application in ITS,” *IEEE Trans. Intell. Transp. Syst.*, vol. 8, no. 2, pp. 181–187, Jun. 2007.

[6] T. Fu, J. Stipancic, S. Zangenehpour, L. Miranda-Moreno, and N. Saunier, “Automatic Traffic Data Collection under Varying Lighting and Temperature Conditions in

Multimodal Environments: Thermal versus Visible Spectrum Video-Based Systems," *J. Adv. Transp.*, vol. 2017, no. May, pp. 1–15, 2017.

[7] A. Sangnoree and K. Chamnongthai, "Thermal-image processing and statistical analysis for vehicle category in nighttime traffic," *J. Vis. Commun. Image Represent.*, vol. 48, pp. 88–109, Oct. 2017.

[8] Y. Iwasaki, M. Misumi, and T. Nakamiya, "Robust Vehicle Detection under Various Environmental Conditions Using an Infrared Thermal Camera and Its Application to Road Traffic Flow Monitoring," *Sensors*, vol. 13, no. 6, pp. 7756–7773, Jun. 2013.

[9] Y. Nam and Y.-C. Nam, "Vehicle classification based on images from visible light and thermal cameras," *EURASIP J. Image Video Process.*, vol. 2018, no. 1, p. 5, Dec. 2018.

[10] L. Kovář, D. Krásenský, V. Polach, and Z. Zouhar, "Diagnostika jedoucích železničních vozidel ," Praha, Nov. 2013.

[11] "FLIR E5 Infrared Camera with MSX® | FLIR Systems." [Online]. Available: https://www.flir.com/products/e5/. [Accessed: 01-Feb-2020].

Corresponding author:

Ing. David Švorc, Department of Vehicles and Ground Transport, Faculty of Engineering, Czech University of Life Sciences Prague, Kamýcká 129, Praha 6, Prague, 16521, Czech Republic, email: svorcd@tf.czu.cz

Comparison of municipalities of the Czech Republic in physical composition of municipal solid waste and their potential in separation

Shuran Zhao[1], L. Richterova[2], V. Altmann[1], V. Vitková[1]

[1]Department of Machinery Utilisation, Faculty of Engineering, Czech University of Life Sciences Prague (CULS), Kamýcká 129, 165 00 Prague 6 – Suchdol, Czech Republic

[2]INCIEN, Institut Cirkulární Ekonomiky, z.ú., Hybernská 998/4, Prague 1, 110 00, Czech Republic

Abstract

Czech Republic is moving from landfill-based system toward resource-based waste management system with an increasing rate of recyclable waste in last years (38.6% of recycling by material and 11.7% of energy recovery in 2018). But landfill is still the popular way of municipal solid waste (MSW) disposal. Therefore a good knowledge of physical composition of MSW is required in order to define strategy plans and improve waste management in municipality. In the Czech Republic, municipal solid waste is collected from households by door to door system or recovery operations (Household Waste Recycling Centre) and only should consists of everyday items, which are further non-recyclable and unreusable. However, a significant amount of recyclable waste can still be found in MSW. This work is aimed to compare the physical composition of MSW in small municipalities in the Czech Republic with population size up to 2 999 inhabitants to recognize the share of recyclable and non-recyclable waste in MSW and designate the potential of separation at source. Composition of MSW was determined by physical assessment of waste collected from households in targeted small municipalities, where a waste sample of approx. 300 kg of MSW collected from both residential and family housing as it may differ in composition of each component of MSW. The physical composition was identified by detailed manual sorting of waste into specific groups (13 categories in total) by their features and weighted to compare later. We found that the real fraction of MSW, which cannot be further reused or recycled, was much smaller than the amount discarded into the black municipal trash bins. Big portion of MSW was made by organic waste together with food waste. This kind of waste is especially useful when people turn it into compost in terms of waste production prevention and it returns the nutrients back to the soil and thus closing the

circle. Rate of recyclable waste was also high in many municipalities of our analysis, which indicated lower separation rate. It reflects an inadequate sorting system in municipality and insufficient education of habitants. On the other hand, it points out a big room of potential in separation at households. To conclude, the assessment highlights the improper proportion of MSW. Much waste can be recycled but once it is thrown into black bins as MSW, there is no chance for it to be reused/recycled. Therefore, it calls for measures of improving in sorting at source, which benefits municipal authorities in term of increasing the recycling rate to meet the regulations as well as gaining profit from selling the recyclable waste as secondary material. We found analysis of physical composition of MSW as a fundamental method for municipalities to verify separation rate at source and it is necessary to conduct this analysis regularly and monitor the development.

Key words: Analysis, physical composition, municipal solid waste, recycling, separation at source, Czech Republic

INTRODUCTION

Czech Republic generated 5 782 thousand tons of municipal solid waste (MSW) in year 2018, it was 544 kg of MSW per person, about 44 kg more than 5 years ago in comparison with year 2015. Only 38.6 % was recycled by material and 11.7 % for energy recovery, 46 % was landfilled (MŽP 2019). Thanks to the low landfill tax, landfilling as a way of waste disposal is still popular for the Czech municipalities, especially for small municipalities with low budget.

This year in March, The European Commission has adopted a new Circular Economy Action Plan which includes revised legislative proposals on waste to stimulate Europe's transition towards a circular economy. The new action plan presents key elements including a target for recycling 65% of municipal waste by 2030 and to reduce landfill to maximum of 10% of municipal waste at the same year. Additionally there is applied a strict ban on landfilling separately collected waste, for example paper, plastics, organic waste, metals, etc. (European Commission 2020). Czech own Waste Management Plan 2015-2024 already set up that landfilling tax should be adjusted in order to divert waste higher up the hierarchy (MŽP 2014). Increase 1850 Kc of landfilling tax from 500 Kc per ton applied in 2030 should shift waste treatment more

to recycling and reuse instead of landfilling. This step would have huge impact on the municipal budget and make small municipalities focusing on waste treatment and trying to find out a new way with municipal waste produced in their region.

Municipal solid waste is primarily produced by households, in small scale can be produced by private sector based on agreement with municipal office. It is waste with no further usage or small usage (for energy recovery) in contrast to recyclable waste which, among other things, bring extra income for municipality. Municipalities joined integral waste separation system by EKO-KOM can get benefits depending on the collected recyclable waste (paper, plastics, glass, etc.). It is a fact, that the more municipality collects from inhabitants and invest into the waste infrastructure system, the more reward they get from the EKO-KOM system. Therefore, it is also from a desire of municipal authority to make steps leading to MSW reduction and increase of collection of recyclable waste.

To come out with an efficient solution for MSW reduction, it is necessary to identify the composition of MSW in the municipality. The composition of produced waste is extremely variable and depends on multiple seasonal and cultural factors, eating habits, and socioeconomic and legislation impacts. This variability makes defining and measuring the composition of waste more difficult and at the same time more essential (Kreith 1999; Diaz et al. 2020; Dehghani et al. 2009). The precise information regarding the quantities and characteristics of the solid waste can be then used for design, implementation, and operation of the best practice in the waste management as well as source control, saving resources, recycling, planning waste collection layout, transport, and disposal system which finally results in protection of the environment against such harmful effects (Heravi et al. 2013; Erami et al. 2015). Assessment of waste composition gives a detail view into municipal waste produced by citizens each day and inspires authorities on further improvements.

For this purpose, the non-governmental organization Institut Cirkulární Ekonomiky z. ú. (INCIEN) in cooperation with JRK Czech Republic s.r.o. (JRK) have been conducting analyses of physical composition of MSW to help the municipalities getting a better knowledge about their waste. Thanks to their work and collected data this paper could arise.

The primary goal of this study was to evaluate all the collected data of 20 small municipalities in the Czech Republic during analysis of physical composition, assess the qualitative and quantitative characteristics of MSW, compare in-between these regions and find the potential in waste reduction and increase of recycling.

MATERIALS AND METHODS

The assessment of physical composition of MSW was performed in 20 Czech municipalities with population up to 2 999 citizens over 4 years. Some analyses were repeated on request in order to monitor the municipal waste composition changes over the year.

All these composition analyses were completed by Institut Cirkulární Ekonomiky, z.ú in cooperation with JRK Czech Republic, s.r.o., whose main goal is about transformation and implementation of circular economy in the Czech Republic.

Analysis is aimed to evaluate the municipal solid waste and its composition of recyclable and nonrecyclable compounds, determine their percentage and find the potential to improve recycling rate.
The methodology was designed by Methodological guideline of waste sampling (Ministry of the Enviroment 2008) and adjusted to meet the goal of waste analysis.

Waste samples were collected during each MSW analysis in field.

All analyses were performed in cooperation with municipal authorities which provided MSW collected just before analysis from households according to the waste collection schedule. For analyzing, a sample of approx. 500 kg of municipal waste, randomly picked from the pack, was taken aside and analyzed. For this study was used household waste both from apartment and family houses. Protective equipment (suit, gloves, glasses, respirators etc.) were used during the whole analysis.

Each sample of MSW was waded through carefully and manually separated into 13 detailed categories (13 black bags) according to their attributes (

Figure *1*). Every separated category was weighted using weighing scale and recorded throughout the analysis followed by calculation of total weight by the end. Then all data were recorded and photographed, the waste sample was discarded into a big container and disposed in compliance with the policy.

Afterall, all the separated waste (paper, plastics, glass, etc.) was counted in percentage (rate), where 100 % is total weight of waste sample from each municipality (Formula below). A profile of MSW in each municipality was processed using data from physical analysis.

$$\frac{weight\ of\ separated\ waste\ category\ (kg)}{waste\ sample\ in\ total\ (kg)} * 100 = rate\ (\%)$$

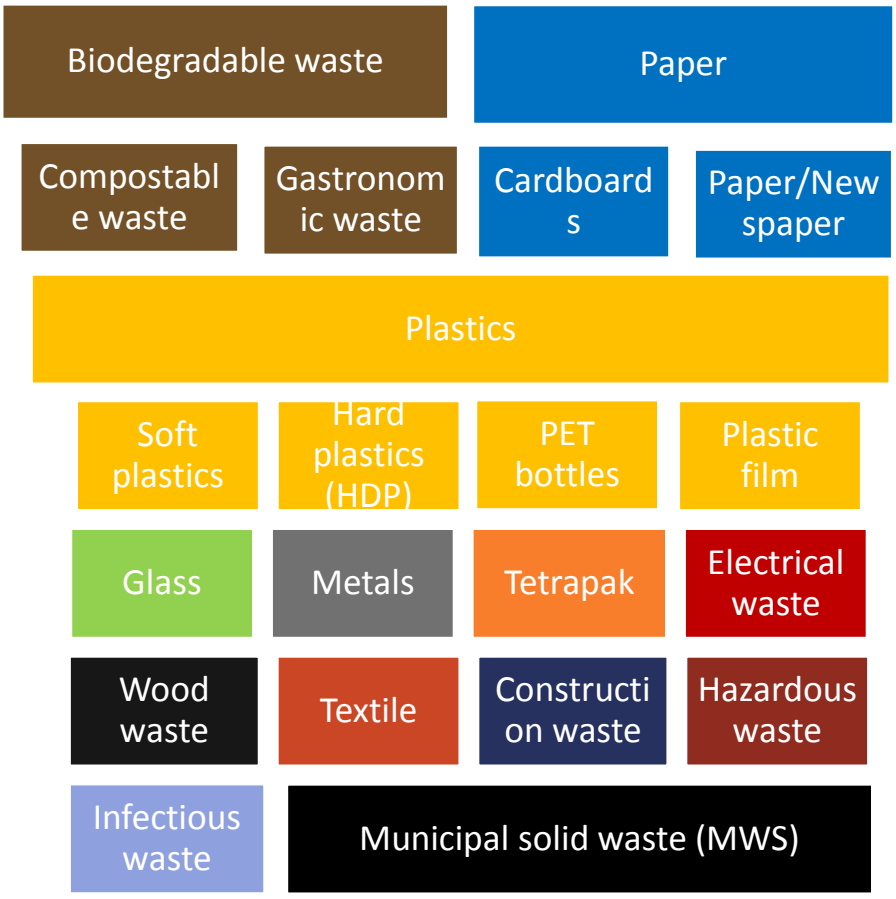

Figure 1: Categories of waste in which waste samples were separated during analysis.

Program R (R Core Team 2016) was used for statistical analysis of gained data to compare the difference in MSW and recycling potential between municipalities. All data were tested for normality assumption of parametric testing using Shapiro-Wilk test (Shapiro and Wilk 1965) but neither one set met the requirements of normality, therefore all data sets were treated as non-parametric and were used non-parametric statistical treatments for testing. Data of wood waste were recorded and used for result

visualization but excluded from statistical analysis due to their insignificant portion in samples over all municipalities as this might distort the statistics.

RESULTS

An overview of average physical composition of MSW is presented in figures below.

Figure 2 provides an overview of the data from analysis of physical composition depicting the average portion of waste compounds found in MSW sample basing on their weight. In the waste samples, non-recyclable part containing real municipal solid waste accompanied by hazardous and infectious waste created only approx. 34 % of MSW (**Chyba! Nenalezen zdroj odkazů.**), the remaining part (66 %) was created by recyclable compounds that should not end up in the black bins designated for non-recyclable waste. Most of recyclable compounds was created by organic waste (29.54 %) followed by plastics (11.38 %), paper (5.93%), textile (5.78 %) and glass (4.62 %). Organic waste was sum of compostable waste and gastronomic waste (=almost not compostable in CZE). Plastic waste included a big amount PET bottle which can be easily recycled. Recently a hot topic associated with PET bottles has arisen in the Czech Republic. According to the practices aboard, PET bottle deposit system is coming to forefront. The main goal of operating the deposit system will be saving the bottles from municipal waste bins and littering, also guaranteeing a good quality of bottles returning back to producers. Beside PET bottles, plastic films, soft and hard plastics were also found in the waste sample. Construction waste occurred in the MSW in less significant amount, but still occupied more than 3 % of MSW. Sometimes the electrical and electronic waste could be found in MSW as well, representing approx. 1 % of waste sample, similarly like tetrapak. Clearly, non-recyclable MSW produced by households represented actually much smaller amount than throwed into the municipal waste bins.

Statistically, data were compared between municipalities to show the difference in municipal solid waste composition. The results demonstrated that there was no evidence of significant differences in waste structure in all municipalities difference (p value > 0.05). It suggests that small municipalities in the Czech Republic with population up to 2999, might have similar waste structure in MSW.

Due to their significant amount representing in MSW, organic waste and plastics were specially tested in-between municipalities (Figure 4). Plastic waste had small range from 3 % up to 7 % of MSW while organic waste was more variable, one municipality had more than 50 % of MSW created by organic waste, another 3 had over 40 % and average rate is 29.5% of total MSW. These results pointed that plastics and organic waste produced from kitchen and gardening is usually throwed into municipal waste bin instead of being recycled. On the other hand, this gives a sign of potential in improving recycling at source.

Statistically, neither of these two components had shown noteworthy difference in composition of MSW (all p value > 0.05) as all tested municipalities had similar waste structure, like it is showed at overall physical composition of MSW above.

Because of the lack of data from municipalities with more population size (>3000 citizens), we decided to not include these data into the present study.

Based on the results from physical composition assessment it is possible to assume the approximal potential for improving. Organic waste represented 29.5 % of total MSW. In year 2018 the production of MSW in the Czech Republic did 5 782 thousand tons. If we deducted 29.5 % from it, which introduces the organic waste, we would get to the level of 4073.93 thousand tons of MSW. Moreover, if we deducted additionally plastics, paper and glass from the total production, we would save 2976.4 thousand tons of waste from landfilling or incineration. This scenario is less likely because we cannot reach 100 % of recycling organic waste etc. Even though, if we improved only 30 % of recycling, means deducted 30 % of organic waste, plastics, paper and glass ended in MSW, we would save 512.42 thousand tons of organic waste from landfilling and 380.5 thousand tons of paper, plastics and glass together. Figure 5 demonstrates, that even improve about 30 % would change the amount of landfilling waste and save some money for the municipal budget as well as contributing to the better environment.

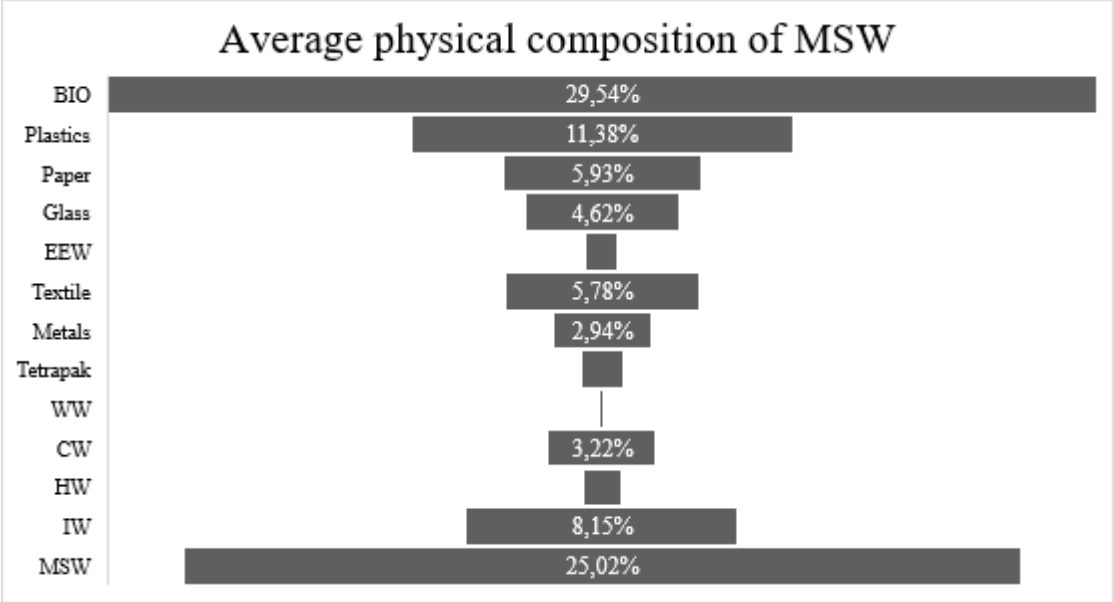

Figure 2 showing the average physical composition of municipal solid waste in the selected municipalities of this study. **Abbreviations**: BIO – organic waste; EEW – electrical and electronic waste; WW – wood waste; CW – construction waste; HW – hazardous waste; IW – infectious waste; MSW – municipal solid waste.

Figure 3: Average portion of recyclable and non-recyclable waste divided according to their attribute. Municipal solid waste is kind of waste with no further use but determined for incineration (energy recovery) and landfilling. According to this figure, there was still more than fifty percent usable/recyclable waste but ended up in bins with municipal waste.

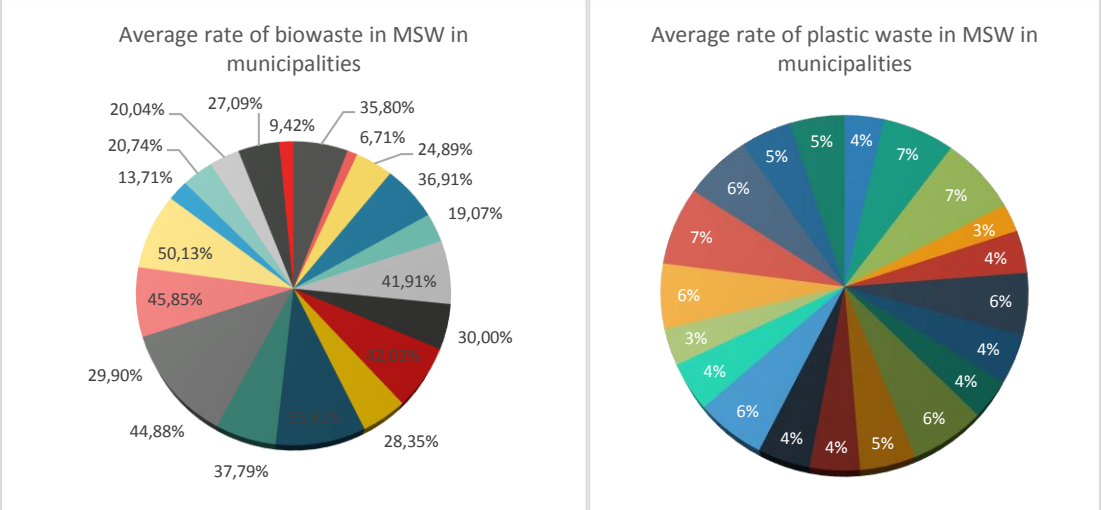

Figure 4: These two figures show average rate of two most abundant components in MSW – organic and plastic waste, in tested municipalities. Each colour represented one municipality. Due to the agreement with municipalities, their names stayed anonymously.

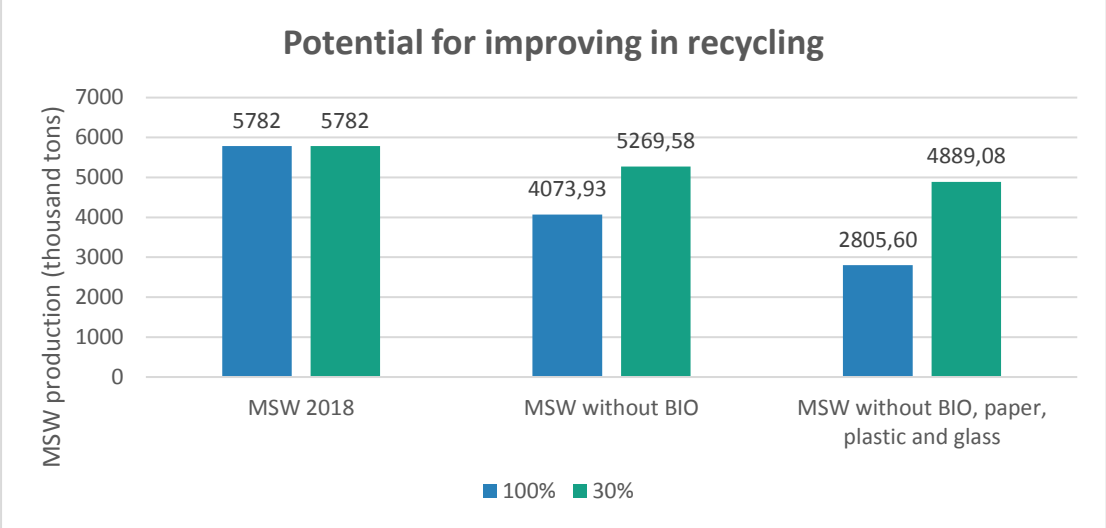

Figure 5: Possible scenario how much would production of MSW decrease when increase the recycling. MSW 2018 means total production of MSW in year 2018 in thousand tons. MSW without BIO means how much would MSW production decrease, if the organic waste ended in MSW would be recycled (removed from MSW) by 100 % or 30 %, specifically MSW 2018 minus organic waste which is multiplied by rate of organic waste from analysis above. MSW without BIO, paper, plastic and glass is like previous information, but from MSW 2018 is deducted organic waste and paper, plastic and glass.

DISCUSSION

Assessment about physical composition of municipal solid waste has goal to define the structure of MSW, i.e. paper, plastics, organic in municipal waste. The structure can tell a lot about the waste management in borough, especially it may reflect the citizen behavior related to waste recycling and disposal.

Our results demonstrate that structure of individual components in MSW is similar between the 20 tested municipalities. Further it is assumed that the ratio of municipal waste and organic waste in the total MSW produced by citizens is similar, as is the ratio of plastics.

This study also pointed out a lot of room for improvement in the sorting of municipal waste directly at source (in households), as usable waste disposed in non-recyclable bins represented up to 65.7% of MSW. Waste discarded in this way can no longer be recycled and can be only incinerated for energy recovery or at worst, landfilled without any use. This huge amount does not bring any income to the municipal authority, or even might burden the city budget by all acts associated with MSW collection, maintenance and landfill tax which means the more MSW is produced the higher tax has to be paid. Therefore the priority is decreasing the amount of MSW by reaching two main targets: preventing waste generation at source (household) and collecting recyclable waste as it can be reused or recycled, while trading with recyclable waste means additional income to city budget.

The biggest portion of MSW was represented by organic waste (food waste, yard waste, leaves) which is also confirmed in the other studies in Crete (Gidarakos et al. 2006), Iran (Dehghani et al. 2009; Phillips, Gholamalifard 2016), Western Algeria (Guermoud et al. 2009) and Ghana (Miezah et al. 2015).

Also there is an exceptional cause calling for an increase in recycling from the national level. According to the present waste law which determines the obligation of separate collection for organic and metal waste since year 2015, municipal authority has to ensure the collection for the whole year at least for compostable organic waste. Recently from this year (January 1st, 2020), a new duty for municipal authority has been applied that used gastronomic oil waste from households should be collected individually and recycled. The Czech legislation has a clear message oriented to circular economy and waste production reduction. This appear to be necessary and essential

how to make changes not only at the municipal levels also with private sectors. It is interesting to note that the present waste law determines the total ban on landfilling of recyclable and usable components of MSW since year 2024, but the new law, which is in preparation process and will come into force soon, is about to defer this ban to year 2030.

Other motivation for waste reduction comes from European Union too, which has released new policies about circular economy in waste management. To meet these requirements, municipal authorities have to come with measures leading to reduction of both total amount of waste and non-recyclable waste.

On the other hand, it is very easy to reduce landfill costs and MSW amount when we found out that there is a striking quantity of recyclable waste waiting for separation which if we redirect it, can be saved. Waste reduction is highly depended on dwellers activities. There are many socio-economic-technically factors affecting their behavior and disabling them in recycling. For example the distance and availability of recycling bins, the volume and repletion of bins, lack of awareness and education, low technology and innovation level, etc. (Lane and Wagner 2013) create barriers for the basic recycling, whereas financial stimulus is the major motivational factor for their active participation. The good site is that can be easily changed by the motivations and efforts from municipal authority (Kattoua et al. 2019). The link between them and citizens needs to be strengthened. Hence, possible activities for inhabitants must focus on these areas bracing education for inhabitants, special education activities for children and schools, organizing events to increase the awareness of recycling and the overall promotion of waste reuse and recycling.

Revaluating waste collecting system opens also new opportunities for municipality. Good way is to check the data from collection companies. Other study from INCIEN showed that many waste bins were collected practically empty or half-empty, but municipality have to pay to companies for each collection regardless of that if the bin was empty or full. Based on this information, optimalization of the number of containers come in handy and can bring further significant budget savings which can be invested into technology, for instance.

CONCLUSION

In summary, this paper evaluated the data about physical composition of MSW in Czech small municipalities, found out the disadvantages of low rate of recycling and pointed out the opportunities of improvement.

This analysis of physical composition of MSW is considered as a fundamental method for municipal authorities to verify separation rate at source and help with design, implementation, and operation of the best practice in the waste management. It is recommended to conduct regularly and monitor the development over years.

ACKNOWLEDGEMENTS

A special thank to Institut Cirkulární Ekonomiky, z. ú. for providing the data for this study.

This research was supported by Internal Grant Agency of Faculty of Engineering, Czech University of Life Sciences Prague, Grant No. 2020:31180/1312/3108.

REFERENCES

1. Dehghani MH, Dehghanifard E, Azam K, et al (2009) A Quantitative and Qualitative Investigation of Tehran Solid Waste Recycling Potential. Knowl Heal 4:40–44
2. Diaz LF, Golueke CG, Savage GM, Eggerth LL (2020) Composting and recycling municipal solid waste. CRC Press
3. Erami S, Maleki A, Shahmoradi B (2015) Municipal Solid Waste Management in Mahabad Town, Iran. ournal Environ Sci Technol 1–9
4. European Commission (2020) Circular Economy Action Plan for a cleaner and more competitive Europe. 28
5. Gidarakos E, Havas G, Ntzamilis P (2006) Municipal solid waste composition determination supporting the integrated solid waste management system in the island of Crete. Waste Management 26:668–679
6. Guermoud N, Ouadjnia F, Abdelmalek F, et al (2009) Municipal solid waste in Mostaganem city (Western Algeria). Waste Manag 29:896–902

7. Heravi HM, Sabour MR, Mahvi AH (2013) Municipal Solid Waste Characterization, Tehran-Iran. Pakistan J Biol Sci 16:759–769
8. Kattoua MG, Al-Khatib IA, Kontogianni S (2019) Barriers on the propagation of household solid waste recycling practices in developing countries: State of Palestine example. J Mater Cycles Waste Manag 21:774–785
9. Kreith F (1999) Handbook of solid waste management. McGraw-Hill, New York
10. Lane GWS, Wagner TP (2013) Examining recycling container attributes and household recycling practices. Resour Conserv Recycl 75:32–40
11. Miezah K, Obiri-Danso K, Kádár Z, et al (2015) Municipal solid waste characterization and quantification as a measure towards effective waste management in Ghana. Waste Manag 46:15–27
12. Ministry of the Enviroment (2008) Metodický pokyn ke vzorkování odpadů
13. Ministry of the Environment (2019) Waste production in the regions of the Czech Republic 2018
14. Ministry of the Environment (2014) Waste Management Plan of the Czech Republic for the period 2015-2024. Prague
15. Phillips J, Gholamalifard M (2016) Quantitative evaluation of the sustainability or unsustainability of municipal solid waste options in Tabriz, Iran. Int J Environ Sci Technol 13:1615–1624
16. R Core Team (2016) R: A Language and Environment for Statistical Computing. R Found Stat Comput Vienna, Austria
17. Shapiro S, Wilk M (1965) An analysis of variance test for normality (complete samples). Biometrika 52:591–611

Corresponding author:
Ing. Shuran Zhao, Department of Machinery Utilization, Faculty of Engineering, Czech University of Life Sciences Prague, Kamýcká 129, Praha 6, Prague, 16521, Czech Republic, tel: +420720364856, email: zhao@tf.czu.cz

Proceeding of 22nd International Conference of Young Scientists 2020

September 14th 2020 – September 15th 2020

Publisher:	Czech University of Life Sciences Prague Kamýcká 129, Prague, Czech Republic
Editors:	Rostislav Chotěborský, Jiří Kuře
Printing house:	CULS Prague
Number of copies:	0
Number of pages:	330
Issue:	First
Year:	2020
ISBN	978-80-213-3037-5